Chinese Hamster Ovary Cell Line Development via Imaging Flow Cytometry and Directed Evolution

Eva M. Pekle

Academic supervisor: Prof. Mark Smales

Industrial supervisors: Claire Pearce, Chris Sellick and Claire Harris

Department of Biosciences

University of Kent

This dissertation is submitted for the degree of

Doctor of Philosophy

September 2019

Declaration

I, Eva Pekle, hereby declare that no part of this thesis has been submitted in support of an application for any degree or other qualification of the University of Kent, or any other university of institution of learning. I declare that the contents of this dissertation are original, and consist of my own work, along with collaborators who have been specified in the text.

Acknowledgements

This thesis represents four years of work at MedImmune towards achieving my PhD and could not have been accomplished without the support of many people, to which I owe my deepest gratitude. Thank you to Professor Mark Smales, Dr. Claire Pearce and Dr. Chris Sellick for giving me the opportunity to work on this project, and to have believed in me throughout those past years, mentored me, and helped me become more confident. Thank you to Claire and Chris for always celebrating my "achievements" throughout the

project and making those little milestones exciting and memorable. Thank you to Dr. Claire Harris to have taken over as my supervisor in the middle of the project, and supported me until the very end, especially with the very helpful feedback for my thesis. Thank you to Dr. Diane Hatton for always carefully reviewing all of my pre-PSO work and giving insightful comments.

Thank you to all the people who have helped me in the lab. A huge thank you to Dr. Guglielmo Rosignoli for taking the time to show me how to use the flow cytometer and assisting me in my experiments. Thank you to Alison Mason for helping with my first Ambr, to Claire, Dr. Maiken Kristiansen and Dorota Kozub for taking care of my cells when I was away, and to the members of the BPA team, Andy Smith, Fabio Zurlo and Matthew Jackson for accommodating my (numerous!) titre requests. Thank you to Dr. Bertie Chi for his help with the mass spectrometry. Thank you to Dr. Charlotte Godfrey for her help with the qRT-PCR. Thank you to Maiken for teaching and helping me with my RNA samples preparation, and to Dr. Luigi Grassi for his invaluable help with the RNA seq data analysis. Thank you to Dr. Raj Mistry for his help with the glutathione assays. A big thank you to the wider CLD and CCFS teams for your support and insights.

These past four years have also been a lot of fun, through the EES team nights out, to working on the End of the Year reviews and Summer Day with Jake Warrington, those were some of my best memories from Medi. Thank you to Dr. Pegah Saremirad and Audrey Vuillemez for the endless lunches, always bringing me food and being up for going on a little walk around Granta Park. Seeing you at work every day always gave me something to look forward to. Thank you to my fellow Medi PhD students, Natalie Talbot and Calum McIntosh, for always bringing me joy during each of your visit at MedImmune, and Andy Martin for the fun week we had while I was down in Kent. Thank you to my conferences and training buddies, Calum, Ricardo Suarez Heredia and Dr. Hirra Hussain, every event attended with you was always the most fun. And thank you to my friends Dr. Elise Bernard Marine Fickinger, Katherino Chao and Alexandra Scanameo, seeing you always gave me something to be excited about.

Finally, a huge thank you to my parents, Valérie and Guy, and my sisters, Sandra and Emmanuelle, which have supported me, encouraged me and never stopped believing in me throughout those past four years. Thank you for the letters and packages that have kept me going through the cold and grey Cambridge days. And none of this would have been possible without the support of Saeid Samimi. Thank you so much for your love and patience with me, I have been so lucky to have you by side. Thank you for moving to Cambridge, for making me silly videos and giving me the hope to achieve what I wanted.

Abstract

Biopharmaceutical technology development is tailored towards the generation of cell expression systems and bioprocesses for the production of recombinant proteins. Regulatory agencies require production cell lines to originate from a single cell. Different methods can be used to achieve clonality, including single cell sorting via flow cytometry. Following cloning, typically hundreds of clones are screened to identify high producers. Therefore, the ability to enrich for cells with high expression of the target recombinant protein of suitable quality during the cloning process could reduce timelines and reduce the number of clones screened. Here flow imaging technology for the isolation of high producing monoclonal antibody expressing Chinese hamster ovary (CHO) cells was used to select cells based upon particular cell attributes and used to establish whether these correlated with antibody titre. Subsequently, a directed evolution approach was undertaken to generate a new CHO cell host pool which was then compared to the original control host for its ability to produce a range of antibody molecules.

Initially, a panel of recombinant CHO cell lines expressing a model antibody (mAb) was characterised in terms of growth, productivity, intracellular recombinant protein and mRNA amounts. Imaging flow cytometry assays, using commercially available dyes, were developed to investigate organelle content, and multiplexed with heavy chain (HC) protein antibody to probe correlations between organelle content and productivity at the cellular level. Correlations at the population levels between the average intensity of the organelle staining and cell culture parameters were also investigated. Lysosome content was identified as having a positive correlation with specific mAb productivity. Cell sorting based on lysosome content (high, mid and low florescence intensity) was performed and, high lysosome content cell sorting led to the isolation of cells with increased productivity compared to unsorted cells. The range of increased titre was molecule dependent, with titre increasing by up to 200% for what was considered an easy to express mAb (ETE), and 30% for a bispecific mAb. Moreover, the increase in titre was due to an increased homogeneity of the heavy and light chain (LC) expressing population and delayed apoptosis of the cells in culture.

Following this, directed evolution of the CHO host was undertaken in an effort to isolate CHO cells with increased lysosome content. To achieve this, the host cell line was subjected to chemical directed evolution with chloroquine (CQ), a chemical known to increase lysosome content in cells. The host cell line was treated with CQ for 15 passages, until CQ-treatment no longer negatively impacted cell growth or culture viability. The initial (control) and evolved hosts were then transfected to generate stable pools expressing an ETE, difficult to express (DTE) mAb and a bispecific mAb. The evolved host outperformed the standard host for all three molecules tested, with increases in productivity ranging from 2 to 5.8-fold whilst maintaining higher culture viability throughout the fed-batch experiments. Mechanistic studies to determine the cellular attributes underpinning the increase in titre following CQ-evolution were then undertaken, including monitoring protein expression of key target proteins in high lysosome content sorted cells and the CQ-evolved cells, and their respective controls. Transcriptomic analysis by RNA-sequencing was also undertaken to investigate differences between the standard and CQ-evolved hosts to understand the mechanism(s) and pathways involved in the underlying increased performance. Surprisingly these did not reveal any specific changes in lysosome activity in the CQ-evolved cell pool on day 7 of the fed-batch culture and thus the mechanism(s) underpinning the improved productivity from these cells is likely to be the result of multiple changes in the expression of different pathways and genes/proteins.

In summary, this thesis presents two strategies to increase recombinant protein productivity from CHO cells through the manipulation of lysosome content. The cell sorting strategy can easily be implemented in the cell line development process to isolate cells with enhanced productivity characteristics based on lysosome content, whereas the CQ-evolution based approach requires the development of a novel host cell pool through directed evolution, in less than two months.

Table of Content

Declaration. i

Acknowledgement ii

Abstract. iii

Table of Contents. iv

List of Figures. xii

List of Tables. xvi

Abbreviations. xviii

Chapter 1 Introduction and Background. 1

1.1 Biopharmaceutical development. 1

1.1.1 Biopharmaceuticals. 1

1.1.2 Expression systems used for biopharmaceutical production. 3

1.1.3 Overview of biopharmaceutical production. 5

1.2 Chinese hamster ovary (CHO) cells. 8

1.2.1 History of CHO cells in bioprocessing. 8

1.2.2 Structure, folding and secretion of mAb. 10

1.2.3 Cellular constraints. 12

1.3 Previous strategies to increase CHO cell productivity and cellular pathway. 12

1.3.1 Host cell line engineering and manipulations. 12

1.3.2 mRNA translation, protein synthesis, translocation and folding pathway. 14

1.3.3 Mammalian target of rapamycin pathway (mTOR) engineering. 18

1.3.4 Lysosomes function and autophagy. 23

1.3.5 Apoptosis. 28

1.3.6 vector engineering for enhanced recombinant protein production. 31

1.4 Flow cytometry in cell line development. 31

1.4.1 Importance of monoclonality. 31

1.4.2 Cell line heterogeneity. 32

1.4.3 Flow cytometry methods to isolate high producers. 33

1.5 Image flow cytometry. 35

1.6 Project aim and objectives. 37

Chapter 2 Materials and Methods. 40

2.1 Mammalian cell culture. 40

2.1.1 Cell lines and cell culture. 40

2.1.2 Cell concentration and culture viability. 40

2.1.3 Cryostorage of cell lines. 41

2.1.4 Thawing of cell lines from frozen stocks. 41

2.1.5 Fed-batch overgrow cultures. 41

2.1.6 Determining cell culture supernatant glucose and lactate concentration. 41

2.1.7 Chloroquine treatment of cells 42

2.1.8 Ambr experiments. 42

2.2 Recombinant protein quantitation. 42

2.2.1 Protein-A affinity purification. 42

2.2.2 Determination of cell specific mAb productivity. 42

2.3 generation of plasmid DNA and transfection of CHO cells. 43

2.3.1 Plasmid DNA transformation. 43

2.3.2 Plasmid DNA purification. 43

2.3.3 Agarose gel electrophoresis. 44

2.3.4 Electroporation of plasmid DNA into CHO cells. 44

2.4 Molecular biology. 44

2.4.1 RNA extraction. 44

2.4.2 qRT-PCR 45

2.5 Flow cytometry and imaging flow cytometry 45
2.5.1 HC and LC mRNA quantification by PrimeFlow RNA. 46
2.5.2 Intracellular HC and LC protein analysis. 47
2.5.3 Organelle assays. 47
2.5.4 Data acquisition and analysis for flow cytometry. 48
2.5.5 Data acquisition and analysis for imaging flow cytometry. 48
2.6 Fluorescence-activated cell sorting. 49
2.6.1 Cell sorting. 49
2.6.2 Cell recovery. 50
2.7 Protein analysis. 50
2.7.1 Protein extraction. 50
2.7.2 Bradford assay to determine protein concentration. 50
2.7.3 SDS-PAGE analysis. 51
2.7.4 Western blotting. 51
2.7.5 Automated western for supernatant analysis. 52
2.7.6 Glutathione measurement assays. 53
2.7.7 Protein digestion for LC-MS/MS analysis. 53
2.7.8 LC-MS/MS. 53
2.8 RNA sequencing. 54
2.8.1 Total RNA isolation using Tri reagent. 54
2.8.2 RNA quality assessment. 54
2.8.3 Library synthesis, sequencing and reference mapping. 55
2.8.4 Differential gene expression analysis and gene ontology analysis. 56
2.9 Statistics. 56

Chapter 3 Application of imaging flow cytometry for the characterisation of intracellular attributes in CHO cell lines at the single cell level. 59

3.1 Introduction. 60

3.2 Results. 61

3.2.1 Preliminary characterisation of a panel of 19 cell lines. 61

3.2.1.1 Cell culture characterisation and comparison of BSF and AMBR systems. . . 61

3.2.1.2 Intracellular HC and LC protein expression. 67

3.2.1.3 HC and LC mRNA expression. 69

3.2.2 ImageStream assay development and validation. 71

3.2.2.1 ImageStream data analysis. 71

3.2.2.2 ImageStream validation against standard flow cytometry. 72

3.2.2.3 ImageStream validation against standard techniques. 75

3.2.3 Investigation of correlations between organelle content and cell culture attributes. . . 77

3.2.3.1 HC protein content comparisons between staining. 78

3.2.3.2 HC and LC protein and message profiles. 78

3.2.3.3 Analysis of correlation at the single cell and population level. 79

3.3 Discussion. 84

Chapter 4 Lysosome content-based cell sorting of CHO cells. 88

4.1 Introduction. 88

4.2 Results. 90

4.2.1 Comparison of lysosome sorted cell characteristics compared to the original cell populations. 90

4.2.2 Mixed cell lines lysosome content sorting: pool sorting based on lysosome content. . . 91

4.2.2.1 Culturing of lysosome content amount sorted cell pools isolated from the mixed cell pool in FBOG conditions. 92

4.2.2.2 Analysis of the intracellular HC and LC content of lysosome isolated cell pools from the original cell mix pool. 94

4.2.2.3 Determining the lysosome content of the Mixed cell pool and subsequent isolation of high, mid and low content lysosome pools. 95

4.2.3 Individual cell lines sorting - Pool sorting based on lysosome content 95

4.2.3.1 Lysosome content cell sorting of individual mAb expressing cell lines 96

4.2.3.2 Intracellular HC and LC content of individual mAb producing cell lines and lysosome sorted pools. 100

4.2.3.3 Lysosome content of individual sorted original cell lines. 103

4.2.4. Bispecific mAb: pool sorting based on lysosome content. 103

4.2.4.1 Lysosome content sorting of bispecific mAb expressing cell lines. 103

4.2.4.2 Lysosome content of the bispecific mAb cell pools isolated based on lysosome content. 105

4.2.5 Characterisation of lysosome sorted pools expressing an ETE mAb by western blotting. 106

4.2.5.1 Autophagy markers. 106

4.2.5.2 mTORC1 markers. 108

4.2.5.3 Apoptosis markers. 110

4.3 Discussion. 112

Chapter 5 Directed evolution of the host cell line using chloroquine. 117

5.1 Introduction. 117

5.1.1 Directed evolution. 117

5.1.2 Chloroquine. 119

5.1.3 Directed evolution of the host cell line using chloroquine. 121

5.2 Results. 122

5.2.1 Development of a novel host via directed evolution using chloroquine 122

5.2.1.1 Initial CQ concentration screening. 122

5.2.1.2 Long-term CQ treatment of CHO cells. 123

5.2.1.3 Chloroquine removal and re-introduction. 123

5.2.2 Strategies for chloroquine treatment of the chloroquine-evolved host post transfection 125

5.2.2.1 Growth profiles of CQ treated recombinant protein expressing pools. 127

5.2.2.2 mAb Productivity of CQ-evolved cells. 129

5.2.2.3 Analysis of the lysosome content in CQ-evolved and control cells. 130

5.2.3 Evaluation of the chloroquine evolved host expressing an ETE mAb. 132

5.2.3.1 Culturing of chloroquine – evolved host expressing an ETE mAb. 132

5.2.3.2 Analysis of intracellular HC and LC content of the chloroquine evolved host expressing an ETE mAb. 134

5.2.3.3 Product quality analysis of ETE mAb expressed from the different hosts. . . 134

5.2.3.4 Analysis of lysosome content of the chloroquine evolved host expressing an ETE mAb. 136

5.2.4 Analysis of the CHO cell chloroquine evolved host expressing a DTE mAb. 137

5.2.4.1 Culturing of the control and chloroquine evolved host expressing a DTE mAb. 137

5.2.4.2 Analysis of intracellular HC and LC content of chloroquine evolved host expressing a DTE mAb. 139

5.2.4.3 Product quality analysis of DTE mAb. 139

5.2.4.4 Analysis of lysosome content of the chloroquine evolved host expressing a DTE mAb. 140

5.2.5 Evaluation of the chloroquine evolved host expressing a bispecific mAb. 141

5.2.5.1 Culturing of chloroquine evolved host expressing a bispecific mAb. 141

5.2.5.2 Analysis of intracellular HC and LC content of control and chloroquine evolved host expressing a bispecific mAb. 143

5.2.5.3 Analysis of lysosome content of the CQ-evolved host expressing a bispecific mAb. 144

5.2.5.4 Product quality analysis of the bispecific mAb. 144

5.2.6 Overall summary of results from the CQ-evolved host. 146

5.2.7 Investigating the mechanisms underlying the improved recombinant protein production and prolonged culture viability of the CQ-evolved host. 146

5.2.7.1 RNA sequencing of the CQ-evolved host and standard host expressing an ETE or DTE mAb. 146

5.2.7.2 PCA analysis of transcript expression and identification of differentially expressed genes. 147

5.2.7.3 Gene ontology analysis. 148

5.2.7.4 KEGG pathway analysis. 151

5.2.7.5 Manual analysis of differentially expressed genes. 151

5.2.7.6 Summary of transcriptomic analyses. 152

5.2.8 Oxidative stress analysis of chloroquine-evolved host and control host expressing an ETE or DTE mAb. 153

5.2.8.1 Glutathione quantification. 153

5.2.8.2 Flow cytometry analysis of oxidative stress. 155

5.2.9 Western blot analysis of specific intracellular proteins in the chloroquine evolved host and standard host expressing an ETE or DTE mAb. 157

5.2.9.1 Analysis of autophagy markers in the ETE mAb expressing cells. 157

5.2.9.2 Assessment of autophagy marker expression in DTE mAb expressing cells. . 159

5.2.9.3 Analysis of mTORC1 markers in ETE mAb expressing cells. 160

5.2.9.4 Analysis of mTORC1 markers in DTE expressing cells. 162

5.2.9.5 Apoptosis markers in the control and CQ-evolved host cells expressing an ETE mAb. 163

5.2.9.6 Apoptosis markers in the control and CQ-evolved host cells expressing a DTE mAb. 164

5.3 Discussion. 165

Chapter 6 Discussion. 173

6.1 Overall discussion. 173

6.2 Future work. 179

References. 182

Appendix A 196

Appendix B. 208

Appendix C. 213

List of Figures

Chapter 1 Introduction and background

1.1 Evolution of the mAb landscape. 2
1.2 Cell line development process workflow. 6
1.3 Overview of the CHO production process. 7
1.4 CHO cell lineage. 9
1.5 Human IgG schematic. 11
1.6 UPR pathways. 16
1.7 mTORC1 and mTORC2 protein complexes. 19
1.8 The role mTORC1 in protein synthesis. 20
1.9 The role of mTORC1 in autophagy. 22
1.10 Schematic of the autophagy pathway. 25
1.11 Schematic representation of the CLEAR pathway. 27
1.12 Schematic of the apoptosis pathway. 30

Chapter 2 Materials and methods

2.1 Schematics depicting the PrimeFlow mechanisms of action. 46
2.2 Imaging flow cytometry analysis workflow. 49
2.3 Bioanalyzer sample results. 55

Chapter 3

3.1 Growth data from the BSF and AMBR experiment. 63
3.2 Titre data from the BSF and AMBR experiment. 64
3.3 Specific productivity data from the BSF and AMBR experiment. 65
3.4 Metabolites profiles for the BSF and AMBR experiment. 66
3.5 IC HC and LC protein quantification by western blotting on day 4 of the FBOG 67
3.6 Comparison of productivity with IC HC and LC protein. 68
3.7 Quantification and comparison of HC and LC mRNA with productivity. 70

3.8 Sample images of the assays developed on the IS and analytical features. 72

3.9 Schematic of the robustness experiment. 73

3.10 Results from the robustness experiment, comparing ImageStream and standard flow cytometry. 74

3.11 HC protein and message quantification by ImageStream, and comparison with final titre. . . 76

3.12 Comparisons of a sample of cell lines with heterogenous and homogenous HC and LC protein/mRNA expression, and HC and LC protein content throughout the FBOG 79

3.13 Sample profiles of ImageStream analysis. 80

3.14 Lysosome content throughout the FBOG and comparison to overall qP. 81

3.15 PCA analysis of the different IS staining on day 3 of the FBOG. 83

Chapter 4

4.1 Schematic showing the sorting strategy based on high-lysosome content. 89

4.2 Cell culture data from preliminary FACS experiment. 91

4.3 Gating strategy for cell sorting based on lysosome content. 92

4.4 Cell culture data comparing high, mid and low lysosome sorted cells. 93

4.5 Intracellular HC and LC protein. 94

4.6 Lysosome content of high, mid and low lysosome sorted cell pools. 95

4.7 Histogram of the lysosome intensity of the individual cell lines. 96

4.8 IVC of individual cell lines, sorted based on lysosome content or unsorted. 98

4.9 Viability of individual cell lines sorted based on lysosome content or unsorted. 99

4.10 Final mAb titre and overall qP of the individual cell lines sorted based on lysosome content. . 100

4.11 Intracellular HC and protein distribution of the individual cell lines sorted based on lysosome content. 102

4.12 Lysosome content of the individual cell lines sorted based on lysosome content. 103

4.13 Bispecific mAb cell culture results. 104

4.14 IC HC and LC protein of the bispecific mAb sorted based on lysosome content. 105

4.15 Lysosome content of the bispecific cell lines sorted based on lysosome content. 105

4.16 Autophagy marker analysis by western blotting in the standard mAb expressing pools. 108

4.17 mTORC1 pathway analysis by western blotting in the standard mAb expressing pools. 110

4.18 Apoptosis biomarker analysis by western blotting in the ETE mAb. 111

Chapter 5

5.1 Conversion of chloroquine to its protonated form. 119

5.2 Chloroquine mechanism of action. 121

5.3 Screening of a range concentrations of CQ for directed evolution. 122

5.4 Long term chloroquine treatment of untransfected cells. 123

5.5 Removal of chloroquine treatment and re-introduction. 124

5.6 Chloroquine treatment strategies following transfection. 126

5.7 Cell culture data comparing the different chloroquine treatment strategies following transfection. 128

5.8 Productivity data comparing the different chloroquine treatment strategies following transfection. 129

5.9 Lysosome content of cell during culture, based on the different chloroquine treatment strategies following transfection. 131

5.10 FBOG cell culture data of cells expressing the ETE mAb. 133

5.11 Intracellular HC and LC protein for the cells expressing the ETE mAb. 134

5.12 N-linked glycan profiles of an ETE mAb. 136

5.13 Lysosome content of cells expressing the ETE mAb. 136

5.14 FBOG cell culture data of cells expressing the DTE mAb. 138

5.15 Intracellular HC and LC protein for the cells expressing the DTE mAb. 139

5.16 N-linked glycan profiles of a DTE mAb. 140

5.17 Lysosome content of cells expressing the DTE mAb. 140

5.18 FBOG cell culture data of cells expressing the bispecific mAb. 142

5.19 Intracellular HC and LC protein for the cells expressing the bispecific mAb. 143

5.20 Lysosome content of cells expressing the bispecific mAb. 144

5.21 Non-reduced HC automated western of supernatant harvested on day 12, showing product aggregates. 145

5.22 PCA analysis of RNA-seq transcriptomic gene expression data comparing all the samples. . . . 147

5.23 Heatmap and MA plot of the RNA-seq analysis. 148

5.24 Schematic outlining the conversion of reduced glutathione to oxidised glutathione and key enzymes involved in that conversion. 153

5.25 Total and oxidised glutathione levels during the culture. 154

5.26 Flow cytometry analysis of the oxidative stress levels. 156

5.27 Autophagy marker analysis by western blotting for the ETE pools. 158

5.28 Autophagy marker analysis by western blotting for the DTE pools. 159

5.29 mTORC1 pathway analysis by western blot in the ETE mAb. 161

5.30 mTORC1 pathway analysis by western blot in the DTE mAb. 162

5.31 Apoptosis markers analysis by western blotting of the ETE mAb. 163

5.32 Apoptosis markers analysis by western blotting of the DTE mAb. 164

Appendix B

1 Cell culture data from the repeat of the BSF FBOG (with IS sampling) 208

List of Tables

Chapter 1 Introduction and background

1.1 Ten bestselling biopharmaceuticals in 2013. 4

1.2 Host cell engineering strategies for improved cell lines. 13

Chapter 2 Materials and methods

2.1 HC and Kappa LC primers for qRT-PCR. 45

2.2 Reagents used for flow cytometry. 48

2.3 List of primary and secondary antibodies used for western blotting. 52

Chapter 3

3.1 Pearson's correlation coefficient between median fluorescence intensity of HC/LC protein and message, and productivity. 77

3.2 Pearson's correlation coefficient between the organelle content on different days and the cell culture growth and productivity values. 81

Chapter 4

4.1 Summary of autophagy proteins based on their function and at which stage of autophagy they are involved. 107

Chapter 5

5.1 Overview of the detected N-glycan structures of a monoclonal antibody. 135

5.2 Biological processes identified as being enriched by the GO analysis. 150

5.3 Cellular components identified as being enriched by the GO analysis. 151

5.4 Differentially expressed genes involved in the glutathione pathway. 152

Appendix B

1 Values for the overall qP, final titre and final IVC for the cell lines in BSF. 209

2 Correlation at the single cell level for individual cell line between mitochondrial content and HC protein, ER content and HC protein, LC protein and HC protein. 210

3 Results from the PCA analysis, showing the importance of the different variables towards each of the components. 211

Appendix C

1 Gene list of up-regulated genes in control compared to CQ-evolved cells. 213

2 Gene list of down-regulated genes in control compared to CQ-evolved cells. 220

Abbreviations

3-MA	3-methyl adenine
4EBP1	4E binding protein 1
ACF	animal component free
AMBRA1	autophagy beclin-1 regulator 1
AMPK	5' adenosine monophosphate-activated protein kinase
AMS	antibody-membrane switch
ATF4	activating transcription factor 64
ATF6	activating transcription factor 6
Atg	autophagy-related gene
Bcl-2	B-cell lymphoma 2
Bcl-xL	B-cell lymphoma xL
BID	BH3 interacting-domain
BiP	binding immnoglobulin protein
BSA	bovine serum albumin
BSF	baffled shake flasks
CD	chemically-defined
CH	heavy chain constant domain
CHO	Chinese hamster ovary
CHO-ori	original CHO cell line
CHOP	C/EBP homologous protein
CL	light chain constant domain
CLD	cell line development
CLEAR	coordinated lysosomal enhancement and regulation

CNV	copy number variation
CQ	chloroquine
CT	cycle threshold
DE	differentially expressed
Deptor	DEP domain TOR-binding protein
DHFR	dihydrofolate reductase
DMSO	dimethyl sulfoxide
DNA	deoxyribonucleic reductase
DTE	difficult-to-express
DTT	dithiothreitol
EDTA	ethylenediaminetetraacetic acid
eEF2K	eukaryotic elongation factor 2 kinase
eIF2	eukaryotic translation initiation factor 2
eIF4E	eukaryotic initiation factor 4E
EMA	European Medicines Agency
ER	endoplasmic reticulum
ERAD	endoplasmic reticulum-associated protein degradation
ERAF	endoplasmic reticulum-associated folding
ETE	easy-to-express
FACS	fluorescent-activated cell sorting
FBOG	fed-batch over-grow
FDA	U.S. Food and Drug Administration
FIP200	focal adhesion kinase family-interacting protein of 200 kDa
FISH	fluorescent in-situ hybridization
FSC	forward scatter
GAPDH	glyceraldehyde 3-phosphate dehydrogenase
GFP	green fluorescent protein

GO	gene ontology
GRP94	glucose-regulated protein 94
GS	glutamine synthetase
GSH	glutathione
GSSG	glutathione disulphide
HC	heavy chain
HEK	human embryonic kidney
HPLC	high performance liquid chromatography
Hsp	heat shock protein
IFC	imaging flow cytometry
IgG	immunoglobulin G
IRE1	inositol-requiring enzyme 1
IRES	internal ribosome entry site
IS	ImageStream
IVC	integral of viable cells
JNK	Jun N-terminal kinases
LAMP2A	lysosomal-associated membrane protein 2A
LC	light chain
LC-MS	liquid chromatography mass spectroscopy
mAb	monoclonal antibody
mLST8	mammalian lethal with Sec-13 protein 8
MMP	mitochondrial membrane potential
M-PER	mammalian protein extraction reagent
mRNA	messenger ribonucleic acid
MSX	methionine sulphoximine
mTOR	mammalian target of rapamycin
mTORC1	mammalian target of rapamycin complex 1

mTORC2	mammalian target of rapamycin complex 2
MTX	methotrexate
NEM	N-ethylmaleamide
NF-kB	nuclear Factor kappa-light-chain-enhancer of activated B cells
OKT3	Orthoclone
p62	sequestosome-1
p70S6K	p70 ribosomal S6 kinase 1
PBS	phosphate buffered saline
PCA	principal component analysis
PDI	protein disulphide isomerase
PEI	polyethyleneimine
PERK	protein kinase -like endoplasmic reticulum kinase
PI	propidium iodine
PI3P	phosphatidylinositol-3-phosphate
PLG	phase lock gel
PRAS40	proline-rich Akt substrate 40 kDa
protein-binding rictor 1	protor 1
protein-binding rictor 2	protor 2
qP	cell specific productivity
qRT-PCR	R quantitative real-time polymerase chain reaction
R	correlation coefficient
Raptor	regulatory associated protein mTOR
RFP	red fluorescent protein
Rheb	Ras-homologue enriched in brain
Rictor	rapamycin-insensitive companion of mTOR
RIN	RNA integrity number
RNA	ribonucleic acid

SDS-PAGE	sodium dodecyl sulphate polyacrylamide gel electrophoresis
SSC	side scatter
mSin1	stress-activated protein kinase-interacting protein 1
TF	transcription factor
TNF	tumour necrosis factor
TRAIL	TNF-related apoptosis-inducing ligand
TSC1	tuberous sclerosis complex 1
TSC2	tuberous sclerosis complex 2
ULK1	unc-51-like-kinase 1
UPR	unfolded protein response
VCD	viable cell density
VH	heavy chain variable domain
VL	light chain variable domain
XBP1	X-box binding protein 1
XBP1s	spliced X-box binding protein 1
XBP1u	unspliced X-box binding protein 1

CHAPTER 1

General Introduction and Background

This introduction initially describes what biopharmaceuticals are and how they are produced. It then focuses particularly on Chinese hamster ovary (CHO) cells as hosts for the expression of biopharmaceuticals and the intracellular pathways that may impact their productivity. The different strategies that have been used to increase CHO productivity are also discussed, with a focus on host cell line engineering. The development and role of flow cytometry in cell line development and methods that have been used to isolate high producing CHO clones is then described. Finally, the role that imaging flow cytometry could potentially play in the cell line development process is discussed.

1.1 Biopharmaceutical development

"We are at the beginning of a new era of immunochemistry, namely the production of 'antibody based' molecules" were Milstein's words during his Nobel Lecture in 1984, as he was awarded the Nobel Prize along with Jerne and Kohler for the discovery of the principle behind monoclonal antibody production. More than 30 years later, his prediction has become reality.

1.1.1 Biopharmaceuticals

Biopharmaceuticals are a class of biological macromolecules that include monoclonal antibodies (mAb) and antibody-derivatives, as well as vaccines, hormones and nucleic acid-products [1]. Antibodies and their derivatives are generally produced from cultured mammalian cell lines by direct secretion into the culture media. Monoclonal antibody and Fc-fusion proteins constitute the most prevalent type of recombinant biotherapeutic proteins commercially produced and the fastest growing group of molecules in clinical trials [2]. The biopharmaceuticals market continues to grow, with over 54 new biologics approved in the past four years and a predicted market for antibodies greater than $150 billion by 2020 [1, 3, 4].

In 1986, the fully murine monoclonal antibody Orthoclone OKT3, used for the prevention of kidney transplant rejection, was the first mAb approved for clinical use [5]. OKT3, specific for the antigen CD3

present on T-lymphocytes, can bind and block T-lymphocyte's response to the foreign kidney. Despite being a potent immunosuppressive drug, it also happened to be strongly immunogenic, causing the human immune system to attack the foreign murine antibodies [6]. This led not only to a decreased drug efficacy, but also increased the risk of complications. Since OKT3 approval, the mAb landscape has evolved from murine chimeric mAbs to humanised mAbs and eventually fully human mAbs (Fig. 1.1), each advancement has been accompanied by an exponential increase in product approvals and sales [2].

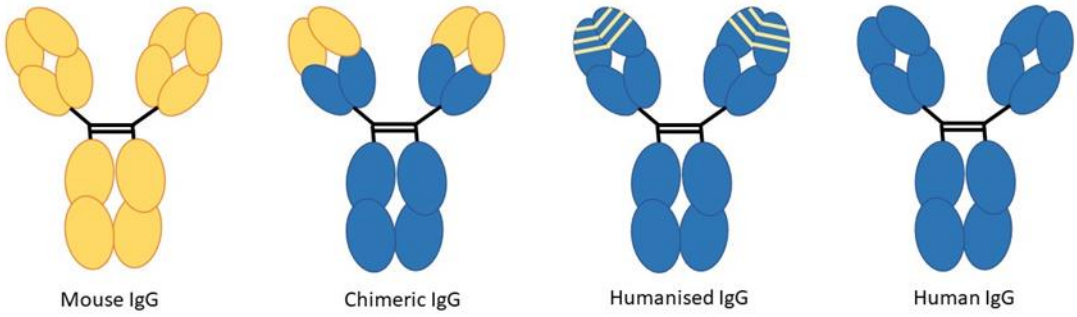

Figure 1.1 Evolution of the mAb landscape. From fully murine IgG (Immunoglobulin G, yellow), to chimeric IgG with a human constant domain and mouse variable region (variable region in yellow), to humanised IgG with murine antigen-binding domains (yellow lines) and finally to fully human IgG (blue).

The need for less immunogenic antibodies was obvious. Scientific progress initially achieved the production of the chimeric antibody, composed of a human constant immunoglobulin G (IgG) region and a mouse variable region, and eventually humanised monoclonal antibodies, composed of a human framework of antibodies to which murine antigen-binding domains are attached (Fig. 1.1), decreasing immunogenic concerns [7]. Despite the use of human and humanised monoclonal antibodies, the problem of immunogenicity has not been completely solved. For instance, Humira, the first fully human antibody, showed immunogenicity in 12% of patients [8]. It is possible that post-translational modifications, product impurities such as aggregates or fragments, and manufacturing process-related impurities can cause this immunogenicity in the human body.

The potential of these mAbs 'magic bullets', a term coined by Paul Ehrlich in 1900 to describe antibodies, has only been made further evident with more recent scientific advances. Antibodies have the ability, in theory, to bind to any extracellular protein target, as long as the antibody has access to the antigen-binding site. With a further understanding of diseases at the molecular level and the easier accessibility to patients next-generation sequencing data to detect new targets faster, mAbs offer a rapid way to activate, inhibit or block specific targets. Therapeutic proteins have become a major part

of treatments in various disease areas such as cancers, multiple sclerosis, asthma, rheumatoid arthritis and orphan diseases [1, 2]. Due to the specific binding nature of antibodies, more recently these have also been used to carry cytotoxic drug molecules to specific cell sites through the development of antibody-drug conjugates [9].

1.1.2 Expression systems used for biopharmaceutical production

Therapeutic proteins can be produced in a wide range of hosts including bacteria, insect, yeast, plant-based systems and mammalian cell lines. Out of the 10 bestselling biopharmaceutical recombinant protein (thereafter also referred to as recombinant proteins) products approved in the United States and Europe in 2013, only three were produced in *E. coli* with the others being produced in mammalian cell lines (Table 1.1) [2]. This prevalence of mammalian cell lines over non-mammalian cell lines correlates with an increase in molecules requiring human post-translational modifications such as glycosylation [1, 10]. Different expression systems have various advantages and drawbacks for the manufacture of a specific biopharmaceutical and having a heterogeneous panel of expression systems allows different production strategies depending on post-translational requirements of the molecule (e.g. glycosylation) and scale of the product required, for example from small quantities for individuals with orphan diseases, to hundreds of kilograms for blockbuster medicines.

Table 1.1 Ten bestselling biopharmaceuticals in 2013 [1]

Product	Molecule type	Production host	Company	Treatment	Sales (U.S.$ billions)
Humira (adalimumab)	mAb	CHO	AbbVie	Arthritis	11
Enbrel (etanercept)	Fc-fusion protein	CHO	Amgen	Arthritis	8.76
Remicade (infliximAb)	mAb	Murine myeloma	Johnson & Johnson	Arthritis	8.37
Lantus (insulin glargine)	Protein	*E. coli*	Sanofi	Diabetes	7.95
Rituxan (riximAb)	mAb	CHO	Roche	Arthritis and cancer	7.91
Avastin (bevacizumab)	mAb	CHO	Roche	Cancer	6.97
Herceptin (trastuzumab)	mAb	CHO	Roche	Cancer	6.91
Neulasta (pegfilgrastim)	Protein	*E. coli*	Amgen	Neutropenia	4.39
Lucentis (ranibizumab)	mAb	*E. coli*	Roche	Macular degeneration	4.27
Epogen (epoetin alfa)	Protein	CHO	Amgen	Anaemia	3.35

Various human cell lines and mouse myeloma cell lines are amongst those used as mammalian expression systems. Human embryonic kidney (HEK) and human embryonic retinal cell line PER.C6 cells have the capability to produce proteins like those native to humans, with the appropriate translational modifications [11]. HEK cells can deliver transient recombinant protein titres up to 0.6 g/L in fed-batch to produce a single chain variable-Fc antibody fragment [12], while PER.C6 titres are closer to those achieved in CHO cells, with stably transfected cell lines reaching up to 8 g/L in fed-batch and 27 g/L in perfusion systems [13]. For non-human mammalian cell lines, NS0 cultured cells typically reach up to ten-fold lower cell concentration and mAb production than CHO cell lines, with reported titres ranging from 0.1 to 0.8 g/L in fed-batch [14]. Despite reducing the risk of human virus transmission, one disadvantage of non-human mammalian cell lines is that they can produce post-

translational modifications that are not present in humans, such as galactose-alpha1,3-galactose and *N*-glycolylneuraminic acid, requiring screening for the appropriate glycan profiles [15-17]. Across the different mammalian cell lines however, CHO cells remain the main expression system used commercially for the production of monoclonal antibodies and is discussed in more detail in section 1.2.

1.1.3 Overview of biopharmaceutical production

Biopharmaceutical manufacturing requires the production of commercially relevant quantities of therapeutic proteins. It is now possible for cultured CHO cell lines to reach specific productivity of over 50 pg/cell/day and an overall titre between 5 – 10 g/L - a 1000-fold titre improvement from the titres achieved in the mid-1980s [16, 18]. Commercial manufacturing is usually performed in large bioreactors, with volumes of 10,000 L or larger, using suspension mammalian cell lines. The production process relies on critical parameters such as the specific growth rate of the cell line, the length of the process to achieve the final desired quantity and quality of product, and consequently the specific production (qP) of the cells [19].

Biopharmaceutical generation starts by delivery of the DNA, usually as part of plasmid DNA, encoding the gene-of-interest into the host cells (Fig. 1.2, Transfection). Transient transfection of the vector is usually used for small scale early characterisation of the efficacy and manufacturability of the molecule [20], but a stable transfection is standard for large-scale production. DNA delivery methods include calcium phosphate DNA co-precipitation, polyethyleneimine (PEI) delivery and electroporation [21, 22].

The transgene vector usually contains a second gene that acts as a metabolic selection marker, although other markers such as antibiotics can be used. The selection agent is added to the culture media a few days post-transfection, therefore only cells that have integrated the vector with the selection marker will survive (Fig. 1.2, Selection). The two most common selection genes in mammalian cells for commercial production of biotherapeutics are dihydrofolate reductase (DHFR) and glutamine synthetase (GS). Cells are cultured in media lacking hypoxantine and thymidine in the case of DHFR and, glutamine in the case of GS, to prevent growth of non-transfected cells. Both systems also have the potential of being exploited for amplification of the gene copy number: supplementing the GS-system with methionine sulphoximine (MSX), an inhibitor of GS activity, permits gene amplification by using MSX additions into the media [23]. Equivalent results can be achieved with the use of methotrexate (MTX) with cells using the DHFR system [24, 25].

The next step in cell line development is cloning, during which single cells are isolated and expanded as clonal populations (Fig. 1.2, Cloning). Proof of monoclonality is required by regulatory agencies [26], and

different methods have been approved, including limiting dilution, single-cell printing, cloning via flow cytometry, and ClonePix [27, 28]. Limiting dilution usually requires two rounds of cloning to achieve the required probability of monoclonality which can be a lengthy protocol. Cells are diluted to very low concentrations and plated into multi-wells plate. Two rounds of limiting dilution can yield a probability of monoclonality up to 99% [29].

ClonePix FL (Molecular devices) uses automation and robotics to monitor protein secretion by measuring fluorescence intensity of secreted proteins retained by semi-solid media around the original colonies [28, 30-32]. Protein production can be assessed by the halo size and intensity of the fluorescence signal, evaluated by images taken, enabling the picking of single cells from high producing colonies [30, 31]. ClonePix is a more rapid cloning method than limiting dilution, although it still requires two rounds of cloning. In three weeks, ClonePix can screen 10,000 clones, in contrast to limiting dilution which can typically process 1,000 clones in eight weeks. Screening a larger number of clones increases the probability of finding higher producing clones. For instance, ClonePix has been able to detect rare high producing clones, with a frequency as low as 0.003% [32]. Cloning via flow cytometry is discussed more in depth later in this chapter (see section 1.4.3).

Following recovery from the cloning process, cell lines are screened and characterised to identify high producers with the optimal growth profile and desired product quality attributes (Fig. 1.2, Screening). Cell culture process development, after cell line generation and selection, requires process and media optimisation. Prior to scaling up into industrial-scale bioreactors, it is important to predict how the cells will behave in culture conditions. This is usually achieved on smaller scale systems, including 24 well-plates and shake flasks (Fig 1.2, Expansion).

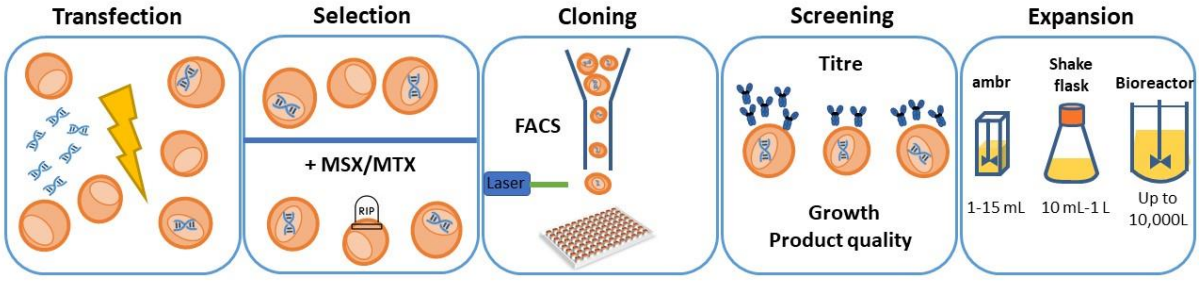

Figure 1.2 Cell line development (CLD) process workflow. Following transfection of the host cell, a selection agent is added to the cells, ensuring that only cells containing the transgene will survive. Cells are expanded and cloned via FACS, ClonePix, single cell printing or limiting dilution, followed by clonal expansion. Clones are then individually characterised in terms of growth, productivity and product quality. The selected clones that meet the desired criteria are then further characterised, for example in the ambr system, shake flasks and eventually bioreactors.

Recent scale-down models, such as the ambr, have been developed to mimic the conditions of large bioreactors. This technology uses single-use bioreactors that only require 10-15 mL of culture media per vessel, and deliver cell culture profiles that mirror those in 200 L stirred tank fed-batch bioreactors [33]. Scale-down bioreactors are monitored individually via an automated workstation. The controlled environment of the ambr includes monitoring and control of dissolved oxygen and carbon dioxide concentrations, pH, temperature, and specific nutrient levels, specifically glucose [33]. Ambr also has specific physical features, enabling different form of gas distribution, as well as rate of stirring of the media and cells, ensuring culture homogeneity.

Following a standard 14-day fed-batch process, the final culture media is harvested by centrifugation for downstream processing. MAb capture and purification, at AstraZeneca, is typically performed by protein A chromatography, which binds the Fc region on the heavy chain of the antibody. Protein A chromatography also includes a low pH elution step for viral inactivation. Typically, purification also includes further purification steps for example, anion-exchange chromatography and cation-exchange chromatography, as well as a final filtration step to remove viruses. The product is then filled into the appropriate vial or device by the formulation team. After the stability of the product has been tested over time and over different storage conditions (ie. Increased temperature), the final product is ready.

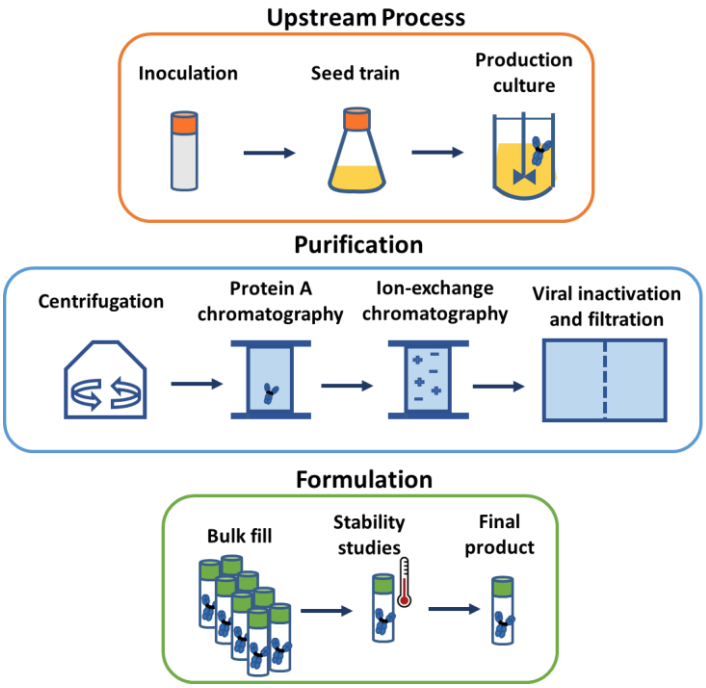

Figure 1.3 – Overview of the CHO production process. from the upstream process which generates the mAb, through purification (downstream process) which purifies the product and, formulation, which finds the optimal formulation for the product and tests its stability, to generate the final product.

1.2 Chinese hamster ovary cells

Prior to their success as the cellular factory of choice for bioprocessing, CHO cells were popular for studies in molecular and cell genetics due to their large chromosomes and the simplicity with which mutations could be distinguished [34]. Their small number of chromosomes, usually ten autosomal pairs and two sex chromosomes, also made them attractive. CHO cell lines were first isolated and developed by Theodore Puck in 1957 from ovarian tissue from an outbred Chinese hamster [35], to reduce homozygosity [34, 36]. The trypsinisation of the ovarian tissue led to a population of predominantly fibroblast cells and was subcultured *in vitro* for ten months. Despite numerous passages, the cells did not display any signs of senescence [37]. At some point throughout the ten months, it was noticed that the original fibroblast morphology of the cells had changed towards an epithelioid morphology and phenotype, which outgrew the fibroblasts and underwent spontaneous immortalization [34]. This new population of cells also happened to be proline-deficient, which suggested that genetic mutations had occurred [38]. The genetic causes underlying the phenotypic change or cellular immortalization are still poorly understood and if a similar cell line generation was performed today, it is unlikely that it would meet regulatory or industrial expectations [34].

1.2.1 History of CHO cells in bioprocessing

Despite the “mystery” surrounding the generation of CHO cell lines, the original CHO (CHO-ori) cell line was shared by Puck [35] with many interested laboratories [39]. CHO cells quickly became renowned for being “hardy” and for their fast doubling time even in media with low foetal bovine serum concentrations, leading to their widespread use. Decades of individual and parallel culture of this genetically unstable host led to sub-families of CHO cells lines (Fig. 1.3), with the most popular in current times being CHO-K1 [40], CHO-DX B11 [41], CHO-Toronto, CHO-S [42], CHO-pro3 and CHO-DG44 [43], all originating from CHO-ori (Fig. 1.3) [34, 44]. These different cell lines can be considered as “quasispecies”: a group of related cells subjected to a high mutation rate environment, and in which most of the descendants carry at least one mutation [34, 45]. Despite originating from an initial clone, this family of cell lines has many differences in terms of their individual phenotypes and optimal cell culture parameters [44]. Moreover, the karyotype of current CHO cell lines varies greatly from that of the Chinese hamster, with genetic changes such chromosomal rearrangements or deletions leading to CHO cells being quasidiploid, as many chromosomes no longer form distinct pairs [45, 46]. Ten years after the isolation of CHO-ori in 1957 [35], the CHO-K1 cell line was generated [40]. To optimise the creation of a stable cell line for recombinant protein production, a selection system was needed. CHO-

DXB11 was created as a derivative of the CHO-K1 system, with the aim of developing a stable cell line for protein production. CHO-DXB11 generation relied on directed mutagenesis to eliminate DHFR activity, resulting in cells with an inability to reduce folate hence halting thymidine and hypoxanthine synthesis [47] [41]. This cell line became the pioneering cell line in biotechnology due to its capacity to enable gene amplification by taking advantage of the DHFR system [48]. However, minimal reversion of DHFR activity was still present in CHO-DXB11, which led researchers to create a new cell line. Using CHO-ori, full deletion of the two DHFR loci on chromosome 2 was performed, creating the CHO-DG44 cell line [43]. CHO-Toronto, a sister cell line of CHO-K1, was later used to develop a suspension cell line, CHO-S [42].

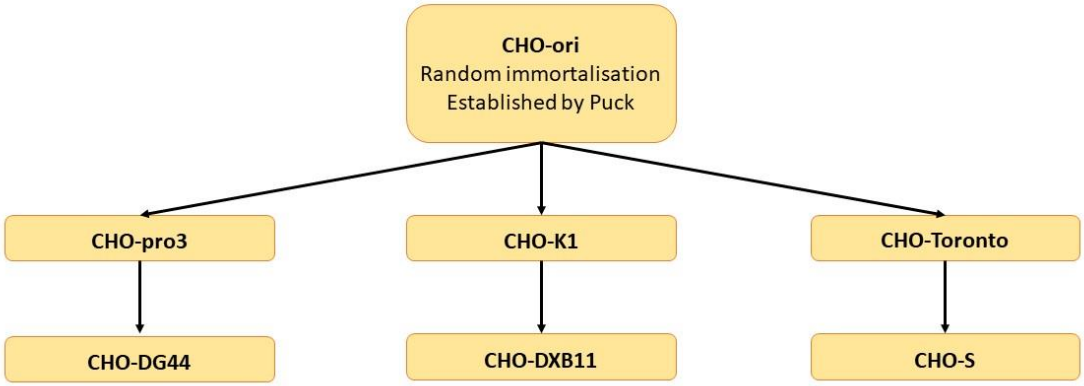

Figure 1.3 CHO cell lineage, with the numerous cell lines originating from the original CHO cell line, CHO-ori, established by Puck in 1957.

In 1987, a tissue-plasminogen activator developed by Genentech, was the first approved therapeutic protein produced in CHO cells [36, 49]. Since then, CHO cell lines have dominated the production pipelines and are the primary choice for production of mAbs and their derivatives, being used for the manufacture of over 70% of currently approved biotherapeutic recombinant proteins [50]. As a cell line that has been heavily used and characterised over the past three decades, the CHO cell platform process for development and manufacturing has been established and continually improved, which has reduced timelines both for generation of cell lines and for approval by regulatory agencies and has increased access to goods like chemically-defined (CD)-media [15].

CHO cell lines have also been demonstrated to be a safe expression system, leading to easier approval to market by regulatory agencies. CHO cells have a reduced risk of being contaminated by certain viral infections compared to other mammalian cell lines and adventitious agent testing has proven to be effective for the detection of viruses [51]. Moreover, CHO cell lines offer rapid growth in suspension,

high productivity, flexibility to be adapted to serum-free CD-media, scalability and the ability to perform post-translational modifications similar to human cell lines [52]. As described previously, high specific productivity can be achieved by taking advantage of the gene amplification systems such as DHFR or GS-mediated gene amplification strategies [23-25]. Over the years, many other approaches have been taken to increase the productivity of this host, which is discussed in greater detail in section 1.3.

Importantly, CHO cells can perform human-like glycosylation such as galactosylation, alpha1,6-fucosylation, bisecting N-acetyl glucosamine and sialylation [16]. This is particularly important as post-translational modifications that are compatible and native to humans are essential for the efficacy of many biotherapeutic recombinant proteins. Indeed, non-glycosylated IgGs have been shown to have low to no efficacy activity and can impact the safety profile of the recombinant protein [17, 53].

1.2.2 Structure, folding and secretion of mAb

Antibodies and antibody-derivatives are some of the main biotherapeutic recombinant protein molecules expressed in CHO cells. The antibody Y-shape serves a dual function: the identification of foreign cells or macromolecules at the N-terminus of the molecule, and the C-terminus is responsible for triggering a response that aids clearance of the foreign molecule. Subcategories of IgG exist that include IgG1, IgG2, IgG3 and IgG4. IgGs share more than a 90% identical amino acid content, yet each subclass has distinct characteristics in terms of antigen-binding, immune complex formation, half-life, complement activation and triggering of effector cells [54]. The IgGs subtypes vary both in their amino acid sequence and the positions of their disulphide bonds. The hinge region of the different IgGs, that connect the two heavy chains (HC), by disulphide bonds, contains a variable number of these bonds: 2 for IgG1 and IgG4, 4 for IgG2, and 11 for IgG3 [55]. The variable region can recognize a potentially limitless number of antigens, giving rise to the extreme heterogeneity of antibodies. Within the variable region exist three hypervariable regions per chain, constituted of 5-10 amino acids, which form the antigen-binding pocket [54].

The antibody constant region affects various physical and chemical characteristics of antibody binding. Studies in which the same variable regions were expressed with different constant regions showed that the constant regions can influence the affinity, magnitude of binding, specificity and kinetics of binding [56]. Such findings are valuable for the design and optimisation of new antibodies and recombinant proteins.

IgG1, the most abundant form of IgG and the type of molecule expressed in the cell lines within this study, will now be referred to simply as IgG. The IgG is a Y-shaped molecule formed of two identical

HC approximately 50 kDa, and two identical light chains (LC) approximately 25 kDa, attached together by disulphide bonds, totalling a molecular weight of approximately 150 kDa. It is subject to post-translational modifications such as phosphorylation, glycosylation and deamidation for example [57]. Both HC and LC are composed of a variable region and a constant region. There are two types of LC, lambda and kappa, which consist of one N-terminal variable domain (VL) and one constant domain (CL) (Fig. 1.4). The HC is composed of an N-terminal variable domain (VH) and three constant domains (CH1, CH2, CH3) (Fig. 1.4), and the hinge region connecting CH1 to CH2, this region differs between the different IgG subclasses. The antibody can further be divided into functional parts. The Fab, the antibody binding regions, consists of one constant and one variable domain of the HC and LC, while the Fc region consists of the two HC domains CH2 and CH3, and binds to various receptors on target cells [3, 58]. Binding of the antibody to its target can lead to different results, such as neutralization (blocking of the target cell signalling pathway), antibody-dependent cell-mediated cytotoxic activity (recruitment of macrophages and natural killer cells for the lysis of the target cell) or complement-dependent cytotoxic activity (lysis of the target cells through the formation of a protein complex [59].

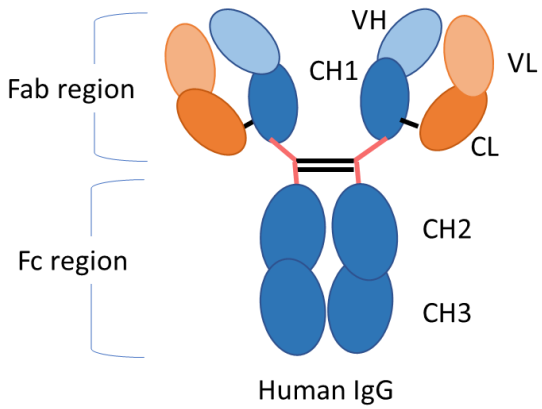

Figure 1.4 Human IgG schematic. Heavy chain in blue; Light chain in orange. VH and VL correspond to the variable region for the heavy and light chain, respectively. CH1, CH2 and CH3 are the constant domains for the heavy chain, and CL the constant domain for the light chain. Disulphide bonds are shown as black lines, and hinge as a pink line

1.2.3 Cellular constraints

Despite being one of the most popular cell lines to produce biotherapeutic recombinant proteins, there are still challenges in generating recombinant cell lines, especially for the production of complex protein formats. Increasing the gene copy number of the transgene has been found to increase protein secretion, however it eventually reaches a plateau where no additional protein is secreted, and higher copy number could cause stability issues in the mAb expression, if cells were to lose copies of the transgene [60]. At low levels of transgene mRNA expression, titre and HC mRNA correlates, however this correlation is not found when factors such as translation and secretory bottlenecks are considered at higher transcript levels. For example, the final titre can be impacted by a cell's inability to handle high amounts of mRNA and polypeptide [60-64].

1.3 Previous strategies to increase CHO cell productivity and modulate cellular pathways

Productivity in cultured mammalian cell lines has improved over the past forty years, with specific productivity reaching over 50 pg/cell/day and harvest titres between 5 – 10 g/L for some antibodies [16, 18]. Many different approaches to targeting different cellular pathways and bottlenecks have been used to generate cell lines with more desirable productivity profiles.

1.3.1 Host cell line engineering

Engineering strategies have been reported to improve protein production from CHO cells, by manipulation of cell growth [65-67], cellular longevity [68, 69], metabolites and pathways that underpin recombinant protein production itself (Table 1.2)[70-73]. Yields can be increased by improving translational pathways to increase the cellular capacity for protein production by specific chaperone proteins or reducing ER stress by limiting the unfolded protein response (UPR) or the endoplasmic-reticulum-associated protein degradation (ERAD) [70-74]. The mammalian target of rapamycin (mTOR), essential for cell proliferation and protein translation, can also be manipulated for improved productivity [65]. Finally, prolonging the duration of the fed-batch by manipulating pathways related to autophagy or apoptosis can lead to increased overall productivity [68, 69, 75]. This section will discuss some of the pathways that have been investigated for cell engineering and some of the strategies developed to produce improved host cell lines or culture conditions that increase productivity.

Table 1.2 Host cell engineering strategies for improved cell lines

Expression	Molecule / Treatment	Recombinant protein	Results	Reference
ER				
Stable	PDI overexpression	interleukin 15	No effect	Davis et al., 2000
Stable	PDI overexpression	Thrombopoietin	No effect	Mohan et al., 2007
Stable	PDI overexpression	mAb	15-27% increased secretion	Mohan et al., 2007
Stable	PDI overexpression	tumor necrosis factor receptor fusion protein	decrease in productivity	Davis et al., 2000
Stable	PDI and BiP overexpression	mAb	decrease in productivity	Borth et al., 2005
Stable	BiP overexpression	mAb	decrease in productivity	Borth et al., 2005
Transient	PDI and ER oxidoreductase overexpression	mAb	55% enhanced qP	Mohan et Lee, 2010
Stable	PDI and ER oxidoreductase overexpression	mAb	No effect	Mohan et Lee, 2010
Transient	PDI overexpression	IgG4	No effect	Hayes et al., 2010
Stable	XBP1 overexpression	SEAP	6-fold increase	Tigges and Fussenegger, 2006
Stable	XBP1 overexpression	Secreted alpha-amylase	4-fold increase in titre	Tigges and Fussenegger, 2006
Stable	XBP1 overexpression	mAb	No effect	Ku et al., 2008
Transient	XBP1 overexpression	interferon gamma	No effect	Ku et al., 2008
Transient	XBP1 overexpression	EPO	2-fold increase in titre	Ku et al., 2008
Transient	XBP1 overexpression	mAbs	0.8-1.7 fold change in titre	Pybus et al., 2014
mTOR				
Transient	mTOR	SEAP	3-fold increase in qP	Dreesen and Fussenegger, 2011
Transient	mTOR	secreted alpha-amylase	3-fold increase in qP	Dreesen and Fussenegger, 2011
Stable	mTOR	mAb	4-fold increase in qP	Dreesen and Fussenegger, 2011
Stable	mTOR	secreted alpha-amylase	4-fold increase in qP	Dreesen and Fussenegger, 2011
	Rapamycin treatment	mAb	16% increase in titre	Courtes et al., 2014
	4EBP1 knocked down	mAb	No effect	Josse et al., 2016
Autophagy / Apoptosis				
Transient	Bcl-xL overexpression	EPO	Enhanced cell viability and culture longevity	Kim et al., 2009
	3-methyl adenine treatment	tissue-plasminogen activator	2.8-fold increase in titre	Jardon et al., 2012
Stable	Bcl-2 and Beclin-1 overexpression	Host cell	increased viable cell concentration and delayed apoptosis	Ha et al., 2013
	Caspase-8/9 inhibition	Host cell	Increase in cell growth	Yun et al., 2017

1.3.2 mRNA translation, protein synthesis, translocation and folding pathway

The ER is the mammalian cell's largest organelle and plays a significant role in secretory protein synthesis, transport and folding. Secretory recombinant proteins are translocated into the lumen of the ER, which contains chaperones and folding enzymes that operate as a quality control system, to be correctly folded and assembled prior to transport to the Golgi apparatus [76]. Post-translational modifications such as N-linked glycosylation and disulphide bond formation are carried out in the ER [77]. Other functions of the ER include intracellular calcium storage and biosynthesis of lipids and steroids.

The ER quality control system is separated into two branches: a generic one, applied to all proteins to confirm structural and biophysical features, and a protein-specific control, involving the recognition of specific proteins by specialized chaperones [78]. Chaperones are a group proteins that assist incorrectly or unfolded proteins to achieve their correct conformation, but are not a component of the final protein [79]. ER chaperones include the family of heat shock protein (Hsp) such as the Hsp70 family, which contains the immunoglobulin heavy chain binding protein (BiP). BiP is a key player in ER quality control and assists in protein folding and is also involved in ERAD and the UPR [78, 80]. BiP is essential for the protection of newly synthesized antibody HC before it assembles with the LC [81]. Other chaperone proteins present in the ER include protein disulphide isomerase (PDI), glucose-regulated protein 94 (GRP94), and two lectins; calnexin and calreticulin [82].

Most glycoprotein folding, and quality control is processed by calnexin and calreticulin, which both prevent aggregation and premature export of incorrectly processed proteins from the ER [83, 84]. Following correct folding, calnexin and calreticulin transfer the protein to enzymes of the PDI family for disulphide bond formation [82, 85]. BiP binds hydrophobic areas of the proteins, preventing aggregation until correct folding occurs, and chaperones both non-glycosylated and glycosylated proteins. The proteins are then transferred to GRP34 that presents the partially folded protein to PDIs to complete folding [82, 86]. When folding conditions are not met, GRP94 stays bound to the unfolded protein, releasing the unfolded protein only when the appropriate folding conditions are restored [87].

Three pathways regulate ER homeostasis: the ER-associated folding (ERAF), ERAD and UPR pathways. Disruption of ER homeostasis can be caused by many factors including an over-load of polypeptide into the ER, abnormal oxidation or calcium levels, glucose deprivation, pH changes, or inhibition of the post-translational modification machinery [88, 89]. These disruptions result in the accumulation of unfolded proteins in the ER, which are detrimental to cells due to non-native hydrophobic patches on their surface that have the capability of aggregating with other proteins. These stresses can activate the ERAD response, autophagy or lead to activation of the UPR pathway [88, 90].

ERAD plays an important role in ER homeostasis, by preventing the accumulation of misfolded proteins in the lumen and membrane of the ER, a main cause of ER stress [91]. ERAD consists of the retro-translocation of the unfolded polypeptide chain into the cytosol, followed by degradation through the ubiquitin-proteasome system [92]. The UPR, on the other hand, increases the protein folding capacity by increasing transcription of genes that encode ER quality control proteins, folding enzymes, and proteins involved in ERAD [89]. Initial response of the UPR starts with adaptation: protein folding is increased by expression of particular chaperones; global mRNA translation is reduced; and finally the degradation of unfolded proteins is increased [93]. If adaptation fails, apoptosis is initiated, leading to removal of the translation machinery, the down-regulation of pro-survival factors, and eventually apoptosis.

Three ER-transmembrane proteins are responsible for activation of the UPR. These proteins are double-stranded RNA-activated protein kinase (PKR)-like endoplasmic reticulum kinase (PERK), activating transcription factor 6 (ATF6), and inositol-requiring enzyme 1 (IRE1) (Fig. 1.5). Each of these sensors, activates its respective transducer: ATF4, ATF6 and X box-binding protein spliced (XBP1s), upon dissociation from BiP.

PERKs key role is to modulate global mRNA translation, yet it is also involved in the transduction of pro-survival and pro-apoptotic signals depending on the cellular environment. Apart from being one of the main sensors involved in UPR signalling, it is also activated under hypoxic and energy-depleted conditions [81]. The accumulation of unfolded or misfolded proteins in the ER leads to the dissociation of BiP from the N-terminus of PERK, consequently activating PERK and phosphorylating the eIF2α subunit of eIF2. Phosphorylation of the eIF2α subunit prevents the dissociation of eIF2α and eIF2β subunits, inhibiting eIF2β, the formation of the ternary complex and translation initiation, and consequently inhibiting general protein synthesis [94]. Decreased translation decreases the protein folding load in the ER while ERAD simultaneously increases the removal of accumulated proteins. ATF4 translation is activated by eIF2α phosphorylation, which promotes expression of pro-survival genes [82, 93, 95].

The dissociation of BiP from ATF6 leads to ATF6 activation, leading to an upregulation of pro-survival transcriptional factors. ATF6 is composed of two homologues: ATF6α and ATF6β, with the former being the primary protein in the transcriptional regulation of pro-survival genes following ER stress [96]. BiP dissociation from the N-terminus of ATF6 is followed by its translocation, and its binding to, the Golgi localization sequences (GLS1 and GLS2), which are in the luminal domain of ATF6. Subsequently, the cytosolic domain of ATF6 in the Golgi is cleaved by site-1 proteases (S1P and S2P), which release the transcription factor ATF6. As a transcription factor, ATF6 upregulates chaperone expression as well as the degradation of unfolded proteins. ATF6 increases the expression of BiP, PDI,

the death transcription factor C/EBP homologous protein (CHOP), and ERAD components as well as X box-binding protein 1 (XBP1) [89, 93, 97].

XBP1 is a simple leucine zipper transcription factor and exists in two forms: the unspliced form, XBP1u, negatively regulates ATF6 transcription, and the spliced form XBP1s which is transcriptionally inactive and is the most abundant isoform under non-stress conditions. XBP1s, when translated, upregulates chaperone activity and genes involved in the UPR and protein degradation [89, 98]. XBP1 can also bind to BiP, enhancing the recruitment of proteins, allowing the ER to cope with high levels of protein expression [98]. As BiP dissociates from the IRE1 receptor, the activated form of IRE1 cleaves 26 nucleotides from the XBP1 transcript, generating the active isoform XBP1s [99]. IRE1 can also activate c-Jun N-terminal kinases (JNK), which can activate apoptosis if the ER stress is not decreased [100].

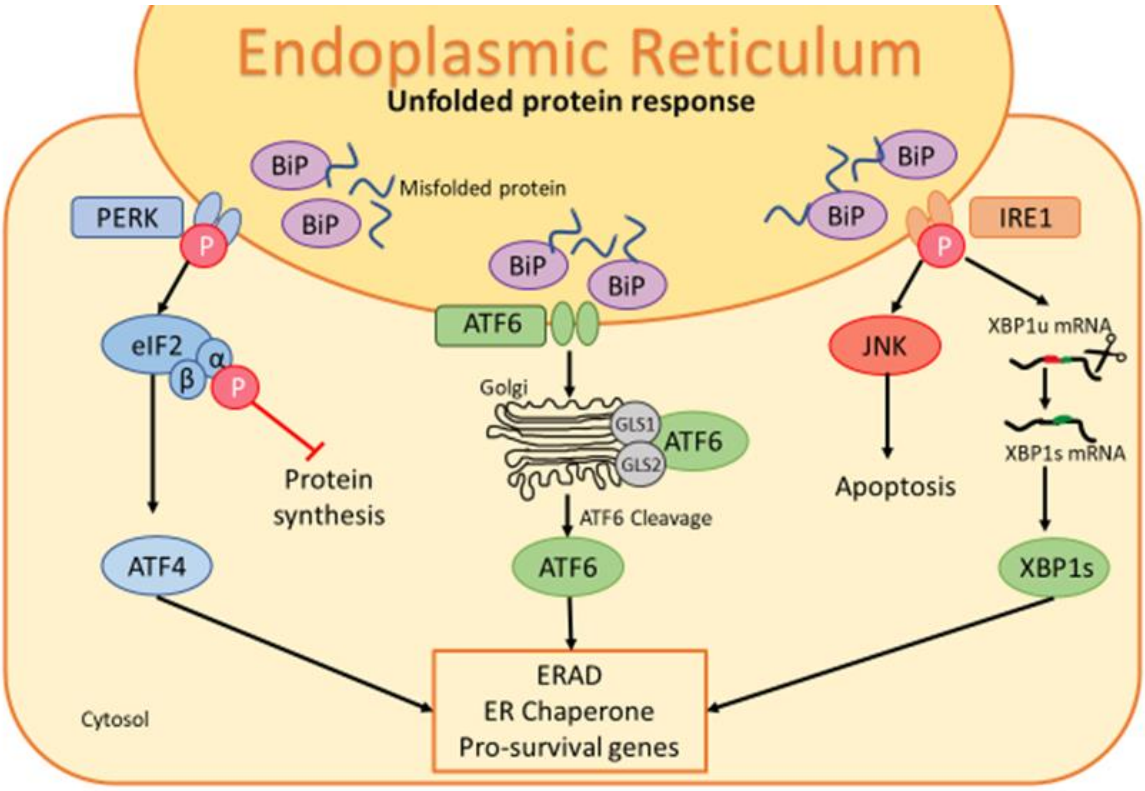

Figure 1.5 UPR pathways. Under normal conditions, BiP is bound to the receptors, inhibiting their signalling activity. Upon detection of ER stress, such as when misfolded proteins accumulate, BiP dissociates from PERK, ATF6 and IRE1 leading to their activation and a subsequent signalling cascade to promote ERAD protein expression, ER chaperone expression and increase in expression of pro-survival genes. UPR activation also inhibits protein synthesis and can trigger apoptosis if ER homeostasis is not restored.

Considering the ER as essential for secretory recombinant protein folding and assembly, strategies have been developed to optimise CHO cell productivity through improved protein folding by overexpression of members of the PDI family and other ER-resident chaperone proteins.

Mixed results were observed with chaperone engineering by PDI overexpression, likely since overexpressed chaperones could have different functions than at their normal physiological concentrations, or the use of a strong promoter for PDI overexpression could give additional translation burden to the cell [71]. No increase in specific productivity was recorded for the expression of interleukin-15 [101] or thrombopoietin [70], and only a minor increase in qP was recorded for mAb producing cell lines [70]. PDI overexpression even resulted in a decrease in productivity for a tumour necrosis factor receptor fusion protein [101]. Overexpression of PDI and BiP, as well as overexpression of BiP alone, has also demonstrated a negative effect on productivity of mAbs [102]. Transient co-overexpression of PDI and endoplasmic reticulum oxidoreductase resulted in an up to 55% enhanced qP, whereas stable co-expression had no effect or a negative effect, possibly due to the altered oxidation state of PDI [71]. In another study performed in CHO cell lines expressing an IgG4, transient PDI overexpression did not have any impact on qP [103]. Controlled expression of other chaperones, such as calreticulin and calnexin, have also been reported to have a positive impact on titre, resulting in significant increase specific productivity without affecting growth [72].

Regarding modifications to the control of UPR signalling, various approaches have been reported around ectopic expression of XBP1 in mammalian cells to increase production of secreted recombinant protein, with mixed results. XBP1s overexpression in CHO-K1 cells increased cell productivity independent of the product expressed or type of promoters used [73, 104]. Ectopic XBP1s expression was accompanied by phenotypic changes, an increase in ER and Golgi content, suggesting a reduction in secretory bottlenecks. There were no advantages however in using this strategy over other standard practises such as low temperature cultivation or controlled proliferation [73]. Ku et al., reported that XBP1s overexpression had no effect on the productivity of CHO cells stably expressing EPO, but noted a significant increase for transiently expressing cells [105]. On the other hand, Pybus et al., highlighted that XBP1s overexpression had the most impact on productivity in cells expressing difficult-to-express (DTE) molecules rather than easy-to-express (ETE), suggesting an improvement is more likely seen in cells with ER bottlenecks at folding and assembly stages [74]. The mixed results highlight the metabolic differences in different host cells as well as the impact of the molecule being expressed.

Confocal visualisation of intracellular bottleneck pathways during production of DTE molecules may inform novel engineering strategies. A DTE bispecific was found to accumulate in the ER, with none of the molecule present in the *cis*-Golgi [106]. ER morphology was also dilated, and aggregates were

found in Russel bodies, where BiP and calnexin reside [106]. Visualisation of bottlenecks in a protein-dependent manner could facilitate the design of interventions that would be tailored to the organelle and molecule of interest.

1.3.3 Mammalian target of rapamycin pathway (mTOR) engineering

Rapamycin was discovered in the Easter Islands from a soil sample, and was quickly recognized for its antifungal, anticancer and immunosuppressive properties, and eventually led to the discovery of the mTOR pathways [107, 108]. These pathways integrate intracellular and extracellular signals to sense nutrients and energy levels, to instruct cell growth and proliferation, protein synthesis, metabolism, autophagy and cell survival [108-110]. Two structurally and functionally distinct complexes are formed around mTOR: a rapamycin-sensitive complex, mTORC1 and a rapamycin-insensitive complex, mTORC2 [111].

mTORC1 signalling is considered as a master regulator of cell growth and, cellular and metabolic pathways such as mRNA translation, ribosome biogenesis and autophagy. mTORC1 is formed of the regulatory associated protein mTOR (raptor), proline-rich Akt substrate 40 kDa (PRAS40), mammalian lethal with Sec-13 protein 8 (mLST8) and DEP domain TOR-binding protein (Deptor) (Fig. 1.6) [111, 112]. The raptor-mTOR association is present under all nutrient conditions, but the stability of the complex changes based on nutrient availability [113]. During starvation or low nutrient conditions, raptor promotes mTORC1 complex formation and increases its stability, consequently decreasing mTORC1 activity such as protein synthesis and cell growth, while activating autophagic pathways [112, 113]. The mLST8 role in mTORC1 is unclear, as its deletion does not affect mTORC1 activity, whereas PRAS40 and Deptor have been reported to be negative regulators of mTORC1 when the activity of mTORC1 is reduced and during growth factor depletion conditions [112, 114-116]. Activation of mTORC1 directly phosphorylates PRAS40 and Deptor, decreasing their interaction with mTORC1 and enabling its signalling [114].

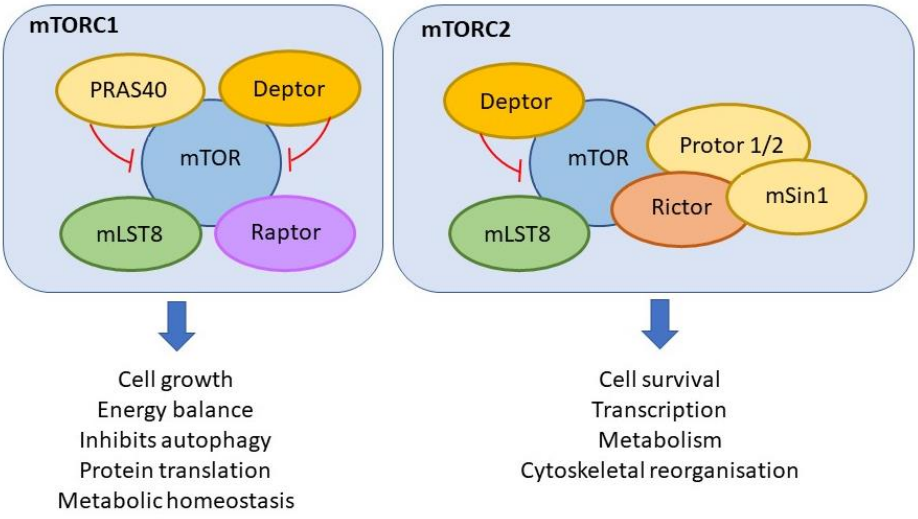

Figure 1.6 mTORC1 and mTORC2 protein complexes. mTORC1 complex comprises of PRAS40, Deptor, mLST8 and Raptor, and regulates cell growth, nutrient sensing, and mRNA translation. mTORC2 complex is composed of Deptor, Protor1/2, mSin1, Rictor and mLST8, and regulates cell survival, transcription and metabolism.

mTORC2 has been associated with cytoskeletal reorganization and cell survival through Akt signalling, as well as transcription, translation, apoptosis and metabolism control [112]. mTORC2 is composed of Deptor and mLST8, but also rapamycin-insensitive companion of mTOR (Rictor), protein-binding rictor 1 and 2 (Protor 1 and 2), and stress-activated protein kinase-interacting protein 1 (mSin1) (Fig. 1.6) [112, 117]. Deptor negatively regulates mTORC2 activity.

mTORC1 enables sensing of cellular resources such as amino acids, growth factors and insulin, as well as energy levels [112]. mTORC1 has been reported at different subcellular localisations, such as the lysosome, mitochondria, plasma membrane, ER and nucleus [117]. Whereas growth factor-activated mTORC1 is found at all subcellular compartments, leucine-induced mTORC1 activity only occurred at the lysosome and nucleus, indicating amino acids sensing mechanisms at these locations [118]. The mTORC1 pathway is regulated by PI3K and Akt and inhibited by AMPK [111, 112]. Protein synthesis and cell growth are activated through parallel pathways. Phosphorylation of 4E binding protein 1 (4EBP1) leads to the dephosphorylation of eukaryotic initiation factor 4E (eiF4E), enabling translation elongation (Fig. 1.7) [112, 119, 120]. In parallel, phosphorylation of p70 ribosomal S6 kinase 1 (p70S6K) by mTORC1 also increases mRNA biogenesis and synthesis of ribosomal proteins through inhibition of ribosomal protein S6 [121]. Phosphorylation of eukaryotic elongation factor 2 kinase (eEF2K) inhibits its ability to phosphorylate elongation factor eEF2, and thus eEF2 remains active and leads to an

increase in translation elongation. This cascade of events leads to phosphorylation of 40S ribosomal subunit, increasing the translational efficiency of mRNAs [112].

Rag GTPases are also amino acid-specific regulators of the mTORC1 pathway [122]. Mammalian cells express four Rag proteins, RagA-D, with dimer formation of RagA/B and RagC/D leading to the activation of mTORC1 [122]. The trimeric protein Ragulator interacts with the Rag proteins to maintain them on the lysosomal surface [123]. The Ragulator-Rag complex acts as a recruiter and an amino acid-regulated docking site on the lysosomal surface for mTORC1.

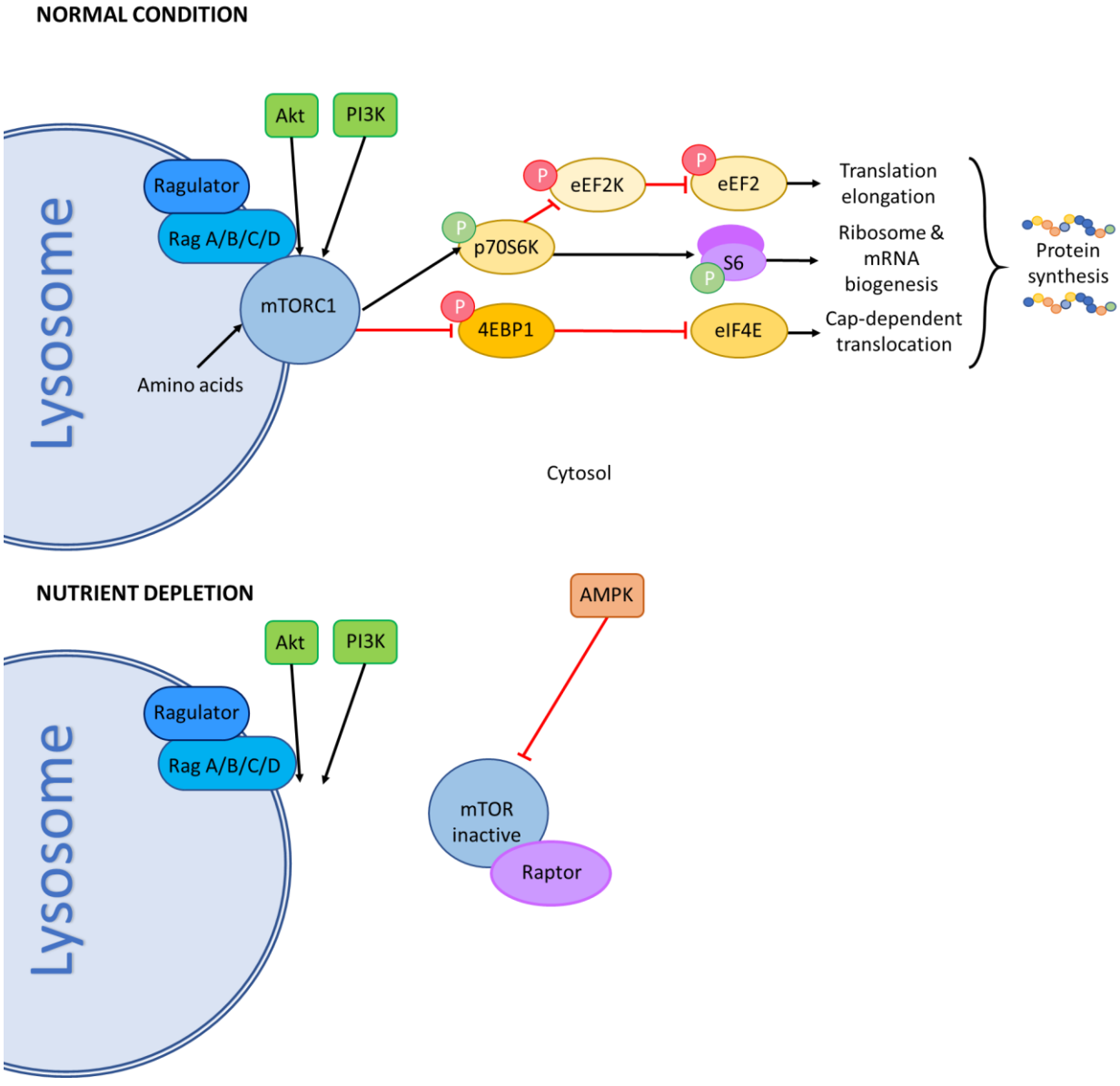

Figure 1.7 The role of mTORC1 in protein synthesis. Under normal (nutrient-rich conditions, top), mTORC1 translocates onto the lysosome, phosphorylating and activating p70S6K (green P), activating translation elongation, as well as ribosome and mRNA biogenesis. mTORC1 also inhibits 4EBP1 through phosphorylation (red P) leading to cap-dependent translocation, and protein synthesis. Under stressed or nutrients-depleted conditions (bottom), mTORC1 is inhibited by AMPK and does not attach onto the lysosome surface, hence reducing protein synthesis rates.

Activated AMPK phosphorylates not only the raptor subunit of mTOR, but also the tuberous sclerosis complex 2 (TSC2), which prevents the formation of the repressive complex TSC1/TSC2. As TSC2 is a GTPase-activating protein and inactivates Ras-homologue enriched in brain (Rheb), an mTORC1 activator, its inhibition allows Rheb to directly activate mTORC1 on the lysosome surface (Fig. 1.8) [124-128]. Rheb overexpression has been shown to not only increase mTORC1 activity, but also negatively regulate ULK1 [129]. A lysosomal proton pump, v-ATPase, has also been identified as part of the lysosomal mTORC1 complex. This pump not only transfers protons inside the lysosome, maintaining a low pH, but is also able to respond to an increase in amino acids inside the lysosome (generated through autophagy for example), leading to a conformational change that weakens v-ATPase binding with Ragulator [130, 131]. As inactive mTORC1 resides in the cytoplasm, mTORC1 activation is directly dependent on its translocation to the lysosome membrane, although negative regulation of mTORC1 also occurs here. [131].

As mTORC1 activity corresponds to cellular nutritional status, its activity is directly linked to the autophagic state: mTORC1 inhibition increases autophagy, whereas mTORC1 activation reduces it (Fig. 1.8). Autophagy initiation is coordinated through unc-51-like-kinase 1 (ULK1) complex, along with autophagy-related gene 13 (Atg13), focal adhesion kinase family-interacting protein of 200 kDa (FIP200) and Atg101 [129, 132]. AMPK signalling can also directly initiate autophagy through phosphorylation of ULK1, whereas mTORC1 activity can repress autophagy through direct phosphorylation of ULK1 and Atg13, which inhibits the protein complex [129]. mTORC1 can also inhibit autophagy through inhibition of the Vsp34 complex, which comprises of Atg14, Beclin-1 and autophagy beclin-1 regulator 1 (AMBRA1) [127, 133]. Activation of ULK1 and Vsp34, when mTORC1 is inhibited, increases the recruitment of additional Atg proteins to phagophore membranes to promote maturation of the autophagosome [110, 134].

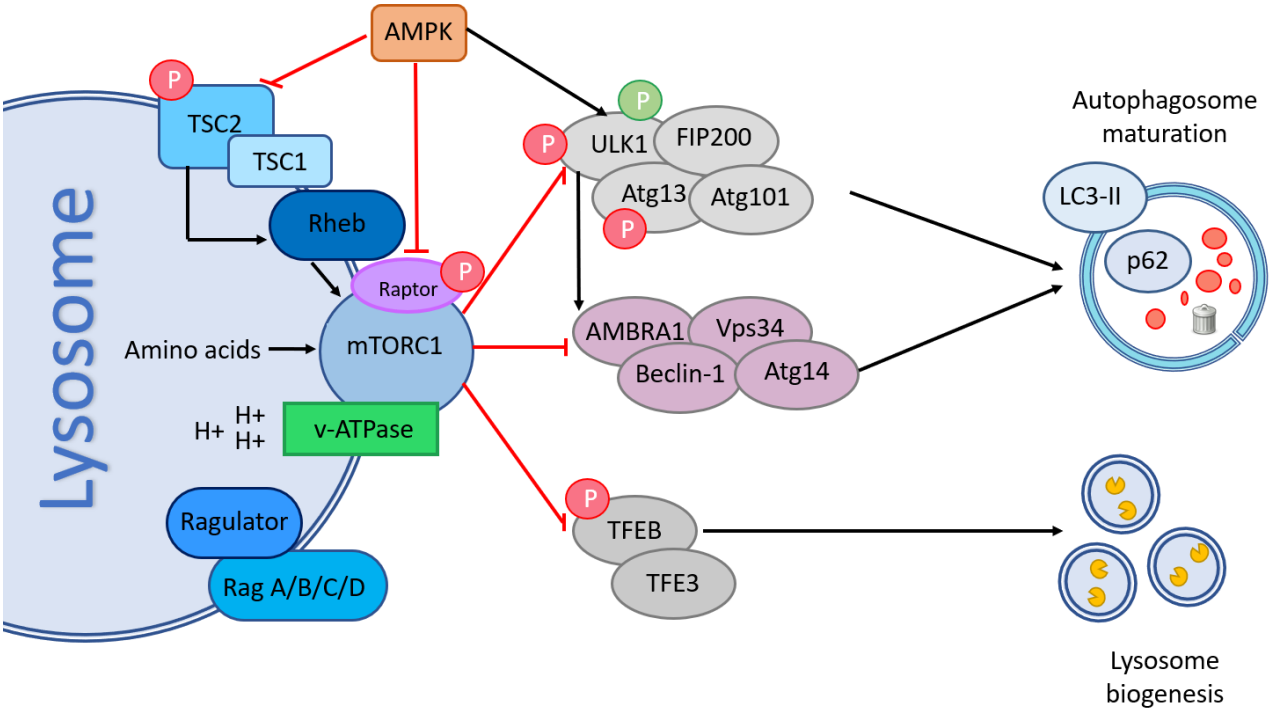

Figure 1.8 The role of mTORC1 in autophagy. During normal or non-stressed conditions, mTORC1 translocates to the lysosomal membrane, where it inhibits ULK1, AMBRA1 and TFEB, hence inhibiting autophagosome maturation, lysosome biogenesis and autophagy. During cellular stress, AMPK, inhibits mTORC1 through inhibition of the TSC2-TSC1 complex which is necessary for mTORC translocation the lysosomal membrane. ULK1 complex, AMBRA1 complex and TFEB/TFE3 can therefore activate autophagy and lysosome biogenesis.

The mTORC1 effect on autophagy and ULK1 regulation is also strengthened through AMPK signalling. Under starvation, AMPK inhibits mTORC1, activating ULK1, this activation is reinforced by AMPK directly binding and phosphorylating ULK1 [132]. AMPK inhibition of mTORC1 proceeds through AMPK phosphorylation of raptor, disrupting the mTORC1 complex as well as the activation of TSC2 through direct phosphorylation [110]. Both mTORC1 and AMPK oppositely regulate ULK1 activity by direct phosphorylation, while ULK1 can both negatively regulate mTORC1 by phosphorylation of raptor, and negatively regulate AMPK by phosphorylation of its subunits [124] .

As mTOR is a master regulator of many cell processes including protein synthesis and cell proliferation, it might be considered an ideal target for manipulation for optimising recombinant protein expression. Dreesen and Fussenegger reported that ectopic expression of mTOR significantly increased cell growth and proliferation, culture viability as well as qP by up to three-fold [65]. Edros et al. further went on to characterise the potential mechanistic pathways underlying this improved host cell [135]. Comparing two CHO cell lines with a 17.4-fold difference in qP, the study investigated the differential expression of the genes and proteins in the mTORC1 pathway. It was reported that a gene of the PI3K

pathway (p110δ subunit of PI3K) was the most overexpressed, with a 71.3-fold increase [135]. Other genes that were significantly overexpressed included RagC, insulin, phospholipase D1, as well as ribosomal protein S6 and the beta subunit of AMPK [135]. Confirming these findings, Godfrey et al. discovered elevated levels of RagC mRNA transcript in the heavy polysome fraction of a highly expressing and fast-growing cell line, further supporting a role of mTORC1 in recombinant protein production [136].

Courtes et al. characterised the impact of mTORC1 on the translational activity of growth and mAb productivity in CHO cells under rapamycin stress by performing polysome profiling [66]. A 30% decrease in maximal growth was recorded in cells treated with rapamycin, but culture viability was maintained for an extra 3 days compared to control cultures, leading to a 16% increase in titre in a batch culture [66]. Others have reported that rapamycin treatment improved culture viability by inhibiting cell death through autophagy induction [68]. Moreover, polysome profiling revealed that mTORC1 activation positively impacted both growth and productivity, with rapamycin treatment leading to mRNAs shifting from polysomes to monosomes, indicating a decrease in mRNA translation [66]. This was further confirmed with reports that elevated levels of 4EBP1 protein, present when mTORC1 is inhibited, were found in a cell line with low mAb expression [137]. It was found that the ratio of eIF4E:4EBP1 positively correlated with cell productivity [137]. However, manipulation of the eIF4E:4EBP1 ratio did not transform a low producing cell line into a high producing one, or vice versa [137].

1.3.4 Lysosomes function and autophagy

Autophagy, from the Greek translated to ‘self-eating’, is a catabolic cellular mechanism that processes the degradation of intracellular components. Autophagy is considered a protective mechanism in response to cellular stress under both normal and stressed conditions. Intracellular recycling and degradation of organelles and proteins is important to maintain cellular homeostasis. Under normal conditions, autophagy occurs at a low basal rate, maintaining homeostasis by cytoplasmic and organelle turnover, and eliminating damaged components that could become toxic [138, 139].

Cytoplasmic cargo, such as proteins, organelles, lipids and nucleic acids, are degraded within lysosomes, acidic membrane-bound organelles containing the hydrolytic enzymes cathepsins [140]. Lysosomes require a pH between 4 and 5 for optimal acid hydrolases activity, and play a critical role in nutrient sensing and signalling pathways involving cellular metabolism and cell growth [141]. Lysosomal genes and functions are differentially regulated under stress, as lysosomes can adapt to both intracellular and extracellular stress cues.

The key cellular role of lysosomes is the degradation of intracellular waste and autophagy. There are three distinct types of autophagy: macroautophagy (hereinafter referred to as autophagy), microautophagy, and chaperone-mediated autophagy. In macroautophagy, the cytoplasmic cargo is delivered to the lysosome by double-membrane bound vesicles, autophagosomes, which fuse with the lysosome to form an autolysosome. For microautophagy, lysosomes themselves take up cytosolic components, without the intermediary autophagosomes [142]. Finally, in chaperone-mediated autophagy, target proteins are transported across the lysosome membrane inside a complex formed with chaperone proteins, which are recognized by the lysosome membrane receptor lysosomal-associated membrane protein 2A (LAMP2A), activating their unfolding and degradation inside the lysosome [140].

Autophagy is a conserved process across species, with many autophagy-related (Atg) proteins expressed in different species, from yeasts to mammals. Formation of the autophagosome requires sensing of environmental stress signals by AMPK, leading to the inactivation of mTORC1. This initiates autophagy through ULK1 signalling, initiate the formation of the phagophore around the target intracellular cargo (Fig. 1.9). mTORC1 inhibition also leads to the hypophosphorylation of Atg13 and its binding to Atg1, leading to recruitment of Atg9 [143-145]. Atg9 begins to collect lipids from different organelles, such as the ER, to form the autophagosome membrane [146, 147].

The nucleation process and formation of the autophagosome is controlled by the PI3K complex, composed of Beclin-1, vesicular protein sorting 34 and phosphatidylinositol-3-phosphate (PI3P) (Fig. 1.9) [100, 148]. Elongation of the autophagosome requires two ubiquitin-like reactions. The first one requires conjugation of Atg12-Atg5, until its formation of the Atg12-Atg5-Atg16 complex, located on the outer membrane, which in turn is responsible for recruiting LC3-II (Fig. 1.9) [149, 150]. LC3-II forms from LC3 cleavage by Atg4 and conjugation with phosphatidylethanolamine. LC3-II is then recruited onto the membrane of autophagosome, to form a mature autophagosome[143, 150]. Sequestosome-1 (p62), an autophagosome cargo protein binds with LC3 for formation of the autophagosome membrane [151, 152]. Mature autophagosomes bind and fuse with lysosomes for degradation and release their cargo. Broken-down products are then released back into the cytosol, for use by the cell for metabolic pathways [153].

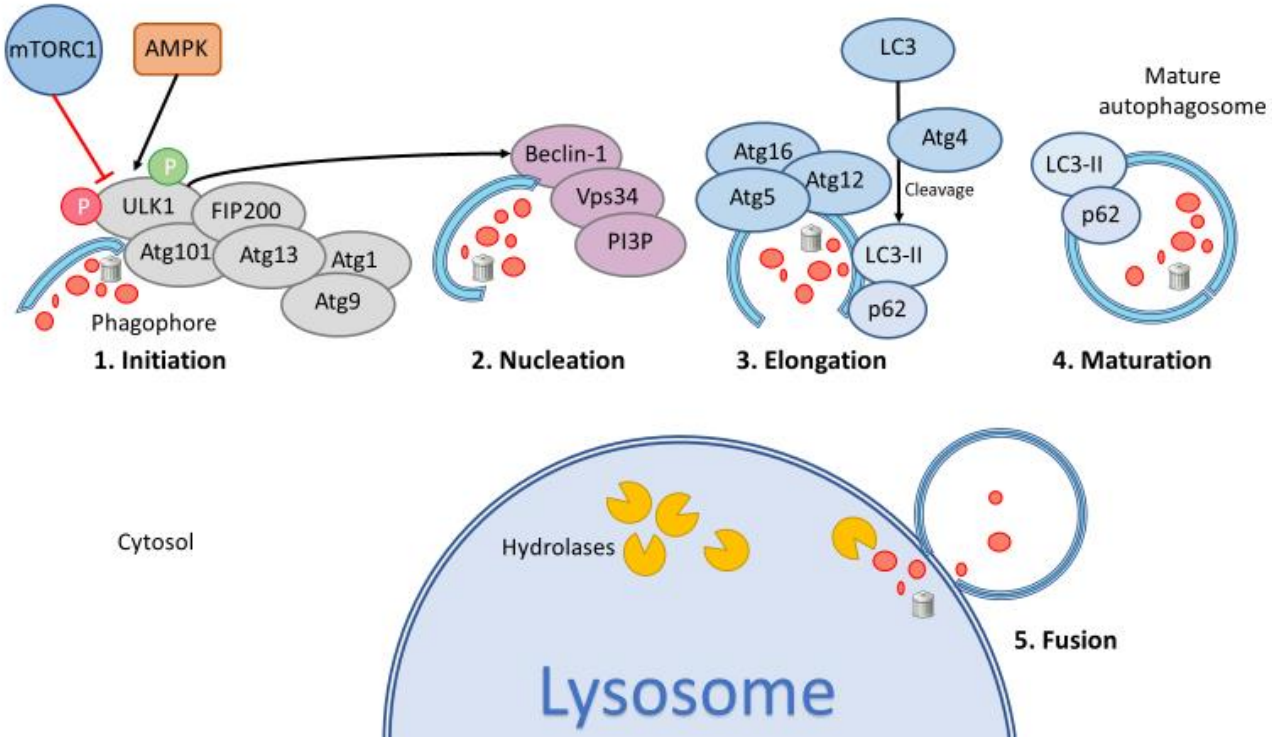

Figure 1.9 Schematic of the autophagy pathway - The different stages and proteins of formation of autophagosomes including the initiation, phagophore nucleation, elongation of the autophagosome membrane, maturation and the final fusion of the mature autophagosome with the lysosome. Autophagosome cargo is unloaded into the lysosome for protein degradation by lysosomal hydrolases.

Autophagy is also initiated by the activation of PERK, IRE1 and cytosolic Ca^{2+} [100, 154, 155]. Additionally, eIF2α phosphorylation is required for autophagy initiated by ER stress, while ATF4 and CHOP have also both been shown to regulate more than a dozen Atg genes [154, 155]. If the UPR fails to restore the ER homeostasis, the cell initiates an alarm signal. Compartment formation, such as Russel bodies or BiP bodies, is triggered by accumulation of misfolded or unfolded proteins [156, 157]. These compartments display different characteristics, such as enrichment of structurally and functionally different proteins (i.e. lectin chaperones, soluble ER-resident proteins), that can be targeted for ER-specific autophagy.

Lysosome biogenesis, homeostasis and other related functions such as autophagy are controlled by a network of genes: the coordinated lysosomal enhancement and regulation (CLEAR) pathway (Fig. 1.10) [158]. This network is controlled by four key transcription factors (TF): microphthalmia-associated TF (MATF), TFEB, TFE3 and TFEC, which bind CLEAR sites in the promotor region of those target genes [158, 159].

TFEB is considered the master gene regulator of the CLEAR pathway, and usually resides in the cytoplasm, alongside TFE3, but can translocate rapidly to the nucleus under starved or stress conditions to initiate lysosome biogenesis [141, 160-162]. Overexpression of TFEB caused an increase in the number of lysosomes per cell, as well as increased number of autophagosomes, and increased clearance of protein aggregates, emphasizing TFEBs role in lysosome biogenesis (Fig. 1.10) [158, 159, 163, 164]. TFEB also stimulates autophagosome formation, the fusion of autophagosomes with lysosomes and the final degradation of the autophagosome- lysosome complex cargo. Overexpression of TFEB has been associated with increased levels of autophagy and activation of TFEB transcriptional targets including lysosomal hydrolases [159, 160]. Finally, Settembre et al. showed that TFEB interacts with the v-ATPase-mTORC1 complex on the lysosomal surface to sense lysosome content, making TFEB both a sensor of lysosomal state and an effector of lysosomal biogenesis as it translocates to the nucleus [162].

Translocation of TFEB and TFE3 is orchestrated by mTORC1 activity. Interestingly, mTORC1 senses environmental and intracellular signals, such as growth factors, nutrient availability, energy status and stress to control cell growth [165]. Under normal conditions, active mTORC1 inhibits autophagy by binding to the lysosome, while promoting mRNA translation, ribosome biogenesis and lipid synthesis [166]. Under cellular stress, such as nutrient deprivation, mTORC1 is inhibited, leading to the dephosphorylation and translocation of TFEB and TFE3, enabling lysosomes to maintain homeostasis, respond to stress cues and promote cell survival [160, 161].

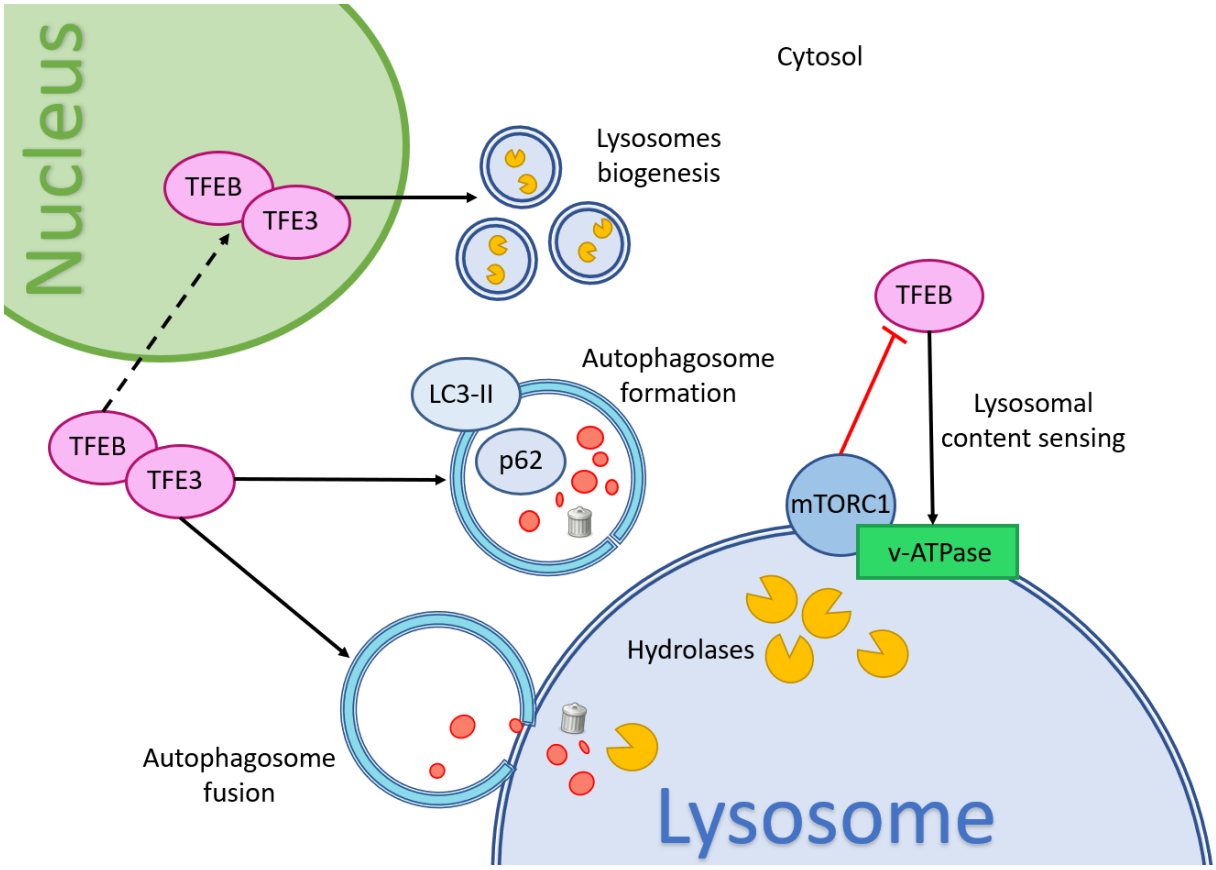

Figure 1.10 Schematic representation of the CLEAR pathway, highlighting lysosome biogenesis through the nuclear translocation of the transcription factors TFEB and TFE3. TFEB and TFE3 translocation is dependent on mTORC1 activity and regulates autophagosome formation and fusion.

Increased autophagy can be interpreted as either the first step towards cell death or cell survival. Genetic engineering of autophagic pathway has been used to prevent and protect cells from cell death. As nutrient deprivation can induce autophagy, reports have highlighted the importance of autophagy for cell survival under nutrient depleted conditions at late stages of the culture [167] [168]. Nutrient feeding can extend culture longevity and increase antibody production. However, this is often not enough to prevent cell death, which can also be caused by hyperosmolality, oxygen limitation, hydrodynamic stress, harmful by-product accumulation, and reactive oxygen species build-up [168, 169]. For example, hyperosmotic stress has been shown to inhibit cell growth and apoptotic cell death in CHO cells, but can induce autophagy through faster conversion of LC3-I to LC3-II [169].

As many pro-apoptotic signals can trigger autophagy, anti-apoptotic proteins have been shown to inhibit autophagy in many mammalian cells [170]. For instance, Bcl-xL overexpression has been associated with improved culture viability and culture longevity. However, as Bcl-xL overexpression inhibits both apoptosis and autophagy, the authors highlighted the limitation that their work did not quantify the proportion of cells dying due to apoptosis and/or autophagy [69]. Moreover, chemical

inhibition of autophagy with 3-methyl adenine (3-MA) led to an up to 2.8-fold increase in titre in CHO cell lines expressing tissue-plasminogen activator [75].

However, other studies have observed that autophagy activation is beneficial. Interactions between Bcl-2 and Beclin-1 maintain autophagy at 'appropriate levels': during nutrient depletion, Bcl-2 binding to Beclin-1 protects against increasing levels of autophagy that could lead to cell death [170]. In CHO cells, co-overexpression of Bcl-2 and Beclin-1 resulted in increased viable cell concentration and delayed apoptosis [171, 172]. The combination of promoting autophagy and inhibiting apoptosis can therefore potentially boost titre by preventing cell death, both programmed and non-apoptotic. Supporting this, chemical induction of autophagy by rapamycin has also led to improved culture viability accompanied by higher titres [68]. Interestingly, Josse et al. observed that for low producing cell lines, autophagy activation was detrimental to the cell line, leading to low recombinant protein production as well as decreased culture viability [137]. Autophagy is a complex pathway regulated by many different mechanisms, and a fine balance between cell survival and cell death. The studies discussed could highlight some fundamental differences between the cellular biology of a high producing cell line and a low producing one.

1.3.5 Apoptosis

Apoptosis is a programmed cell death defined by the condensation of the nucleus and cytoplasm, the association of chromatin with the nuclear periphery, DNA fragmentation, cell shrinkage and membrane blebbing [173]. Multiple physiological and chemical stimuli can induce cell death by apoptosis, and at least two initiation pathways have been identified: the extrinsic pathway and intrinsic pathway, also known as the mitochondria-mediated pathway [174].

The extrinsic apoptosis pathway requires the activation of death receptors found on the cell membrane surface, such as death receptors from the tumour necrosis factor (TNF) family, including CD95 (APO1/Fas) or TNF-related apoptosis-inducing ligand (TRAIL) [174, 175]. These transmembrane receptors activate a downstream cascade of events, with the activation of the initiator caspases 8 and 9, leading to the direct cleavage of downstream effector caspases such as caspases 3 and 7 (Fig. 1.11) [175]. Caspases 8 and 9 also activate the BH3 interacting-domain (BID), a pro-apoptotic protein from the Bcl-2 family. These pro-apoptotic Bcl-2 family members induce mitochondrial damage, committing the cell to death by initiating the mitochondrial pathway of apoptosis [174].

The mitochondrial pathway of apoptosis is controlled by the Bcl-2 protein family. These proteins control the permeabilisation of the mitochondrial outer membrane, leading to mitochondrial membrane potential loss, and eventually causes the release of cytochrome c and other apoptotic

factors directly into the cytosol, activating caspases and committing the cell to die [174, 176]. The *bcl-2* gene is often found overexpressed in cancer cells and affects viability without affecting cell growth [177].

The Bcl-2 protein family is composed of three subgroups: (1) the pro-survival proteins, such as Bcl-2, Bcl-xL, Bcl-w, Mcl-1 and A1, which inhibit cell death through interactions with pro-apoptotic proteins; (2) the executioners Bax and Bak that cause the mitochondrial outer membrane permeabilisation; and (3) the BH3-only proteins which all have the BH3 domains, such as Bim, which sense cellular stresses and initiate apoptosis accordingly [176, 178]. Under basal conditions, BH3 protein levels are low, and increase in the presence of cellular stress or apoptotic stimuli, activating Bax and Bak. Bcl-2 and Bcl-xL are attached to the membranes of the mitochondria, ER and nucleus, whereas other proteins from the Bcl-2 family are found in the cytoplasm. Apoptosis via mitochondrial permeabilisation can be prevented by Bcl-2 and Bcl-xL binding Bax at the mitochondria [171, 179].

Bcl-2 activation can be mediated by prolonged or severe UPR, emphasized by increased expression and/or activation of PERK, ATF6 and IRE1 [155]. ATF6, ATF4 and XBP1 all instigate the expression of CHOP, which downregulates the expression of Bcl-2. If the UPR restores homeostasis of the ER before the levels of Bcl-2 fall below a critical threshold, the UPR will be deactivated by binding of BiP to the stress sensors. However, if the UPR fails to restore homeostasis before Bcl-2 falls below the critical threshold, apoptosis will be initiated.

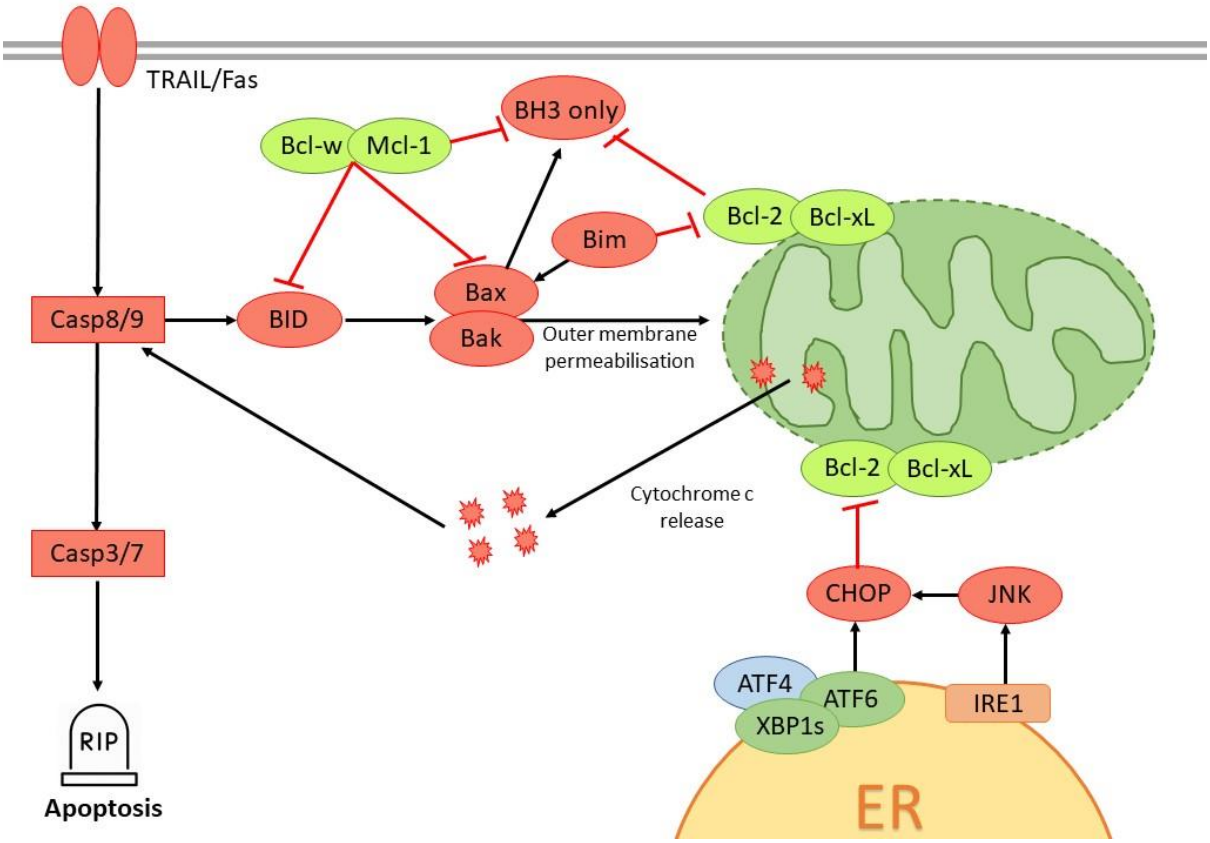

Figure 1.11 Schematic of the apoptosis pathway. Activation of the TRAIL/Fas receptors under appropriate conditions activates caspases 8/9. These activate pro-apoptotic proteins, which in turn can inhibit pro-survival proteins, leading to apoptosis through caspases 3/7 activation, and release of cytochrome c from the mitochondria. ER stress can also trigger apoptosis by inhibiting the pro-survival proteins.

Manipulation of the apoptotic pathways is one of the strategies that has been investigated to improve recombinant protein production. Since apoptosis can account for up to 80% of cell death in a bioreactor, induced by nutrient and oxygen depletion, toxin accumulation and sheer stress, its delayed onset maintains viable cell concentration, and consequently, increase in titres [180, 181]. Moreover, cell death can compromise the quality of the recombinant products and increase the workload for downstream processes and purification. As apoptosis is genetically controlled and regulated through molecular signal transduction, many approaches have sought to inhibit or delay apoptosis by manipulating pro- and anti-apoptotic proteins.

Overexpression of anti-apoptotic proteins such as Bcl-2, Mcl-1 and Bcl-xL can delay apoptosis by lowering the rate of decline in culture viability, hence keeping viable cell concentration high and consequently increasing production of recombinant protein. Overexpressing these genes has also led to cell lines being more resilient, less susceptible to hyperosmotic pressure, and limited lactate production, promoting an increase in lactate consumption and ultimately limiting the adverse effects of the accumulation of this metabolite in the media [177, 179-183].

As previously described, caspases involved in the apoptosis cascade can be divided into two functional groups, the initiator caspase and effector caspase. Inhibition of the initiator caspases caspase-8/9 by overexpression of a dominant negative mutant has been shown to result in an increase in cell growth [67]. Down-regulation of the effector caspases, caspase-3/7, by introduction of small interfering RNA or antisense RNA also demonstrated positive effects on extending cell culture longevity [184]. Other strategies to decrease the effect of apoptosis, focusing on the overexpression of the human telomerase reverse transcriptase has led to an increase in culture viability, and higher viable cell concentrations under stressed conditions [185].

1.4 Flow Cytometry in Cell Line Development

1.4.1 Importance of monoclonality

The U.S. Food and Drug administration (FDA) is one of the regulatory agencies responsible for drafting federal regulations. Drug development, including biologics, must observe title 21 of the Code of Federal Regulation. More specific to antibodies is the "Points to consider in the Manufacture and testing of Monoclonal Antibody Products for Human Use", which describe the FDA current guidelines [186]. The International Conference on Harmonisation is another organization publishing regulatory documents on drug development, comprising of international scientists from the U.S, Europe and Japan [26].

Biopharmaceutical production is under rigorous rules and guidelines, requiring proof of product quality and consistency. Production of biologics in animal cells has the potential risk to be directly exposed to contaminants from the cell, such as viruses, cellular nucleic acid and growth-promoting proteins, and harmful impurities that can arise from the manufacturing process itself [26].

The FDA, the European Medicines Agency (EMA), as well as the International Committee on Harmonisation guidelines require that the production cell line originates from a single cell [187]: "For recombinant products, the cell substrate is the transfected cell containing the desired sequences, which has been cloned from a single cell progenitor". The theory behind this regulation is that cells within a population originating from a single cell should be homogeneous, with an identical genotype and phenotype, hence guaranteeing the safety and efficacy of the product [188-190]. However, the reality is quite different, and monoclonality does not guarantee population homogeneity. More importantly, many industrial cell lines such as CHO or NS0 can show large variability in growth and productivity profiles between batches [188, 191]. Further characterisation is required post-cloning to demonstrate the phenotypic stability of the chosen cell line and proof of the consistency of the manufactured produced therapeutic protein must be provided [192].

1.4.2 Cell line heterogeneity

Artificially immortalized cell lines such as CHO cell lines are particularly known for their heterogeneity and inherent gene instability. Changes in chromosomal arrangement, gene copy number, and transcriptional activity are some elements that create such diversity [193, 194]. Lewis et al reported missing genes and a high variability in copy number variation (CNV) across different cell lines, with 48% of CNV being unique to each cell line [195]. Most of the different mutations across cell lines were in genes related to processes that might impact the bioprocessing of recombinant proteins, like apoptosis [195].

Analysis of a cell lines stability with or without continued selective pressure has revealed high levels of variation in productivity and growth [196]. However, experiments assessing population homogeneity based on growth profile, in both transfected and untransfected cell lines, have revealed that heterogeneity is an intrinsic cell attribute, and does not arise from a metabolic pressure caused by the production of recombinant proteins or by the effect of selective pressure [25, 188, 196].

CHO cells have a high mutation rate, a natural process during which a population of cells acquire different mutations, leading to diversity and heterogeneity over time. Heterogeneity can prevent cell lines from reaching optimal productivity, and it has been observed that with an increase of passage number, a decline in specific productivity is often observed. This can be due to a mix of high producing cells with a non-producing population or low producing population: the subpopulations eventually outgrow the high productivity cells, as they do not have the burden of expressing the recombinant product [197, 198]. Indeed, when a clonal cell line expressing an IgG1 was sorted via flow cytometry, the non-producer population had a faster growth rate than the producing cells [198]. This non-producing population could result from loss of chromosomes or sections of DNA, or gene silencing through methylation, that contain the HC and LC genetic information. A more recent study reported cell lines that maintained the same transgene copy number, while there was an increase in the proportion of cells that lost HC protein expression, due to apparent gene silencing [199]. Krebs et al. describe a cell line characterisation process that ensures early selection of a cell line that will not be impacted by loss of mAb expression. This includes measurement of intracellular HC and LC protein levels by an automated flow cytometry process, and single-cell quantitative PCR transgene analysis, to assess both the cell's genetic and phenotypic characteristics [199].

Levels of expression of IC LC and HC, measured by flow cytometry, between cells from the same clonal population can vary drastically, with standard deviations that are 50 to 70% of the mean [200, 201]. Population noise (a stable intrinsic cell-to-cell variability) or temporal noise (protein expression levels fluctuating over time, due to random protein synthesis or breakdown) can also account for non-

genetic differences between cells, and can lead to mistaking a low-producer for a temporarily high producer [200, 201].

A CHO cells' genetic instability is also related to their ability to accept transgenes and adjust to different process conditions, such as their adaptation from basal culture media to growth media conditions. Each single cell may respond to changes in the culture or process differently, emphasizing the fact that 'clonal' cell lines in the strict term of the sense may never be accomplished, and many have suggested that the term 'clonally-derived' may be more accurate [189, 202].

1.4.3 Flow cytometry methods to isolate high producers

Flow cytometry is a commonly used cloning method, which has the advantage of being high-throughput and able to assess cell characteristics at the single-cell level. Cloning via flow cytometry combines screening to enrich the productivity of selected clones with a more time-efficient cloning method, reducing timelines (Manz et al., 1995; Carroll and Al-Rubeai, 2004). Many flow cytometry-based screening methods have been described in the literature, including the monitoring of IgG production by capture of the antibody via binding to the cell surface using microbead technology [203] or surface affinity matrix [204-206], introducing fluorescent markers into the vector [207-210] and other vector modifications to enable the secreted mAb to bind to cell surface proteins, such as the development of an antibody-membrane switch [211-213].

Extracellular cell surface staining of secreted mAbs has had mixed results in terms of isolating high producing cell lines. Okumura et al., tried to isolate high-expressers with an antibody that binds the mAb presented on cell surface, without success [214]. However, others report isolating high producing clones with similar methods, especially with the incubation of CHO cells at 4^{o}C, which leads to a transient association of secreted mAbs to the cell surface [215, 216]. Retaining secreted proteins on the cell surface has also been successful with the use of microbeads. Microbead technology relies on the formation of agarose microdroplets around single cells, creating a microenvironment that would retain secreted proteins [203]. Despite isolating high-expressers, this method requires the equipment for bead formation, which are between 80 – 500 µm in size, and a flow cytometer equipped with a 200 µm nozzle. Another strategy, surface affinity matrix, uses the capture of secreted proteins with antibodies linked to cell surface protein using biotin-avidin bridge [204]. This method has proven successful in enriching populations with high-expressers in an immunological context, as well as in CHO cells [204, 205].

Many co-expression methods have been described in the literature to produce surface displayed Abs, or to use other cellular markers to correlate with productivity. DeMaria et al., described the co-expression of the mAb and the cell surface protein CD20, which is usually not expressed in CHO cells, where expression of the two proteins was linked by an internal ribosome entry site (IRES). CD20 expression levels were shown to correlate with the expression of the recombinant protein, and could rank clones effectively based on their mAb productivity [217]. The antibody-membrane switch (AMS) technology, described by Yu et al., relies on alternative splicing of the HC, by introducing a membrane-anchoring domain in the HC CH3 domain, anchoring the secreted antibody onto the cell surface [211]. By staining cells with an anti-human Fc antibody, it is possible to isolate high producers, and following cell sorting, cells can be switched back to 'production' mode by transfection with a Cre recombinase. This inhibits the expression of the AMS, hence focusing cellular resources on transcription and translation of the recombinant protein of interest [211]. Similarly, surface display of HC was also achieved with a vector containing a leaky translation termination signal at the 3' end of the HC followed by a transmembrane and cytoplasmic domain [212]. Cells enriched in this manner had increased productivity when compared to cells cloned by limiting dilution or cloned by flow cytometry using a cold capture staining method [212]. Chakrabarti et al. also developed a switchable membrane-associated domain to anchor the antibody to the cell surface. By assigning an amber stop codon to a non-natural amino acid, the addition of the non-natural amino acid into the media 'switches on' the attachment of the mAb to the cell surface, increasing productivity by ~2-fold [213].

Co-expression of the recombinant protein and GFP has also been used. Expression of GFP in an expression cassette, and DHFR and the recombinant protein in a second expression cassette showed a correlation between GFP signal and recombinant protein expression, enabling cell sorting of high producing cell lines based on GFP fluorescence [210]. Co-expression of a mAb and GFP linked by an IRES has shown similar results [209]. Yoshikawara et al. used a fluorescein methotrexate reagent, which binds to DHFR, and fluorescence was found to correlate with MTX resistance and so could be used to isolate high producers [218]. Despite successfully isolating high producers, this method is limited to cell lines that use DHFR as a selection marker. Finally, split-GFP, with half of the GFP on the HC and the other half on the LC, is only active when HC and LC are combined and was also an efficient indicator of mAb production [207]. However, for methods relying on intracellular measurements, it is important to remember that increased intracellular expression may not always correlate with an increase in protein secretion, due to accumulation of proteins in the ER if secretory bottlenecks are present [215].

Finally, it was reported that cells isolated based solely on gating on forward scatter (FSC) and side scatter (SSC) had a 3.4-4.7-fold higher final titre than ungated cells [214]. The FSC corresponds to the

amount of laser beam that passes around the cell, indicating its relative size, whereas the SSC measures the amount of laser beam that is deflected from particulates inside the cells, reflecting the granularity of the cells. Gating based on the smallest cells, based on FSC, and cells with the lowest granularity, based on SSC, resulted in the highest expressers in fed-batch over-grow cultures (FBOG). This is the only strategy reported in the literature that does not rely on vector modifications and that is reagent-free, potentially making it easier for regulatory agencies to approve of the process.

1.5 Imaging flow cytometry

In recent decades, novel advances in the field of flow cytometry have been made with the development of a commercially available imaging flow cytometer, the ImageStream (referred to as the IS, Amnis/Merck). The key feature of the IS technology is that it combines the workflow and high-throughput of a conventional flow cytometer with the acquisition of up to 12 images per cell, thus enabling spatial resolution and quantitative morphology analysis that can be achieved with microscopy [219]. Three objective lenses are available; 20 x, 40 x and 60 x. ImageStream analyses a flow of suspension cells and collects dark-field (side scatter) images, brightfield images and up to nine fluorescent images. This feature is one of the greatest advantages of IS: for each collected event, images of each cell are available. For each 'dot' displayed on a two-dimensional dot plot, it is possible to retrieve the images corresponding to that cell. Unlike conventional flow cytometry, in which gating is limited to light scattering and fluorescence, imaging flow cytometry (IFC) offers different gating strategies such as aspect ratio of a cell (a ratio of cell diameter, reflecting cell circularity), cell diameter, cell volume and many other morphological features. Moreover, the data software, IDEAS (Amnis/Merck) includes multiple data-processing algorithms for image analysis. For instance, new and complex features can be created using Boolean logic or combining two-dimensional masks, to investigate morphological features, intensity threshold, colocalization and spot counting. Imaging flow cytometry has been used in a wide range of studies ranging from the analysis of microparticles [220, 221], the intracellular localisation of probes [222], fluorescent *in situ* hybridization (FISH) studies [219], to the analysis of cells in early or late stages of apoptosis and necrosis [223-225].

Unlike a standard flow cytometer, the IS provides increased sensitivity for smaller particles, as it is able to distinguish particles ranging from 1 μm to 20 nm [221, 226]. This is particularly important for the detection of microparticles, and cellular content. IS also offers visual confirmation, providing verification of the phenotypes of interest, and validating that unwanted cells, such as small cells or aggregates are excluded.

George et al. described a method to quantify the nuclear translocation of Nuclear Factor kappa-light-chain-enhancer of activated B cells (NF-kB) by visually comparing per cell, the colocalization of a nuclear dye and the staining pattern of NF-kB with overlap of the two signals considered as translocation of NG-kB [222]. This method relied on the built-in similarity score feature, based on the Pearson's correlation coefficient (R), which compares pairs of pixel intensities at the same location on the fluorescent image. The correlation coefficient ranges from – 1 to 1, where a positive value indicates a positive correlation between the two signals (i.e. Translocation of NF-kB), whereas a negative value indicates a negative correlation (i.e. untranslocated NF-kB). One limitation of the correlation coefficient is that distribution of extreme values at each end of the spectrum are compressed: cells that are highly translocated would be assigned the same correlation coefficient, despite having different staining pattern by visual inspection. The similarity score solves this problem by offering a more dynamic range, not being bound positively or negatively [222].

$$Similarity = \ln(\frac{1 + R}{1 - R})$$

Compared to the correlation coefficient, a negative similarity score signifies signal localisation in different areas, a positive score indicates co-localisation and 0 indicates no correlation.

Finally, different reports have also described the analysis of cell death and necrosis, combining fluorescent and morphologic features to discriminate cell types and features. Combining annexin V/propidium iodine (PI) staining (annexin V binds to phosphatidylserine, a membrane marker of apoptosis, while PI is unable to permeabilise live cell membranes, and hence is used to detect dead cells) and the morphological analysis, researchers were able to show that nuclear condensation and fragmentation correlates with annexin V and caspase staining [225], and using PI threshold intensity and staining morphology, secondary necrotic/late apoptotic and necroptotic cells could be distinguished [224]. Live, early apoptotic, late apoptotic and necrotic cells could be distinguished by measuring the size of cytoplasm (brightfield area minus nucleus area) and combining this data with annexin V signal [223].

IFC does come with its own limitations, especially when compared to flow cytometry or microscopy. Traditional microscopic methods have better spatial resolution than IS, and allow for time-lapse experiments, and spatial-temporal analysis of the sample [226]. Moreover, IS has a maximum speed of 300 events/sec, which can only be reached with high sample concentrations of 10^8 cells/mL. Samples with a low concentration can take tens of minutes to acquire or may not even reach their acquisition target, this is drastically different from the high-throughput of standard flow cytometry.

One of the most time consuming tasks during IFC event collection is focusing the cells, as out of focus cells would be excluded from analysis [226].

1.6 Project aim and objectives

The main aim of the work described in this thesis was to develop IFC assays to characterise cell lines and identify cell attributes that correlate with cell culture parameters such as productivity, cell growth, or product quality. The initial work started by the organelle content characterisation of a panel of cell lines, to investigate whether organelles essential in protein synthesis and autophagy might be differentially expressed between low and high producers. Such cell attributes could then be used as a screening parameter during the FACS cloning step of the CLD process to increase the proportion of cells with a desired attribute. Moreover, this cell attribute could be targeted in the host cell line to engineer a host with improved qualities. Specific aims were to;

1. ImageStream Assay development (Chapter 3)
    - Confirm robustness of IFC when compared to standard flow cytometry
    - Optimise assays for IFC

2. Characterisation of recombinant mAb expressing cell lines (Chapter 3)
    - Characterise a panel of 19 cells lines with different growth and productivity profile, including mAb mRNA and intracellular protein
    - Identify a marker of productivity at the single cell level
    - Characterise the panel of cell lines in terms of intracellular organelle content at the single cell level, as well as mAb mRNA and intracellular protein
    - Investigate correlations at the single cell level between organelle content and HC content
    - Investigate correlations at the population level between organelle content and cell culture parameters

3. Targets for cell sorting (Chapter 4)
    - Explore the effect of cell sorting a mix of clones based on lysosome content-
    - Explore the effect of cell sorting individual clones based on lysosome content

4. Directed evolution of the host cell using chloroquine (Chapter 5)

- Determine optimal concentration of chloroquine, a lysosomotropic agent used to increase lysosome content, for directed evolution
- Investigate the potential of the evolved host vs. standard host for mAb productivity and product quality
- Mechanistic studies of the two hosts, exploring the differences in transcript and protein expression

CHAPTER 2

Materials and Methods

2.1 Mammalian cell culture

2.1.1 Cell lines and cell culture

AstraZeneca proprietary host CHO cells were cultured in chemically defined (CD), protein free CD-CHO medium (Life Technologies, Carlsbad, CA, USA) supplemented with 6 mM L-glutamine (Life Technologies, Carlsbad, CA, USA). Recombinant CHO cell lines were selected and cultured in CD-CHO medium containing 50 µM methionine sulfoximine (MSX) without glutamine, before being adapted to AstraZeneca proprietary production medium for fed-batch overgrown (FBOG), supplemented with 50 µM methionine sulfoximine for the passages prior to the FBOG (MSX; Sigma-Aldrich, St. Louis, MI, USA). Cultures were grown at 36.5^{o}C in a humidified shaking incubator (Kuhner AG, Birsfelden, Switzerland) at 140 rpm (revolutions per minute), 70% humidity and 6% CO_2 environment. Cells were sub-cultured every 3-4 days in 250 mL vented Erlenmeyer flasks (Corning, NY, USA) in 50 mL culture volume at a seeding density of 3.0 x 10^5 viable cells per mL.

2.1.2 Cell concentrations and culture viability

Cell concentration and culture viability were acquired using a Vi-CELL™ cell counter (Beckman Coulter, Brea, CA, USA) instrument by sampling cell culture media, using phosphate buffered saline (PBS; Life Technologies, Carlsbad, CA, USA) as a diluent when necessary. The Vi-CELL cell counter uses the trypan blue dye exclusion method: live cells possess intact cell membranes which inhibits trypan blue from entering the cells, whereas dead cells do not. A cell suspension is mixed with trypan blue, and the Vi-CELL cell counter automatically counts the number of live and dead cells.

The integral of viable cell concentration (IVC) was determined using the following equation:

$$IVC = \Sigma \frac{(x_i - x_{i-1})}{2} \times (t_i - t_{i-1})$$

With x being the viable cell concentration (cells per mL) and t the culture time (day) and i being the timepoint measured.

2.1.3 Cryostorage of cell lines

A total of 3.0 x 10^7 viable cells was harvested during the mid-exponential phase (day 3-4) of growth when culture viability was >95%, centrifuged at 130xg for 5 min and the supernatant removed. Cell pellets were then resuspended in 1 mL 4^{o}C culture media supplemented with 7.5% (volume/volume, v/v) dimethyl sulfoxide (DMSO; Sigma-Aldrich, St. Louis, MI, USA). Cryovials were placed inside Mr Frosty containers (Sigma-Aldrich, St. Louis, MI, USA) filled with 100% isopropyl alcohol, which was then placed into a -80^{o}C freezer for 24 hours before transfer of the cryovials into cryostats containing liquid nitrogen (-196^{o}C) for long term storage. The Mr Frosty enables a controlled cooling rate of approximately 1^{o}C/min, preserving cellular integrity.

2.1.4 Thawing of cell lines from frozen stocks

Frozen cryovials were quickly thawed in 70% ethanol warmed in a 37^{o}C water bath, to avoid cells' exposure to ice crystals, until partially thawed. Warmed culture media was added drop-wise to the thawed cells, to reach a seeding density of 3.0 x 10^5 viable cells per mL in a shake flask.

2.1.5 Fed-batch overgrow cultures

For FBOG experiments, cell cultures were seeded at 0.7 x 10^6 viable cells per mL in 50 mL or 70 mL of media without MSX in 250 mL vented baffled Erlenmeyer shake flasks (Corning, NY, USA). Feeds were added every other day using AstraZeneca proprietary feeds over a 14-day period.

2.1.6 Determining cell culture supernatant glucose and lactate concentration

During FBOG experiments, glucose and lactate concentrations in the culture supernatant were monitored using a YSI 2900 biochemistry analyser (Xylem Analytics, Beverly, MA, U.S.A) by sampling

200 µL of culture media which was centrifuged at 2,200xg for 5 min. When glucose levels were lower than 5 g/L, glucose was supplemented to give a concentration of 8 g/L.

2.1.7 Chloroquine treatment of cells

Chloroquine (CQ) powder (InvivoGen, San Diego, CA, USA) was reconstituted in sterile water to a working concentration of 100 mM. For directed evolution of host cell lines, various amounts of CQ were added directly into the media at each passage to give the desired final concentration in the culture.

2.1.8 Ambr experiments

Experiments were conducted using an ambr15 system (Sartorius Stedim TAP, Royston, UK), with 24 vessels. Process programs for the ambr15 were created using an in-house software (AstraZeneca, Cambridge, U.K.). Bioreactors were inoculated at 7.0 x 10^5 cells/mL in each vessel. Cells were fed with AstraZeneca's proprietary feed on days 2,4,6,8,10 and 12.

2.2 Recombinant protein quantitation

2.2.1 Protein-A affinity purification

Supernatant samples were taken throughout the FBOG culture and centrifuged at 8,000xg for 5 min. Immunoglobulin G (IgG) content in the supernatant was then quantified by protein-A HPLC (high performance liquid chromatography) affinity chromatography on an Agilent HP1100 (Agilent Technologies, Santa Clara, CA, USA).

2.2.2 Determination of cell specific mAb productivity

The cell specific mAb productivity (qP) corresponds to the mAb production per cell rate over time. qP was calculated from the linear slope of the plot of antibody titre versus the integral of viable cell concentration. The overall qP was the average of the individual qPs between the days sampled.

2.3 Generation of plasmid DNA and transfection of CHO cells

2.3.1 Plasmid DNA transformation

DNA was transformed into animal component free (ACF) Z-competent cells (in-house, AstraZeneca, Cambridge, UK) and spread onto ACF PYAG plates. A single colony was picked and used to inoculate cultures using ACF broth containing ampicillin (in-house, AstraZeneca, Cambridge, UK). Cultures were incubated overnight at 37^{o}C, 300 rpm in a shaking incubator (Kuhner AG, Birsfelden, Switzerland). The following day, cells were centrifuged at 3600xg at 4^{o}C for 30 minutes. DNA was purified using the QIAGEN Plasmid Plus Maxi kit (Qiagen, Hilden, Germany) according to the manufacturer's instructions. DNA concentration at the 260 nm absorbance was then measured using a Nanodrop 1000 (Thermo Fisher, Waltham, MA, USA). To verify DNA purity, the ratio of A260/A280 was also calculated: good quality DNA will have a A260/A280 ratio between 1.7 and 2-.0. Linearization of plasmid DNA was undertaken by adding 30 µL of BSA free Pvu-1 enzyme (Sigma-Aldrich, St. Louis, MI, USA) and 45 µl buffer H (Sigma-Aldrich, St. Louis, MI, USA) for every 100 µg DNA, with incubation overnight at 37^{o}C.

2.3.2 Plasmid DNA purification

Purification of DNA was achieved using a phase lock gel extraction and ethanol precipitation. The DNA was added to a 5Prime phase lock gel (PLG) tube (VWR, Radnor, PA, USA) with addition of an equal volume of organic extraction solvent (phenol: chloroform: isoamyl alcohol 25:24:1; Invitrogen, Carlsbad, CA, USA). The organic and aqueous phases were mixed by rapid inversion to form a homogenous suspension. Tubes were centrifuged at 13,000xg for 5 min to separate the phases. The top nucleic acid layer was transferred into a new PLG tube, and an equal volume of chloroform (VWR, Radnor, PA, USA) was added to the sample and mixed thoroughly by inversion. Following centrifugation, the top nucleic acid containing layer was transferred to a fresh Eppendorf tube. Nucleic acids were precipitated by adding 2 volumes of ice cold 100% ethanol (VWR, Radnor, PA, USA) and 0.1 volume of 3 M sodium acetate (Sigma-Aldrich, St. Louis, MI, USA), and mixed by inversion. Samples were centrifuged for 30 min at 13,000xg at 4^{o}C to pellet the DNA. The cell pellet was then washed in 1 mL of 70% ethanol, and centrifuged for 10 min. In a sterile cabinet, the supernatant was then removed by aspiration, and the pellet was allowed to air dry for 10 min. DNA was resuspended in endotoxin-free sterile water (Sigma-Aldrich, St. Louis, MI, USA), and after solubilisation, the DNA concentration was measured at 260 nm using a Nanodrop 1000 instrument (Thermo Fisher, Waltham, MA, USA). The final concentration was adjusted to 400 µg/mL in water and the concentration confirmed using a Nanodrop 1000 instrument.

2.3.3 Agarose gel electrophoresis

A 0.8% agarose E-gel (Invitrogen, Carlsbad, CA, USA) was used to check DNA linearization from 50 ng of uncut vector, 50 ng of linearized vector and 5 µL of digested non-purified vector mixed with 1 µL of loading buffer (Invitrogen, Carlsbad, CA, USA), DNA was separated using a voltage of 80 V for 40 min.

2.3.4 Electroporation of plasmid DNA into CHO cells

CD-CHO medium (Life Technologies, Carlsbad, CA, USA) was pre-gassed and pre-warmed. Stable cell lines, from shaking pools, were generated via electroporation using the Amaxa Cell Line Nucleofector Kit system (Lonza, Basel, Switzerland). For each pool, $2.2x10^7$ viable cells were harvested and centrifuged at 130xg for 5 min. Two transfection events were required per pool, using 5 µg of DNA per transfection. Cells were resuspended in 100 µL Amaxa Nucleofector solution, the DNA added, and the mix was transferred into a cuvette. Cells were electroporated using program U-024, the transfected cells were gently added to 41 mL of CD-CHO media without MSX selection. The following day, 8 mL of fresh media containing 48 µL 50 mM stock MSX was added to each shake flask to give a final concentration of 50 µM. Cells were then left to recover for two weeks before being assessed for the emergence of stably expressing pools of cells.

2.4 Molecular biology

2.4.1 RNA extraction

Total RNA was extracted from cell pellets using the commercially available RNeasy kit (Qiagen, Hilden, Germany) and treated with DNase to remove any undesired DNA following the manufacturer's instructions. RNA concentrations were quantified using a NanoDrop 1000 instrument (Thermo Fisher, Waltham, MA, USA) with the RNA-40 program, at 260 nm absorbance wavelength. For RNA, a A260/A280 of ~2.0 is considered good purity.

2.4.2 qRT-PCR

Primers were designed for HC and LC mRNA quantification by qRT-PCR (quantitative real time polymerase chain reaction) using the OligoPerfect Designer™ (ThermoFisher, Waltham, MA, USA), the generated primer sequences are below (Table 2.1).

Table 2.1. HC and Kappa LC primers used for qRT-PCR

Gene	Primer Forward – Reverse (5'-3')
Heavy Chain	Forward CAAGTGCAAGGTCTCCAACA
	Reverse ACCAGACAGGTCAGGGACAC
Kappa Light Chain	Forward GCAAGGACTCCACCTACAGC
	Reverse TGTTGAAGCTCTTGGTCACG
GAPDH	Forward GCCAAGAGGGTCATCATCTC
	Reverse CCTTCCACAATGCCAAAGTT

qRT-PCR was carried out using the Qiagen Quantifast SYBR green RT-PCR kit (Qiagen, Hilden, Germany) according to the manufacturer's instruction, and the Bio-Rad Chromo4 thermocycler (Bio-Rad, Hercules, CA, USA). PCR conditions; reverse transcription at 50^{o}C for 10 minutes, followed by a 5 minutes incubation at 90^{o}C and 40 cycles of 10 seconds at 95^{o}C and 30 seconds at 58^{o}C using the primers in Table 2.1, and the housekeeping gene glyceraldehyde 3-phosphate dehydrogenase (GAPDH) as a reference gene. Expression levels of HC and LC were normalized to GAPDH levels. Opticon Monitor 3.1 software (Bio-Rad, Hercules, CA, USA) was used for data analysis of the cycle threshold (C_T) and melting curve. Relative quantification was used by comparative C_T method [227].

2.5 Flow cytometry and imaging flow cytometry

Sample preparation for both standard flow cytometry and imaging flow cytometry was identical. Imaging flow cytometry samples contained a minimum of 2 million viable cells whereas samples for flow cytometry contained 1 million cells. Centrifugation steps were performed at 400xg for 5 min, and cells were washed in PBS, unless specified otherwise. Individual staining, unstained and host cell

(negative control for HC and LC protein and mRNA) samples were prepared to aid set up of the flow cytometer.

2.5.1 HC and LC mRNA quantification by PrimeFlow RNA

Two custom probes were designed by Affymetrix to target the variable region of the HC and LC antibody mRNA (Affymetrix, Santa Clara, CA, USA). Samples were prepared according to the manufacturer's protocol. Briefly, cells were fixed and permeabilized, and incubated with the gene-specific probe set for target hybridization. Signal amplification was performed by incubating samples with pre-amplifier, and amplifier DNA. Finally, florescence-labelled probes were added, which bind to the amplifier DNA, this achieves 8,000 to 16,000-fold signal amplification (Fig. 2.1).

For multiplexing of HC mRNA and IC HC protein, following permeabilization, samples were stained with 1:20 goat f(ab')2 anti-human IgG conjugated to Alexa Fluor 488 (Invitrogen, Carlsbad, CA, USA) for 30 minutes at 8^{o}C.

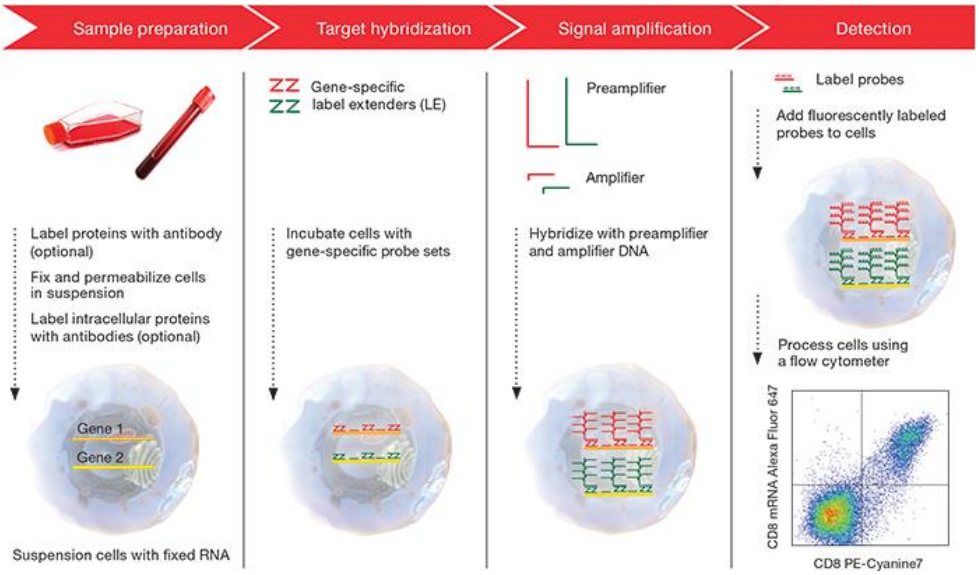

Figure 2.12 Schematics depicting the PrimeFlow mechanisms of action (source: Merck), starting with sample preparation, target hybridization, signal amplification and finally detection of the probes

2.5.2 Intracellular HC and LC protein analysis

Cells were fixed using a 1:1 solution of Fixation Medium A (Invitrogen, Carlsbad, CA, USA) and flow cytometry buffer (PBS with 5% (w/v) BSA) for 15 min at room temperature. Cells were then permeabilised and stained with Permeabilisation Medium B (Invitrogen, Carlsbad, CA, USA) containing 1:20 goat f(ab')2 anti-human IgG conjugated to Alexa Fluor 488 (Invitrogen, Carlsbad, CA, USA) and goat f(ab')2 anti-human kappa conjugated to APC (Allophycocyanin, Biolegend, San Diego, CA, USA). Samples were incubated for 15 minutes at room temperature and washed with PBS prior to flow cytometry analysis.

2.5.3 Organelle assays

The organelles investigated included Golgi apparatus, ER, lysosome and mitochondria. Quantification of the specific organelle content was performed using the following dyes: Golgi-ID Green, ER-ID red, Lyso-ID red, MITO-ID red detection kit (Enzo Life Sciences, Farmingdale, NY, USA) and MitoTracker Deep Red (Invitrogen, Carlsbad, CA, USA). Staining was performed using the recommended protocol from the manufacturer. ER-ID and Mito-ID were multiplexed with goat f(ab')2 anti-human IgG conjugated to Alexa Fluor 488 (Invitrogen, Carlsbad, CA, USA) to investigate the correlation at the single cell level between productivity and organelle content. Golgi-ID was not multiplexed with HC protein due to the apparent loss of specificity of the staining following permeabilization. Cells were also stained with DAPI or Sytox Blue nuclear counter-stain. Lysosome quantification was performed using LYSO-ID in live cells (Enzo Life Sciences, Farmingdale, NY, USA) according to the manufacturer's protocol. Finally, oxidative stress of the cells was also measured using CellROX green kit (Thermo), following the manufacturer's protocol. Staining was performed in fresh cell culture media, as PBS use was not recommended. Excitation and emission values, lasers used and IFC collection channels are listed in Table 2.2.

Table 2.2 Reagents used for IFC or FC with the excitation and emission, laser used, and the IFC collection channel

Reagent	Ex/Em	Laser	IFC collection channel
PrimeFlow HC	650/665	642 nm	11
PrimeFlow LC	495/519	488 nm	2
HC protein	495/519	488 nm	2
LC protein	650/660	642 nm	11
Golgi-ID Green	450/550	488 nm	2
ER-ID Red	550/660	561 nm	5
MITO-ID red	558/690	561 nm	5
MitoTracker Deep Red	644/665	642 nm	11
DAPI	358/461	405 nm	7
Sytox	444/481	405 nm	7
LYSO-ID Red	564/660	561 nm	5
CellRox Green	500/550	488 nm	N/A

2.5.4 Data acquisition and analysis for flow cytometry

Flow cytometry was performed using a BDCanto or LSRFortessa flow cytometer (BD Biosciences, San Jose, CA, USA), with the BD FACSDiva™ software. Unstained controls were used to set the laser intensity. Doublets and debris were removed by gating on forward and side scatter dot plots, and 10,000 events were acquired. FlowJo software (FlowJo LLC, Ashland, OR, USA) was used for statistical analysis of the samples.

2.5.5 Data acquisition and analysis for imaging flow cytometry

An ImageStream® imaging flow cytometer (Merck, Kenilworth, NJ, USA) with the INSPIRE® software was used to collect 10,000 events (or 10 minutes of acquisition, whichever ended first). Images for each event were captured using a 60X objective with the lasers and collection channels described in Table 2.2, alongside channel 1 and 9 for brightfield and channel 6 for darkfield. Cell classifier, the IFC equivalent of a size gate, was set to 50 on area-lower limit of the brightfield channel to avoid debris acquisition. Analysis was performed using IDEAS® software (v6.2). Compensation settings were calculated using the built-in software algorithm in best-fit mode and refined manually. Focused cells were gated using the plot of contrast versus gradient RMS features in the brightfield channel (Fig.

2.2A). Single cells were gated using a dot plot of the aspect ratio versus cell area for the brightfield channel (Fig. 2.2B). Intensity gates were set based on the negative control intensity (Fig. 2.2C), and samples were analysed using those gates (Fig. 2D). Staining intensity was normalised to cell size.

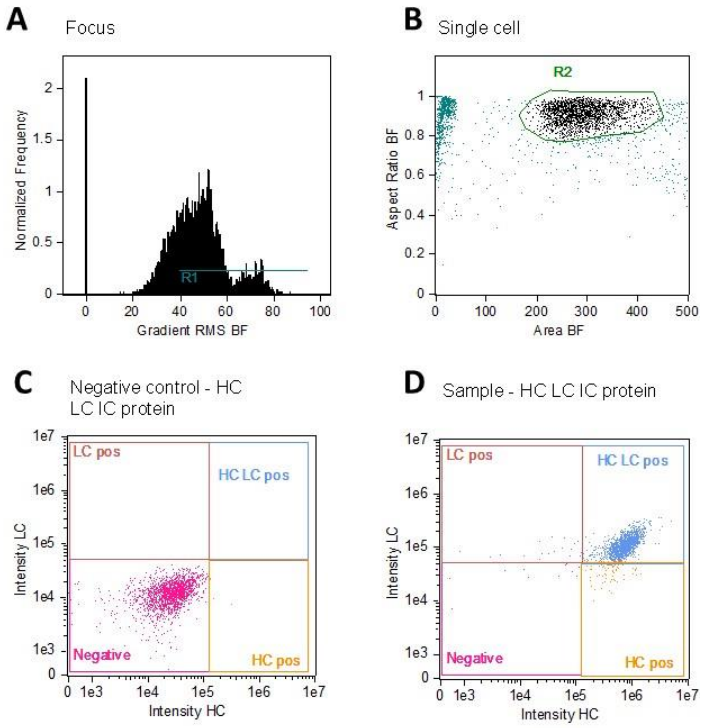

Figure 2.13 IFC data analysis workflow – A) Gating of the images that are in focus. B) Gating of the single cells. C) In this example, the stained host cell line (untransfected) was used to set-up the gates for protein expression. D) Example of HC and LC protein profile for a cell line expressing a standard mAb.

2.6 Fluorescence-activated cell sorting

2.6.1 Cell sorting

Fluorescence activated cell sorting (FACS) was performed with a BD FACSAria sorter II (BD Biosciences, San Jose, CA, USA) equipped with a 100 µm nozzle and default pressure of 120 psi. Stream and drop delay were set-up using beads (BD Biosciences, San Jose, CA, USA). Unstained and LYSO-ID stained cells were gated based on forward and side scatter and based on lysosome signal intensity. Pools of 20,000 cells were generated. Cells were sorted into 15 mL Falcon tubes (BD Biosciences, San Jose, CA, USA) into 1 mL of CD-CHO media supplemented with 50% conditioned media. Conditioned media was harvested fresh on the day of sort, 2-3 days post-split, from AstraZeneca's host cell line cultured in CD-CHO media + L-glutamine. Cells from the conditioned media were removed by centrifugation and

filtration through a Nalgene 0.2 µm filter (Thermo Fisher, Waltham, MA, USA). A post-sort quality check, from the generated pools, was performed acquiring 500 events to monitor the accuracy of the sort.

2.6.2 Cell recovery

Cells were transferred from the 15 mL Falcon into a 24-well plate and allowed to expand and grow in a static incubator at 37^{o}C for more than one week. As the cell concentration increased, cells were subsequently transferred into 12-well plates, 6-well plates and eventually shake flasks. Fresh media was used with each transfer into a new vessel. Cell growth was monitored by visual inspection using a bench-top microscope (Zeiss, Oberkochen, Germany).

2.7 Protein analysis

2.7.1 Protein extraction

Cell pellets containing a minimum of 1x10^{6} viable cells were thawed on ice and resuspended in a solution of mammalian protein extraction reagent (M-PER, Thermo Fisher, Waltham, MA, USA) supplemented with a cocktail of phosphatase inhibitors (Thermo Fisher, Waltham, MA, USA), protease inhibitors (Thermo Fisher, Waltham, MA, USA) and EDTA (Thermo Fisher, Waltham, MA, USA). M-PER is a mild lysis detergent that dissolves cell membranes, allowing the extraction of total intracellular protein. Samples were incubated on ice for 30 min, followed by centrifugation at 4^{o}C for 10 min at 14,000xg. Supernatants were transferred into fresh Eppendorf tubes and kept on ice.

2.7.2 Bradford assay to determine protein concentration

The Bradford assay is used to measure the total protein concentration of a sample. A Coomassie dye is added to the whole protein extract, and under acidic conditions, the colour of the dye changes from brown to blue. This colour change is dependent on the presence of the following amino acids: arginine, lysine and histidine, which bind to the dye.

A bovine serum albumin (BSA) standard was serially diluted in water using Quick Start Bradford Protein Assay (Bio-Rad, Hercules, CA, USA), producing a standard curve from 2 mg/mL down to 0 mg/mL, with 6 concentrations in between. Standards and samples were measured in duplicate by pipetting 3 µL of

each sample into an Eppendorf containing 1 mL of Quick Start Bradford 1x Dye Reagent (Bio-Rad, Hercules, CA, USA). After 10 min incubation, 200 µL of sample was transferred into a 96-well plate. Absorbance readings were measured by a PolarStarOptima plate reader (BMG Labtech, Ortenberg, Germany), at a wavelength of 595 nm.

2.7.3 SDS-PAGE analysis

SDS-PAGE (sodium dodecyl sulphate-polyacrylamide gel electrophoresis), is a method that separates proteins based on their mass. For detection of HC and LC polypeptides, both non-reduced and reduced conditions were used. Protein extracts were mixed with water, gel loading buffer (Thermo Fisher, Waltham, MA, USA) and either reducing agent (Thermo Fisher, Waltham, MA, USA) or N-Ethylmaleimide (NEM, Sigma-Aldrich, St Louis, MI, USA) to obtain a final sample containing between 20 and 40 µg of protein. Reduced samples were heated at 100^{o}C for 5 min, to denature the protein samples, reducing the disulphide bonds. Samples were then loaded onto a 4-12% NuPAGE Bis-Tris SDS gel, with running buffer containing 950 mL MilliQ water and 50 mL SDS buffer (Thermo Fisher, Waltham, MA, USA). A visible Novex Sharp pre-stained protein ladder (Thermo Fisher, Waltham, MA, USA) and a Magic Mark XP western protein ladder (Thermo Fisher, Waltham, MA, USA) were run alongside samples for estimation of molecular weight. Gels were run for 40 min at 200 V and 400 A.

2.7.4 Western blotting

Protein samples were transferred to nitrocellulose membranes using the iBlot 7-minute blotting system (Thermo Fisher, Waltham, MA, USA). Membranes were blocked in 5% (w/v) BSA (Sigma-Aldrich, St Louis, MI, USA) in PBS Tween solution for 30 min. Membranes were then washed three times with PBS Tween, and incubated overnight with the desired antibodies (Table 2.3). Anti-GAPDH rabbit antibody was used to detect hamster GAPDH as a housekeeping protein for normalisation of protein expression. Overnight incubation was followed by three washes in PBS Tween to remove unbound antibodies prior to membrane development.

Western blot membranes were incubated for 1 min in chemiluminescent Amersham ECL reagent (GE Life Sciences, Marlborough, MA, USA) and proteins were detected using an ImageQuant-LAS 4000 ECL set on chemiluminescence, using a charge-coupled device camera (GE Life Sciences, Marlborough, MA, USA). Acquired images were analysed using ImageJ (NIH, Bethesda, MD, USA), quantifying the bands intensity and normalising the protein of interest levels to GAPDH expression levels.

Table 2.3 List of primary and secondary antibodies used for western blotting

Antibody	Dilution	Molecular weight	Distributor
Primary			
HRP - conjugated human anti - IgG (Fc)	1:10,000	50	The Binding Site
HRP - conjugated human anti-Kappa	1:10,000	25	The Binding Site
Anti-GAPDH rabbit	1:2,000	35	Cell Signalling Technology
Anti p62/SQSTM1 rabbit	1:1,000	60	Cell Signalling Technology
Anti-Lamp 1 rabbit	1:1,000	100	Cell Signalling Technology
Anti-Lamp2A rabbit	1:1,000	100	Abcam
Anti - LC3B rabbit	1:2,000	20	Cell Signalling Technology
Anti - Bcl-xL rabbit	1:1,000	30	Cell Signalling Technology
Anti Atg12 rabbit	1:1,000	20 and 50-60	Cell Signalling Technology
Anti - phosphorylated mTOR	1:1,000	250	Cell Signalling Technology
Anti - phosphorylated 4EBP1	1:1,000	15-20	Cell Signalling Technology
Anti - p70 S6 (Thr389)	1:1,000	70-85	Cell Signalling Technology
Anti - Lamtor1	1:1,000	18	Cell Signalling Technology
Anti-caspase 3	1:1,000	32	Cell Signalling Technology
Anti - cleaved caspase 3	1:1,000	17-19	Cell Signalling Technology
Secondary			
Peroxidase - conjugated anti-rabbit	1:10,000		Jackson ImmunoResearch

2.7.5 Automated western for supernatant analysis

The automated, high throughput capillary electrophoresis western system, Peggy Sue (Protein Simple, Minneapolis, MI, USA), was used to quantify proteins in the crude supernatant, harvested on day 14 of the FBOG. Proteins are moved through a capillary tube and immobilized by photochemical capture based on their molecular weight. Detection antibodies come in contact with the immobilized proteins, similarly to the traditional western blotting method [228].

The experiment was conducted following the manufacturer's user guide instructions. Based on titre data, samples were diluted in PBS to 1 µg/mL in water and mixed with the 5x Master Mix containing SDS and dithiothreitol (DTT). Samples were incubated at 100^{o}C for 5 min for protein reduction and denaturation. Samples and the ladder (provided in the kit), were loaded onto the plate. Antibody solutions (anti HC – HRP conjugated), blocking solution (antibody diluent), detection solution (a mix of luminol and peroxide), stacking and separation matrices were loaded onto the plate as well, into their respective wells. A box of single-use silica capillaries was loaded onto the Peggy Sue to start sample analysis.

2.7.6 Glutathione measurement assays

To evaluate oxidative stress in cells, the ratio of glutathione (GSH) and glutathione disulphide (GSSG) was measured using a luminescence-based assay (Promega, Madison, WI, USA). The assay was performed according to the manufacturer's protocol. Briefly, live cells were aliquoted into a 96-well plate, and incubated with a lysis reagent, either for total glutathione or for oxidised glutathione. For total glutathione measurement, both GSH and GSSG were reduced, whereas for oxidised glutathione, a reagent was added that blocks GSH, and reduces GSSG to GSH. Luciferin generation and detection reagents were then added into the wells. GSH converts the luciferin-reagent, a GSH probe called Luciferin-NT, to luciferin by a glutathione S-transferase enzyme coupled to a firefly luciferase reaction. The luminescence signal was measured with an EnVision plate reader (PerkinElmer, Waltham, MA, USA). The ratio of GSH:GSSG was calculated from the luminescence measurements.

2.7.7 Protein digestion for LC-MS/MS analysis

Cell culture supernatant samples from day 14 of the FBOG were diluted to 1- 5 mg/mL in water, and 20 µL samples were mixed with 30 µL 8 M urea (Sigma-Aldrich, St. Louis, MI, USA). DTT (Thermo Fisher, Waltham, MA, USA) stock at 500 mM was added to give a final DTT concentration of 10 mM. Samples were then denatured for 10 min at 50^{o}C. Trypsin (Thermo Fisher, Waltham, MA, USA) was reconstituted in 100 mM Tris buffer pH 7.2 and added at a 1:20, enzyme: substrate ratio. Samples were then incubated at 37^{o}C for up to 4 hours.

2.7.8 LC-MS/MS

LC-MS/MS (liquid chromatography mass spectroscopy) analysis was carried out using a Triple Quadrupole Mass Spectrometry (Waters, Milford, MA, USA) to assess protein, peptide and glycan profiles. An aliquot of 7.5 µg of digested protein was loaded onto a carbon C_{18} column at 55^{o}C (Waters, Milford, MA, USA). The buffers used were the following:

- Mobile phase A: 0.02% TFA (v/v) in water
- Organic phase B: 0.02% TFA (v/v) in acetonitrile

Each sample cycle lasted 10 min. During the first three minutes, samples were desalted at a flow rate of 0.200 mL/min in 5% B and the flow-through discarded. After 3 minutes, the percent of buffer B increased linearly to elute the sample up to a percentage of 30% over 5 mins. The flow-through was

directed into the MS for analysis. At 8 minutes, the column was washed with 90% buffer B for 1.6 min followed by equilibration back to 5% buffer B for 0.2 minutes.

Samples directed for MS analysis were ionized by the source going through an electrospray capillary voltage of 3 kV, cone voltage 20 V, source temperature 70^{o}C. Samples were then directed onto the first quadrupole (Q1), followed by fragmentation in Q2, and finally daughter ions were captured and recorded in Q3. Data analysis was performed using the MassLynx software (Waters Milford, MA, USA).

2.8 RNA sequencing

2.8.1 Total RNA isolation using TRI reagent

Triplicate cell pellets for RNA sequencing were sampled from the evolved host and standard host on day 7 of the FBOG. Cell pellets were flash frozen in liquid nitrogen and stored in -80C° until ready to be used. Total RNA was extracted using the Direct-zol RNA MiniPrep kit (Zymo Research, Irvine, CA, USA) according to the manufacturer's protocol. Briefly, cells were resuspended in TRI Reagent, centrifuged, and an equal volume of 95-100% ethanol was added to the supernatant. The mix was then transferred onto a Zymo-Spin IIC column. In column DNase I treatment was performed on column, removing contaminating genomic DNA. RNA was eluted in DNase/RNase free water. RNA content was quantified using the RNA-40 NanoDrop 1000 program (Thermo Fisher, Waltham, MA, USA), at 260 nm wavelength.

2.8.2 RNA quality assessment

RNA quality was assessed using the Agilent 2100 Bioanalyzer (Agilent Technologies, Santa Clara, CA, USA), a microfluidics-based platform using miniature chips. RNA samples were diluted to approximately 1 ng/µL in water, and 5 ng of RNA was loaded on the LabChip, followed by addition of the RNA 6000 Pico marker. The RNA ladder was also loaded onto the chip for size estimation (Fig. 2.3). The microchip was then quickly vortexed and loaded onto the bioanalyzer. The fluorescence was measured and displayed in a gel-like manner or electropherograms showing 18S and 28S RNA peaks. The ratio of 28S to 18S permits the calculation of the RNA integrity number (RIN), an indicator of RNA quality and degradation, ranging from 0-10, with 10 indicating intact RNA (Figure 2.3). RNA sequencing was performed with samples that had a RIN higher than 8.

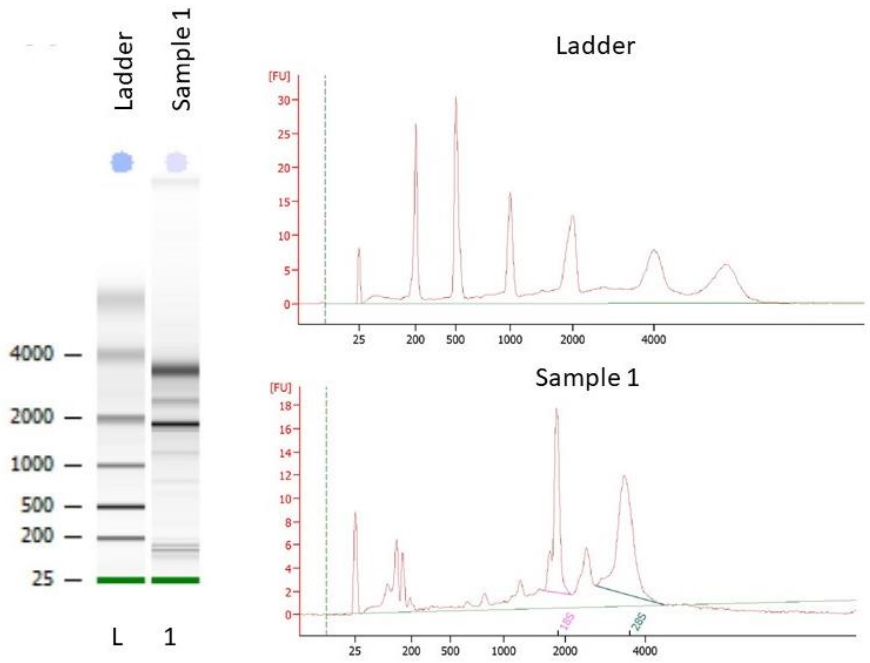

Figure 2.14 Bioanalyzer sample results. A) Gel-like and B) electropherograms showing the RNA peaks of the ladder and of an RNA sample. The area under the curve of the 18S and 28S peaks are calculated to determine the RIN.

2.8.3 Library synthesis, sequencing and reference mapping

Messenger RNA purification and library preparation were performed by Leeds Institute of Molecular Medicine (Leeds, UK). Sequencing data was collected on one lane of a HiSeq 3000 (Illumina, San Diego, CA, USA) using a 2 x 250 bp, paired end read type. The sequence reference of the easy to express (ETE) and difficult to express (DTE) mAb were prepared in house and included both heavy and light chains. Sequence data was analysed for quality using the FastQC software (Babraham Institute, Cambridge, UK). Raw sequences were cleaned of adapters and primers using Cutadapt (https://doi.org/10.14806/ej.17.1.200) and Trimgalore (Babraham Institute, Cambridge, UK) to remove primers, adapters, and low-quality bases. The trimmed reads were mapped onto the annotated CHOK1-GS transcriptome [229] using the STAR read aligner [230]. BAM files were generated using SAMtools [231]. BAM files are used to generate count matrices. All the bioinformatics analysis was carried out by Luigi Grassi at AstraZeneca, using R studio.

2.8.4 Differential gene expression analysis and gene ontology analysis

Transcript expression was quantified using the Salmon tool [232] and FeatureCounts [233], which assigns reads to the target genes and summarizes the data into a table. Differential gene expression analysis was performed from this dataset using edgeR [234] and DESeq2 [235], two count-based statistical methods downloaded from Bioconductor [236]. The software edgeR can account for biological and technical variability of replicate samples through a negative binomial reference distribution and an empirical Bayes method, stabilising overdispersion across genes [234]. DESeq2 software also relies on a negative binomial distribution and Bayesian approach, enabling the quantitative analysis of RNA-seq data using shrinkage estimators for dispersion and fold-change, focusing on the strength of the differentially expressed genes rather than just their presence [235].

Principal component analysis (PCA) analysis was performed to visualise the distribution of the triplicate samples. This allowed comparison across triplicates, based on the molecule expressed, and control vs. CQ-host. Differentially expressed genes were visualised using the pheatmap (https://CRAN.R-project.org/package=pheatmap) R-package, which generates heatmaps.

Gene ontology (GO) enrichment analysis was performed using Fidea [237] a web-based software program. This software maps gene symbols to their molecular function, KEGG pathway, biological process and cellular component. The GO enrichment analysis was performed both with and without a threshold for fold-change. For the threshold-based analysis, differentially expressed genes identified from DESeq2 analysis were input. Thresholds for fold change (1.5 or 2-fold change) and adjusted p-values (p-adj < 0.05 or p-adj < 0.1) were investigated. P-adj controls for the false discovery rate of a list of genes using Benjamini-Hochberg algorithm [238], allowing a more stringent selection of differentially expressed genes. Finally, manual screening of genes and gene pathways was performed to identify target genes of the CQ-treatment.

2.9 Statistics

To analyse the impact of the organelle content on cell culture parameters such as titre, PCA analysis was performed using Minitab software (Minitab, PA, USA). Data from each cell line including the content of Golgi, ER, mitochondria, lysosome, HC and LC protein and mRNA, were input to assess their effect on productivity. Different days were analysed independently or combined.

Excel (Microsoft, WA, USA) was used for most of the data analysis and graph generation. The Pearson correlation coefficient (R) was used to determine the strength of any relationship between two variables, and was calculated with the following equation:

$$r = \frac{\sum (x - \bar{x})(y - \bar{y})}{\sqrt{\sum (x - \bar{x})^2 \sum (y - \bar{y})^2}}$$

with $\bar{x}$ and $\bar{y}$ the average.

Finally, t-tests were performed to determine if the differences between the means of two different conditions were statistically significant.

CHAPTER 3

Application of imaging flow cytometry for the characterisation of intracellular attributes in CHO cell lines at the single cell level

Declaration of contribution

Part of the work described in this chapter has been published as:

Pekle E, Smith A, Rosignoli G, Sellick C, Smales CM, Pearce C. (2019) Application of Imaging Flow Cytometry for the Characterization of Intracellular Attributes in Chinese Hamster Ovary Cell Lines at the Single-Cell Level. Biotechnol J. Mar 29:e1800675. doi: 10.1002/biot.201800675.

For this publication, all the experimental work was conducted by me, except for titre analysis which was completed by Mr Andrew Smith at MedImmune. I was also central to the experimental design, performed the data analysis, wrote the first draft of the paper, as well as editing subsequent drafts along with the paper's co-authors. For this chapter (Chapter 3), the content of the paper has been modified to align with the thesis' format and, to allow the inclusion of additional data that was not included in the paper. The complete publication can be found in Appendix A.

3.1 Introduction

Mammalian cells are the expression system of choice for the commercial manufacture of therapeutic glycoproteins, such as monoclonal antibodies (mAbs), with over 70% being produced using CHO cells [50]. During cell line development, random integration of the expression plasmid and host cell heterogeneity results in varied expression levels of the transgene, requiring extensive screening to identify highly productive and stable clones [200, 239, 240]. Strategies to identify cell lines with an increased probability of a high final titre at the cloning step could reduce timelines and diminish the total number of cells required to be screened to isolate such clones. FACS is commonly used for cell cloning in cell line development, having the advantage of being a high-throughput method that can deposit single cells into wells of multi-well plates, supporting the regulatory demands for clonality, and allowing assessment of cellular characteristics at the single-cell level. Combining FACS with post-sorting visualisation by fluorescent imaging showed that >99.5% of cells were clonal [241]. Various flow cytometry-based screening methods have been developed to enable selective isolation of high producing clones. These include the capture of secreted mAb via binding to the cell surface using microbead technology [242], surface affinity matrix [204], introducing fluorescent markers into the vector [208] and vector modifications to enable secreted mAb to bind to cell surface proteins [211, 212]. Although such approaches give enrichment of high producing clones, they tend be labour intensive and time consuming.

Recent advances in flow cytometry have been made with the development of a novel imaging flow cytometer, ImageStream (IS, Amnis/Merck). A key feature of IS is that it combines the workflow and high throughput of conventional flow cytometers with the acquisition of up to 12 images per cell, enabling the spatial resolution and determination of quantitative morphology that can be achieved with microscopy [219]. Imaging flow cytometry (IFC) images that may be obtained include side-scatter, brightfield and up to nine fluorescent images, and such data has been used in a range of studies including assessing nuclear translocation [222], detection and discrimination of tumour cells and FISH studies [219]. The current study describes a novel approach to study recombinant CHO cell lines using IFC technology to identify cellular characteristics that correlate with productivity at the single cell level, with the potential of being integrated into the CLD platform.

3.2 Results

3.2.1 Preliminary characterisation of a panel of 19 cell lines

To investigate cellular differences between high and low producing cell lines and determine any correlations between organelle content and cell culture parameters, it was important to study cell lines with a range of titre and growth profiles. A panel of 19 cell lines were chosen from an initial large panel of cell lines. These cell lines express a model IgG1 mAb and were initially characterised in terms of growth, productivity, intracellular protein and mRNA levels over a 14-day FBOG in baffled shake flasks (BSF). Moreover, a subset of these cells lines (all except 1, 5, 8) were cultured in the AMBR microbioreactor system. As the AMBR offers a controlled environment in terms of pH, dissolved oxygen, and constant impeller speed, it was important to understand whether data from the BSF was predictive and consistent with those under controlled bioreactor conditions.

3.2.1.1 Cell culture characterisation and comparison of BSF and AMBR systems

Growth

Cell counts, measured by Vicell, were taken on days 0, 1, 2, 3, 7, 8, 9, 10, 11 and 14 for the BSF, and every 2 days for the AMBR. The cell lines exhibited a range of growth profiles, with maximum VCD ranging from $115x10^5$ cells/ml to $470x10^5$ cells/ml in BSF (Fig. 3.1 A). Compared to the BSF, results from the AMBR show a more consistent VCD, without the fluctuations that were observed in the BSF (Fig. 3.1 B). The ranking of cell lines' maximum VCD was consistent between the two systems, and the Pearson's correlation coefficient (R) for the maximum VCD reached between AMBR and BSF was 0.84, indicating a strong correlation (Fig. 3.1 C).

Cell lines 1, 8, 14 and 15 had the highest maximum VCD and highest final IVC, peaking at over $7500x10^9$ cells x hour/L on day 14 (Fig 3.1 D). At the lower end of the spectrum, cell lines 16, 18 and 19 had the lowest maximum VCD, and their IVC barely reached over $2000x10^9$ cells x hour/L by day 14. The remaining cell lines IVC on day 14 ranged from 3036 to $6088x10^9$ cells x hour/L. Final IVCs in the AMBR (Fig. 3.1 E) were consistent with the BSF experiment with a strong positive correlation between the two systems, although for some cell lines, the values were lower in the AMBR compared to the BSF (R = 0.71; Fig. 3.1 F; App. B Table 1).

For the BSF, all cell lines had a starting culture viability above 90%, which was maintained for all until day 7 (Fig. 3.1 G). The final range of culture viabilities on day 14 was between 20 to 82%. The decreased culture viability was most pronounced between day 10 and 14, accentuated by the lack of cell counts between these days. For the AMBR, initial viabilities were above 94% (Fig. 3.1 H). Most cell lines

maintained a culture viability above 90% until day 8, except for cell lines 2, 7, 13 and 17, for which culture viabilities ranged from 80 to 89% on day 8. Culture viability started to decline in all cell lines after day 8, and most cell lines had a final culture viability between 70 and 88%, higher than the BSF final culture viabilities.

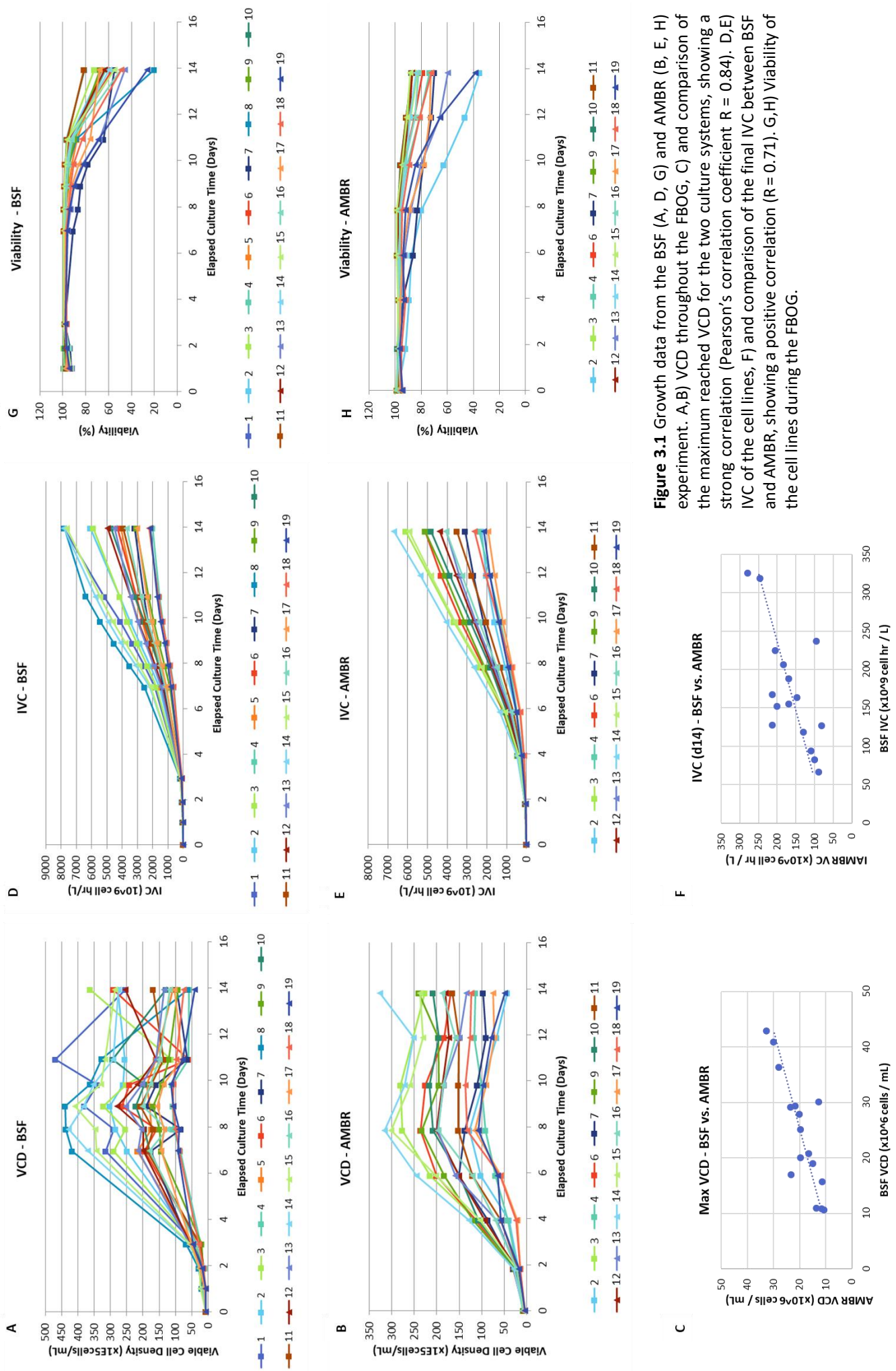

Figure 3.1 Growth data from the BSF (A, D, G) and AMBR (B, E, H) experiment. A,B) VCD throughout the FBOG, C) and comparison of the maximum reached VCD for the two culture systems, showing a strong correlation (Pearson's correlation coefficient R = 0.84). D,E) IVC of the cell lines, F) and comparison of the final IVC between BSF and AMBR, showing a positive correlation (R = 0.71). G,H) Viability of the cell lines during the FBOG.

Productivity

Product titre samples were taken on days 7, 9, 11 and 14 for the BSF, and on days 8, 10, 12 and 14 for the AMBR. In BSF, the highest titres reached were 7418 and 5201 mg/L by cell line 7 and 12, respectively (Fig. 3.2 A; App. B Table 1). Most titres ranged from 2000 to 4000 mg/L. Cell lines with the lowest productivity included 1, 3, 5 and 19, which had final titres lower than 1500 mg/L.

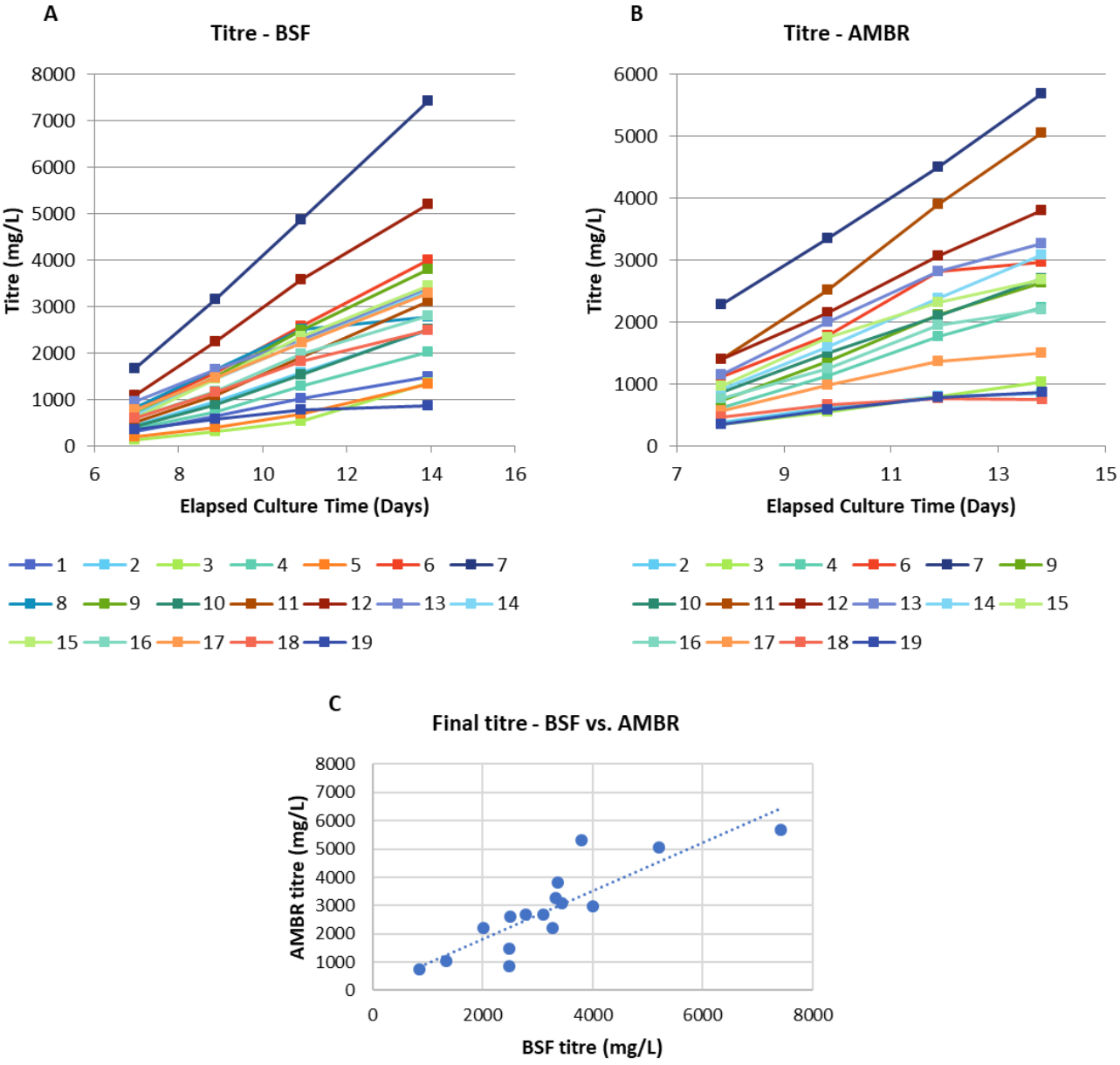

Figure 3.2 Titre data from the BSF and AMBR experiment: FBOG cell lines titre in A) BSF and B) AMBR. C) Comparison of the final titre between BSF and AMBR, showing a strong correlation between the two systems, Pearson's correlation coefficient R = 0.82.

Similarly, in the AMBR system, cell line 7 had the highest titre, 5678 mg/L, although lower than in the BSF (Fig. 3.2 B). The trend of the harvest titre for the different cell lines is consistent between AMBR and BSF, with the BSF titres generally higher than the AMBR titres (R= 0.86; Fig. 3.2 C). Cell line 7, which had the highest titre, also had the highest qP both in the BSF and AMBR (Fig. 3.3 A; App. B Table 1). Overall qPs were similar and consistent between the two systems (R = 0.91; Fig. 3.3 A, B).

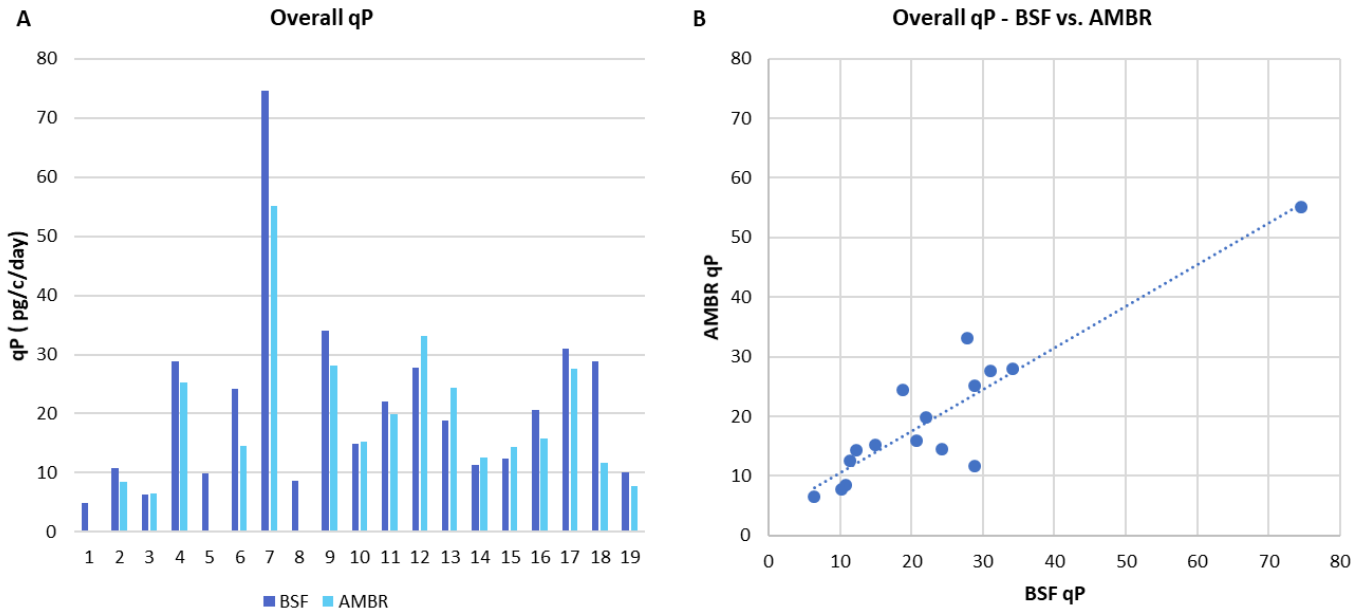

Figure 3.3 Specific productivity data from the BSF and AMBR experiment, A) Overall qP in the 19 cell lines for BSF and AMBR. Cell line number is on the x-axis. B) Comparison of the overall qP between the two systems, showing a strong correlation, with Pearson's correlation coefficient R = 0.91.

Metabolites

Glucose and lactate levels were monitored during the FBOG (Fig. 3.4). Glucose concentration reflects the energy available, whereas lactate informs on the accumulation of metabolic by-products that could deteriorate culture environment, inhibiting cell growth and mAb production [243]. As the culture switches from growth phase to production phase, lactate secretion decreases and there is usually a metabolic shift to lactic acid consumption, increasing pH [244].

Metabolites were more closely monitored in the AMBR; however, reduced sampling for BSF did not have a negative impact on growth or productivity for cells in BSF. Differences in glucose consumption can be observed between the different cell lines (Fig 3.4 A, B), consistent with the differences in growth and productivity. Despite less frequent monitoring of glucose levels in the BSF, it did not negatively impact productivity or growth, as both showed a strong positive correlation with profiles

observed in the AMBR. Lactate measurements ended on day 10 of the FBOG for the BSF (Fig. 3.4 C), and lactate levels decrease from most cell lines from day 3 onwards. Measurements of lactate in the AMBR (Fig. 3.4 D) during the late stage of the FBOG revealed lactate spike in a few cell lines (cell lines 16, 18 and 19). Lactate is usually produced by the cell during the exponential phase, while when the cells enter the stationary phase, cells shift towards lactate consumption [245]. This metabolic shift however does not always happen, and some cell lines continue to produce lactate even in the later culture stages, and the cues that trigger the metabolic shifts remain unknown [245]. Many culture parameters are thought to be involved in the metabolic shift, such as pH, pyruvate availability and mitochondrial function [246, 247].

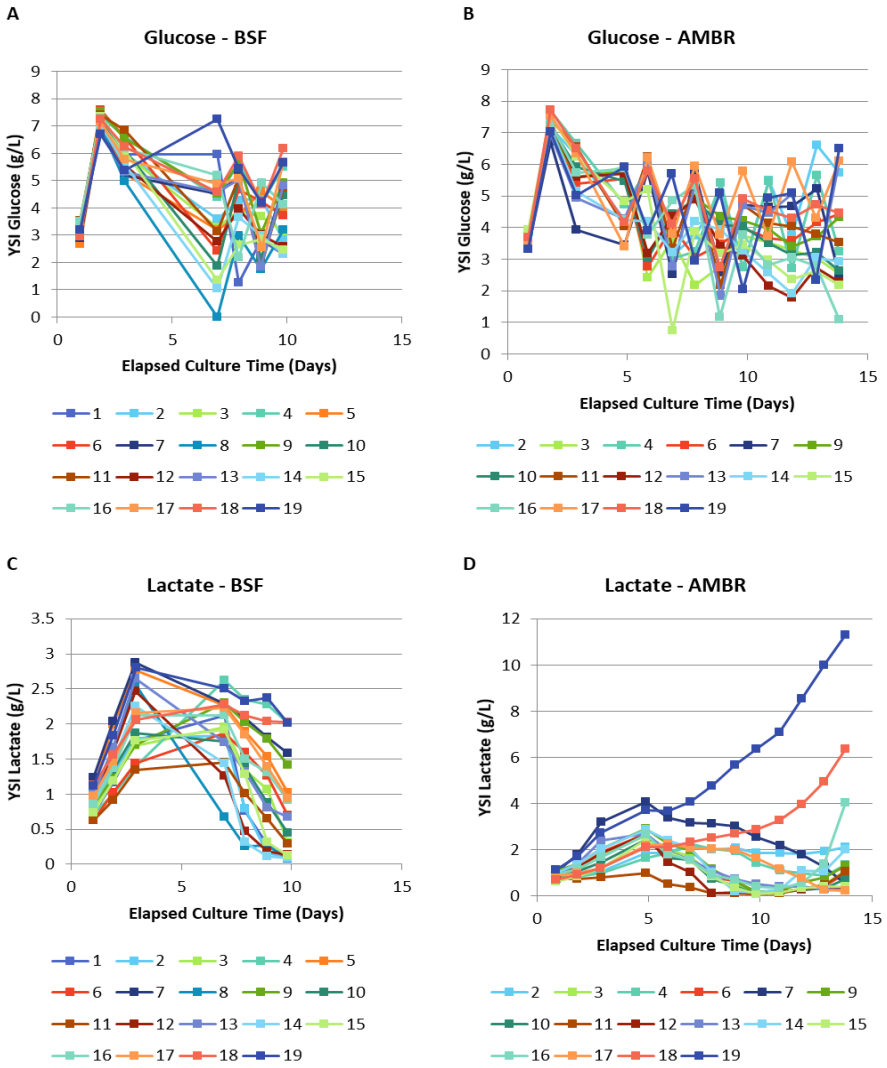

Figure 3.4 Metabolites profiles for the BSF and AMBR experiment: glucose concentrations throughout the FBOG for A) BSF and B) AMBR cultures. Lactate concentrations for the C) BSF and D) AMBR. Last measurement is on day 10 for the BSF, and day 14 for the AMBR. Glucose and lactate concentrations were measured using a YSI bioanalyzer.

Conclusion

When considering both the growth and productivity of the cell lines, the trends observed between cell lines are consistent between the BSF and AMBR. The differences in the controlled environment of the AMBR compared to the BSF does have some impact on growth and productivity. Generally, titres were higher in the BSF than in the AMBR, which for some cell lines could be caused by the increased growth. The overall ranking performance of the cell lines were consistent between the two systems, indicating that for experiments, observations made in BSF are likely to be predictive of how the cell lines would behave in the more controlled, microbioreactor environment.

3.2.1.2 Intracellular HC and LC protein expression

Cell pellets were taken on day 4, 7 and 9 of the BSF FBOG for intracellular (IC) protein quantification by western blotting. Both reduced and non-reduced conditions were analysed (Fig 3.5 A. B). Quantification of both HC and LC was performed using the reduced western blot, by measuring the HC and LC bands intensity using ImageJ, and normalising to the house keeping protein GAPDH.

Western blot analysis revealed that cell lines 3 and 5 expressed an aberrant HC protein as can be seen on both the reduced and non-reduced image, with the HC band on the reduced blot presenting itself at a lower molecular weight. Other cell lines showed a varied range of expression levels for both IC HC and LC protein.

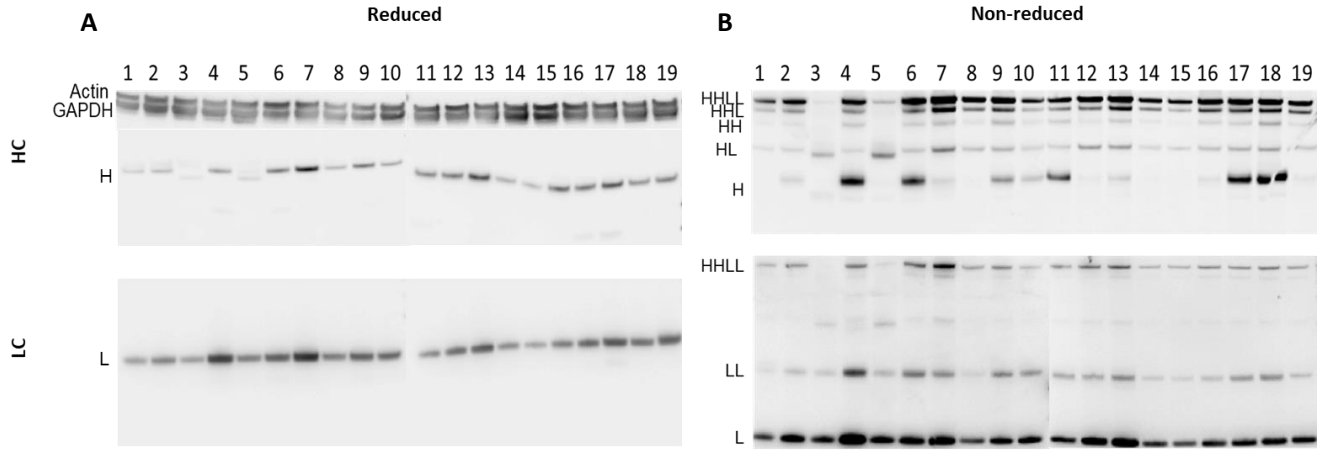

Figure 3.5 IC HC and LC protein quantification by western blotting on day 4 of the FBOG, for A) reduced (left) and B) non-reduced (right) conditions. Cell line numbers are indicated at the top of each blot. Housekeeping genes Actin and GAPDH quantification can be found at the top of the reduced gel. H refers to heavy chain and L to light chain, so HHLL is the intact mAb, HL is a half mAb, HH is the HC dimer, LL is the LC dimer.

Correlations between IC protein subunit expression and IgG titre were then investigated (using the Pearson's correlation coefficient R). Day 4 IC HC protein had a strong positive correlation with final titre (R=0.70; Fig. 3.6A) whereas LC had a weaker correlation (R=0.51; Fig. 3.6B), and later timepoints showed weaker correlations than day 4 (on day 7, R = 0.50 for HC, R = 0.27 for LC; on day 9, R= 0.49 for HC, R = 0.41 for LC). Correlations with qP were strong for both IC HC and LC on day 4 (Fig. 3.6C, D; R= 0.78 for HC, and 0.77 for LC), and decreased with culture time (on day 9, R= 0.41 for HC, and 0.21 for LC). Considering these results, early culture (day 4) IC HC protein would seem to be a predictor of overall productivity and final titre.

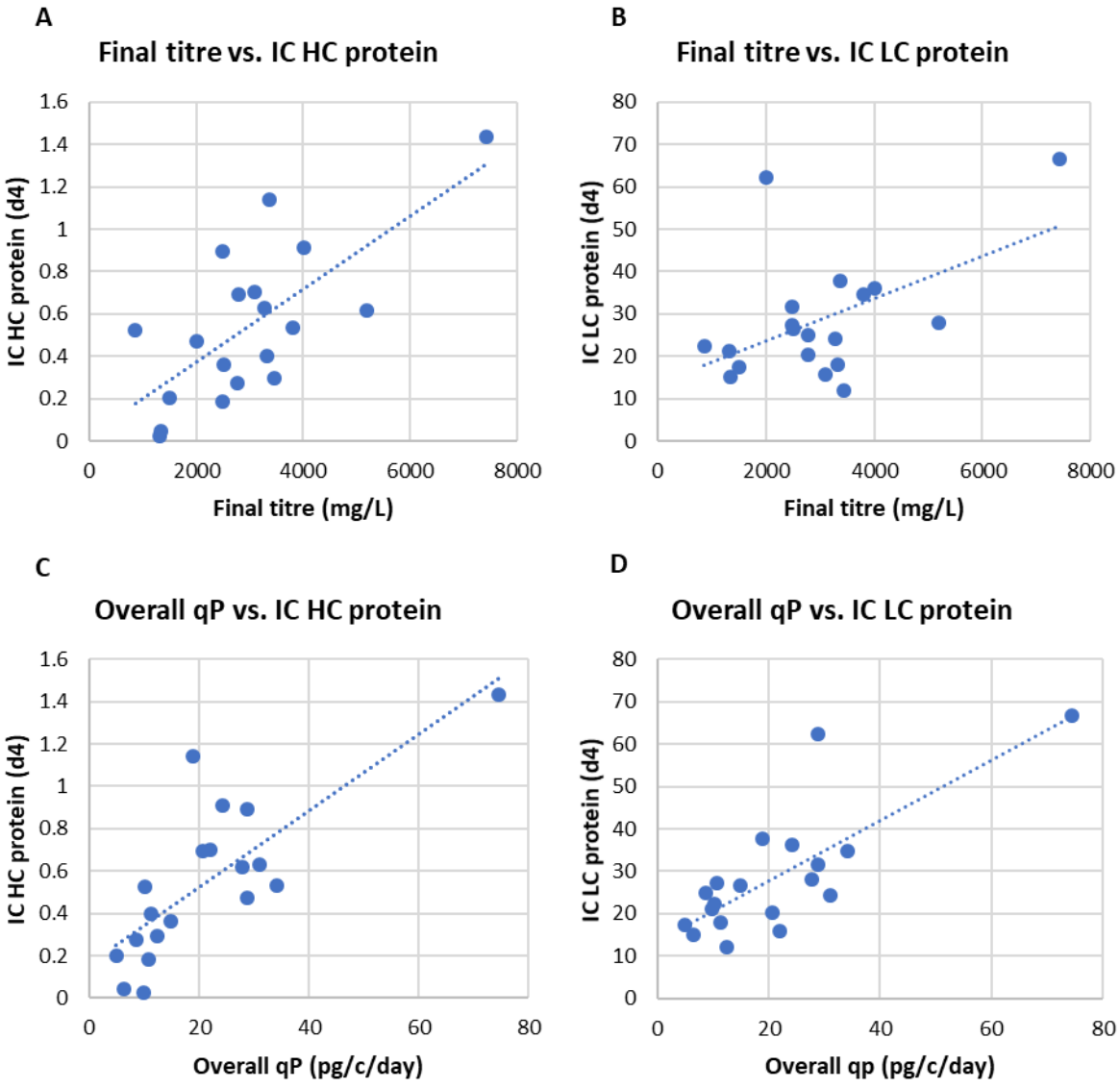

Figure 3.6 Comparison of productivity with IC HC and LC protein, A) Comparison of final titre with IC HC protein on day 4, showing a positive correlation (Pearson's correlation coefficient R = 0.70), whereas a weak correlation was observed with the B) IC LC protein content (R= 0.51). Comparison of overall qP with A) IC HC protein on day 4 (R=0.78) and D) IC LC protein (R=0.77). HC and LC protein were quantified by band intensity on their respective reduced western and normalised to GAPDH protein expression.

3.2.1.3 HC and LC mRNA expression

Cell pellets were also collected on day 4 and 9 of the culture for quantification of relative HC and LC message expression (mRNA) using qPCR, normalised to GAPDH. A wide range of expression of HC and LC mRNA was observed across the cell lines (Fig 3.7 A). Consistent with observations made at the protein level, day 4 HC mRNA levels showed a positive correlation with final titre, with a Pearson's correlation coefficient of R=0.75 (Fig 3.7 B, R = 0.58 for day 9). On the other hand, LC message showed no correlation with final titre (Fig 3.7 D, R = 0.25 for day 4, and R = 0.41 for day 9). A strong correlation was also observed between HC message and qP on day 4 (Fig 3.7 C, R = 0.82 on day 4, and R = 0.51 for day 9), and a weak correlation was observed with the LC (Fig 3.7 E, R = 0.43 on day 4, and R = 0.47 on day 9).

Drawing from the results observed both with the HC protein and message, it can be concluded that both could be used as a marker of productivity. It was crucial to confirm that these results could be replicated with the HC and LC protein and mRNA assays compatible with IS. If these results were reproducible, HC could be used to predict productivity at the single cell level and further, could be multiplexed with other assays.

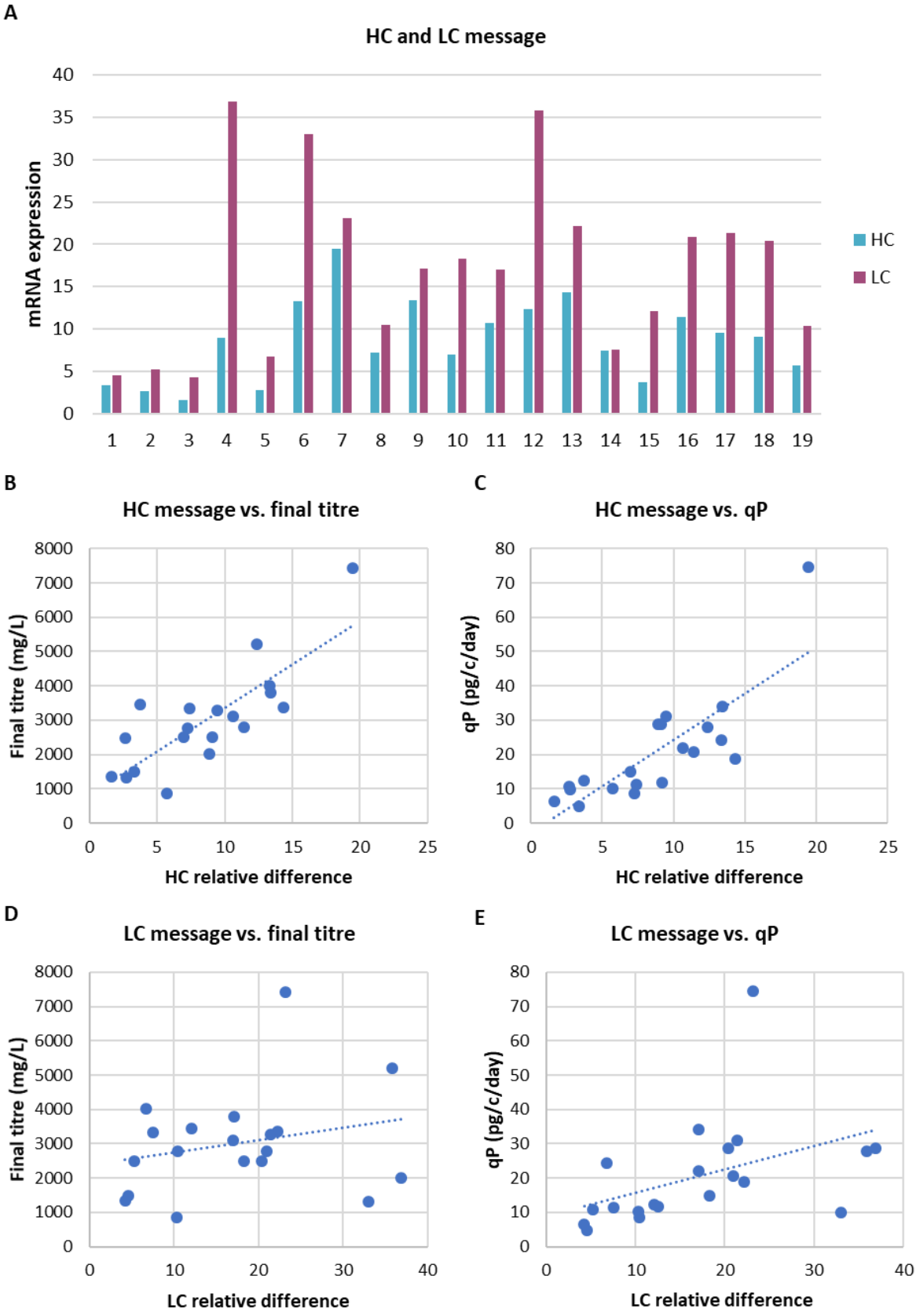

Figure 3.7 Quantification and comparison of HC and LC mRNA with productivity, A) HC and LC mRNA relative expression, normalised to GAPDH. B) HC mRNA content has a positive correlation with final titre (Pearson's correlation coefficient R = 0.75) and C) with overall qP (R=0.82) whereas D) LC mRNA does not show a correlation with the final titre (R = 0.25) nor with the E) overall qP (R=0.43).

3.2.2 ImageStream assay development and validation

The first step of the IS characterisation was to develop IFC assays to investigate the content of IC HC and LC polypeptide, HC and LC mRNA, and for specific organelle assessment. The aim of the assay development was to multiplex a productivity marker or predictor, such as IC HC, which is usually only quantifiable in fixed cells, with an organelle dye that can be used in both fixed and live cells. If a correlation at the single cell level, or population level, between IC HC and an organelle was observed, the organelle dye could then be used to stain and select for live cells by flow cytometry, thus increasing the proportion of high producing cell lines. The organelles chosen were the ER, the mitochondria, the Golgi apparatus, the lysosome and the nucleus (Fig. 3.8 A). These organelles are the main organelles and have commercially available dyes. Moreover, these organelles are essential for processes linked to increased productivity. ER and Golgi are involved in protein synthesis and quality, mitochondria are at the heart of metabolism, the nucleus can inform on the subcellular locations of the different staining (in the nucleus or in the cytoplasm), and lysosomes are directly involved in autophagy. For each organelle, a range of dye concentrations was tested for both live and fixed cells, to identify the optimal staining conditions, with high stain intensity and low background.

3.2.2.1 ImageStream data analysis

The analysis software, Ideas (Amnis, Merck), has built-in functions that enable spot counting (Fig. 3.8 B), for counting spots in punctuated staining such as the Golgi apparatus. Another feature is masking, to determine cell size by creating a mask on the brightfield, or the size of an organelle (Fig. 3.8 C). Masks can be created based on a threshold of fluorescence intensity. Finally, a colocalization score can also be calculated to determine whether two signals are colocalized, with a score of 0 indicating no colocalization and scores above 2 indicating colocalization (Fig. 3.8 D).

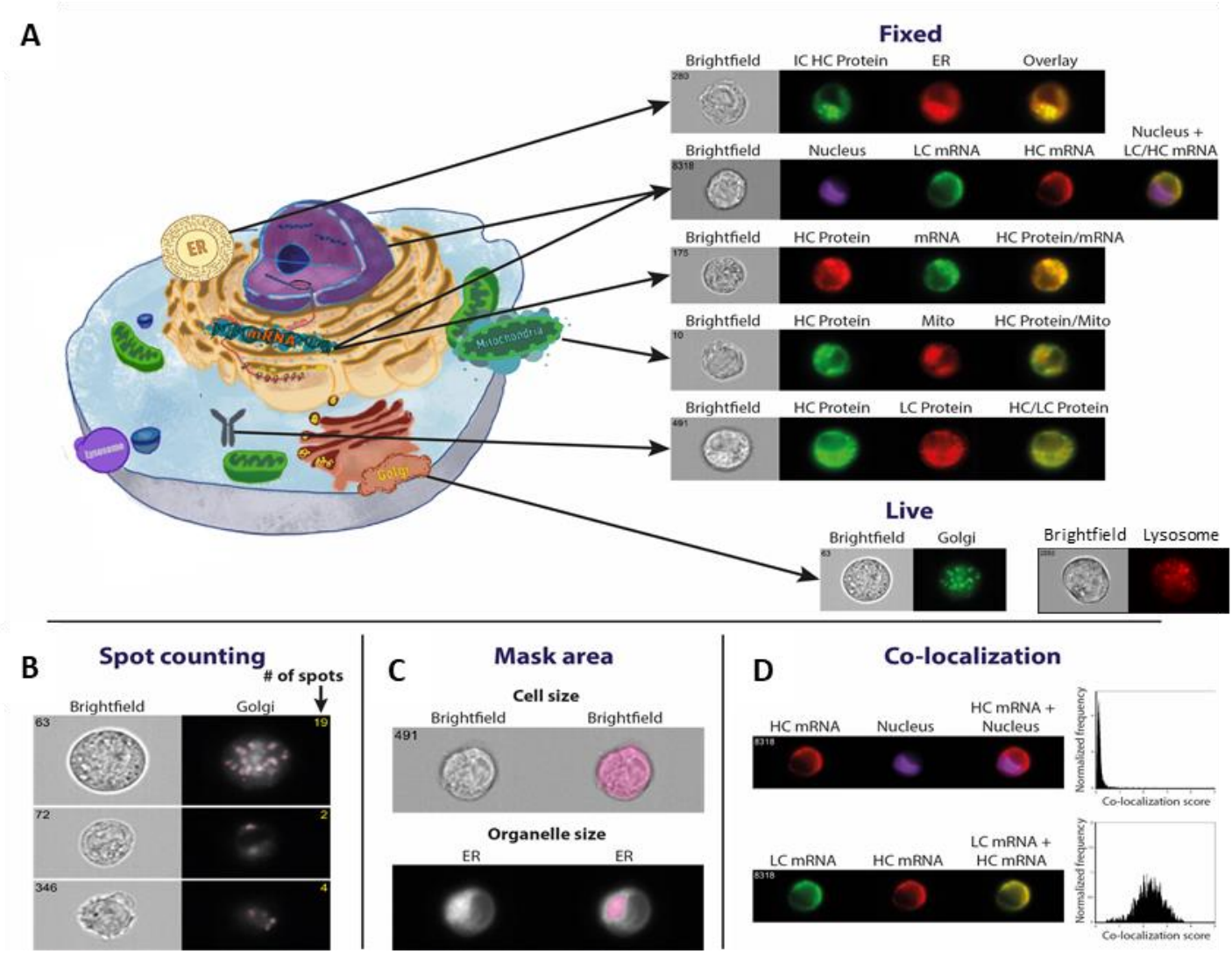

Figure 3.8 Sample images of the assays developed on the IS and analytical features. A) Images show bright field, fluorescent staining, and an overlay of the staining. B) Sample images featuring spot counting of the Golgi apparatus, with bright field and fluorescent channel images with the number of spots on the right corner of the image. C) Masking of the cell size based on the bright field image, and of the organelle size based on the threshold of the ER intensity. D) Colocalization of HC mRNA and nucleus, which shows no colocalization, and HC and LC mRNA, which show strong colocalization.

3.2.2.2 ImageStream validation against standard flow cytometry

Standard flow cytometry is widely accepted as a robust method for investigating cellular attributes, however IFC is a relatively new technology and has not been as extensively used. We therefore assessed the reproducibility and consistency of results between standard flow cytometry and IFC. To do this, three separate vials of a recombinant CHO cell line were thawed and independently cultured in shake flasks. After the first passage, triplicate samples were taken from each flask on three separate

days and stained with MitoTracker and DAPI, with the plate loaded in reverse order on the last day to avoid order bias (Fig. 3.9, Fig 3.10 A).

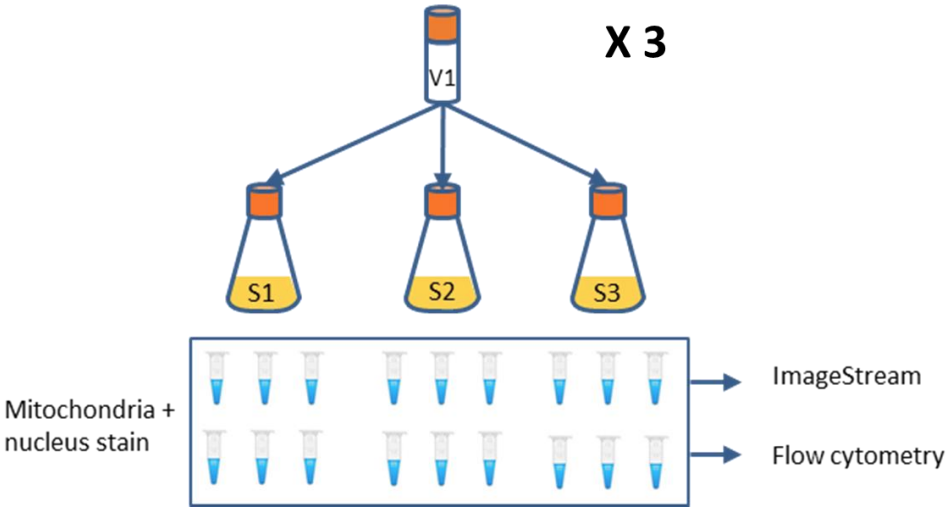

Figure 3.9 Schematic of the robustness experiment. This represents what was done for one vial, but three individual vials were thawed. From each thawed vial, three separate shake flasks were inoculated. Triplicate samples were taken for staining with a mitochondria dye (MitoTracker) and a nucleus dye (DAPI) and analysis on ImageStream and standard flow cytometer.

The percentage of double positive cells across instruments and days, ranged from 94.8% to 100% (Fig. 3.10 B, C). One-way ANOVA followed by Tukey test revealed that some of the differences between means were statistically significant, meaning any variations in percentage of double positive population below 6% can be accounted for by variation between instruments or days.

The intensity of the nuclear staining was consistent between instruments and between shake flasks originating from the same vial, showing no statistical difference (Fig. 3.10 D, E). For the mitochondrial staining, differences in intensity were present between shake flasks originating from the same vial and between vials, despite no differences in growth or viability. These differences which could be due to intrinsic differences between cultures (Fig. 3.10 F, G), and were consistent between IS and standard flow cytometry, with a strong correlation between the signal intensity recorded by the different instruments for both dyes (Fig.3.10 H, I; R^2= 0.42 DAPI and 0.97 MitoTracker). There was thus confidence that any observations made on the imaging flow cytometer could be transferred to standard flow cytometry.

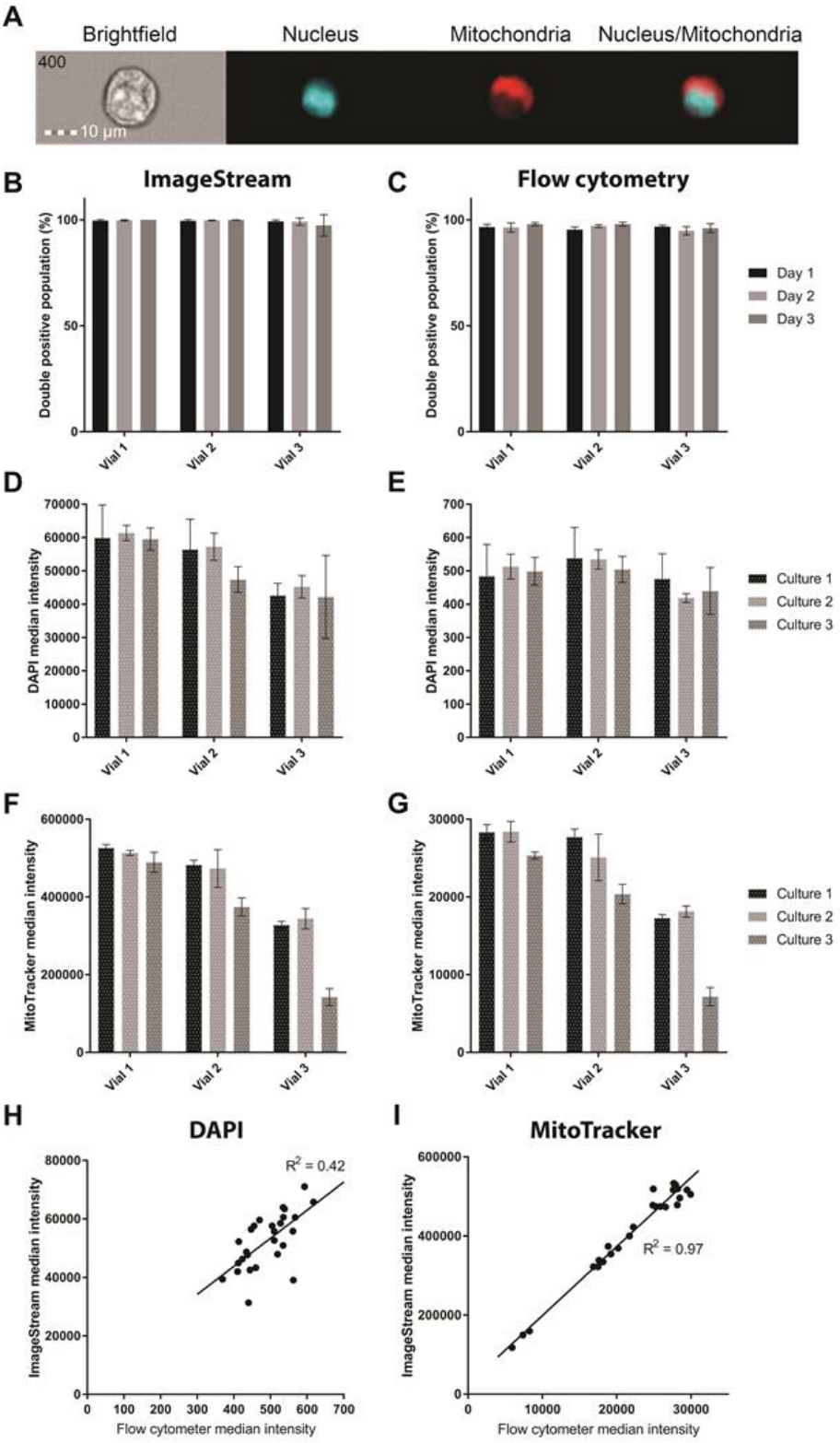

Figure 3.10 Results from the robustness experiment, comparing ImageStream and standard flow cytometry, A) Sample IS images showing the bright field, nuclear staining (DAPI), mitochondria staining (MitoTracker), and composite images. B, C) Average percentage of cells positive for both nuclear and mitochondrial staining for each vial on different days on IS B) and flow cytometry C). D-G) Average of DAPI median intensity D, E) and MitoTracker median intensity F, G) of individual shake flasks on day 3, representative of observations on other days for IS D, F) and flow cytometry E, G). H, I) Overall, there was a strong correlation between the signals measured by both instruments (Pearson's correlation coefficient R = 0.65 for nuclear stain and R = 0.98 for mitochondrial stain), R^2 is the coefficient of determination.

3.2.2.3 ImageStream validation against standard techniques

Having validated that IFC was as robust as standard flow cytometry, it was essential to verify that the correlations observed between HC content, both protein and message, and productivity were replicable with the IFC assays. Another FBOG in BSF of initial panel of 19 cells expressing the same mAb was initiated. Samples for IFC analysis were taken on day 3, 7 and 10 of the FBOG in BSF. Confirming the data obtained by western and qRT-PCR, HC protein intensity and message on day 3 correlated very strongly with both titre and qP (Fig. 3.11 A, B, Table 3.1). LC protein and message also showed a positive correlation with productivity early in the culture, although weaker than the correlation observed with the HC (Table 3.1).

Next, we investigated multiplexing HC mRNA and HC protein at the single cell level. A positive correlation between HC message and protein at the single cell level was observed (Fig 3.11C, R=0.65). Moreover, images obtained via imaging flow cytometry revealed different localisation of the HC protein and HC mRNA (Fig. 3.11D). Since both HC mRNA and protein early in the culture showed positive correlation with final titre, and between each other, HC protein was chosen as the predictor of productivity at the single cell level for this study. HC protein was then multiplexed with the different organelle assays, being more time and cost efficient than the mRNA assay.

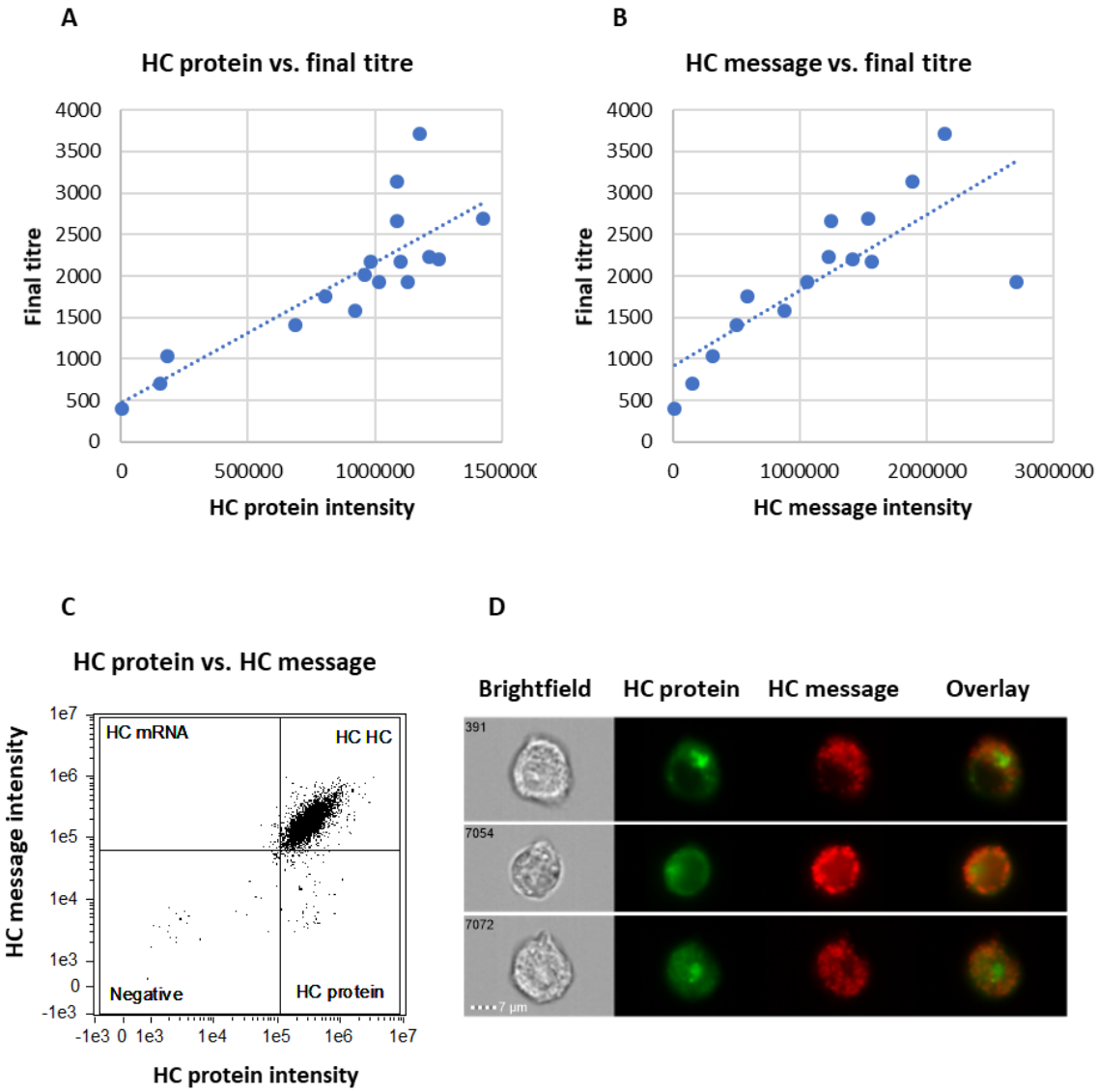

Figure 3.11 HC protein and message quantification by ImageStream, and comparison with final titre Both A) HC protein and B) HC message showed a strong positive correlation with final titre. C) HC protein and message show a positive correlation at the single cell level. D) Sample images of HC protein and message staining by IS.

Table 3.1 Pearson's correlation coefficient between median fluorescence intensity of HC/LC protein and message, and productivity.

	Final titre	Overall qP
D3		
HC protein	0.84	0.60
HC message	0.79	0.92
LC protein	0.61	0.44
LC message	0.73	0.78
D7		
HC protein	0.13	-0.10
HC message	0.32	0.55
LC protein	-0.02	-0.12
LC message	0.12	0.34

3.2.3 Investigation of correlations between organelle content and cell culture attributes

Having developed appropriate IFC assays, a FBOG with the 19 cell lines was repeated in baffled shake flasks, for 14 days. Samples for IS analysis were taken on day 3, 6 and 10 of culture. The following assays were performed in triplicate: ER-HC protein, mitochondria-HC protein, HC-LC protein, and Golgi apparatus (day 6 and 10 only). The Golgi dye was not multiplexed with HC protein, as permeabilization of the cell membrane caused diffusion of the dye into non-specific cellular locations. HC-LC mRNA assay was not done in triplicate, due to the lengthiness of the protocol and the cost of the reagents. Lysosome staining required live cells, and hence was not multiplexed with HC protein, and single samples were taken. Cell lines 18 and 19 had to be discarded after day 6 due to a feeding error.

Correlations from this experiment were then investigated between HC and cell attributes at the single cell level; and at the population level between median intensity of organelle and culture parameters, such as growth, titre and specific productivity (qP). Trends in the cell culture data obtained from this fed-batch was consistent with the data from the previous FBOG (App. B Fig. 1), with high correlation coefficients between final titres and qP ($R = 0.86$ and $R = 0.79$, respectively), with titres and qP lower in this experiment compared to the initial FBOG. Samples acquired required large volumes of cultures (7.5 mL on day 3, equivalent to 10% of the overall culture volume, and 4.8 mL on day 6), which could have negatively impacted final titre.

3.2.3.1 HC protein content comparisons between staining

The effect of multiplexing organelles dyes on HC staining was investigated by comparing HC intensity across the different multiplexed assays (LC protein, mitochondria and ER). Strong correlations were observed between HC intensities from different multiplexing (R ranging from R = 0.83 to R = 0.98 on day 3, R ranging from R = 0.91 to R = 0.95 on day 6, and R ranging from R = 0.87 to R = 0.92 on day 10). Multiplexing HC antibody with the dyes did not impact the integrity of the HC staining.

3.2.3.2 HC and LC protein and message profiles

IFC analysis of HC and LC protein and message revealed not only cell lines with a wide range of expression, but also some cell lines with multiple distinctive populations: a sub-population that expressed HC and LC, a sub-population that only expressed one of the chains, and a sub-population that expressed neither (Fig. 3.12 A). Cell lines with a mixed population include cell line 1 (~14% HC/LC positive, ~85% non-expressing), cell line 3 (~ 50% HC/LC positive, ~35% negative and ~ 15% HC only), cell line 4 (~75% HC/LC positive, ~25% non-expressing), cell line 5 (~50% HC/LC positive and ~35% negative) and cell line 18 (~65% HC/LC positive and ~ 25% negative). These mixed populations were also present at the message level, except for parent 1, for which the population that was negative for HC/LC protein was positive for LC mRNA. The other parents all had a single HC/LC population.

One possible reason for these cell lines to have a mixed population could be due to the cell line not being monoclonal, as these cell lines underwent only one round of cloning. Another possibility is loss of transgene copies or transcriptional silencing of promoter [248]. Interestingly, on day 10, the intensity of HC and LC protein was significantly lower than on day 3 and 6 across most cell lines, except 1, 3, 5 and 17 (Fig. 3.12 B, C). Staining fluorescence intensity are normalised to cell size: as cells get bigger with culture time, the ratio of signal intensity to cell size would decrease and could explain some of the lower HC and LC intensity. Another possibility to explain this decrease in HC and LC protein later in the process could be caused by an increase in mAb secretion, as the cells have exited the growth phase and can concentrate cellular resources on mAb production.

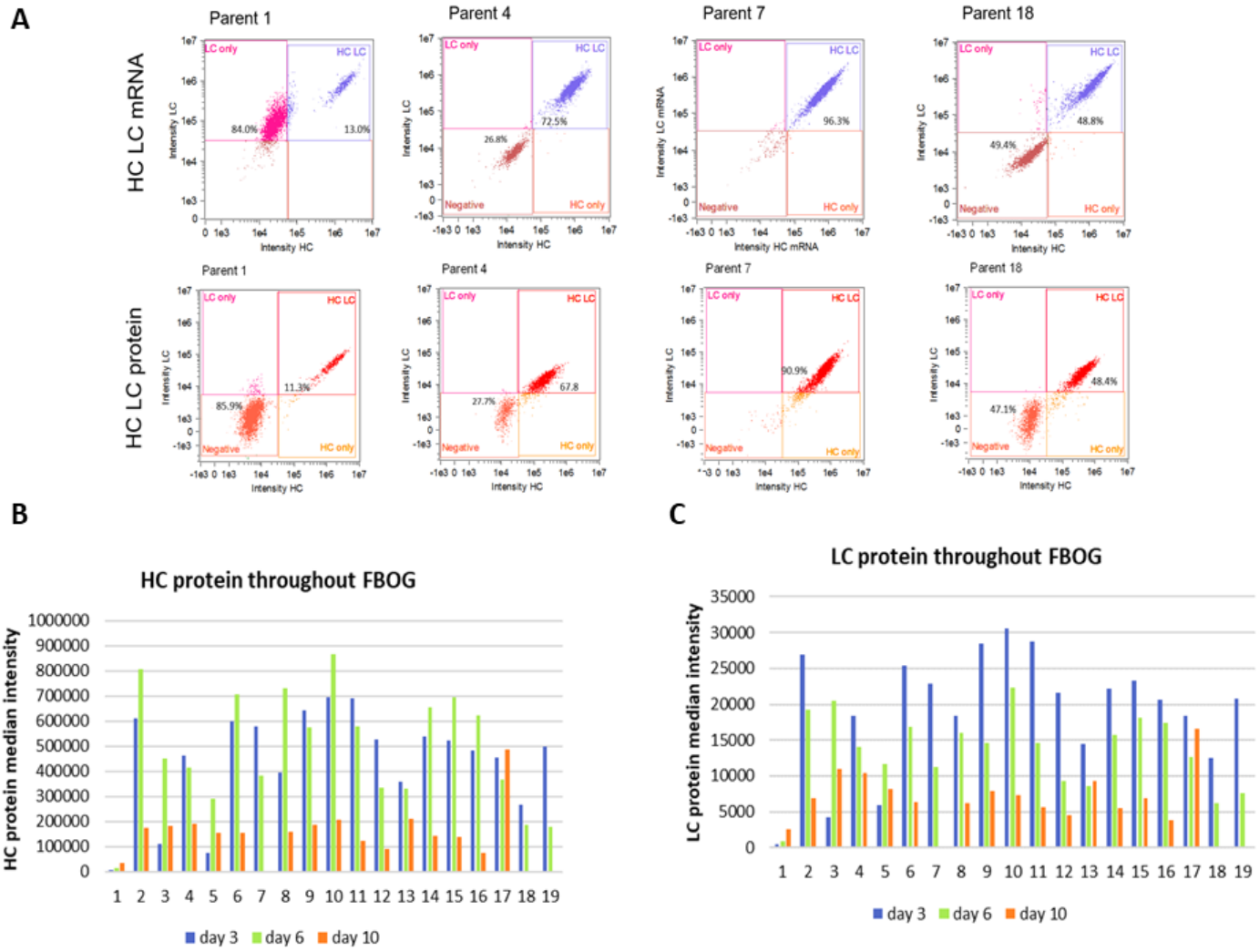

Figure 3.12 Comparisons of a sample of cell lines with heterogenous and homogenous HC and LC protein/mRNA expression, and HC and LC protein content throughout the FBOG, A) HC/LC mRNA and protein profiles of cell lines 1, 4, 7 and 18, showing heterogenous and homogenous populations. B) HC and C) LC protein content on days 3, 6 and 10 of the FBOG.

3.2.3.3 Analysis of correlation at the single cell and population level

As previously seen, the cell lines studied here had a wide range of mAb protein expression. The differences in productivity between cell lines can be explained not only by a diverse range of mRNA levels, but also by differences in the cellular properties that govern the growth and biosynthetic capacities of individual clones. Energy metabolism [249] and protein synthesis [61], folding [71], and secretion [250] pathways can influence the final production and secretion of mAb. We therefore investigated with IS whether productivity differences observed between cell lines were correlated with variations in the mitochondria, ER, lysosome and Golgi content of cells, as well as HC and LC polypeptide and mRNA (Fig. 3.13). For ER and HC, the colocalization score was also analysed, corresponding to the relative amount of HC residing in the ER. Correlations were investigated at the

population (population median intensity vs final titre for all cell lines) and the single-cell (intensity organelle vs intensity HC) level.

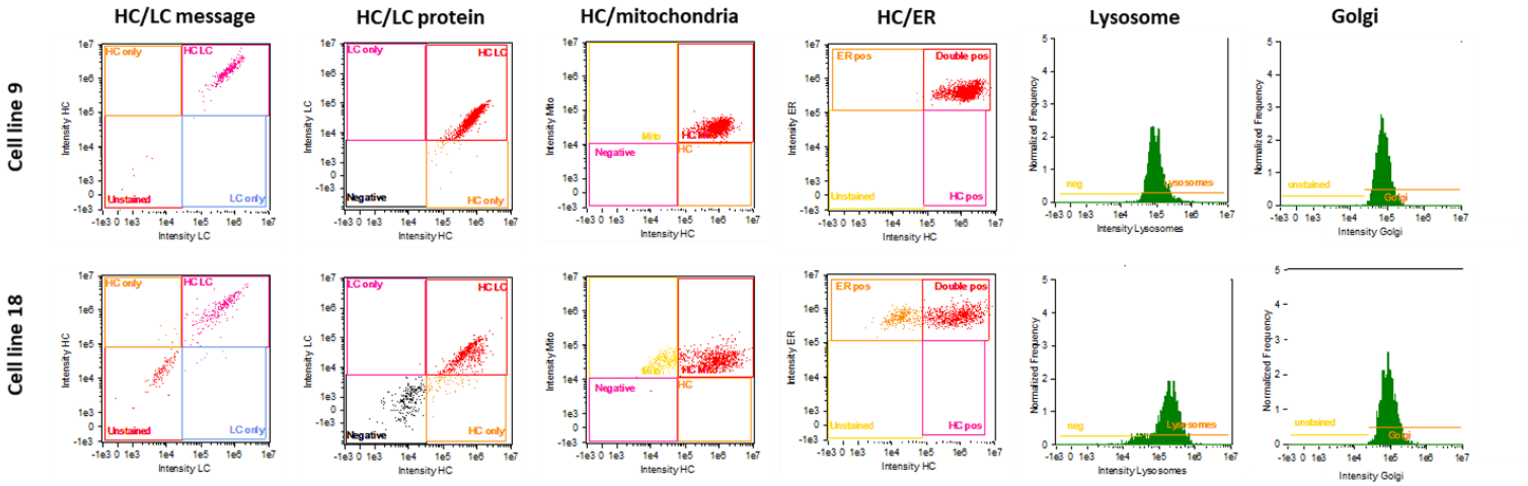

Figure 3.13 Sample profiles of ImageStream analysis: of cell line 9 (top) and 18 (bottom) for the various IS assays used, from left to right: HC and LC message, IC HC and LC protein, HC protein and mitochondria, HC protein and ER, lysosome content and Golgi content.

No linear correlations were found for individual cell lines between the mitochondrial content and HC protein at the single-cell level on any sampled days (App. B Table 2). Moreover, no relationships were found at the population level between mitochondrial content and productivity, or specific productivity on any of the days investigated. Additionally, no correlations were observed between the HC content and the ER content at the single-cell level or at the population level between the ER or Golgi content and titer or specific productivity (App. B Table 2, Table 3.2).

The colocalization score between ER and HC showed a strong negative correlation with productivity on day 3 (Table 3.2). This indicates that as more HC protein accumulates in the ER, cell line productivity was decreased. There was however no correlation at the single cell level between the colocalization score and ER or HC protein amount, indicating that the amount of IC HC protein or ER do not predict the ER folding capacity.

Table 3.15 Pearson's correlation coefficient between the organelle content on different days and the cell culture growth and productivity values. *This value corresponds to the Pearson's correlation coefficient when cell line 7 is excluded as an outlier, due to high titre.

	Mitochondrial content			ER content			Golgi content		Lysosome content			ER / HC colocalisation score		
	d3	d6	d10	d3	d6	d10	d6	d10	d3	d6	d10	d3	d6	d10
Final Titre	-0.22	0.23	-0.03	0.16	0.12	-0.48	-0.11	-0.49	0.24	0.08	-0.11	-0.64	-0.48	0.34
qP	-0.04	0.25	0.09	0.36	0.4	-0.4	0.26	-0.27	0.54 (0.84*)	0.46	0.05	-0.75	-0.43	0.22
Final IVC	-0.32	-0.69	-0.07	-0.64	-0.43	0.36	-0.48	0.18	-0.56	-0.55	0.02	0.65	0.47	0.05

Lysosome content increased with culture time (Fig. 3.14 A). No correlations were found between titre and lysosome content on day 3 (R = 0.23), however there was a positive correlation with overall qP (Fig. 3.14 B, R = 0.84, excluding cell line 7 as an outlier due to high titre; and R = 0.56 when including cell line 7). No other correlations were found on other days of the FBOG.

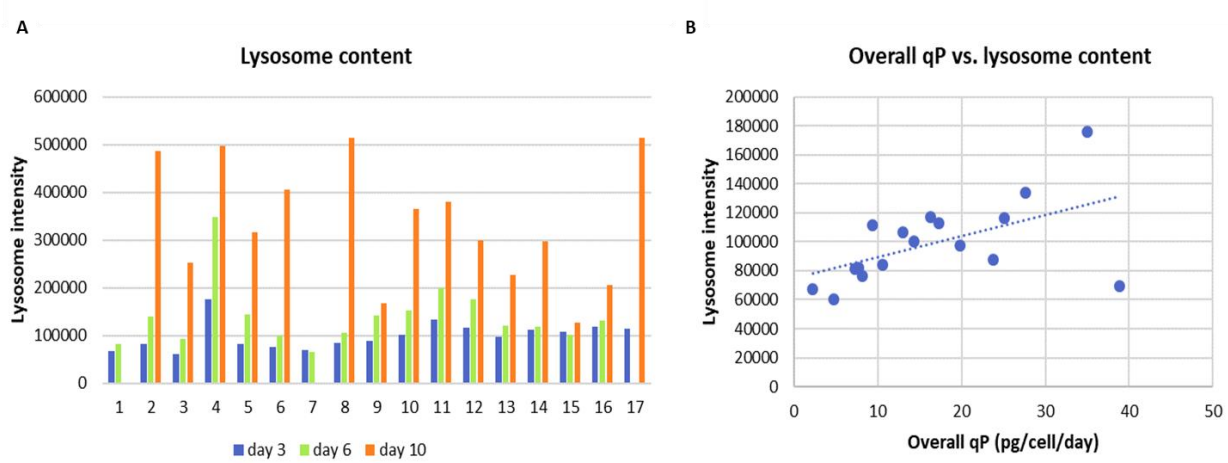

Figure 16.14 Lysosome content throughout the FBOG and comparison to overall qP; A) Lysosome content of cell lines throughout a 14 days FBOG on day 3, 6 and 10. B) Overall qP vs. lysosomal content on day 3, Pearson's correlation coefficient R = 0.85.

Finally, principal component analysis (PCA) was performed to confirm the correlations that were observed on day 3. The median intensity of the organelles and HC/LC protein and mRNA were included in the PCA analysis, as well as cell size, HC/LC ratio for IC protein and mRNA, and the colocalization score between ER and HC. Biplot on day 3, comprising of all the organelles and HC and LC protein and mRNA medians, is separated into two components (Fig. 3.15A). Cell line positions obtained from the biplot were then tagged based on their IVC (Fig. 3.15B), qP (Fig. 3.15C) and final titre (Fig. 3.15D). This allows the visualisation of the impact of the different organelles and HC/LC protein and mRNA on the different culture parameters.

Along the first component, HC and LC protein and mRNA, as well as lysosome content were found to relate in the positive direction, whereas the colocalization score between HC and the ER had a negative value (Fig. 3.15 A, App. B Table 3). When looking at the IVC, high and low IVC were divided across the first component, whereas the second component did not seem to relate to growth (Fig. 3.15 B). Similarly, high producing cell lines, both in terms of qP (Fig. 3.15 C) and final titre (Fig. 3.15 D), are separated from lower producing cell lines across the first component. Considering both the biplot and score plot, high amounts of HC and LC mRNA and protein, as well as lysosome content, had a positive relationship with productivity, whereas a high colocalization score between ER and HC had a negative relationship with productivity. This is consistent with the results obtained from the Pearson's correlation coefficient analysis. Along the second component, only mitochondria content points in the positive direction. However, no clear differentiation is made along the second component for either the growth or productivity.

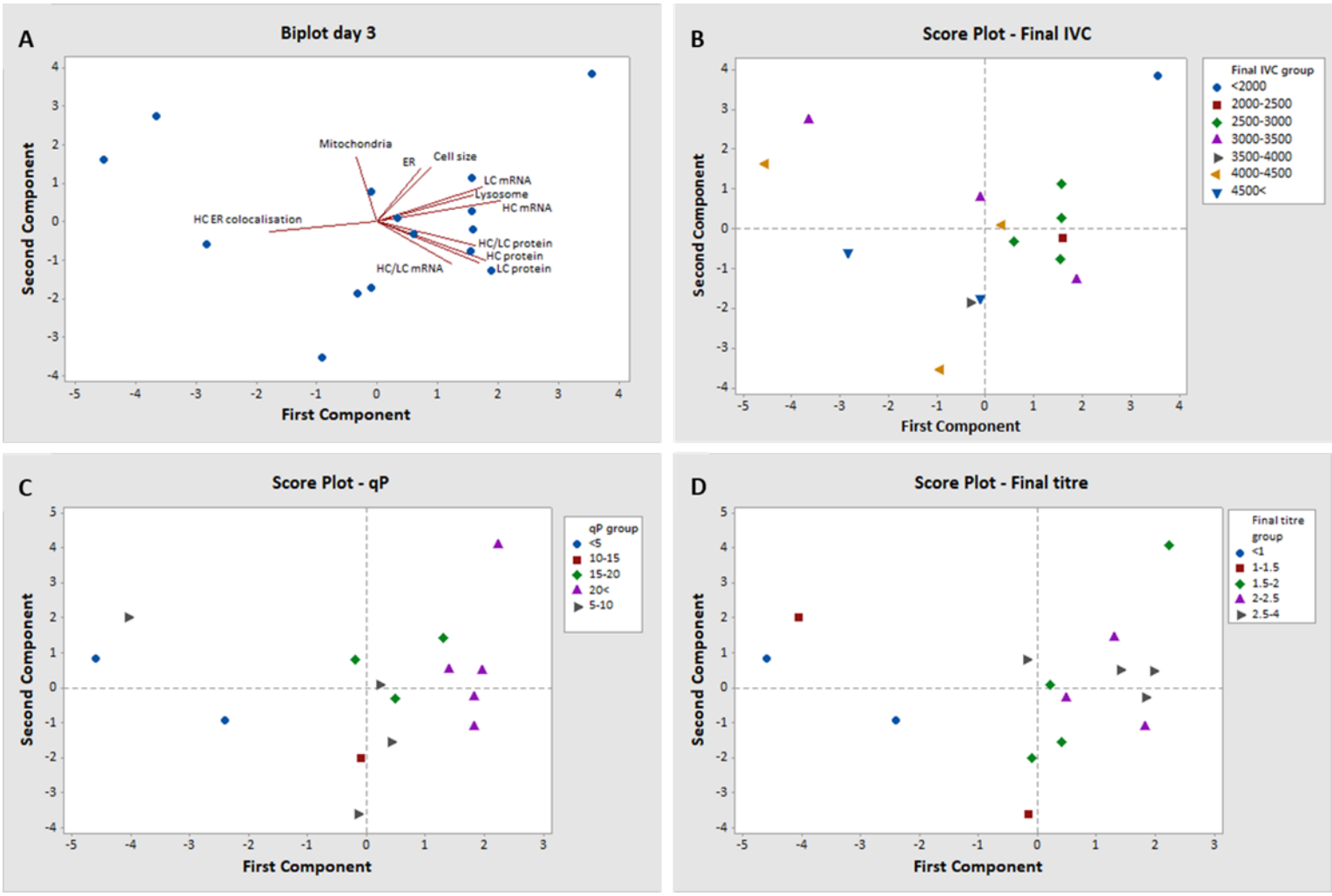

Figure 3.15 PCA analysis of the different IS staining on day 3 of the FBOG. The analysis was performed with 15 cell lines, due to some data being missing for some of the cell lines. A) Biplot showing the influence of each of the parameters. Score plots showing the different cell lines based on their B) final IVC, C) qP and D) final titre.

3.3 Discussion

To investigate the cellular differences between high and low-producing cell lines, a panel of 19 cell lines expressing a model IgG1 mAb with a range of titres, specific productivities and growth in fed-batch culture was characterised. Moreover, cell line organelle content was characterised with IFC. IFC has limitations in its application to sorting and isolation of cells in a cell line construction process. Currently, IFC does not offer a high spatial resolution compared to traditional microscopes, which also allow for time-lapse experiments and spatial-temporal analysis of the sample. A further limitation of IFC is its maximum speed of 300 events s^{-1}, which can only be reached with a high sample concentration of 10^8 cells mL^{-1}. This is quite different to the high throughput of standard flow cytometry. The slow acquisition is mostly the result of limitations in focusing of cells, as out-of-focus cells are excluded from analysis [226]. Finally, there are currently no commercially available IFCs that have the ability to sort cells based on image features, although that may change in the near future following the recent work by Nitta et al. [251] on intelligent image-activated cell sorting. Despite these limitations, IFC remains a powerful tool for single cell analysis.

Prior to performing IS analysis, it was necessary to identify a predictor of productivity that could be used at the single cell level. Cell lines revealed that IC HC and LC protein content and mRNA expression not only varied across the cell lines but also within individual cell lines at different time points of a fed-batch culture. The amounts of HC protein and mRNA on day 4, as determined by western blotting and qPCR, respectively, were both predictive of the final titre, as well as the overall qP. No correlation was found between the titer and the LC content or between the HC protein and the titer later in the culture. From these results, it was evident that the IC HC protein, and mRNA at earlier stages of the culture could be used as markers of cellular productivity.

Results obtained by standard qPCR and western blotting methods were confirmed by IFC. HC protein and mRNA contents on day 3 showed a strong correlation with the final titre, but at later time points no such correlation was found. This suggests that the IC HC protein and mRNA contents are predictive of final titre early in the fed-batch culture; however, this predictive power is lost as the culture progresses as other factors begin to play a role in determining the final titer, e.g., availability of translation machinery, folding/secretion, and energy status of cells. LC protein amounts showed weaker correlation with the final titer or qP, although the LC mRNA content showed a positive correlation with the final titre and qP. Overall, these results are consistent with previous reports that the IC HC protein and mRNA contents show a stronger correlation with mAb productivity than the LC content, as LC protein was present in excess as seen in the western blots, indicating that HC can be a limiting factor for the final titer [61, 102, 252-254].

Although the correlation with LC was lower, there was some correlation between LC transcript and the final titer; this is not unexpected as LC protein is necessary to drive HC constant domain 1 (CH1) folding, mAb assembly, and secretion [255, 256]. The reported differences as to whether HC or LC are limiting may reflect molecule- and host cell-dependent differences. We note that the cell line with the highest HC mRNA content on day 3 did not have the highest titer. This cell line also had a high amount of LC mRNA on day 6, suggesting that above a certain transcript threshold, there might be potential bottlenecks further down the translation and secretion pathways [61, 136, 257].

As cellular metabolism, protein folding, and assembly could influence overall mAb production, we characterised the organelle content of a panel of cell lines. The dyes used for the quantification of organelle content were commercially available, although the exact mechanisms by which they function were not always publicly available. The Mito-ID dye reflects the mitochondrial mass and morphology, regardless of the mitochondrial energy state. It has been shown to colocalise with EGFP-cytochrome C oxidase, validating the specificity of the dye [258]. The Golgi-ID is selective for the Golgi apparatus, and colocalises with RFP-N-acetylgalactosaminyltransferase-2, an enzyme that is abundantly found in the trans-Golgi [259]. The ER-ID dye has been shown to colocalise with EGFP-calreticulin chimeric protein, validating its selectivity for the ER. Lyso-ID is a cationic amphiphilic fluorophore tracer that rapidly partitions into live, through passive diffusion across the various lipid bilayers. Lyso-ID design is a pH clamp that allows detection of acidic vesicle: once inside the lysosome, the dye become protonated and trapped.

No correlations were found between Golgi, ER and mitochondria content and productivity. Mitochondrial content itself is not always reflective of cellular metabolism, as significant changes in the mitochondrial membrane potential (MMP) can occur without fluctuations in mitochondria numbers [260-262]. Studies have linked either high [261] or low [260] MMP with increased final titer; however, we only considered mitochondrial biomass in this study.

Regarding the ER and Golgi content, other studies report a lack of correlation between ER and Golgi content during the growth phase [50, 252], while our results show that neither the ER content nor the Golgi content correlates with productivity during the growth phase or at later stages of batch culture. We note reports that host cells with higher ER content prior to transfection result in the isolation of recombinant cells with higher titer [263]. A negative correlation was observed between the amount of HC protein residing in the ER, based on the colocalization score, and final titre, indicating mAb not being secreted. No correlations were observed at the single cell level between the colocalization score and ER size, indicating that the accumulation of HC protein in the ER may not have activated ER stress yet. ER stress and activation of the UPR is usually accompanied by an expansion of ER size to increase

folding capacity, and reports have shown that overexpression of Xbp-1 leads to expansion of the ER and Golgi, and higher titre [73, 99, 264]. As no correlation was observed later in the culture between the HC accumulation in the ER and productivity, cells may have activated the stress response to increase their folding capacity and mAb production.

Interestingly, the lysosome content was a strong a predictor of productivity as HC or LC content. Lysosomes play a key role in autophagy and the degradation of intracellular waste. Initiation of autophagy can either be the first step towards cell death or cell survival. Genetic manipulation of the autophagic pathway has shown positive effects with either inhibition or induction of autophagy. Over-expression of the autophagic protein Beclin1 and the anti-apoptotic protein Bcl-2 has shown increased benefits compared to overexpression of Bcl-2 alone in different stressed-induced situations, such as nutrient deprivation or chemical stress, inhibiting cell death and increasing VCD [171, 172]. Moreover, autophagy induction by rapamycin treatment, a specific mTOR inhibitor, has also been reported to improve culture viability accompanied with higher titres [68]. Other studies have reported that inhibition of autophagy results in positive effects on cell culture. Bcl-xL overexpression has led to higher titres, however the authors highlight that they did not quantify whether Bcl-xL overexpression worked through the apoptosis or the autophagic pathway [69]. Jardon et al. have reported that chemical inhibition of autophagy with 3-methyl adenine (3-MA) led to up to a 2.8-fold increase in titre [75]. Mechanistic analysis needs to be performed to understand the mechanisms underlying the relationship between lysosome content and productivity observed in our study.

In conclusion, with the studied cell lines, high and low producers are not only differentiated by their HC/LC message and protein content, but also by lysosome content on day 3. Having observed this correlation, it would be interesting to investigate whether lysosome content could be used to isolate high producing cell lines. Other organelle content did not differ between high and low titre cell lines. However, since the mAb that is expressed by these cell lines was easy-to-express, it is possible that cellular organelle amounts might differentiate between the productivity of cell lines making more difficult-to-express molecules. Moreover, the IFC tools described here could be applied to the characterization of host cell populations and to identify potential targets for host cell engineering. Consistent with previous reports, we show that the HC protein and mRNA are markers of productivity early in culture—this highlights a need for the development of new flow cytometric methods that allow the measurement of HC polypeptide or mRNA amounts in live cells, which could be used to enrich the proportion of high producers and improve the efficiency of cell line development.

CHAPTER 4

Lysosome content - based cell sorting of CHO cells

4.1 Introduction

Increased recombinant protein production, with appropriate quality of product, is a priority for the biotherapeutic manufacturing industry, with productivity of CHO cells reaching titres >10 g/L, a 1000-fold improvement over the past four decades [16, 18]. Considerable efforts have led to these improvements in titre, including those in process optimization, high throughput screening of cell lines, and the development of novel cell lines through genetic engineering.

The majority of manufacturing processes for biotherapeutic recombinant proteins use CHO cells for expression of the target protein of interest, however, artificially immortalized CHO cells are heterogeneous and have inherent gene instability, requiring proof of monoclonality by the regulatory agencies [187]. Flow cytometry-based cell sorting is a commonly used cloning method for clonal cell line generation, which has the advantage of being high-throughput and able to assess cells characteristics at the single-cell level. Cloning via flow cytometry can combine screening to enrich high-producing clones with a more time-efficient cloning method compared to traditional limiting dilution cloning, reducing timelines [204, 265]. Many flow cytometry-based screening and sorting methods have been described in the literature for improved productivity, as previously discussed.

As the results described in Chapter 3 from the IS characterisation identified a positive correlation between lysosome content and qP, here the isolation of cells with high lysosome content to increase productivity was investigated. The aim of this investigation was to assess whether cells with a high lysosome content during routine sub-culture could be isolated and subsequently be demonstrated to be high-producing cell lines when assessed under FBOG conditions. Although not directly involved in protein production, lysosomes are essential for the maintenance of cellular homeostasis, through autophagy and recycling of damaged cellular components [266]. A key component in the mTOR pathway, lysosomes are at the centre of nutrient sensing, and the consequent mTORC1 activation [130], leading to growth and protein synthesis. Alternatively, lysosome activity can be associated with autophagy and increased protein yields have been associated with both manipulation of autophagy [68, 75, 171, 267] and the mTORC1 pathway [66, 68, 135, 137, 268].

Based on the correlations observed during the FBOG described in Chapter 3 previously, five cell lines from the initial panel (1, 2, 4, 10 and 17) expressing the standard easy-to-express (ETE) mAb with different expression levels and lysosome content were selected for further study (Fig. 4.1). Initially, an equal number of cells were mixed together on the day of sorting based upon lysosome content. This 'mix' was then stained with the lysosome dye, and triplicate pools of 20,000 cells sorted based on high, mid and low lysosome content. The individual cell lines were also FACS sorted (FS) without gating, while the panel of cell lines were kept as single clonal cultures simultaneously (non-sorted, NS), to assess the effects of the process of FACS sorting on the cell lines. Moreover, in another experiment, individual cell lines were stained with the lysosome dye and sorted based on high and mid dye intensity, to evaluate if more productive cells could be isolated and maintained from the original individual cell lines based on lysosome content. Lysosome content-based cell sorting was also investigated by mixing of two cell lines expressing a bispecific mAb, considered more difficult to express, to determine if isolation of cells with increased lysosome content led to increased productivity over that from the original cell lines.

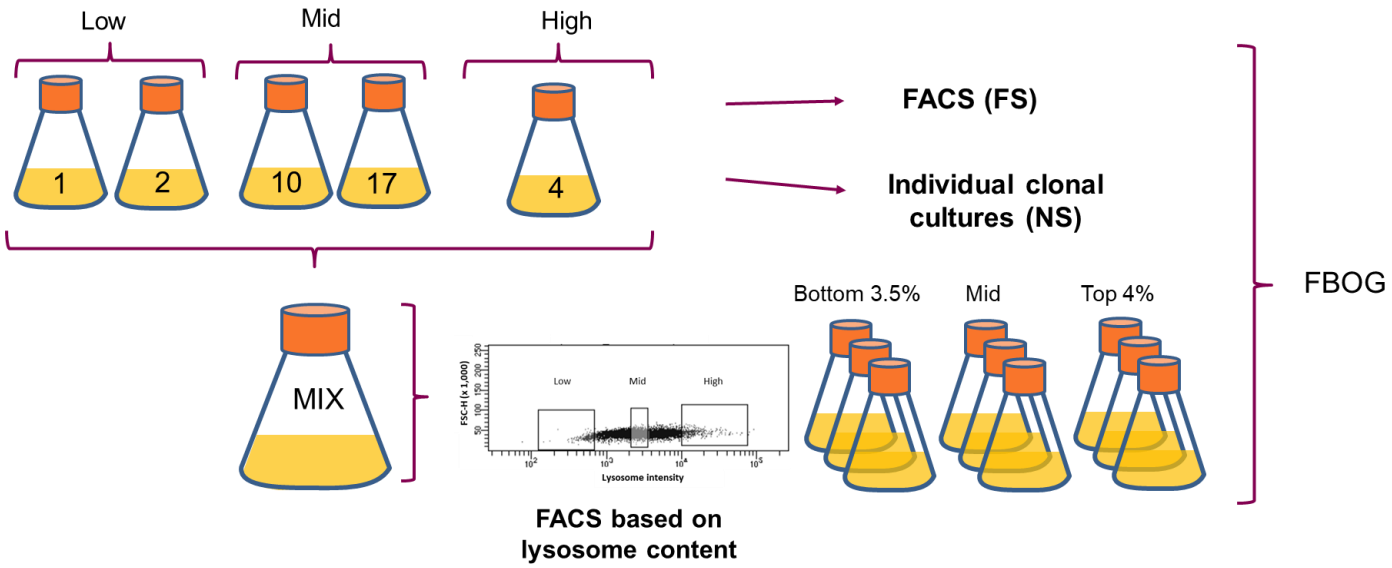

Figure 4.1 Schematic showing the five individual cell lines chosen for the mix, with low qP and lysosome content (1,2), medium qP and lysosome content (10, 17) and high qP and lysosome content (4). The mix was stained with a lysosome dye and sorted based on lysosome intensity, in triplicate pools of 20,000 events. Individual cell lines were either kept in shake flasks, or pools were sorted by FACS without any gating, to investigate the impact of cell sorting on cells. After recovery, cells were cultured in FBOG.

4.2 Results

4.2.1 Comparison of lysosome sorted cell characteristics compared to the original cell populations

To initially assess whether stress imparted on cells during FACS could have an impact on the performance of a cell line, 5 cell lines were sorted by FACS, without any gating, while simultaneously being subcultured routinely in shake flasks. Following recovery, cell growth and productivity characteristics were investigated under FBOG conditions. FACS sorting did not have any appreciable negative impact on growth (Fig. 4.2A), culture viability (Fig. 4.2B) or recombinant protein productivity (Fig. 4.2C, D). Cell lines 4 and 17 had higher titre in FACS sorted (FS) cells than the original non-sorted (NS), cell line 4 qP was higher in the FS cells, whereas this was higher in NS cells for cell line 17 (Fig. 4.2). Cell lines 1, 2 and 10 had similar qPs between both NS and FS cells. Collectively, the data suggests that the FACS did not negatively impact the cells' performance.

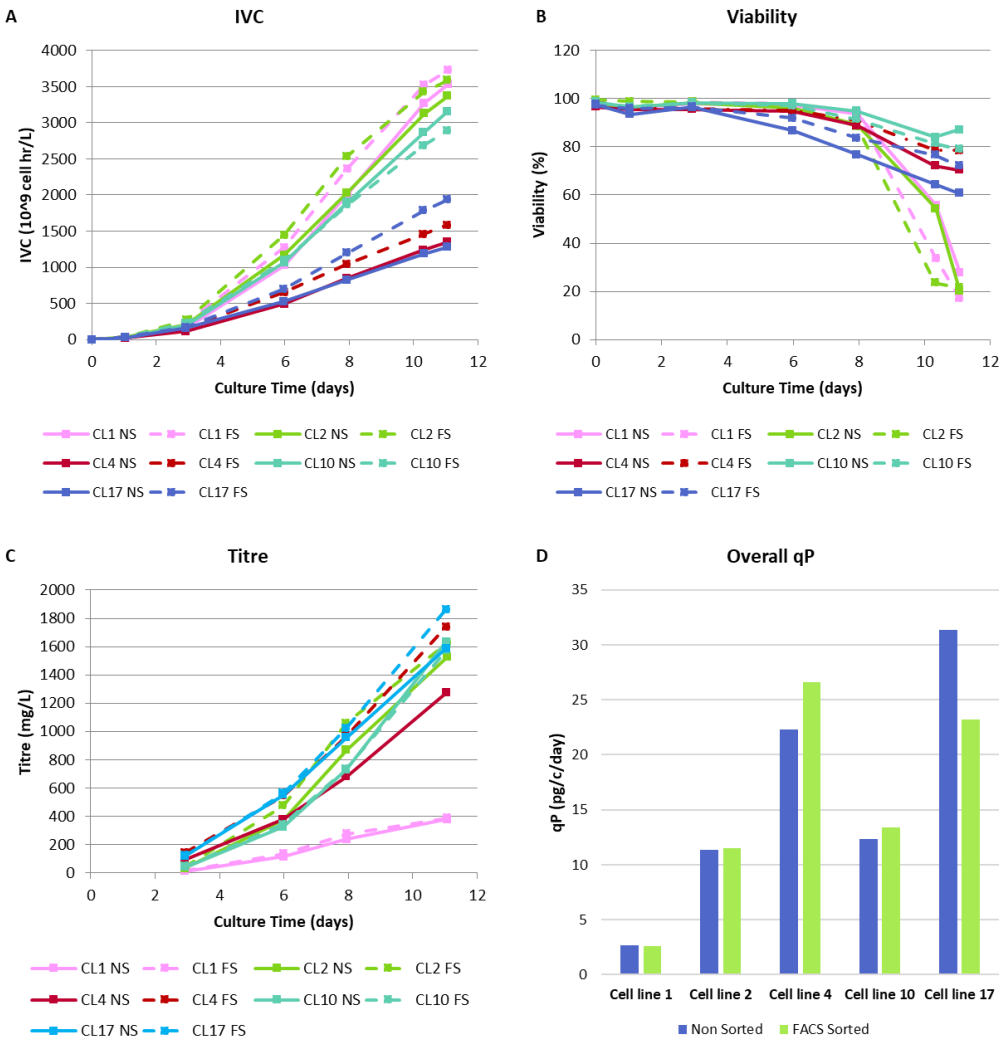

Figure 4.2 Cell culture data from preliminary FACS experiment, comparing non-sorted clonal cell lines (NS, solid line) and FACS sorted pools (FS, dashed line) cell culture parameters including A) IVC, B) Culture viability, C) Titre and D) overall qP. Cells were harvested on day 12, rather than the standard 14-days FBOG process. NS indicates non-sorted cells, that were subcultured in shake flasks (blue in D). FS indicates cells that have been sorted by FACS (green in D), in pools of 20,000 cells.

4.2.2 Mixed cell lines lysosome content sorting; Pool sorting based on lysosome content

Cells from a mixed pool of cell lines (see details above) stained with Lyso-ID were gated and sorted based on lysosome intensity as follows: bottom 4% (low), median (mid) and top 4% (high) (Fig 4.3). Accuracy of the sorts was verified by checking lysosome content of 500 cells post sorting. The pool of cells sorted from the 'low' gate did not recover in the first FACS experiment, but did recover in a second sorting, with a very slow recovery and cell growth.

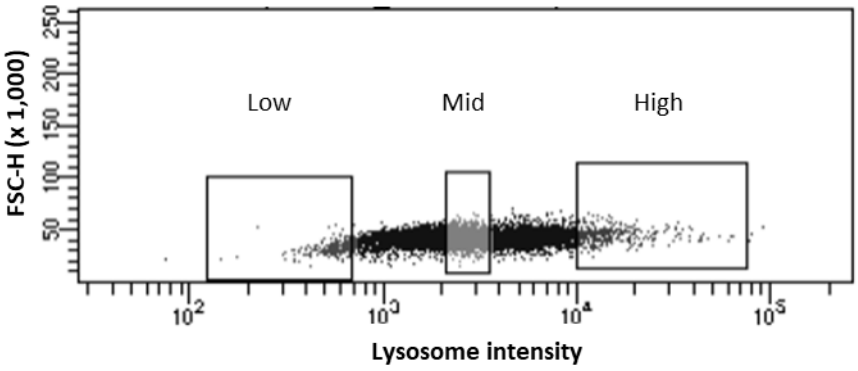

Figure 4.3 Gating strategy for cell sorting based on lysosome content. Mixed cells were stained with Lyso-ID dye. The intensity of the dye shows a wide range of lysosome content across the cells. Pools referred to as low, mid and high were isolated as indicated.

4.2.2.1 Culturing of lysosome content sorted cell pools isolated from the mixed cell pool in FBOG conditions

Pools isolated from the lysosome sorting experiment were assessed in FBOG conditions. High lysosome content sorted cells had the highest IVC (Fig. 4.4A, with a final IVC of 4340x10^9 cell *hour/L for the high lysosome content sorted cells vs. 3713x10^9 cell*hour/L for the mid lysosome content sorted cells) and maintained a higher culture viability for longer (Fig. 4.4B) compared to both the mid and low lysosome sorted cell pools. Cell sorting based on high lysosome content also led to a significant increase in final titre (3740 mg/L vs. 1449 mg/L for the mix, and 2591 mg/L for Mid, p = 0.021) compared to the initial cell lines and mid and low lysosome content sorted cells (Fig. 4.4 C, D). Low lysosome content isolated cells performed poorly in FBOG, with a low final titre (446 mg/L) and overall qP (2.6 pg/c/day) and exhibited an earlier drop in culture viability than the mid or high lysosome content isolated cell pools. Cell specific mAb productivity (Fig. 4.4E) was higher in the high lysosome content cell pools compared to the mid (20.55 vs 17.49 pg/c/day, p = 0.06) and low lysosome content sorted cells and was also higher than the qP of the initial cell lines in all cases except for cell line 17. The high lysosome sorted cells achieved higher cell concentrations and delayed cell death/prolonged culture viability, which would partly explain the increased titre of high lysosome content sorted pools compared to the original cell lines and mid and low sorted lysosome pools.

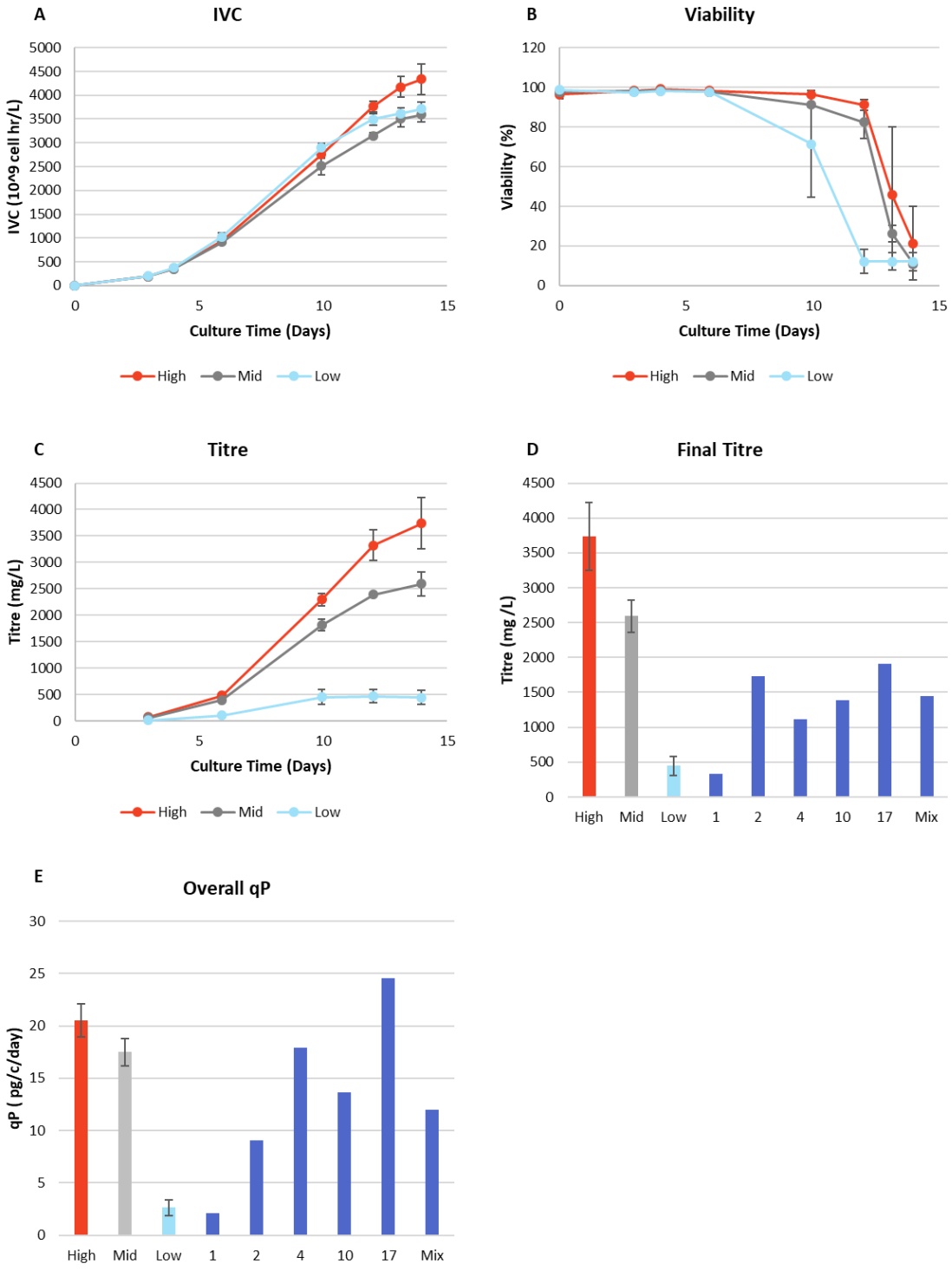

Figure 4.4 Cell culture data comparing the high (red), mid (grey) and low (light blue) lysosome sorted cell pools in terms of A) IVC, B) culture viability, C) mAb titre throughout culture, D) Final titre and E) qP. In panels D and E the data for the original cell lines used to create a mixed pool (1,2,4,10, and 17) and the actual Mix (blue) are shown. For high, mid and low, n=3, mean is shown with error bars = standard deviation.

4.2.2.2 Analysis of the intracellular HC and LC content of lysosome isolated cell pools from the original cell mix pool

Intracellular HC and LC protein were quantified by flow cytometry on day 3, 6 and 10 for the lysosome sorted cell pools and the original mixed pool. The analysis revealed that selecting cells based on high lysosome content led to a more homogeneous expressing population in terms of the amount of HC and LC protein intracellularly (IC). Mid and low lysosome sorted cell pools were composed of two distinct populations of cells expressing different amounts of HC and LC, including one negative for IC HC and LC protein expression (Q3, Fig 4.5). The negative population, in Q3, was particularly significant for low lysosome sorted cells, with over 60% of cells being classified as non-expressing in both HC or LC by this assay. The high proportion of non-expressors in the low pool is likely the result of cells derived from line 1, which had a low lysosome content, and mixed populations of cells expressing HC and LC protein, and cells that did not. Distribution of the % of expressing and non-expressing cells was similar across samples from all three timepoints. In the cell lines used to create the Mixed pool, cell line 1 had the lowest productivity, and the lowest lysosome content. It is interesting to note that high lysosome-based cell sorting excluded most non-expressing cells, further explaining the increased yield in the high lysosome sorted pool.

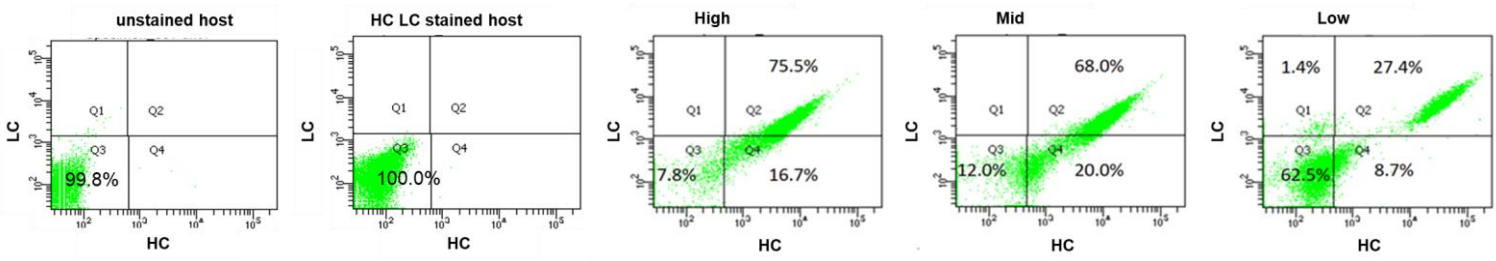

Figure 4.5. Intracellular HC and LC protein. Negative controls: unstained host (untransfected) and IC HC LC protein stained host (untransfected), used for setting the gates. High sorted cells had a more homogenous population expressing HC and LC, whereas Mid and Low lysosome sorted pools showed two distinctive populations, including one that does not express HC and LC protein on day 3 of the FBOG.

4.2.2.3 Determining the lysosome content of the Mixed cell pool and subsequent isolation of high, mid and low content lysosome pools

Lysosome content was measured by flow cytometry during FBOG in the original mixed pool and the lysosome sorted high, mid and low pools. Lysosome content was measured by flow cytometry on live cells, on day 3, 7 and 10 of the FBOG. High lysosome content cells had a small increase in lysosome content on day 3 (Fig. 4.6A, blue bars) compared to mid (p=0.11) and low (p=0.047) lysosome sorted pools. This increase appeared more pronounced by day 10 of culture (Fig. 4.6A, orange bars) where the high lysosome sorted pools had an appreciable higher lysosome content than either the original mixed pool or the low (p=0.028) and mid (p=0.0026) lysosome content sorted pools. There was also a positive correlation between day 3 lysosome content and qP of the sorted pools based on lysosome intensity (R = 0.71, Fig. 4.6B).

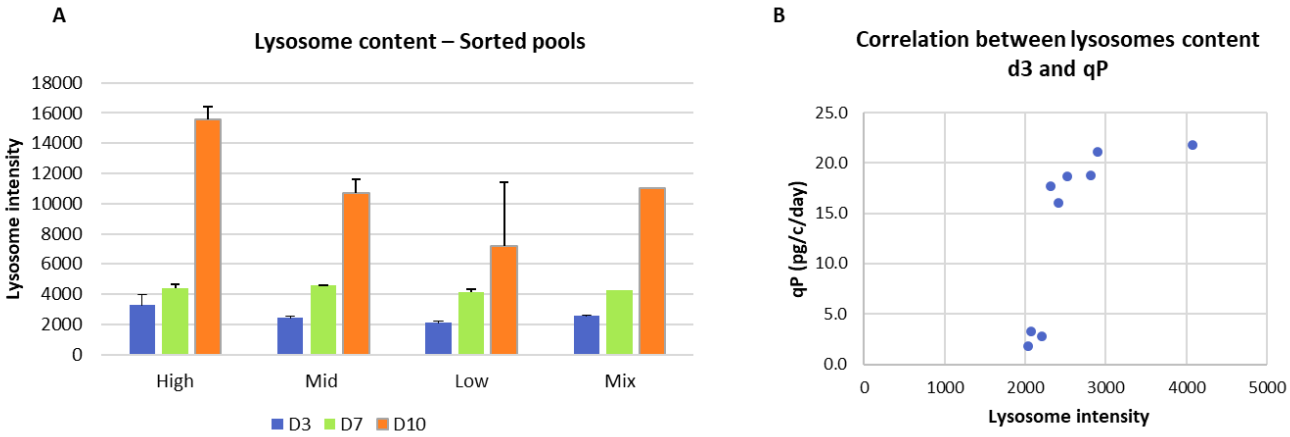

Figure 4.6 A) Lysosome content of high, mid and low lysosome sorted cell pools and the original Mix (control) throughout the FBOG, measured by flow cytometry. Blue indicates day 3 of the FBOG, green represents day 7 and orange day 10 (n=3, mean is shown with error bars = standard deviation) B) Lysosome content of the sorted pools and original cell lines vs. qP, Pearson's correlation coefficient R = 0.71

4.2.3 Individual cell lines sorting - Pool sorting based on lysosome content

Since cell sorting on the mix of cell lines based on high lysosome content gave positive results, the effect of cell sorting individual cell lines without mixing to increase productivity was investigated. Nine cell lines (1, 2, 3, 4, 7, 10, 11, 12 and 17) were stained with Lyso-ID, and the top 3% of lysosome intensity (high) and middle intensity (mid) were sorted. Sorting based on low lysosome content was excluded, as it did not result in any increase in productivity nor improved viability. The original cell line (Original CL) was kept in culture as a control. Individual cell lines had a range of lysosome content prior to the sort (Fig 4.7).

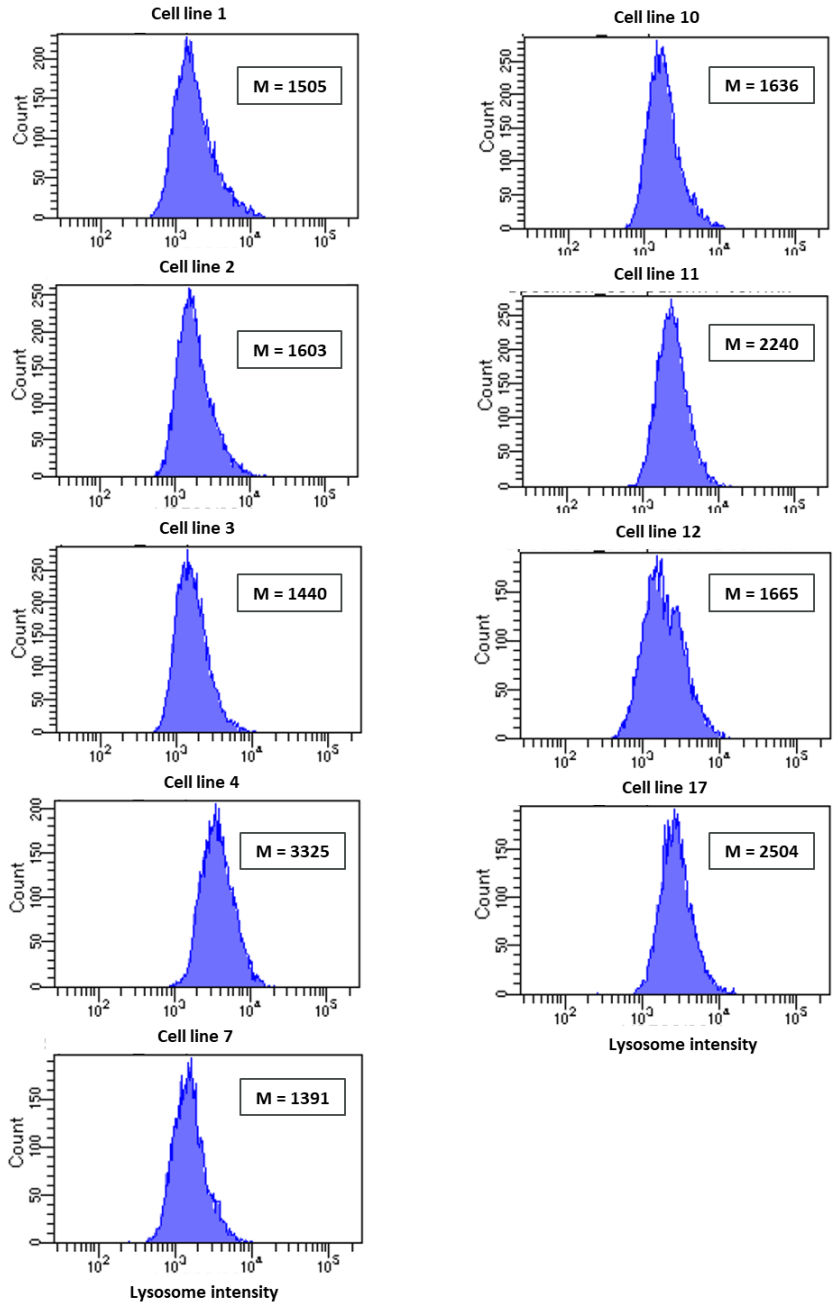

Figure 4.7 Histogram of the lysosome intensity of the individual cell lines, with the median fluorescence intensity (M)

4.2.3.1 Lysosome content cell sorting of individual mAb expressing cell lines

The cell lines shown to have a mixed population of HC and LC expressing cells in IC flow cytometry (1, 3, 4 whereby there was a population of non-expressers and a population of expressers) were sorted by FACS on lysosome content to determine if this resulted in an increase in the proportion of expressing cells within the population. Other cell lines with a homogenous HC and LC expressing population were also sorted to assess if titre could be increased. Following the recovery from sorting,

cells were cultured in a 14-day FBOG and assessed for growth and productivity characteristics. The FBOG growth data did not show any specific trend between the different sorted pools (Fig. 4.8 A-I). Some of the sorted cell pools had similar growth rates across all three lysosome content pools (those isolated from cell lines 1, 2, 7, 11 and 12; Fig.4.8 A, B, E, G and H), whereas in others the mid (from cell lines 4, 10; Fig.4.8 D and F) or High (from cell line 17, Fig4.8 I) lysosome content pools displayed increased growth. The cell sorting did not have any consistent impact on culture viability (Fig. 4.9 A-I). Some of the cell pools isolated on the basis of lysosome content had higher culture viabilities in the high and mid lysosome content pools (those from cell lines 3, 4, 10, 11, 12; Fig.4.9 C, D, F, G and H), whilst others it was the mid lysosome content pool (those from cell lines 2, 7; Fig.4.9 B and E) and for others the highest culture viability was observed in the original cell lines (cell lines 1, 17; Fig4.9 A and I). Further analysis of the lysosome content of the cell lines during the FBOG (described below in 4.2.3.3) showed that there was no difference in the lysosome content between the lysosome-sorted conditions and the control for most cell lines. The lack of differences in the lysosome content could explain the lack of differences between the three conditions for the growth and viability.

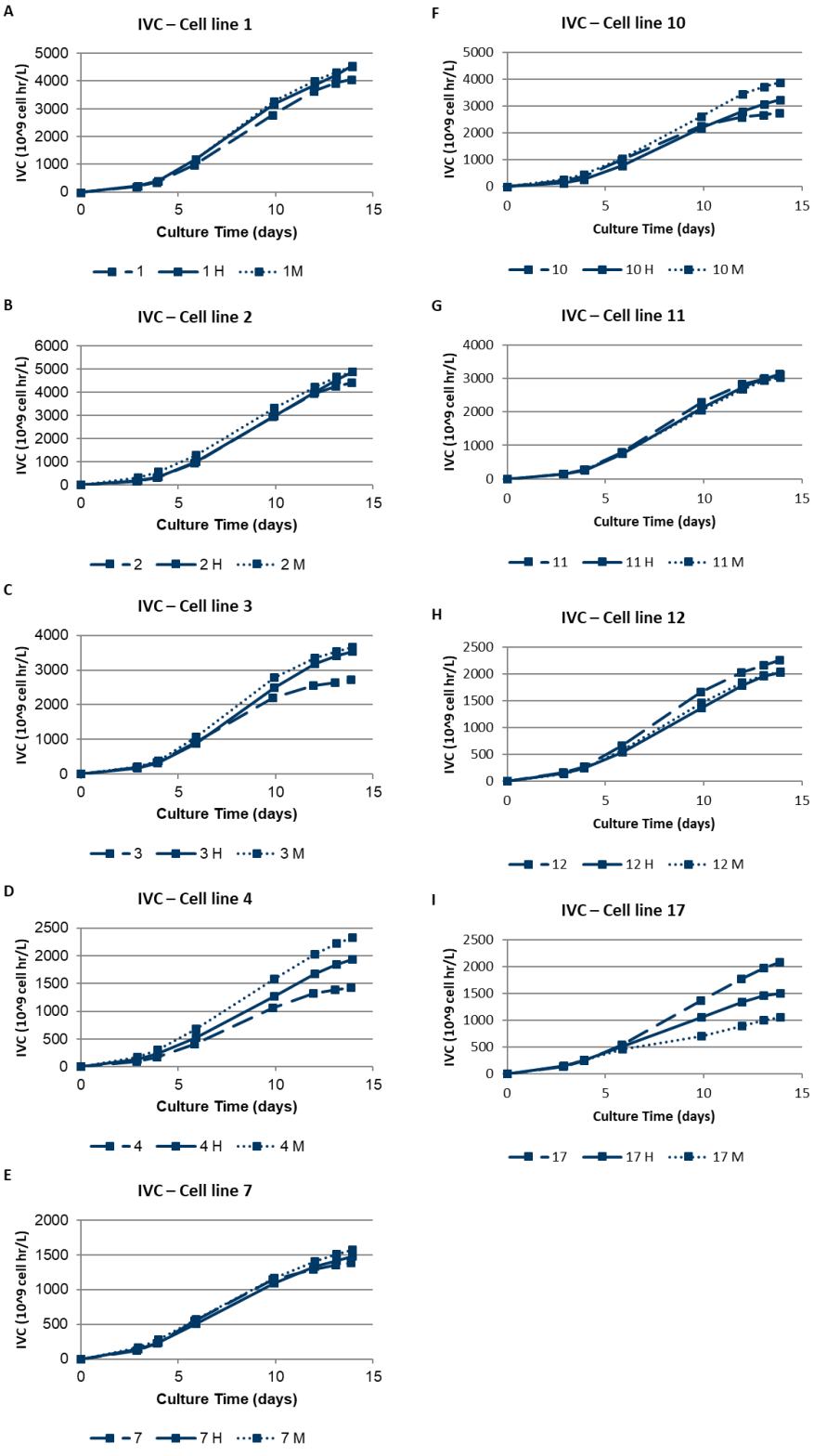

Figure 4.8 IVC (A-I) of individual cell lines that were either non-sorted (dashed line), sorted based on high lysosome content (full line) or sorted based on mid lysosome content (dotted line).

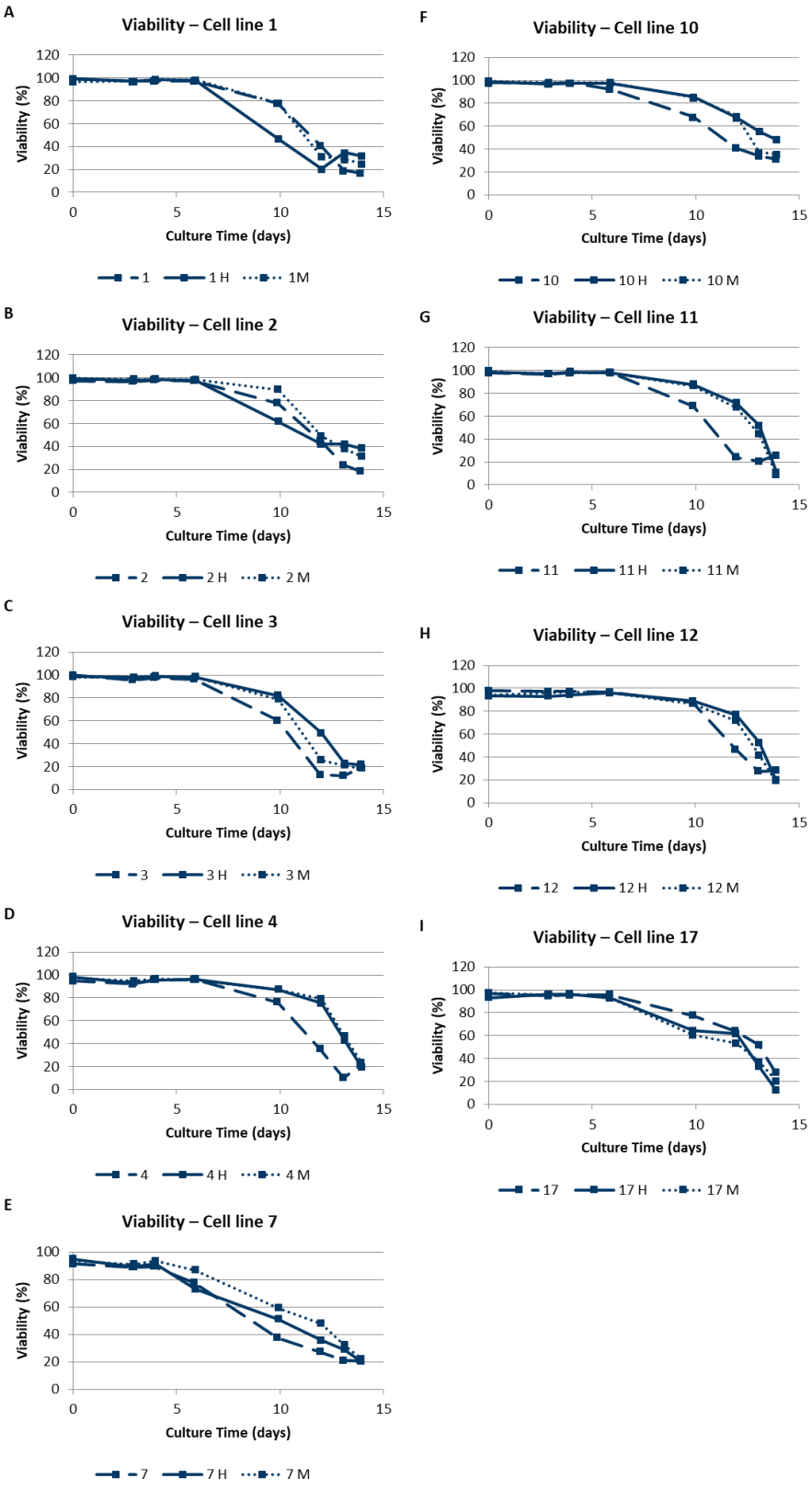

Figure 4.9 Viability (A-I) of individual cell lines that were either non-sorted (dashed line), sorted based on high lysosome content (full line) or sorted based on mid lysosome content (dotted line).

In most cases, lysosome-based cell sorting did not result in increased recombinant protein productivity. Exceptions include pools isolated from cell lines 4 and 10, where there was a small increase in titre in high and mid lysosome content pools compared to the original cell line, but qP was similar to the original cell line, highlighting that the increased titre was driven by increased growth (Fig. 4.10 A, B). For cell lines 3, 11 and 17, qP was increased in one or both of the lysosome-sorted conditions compared to control.

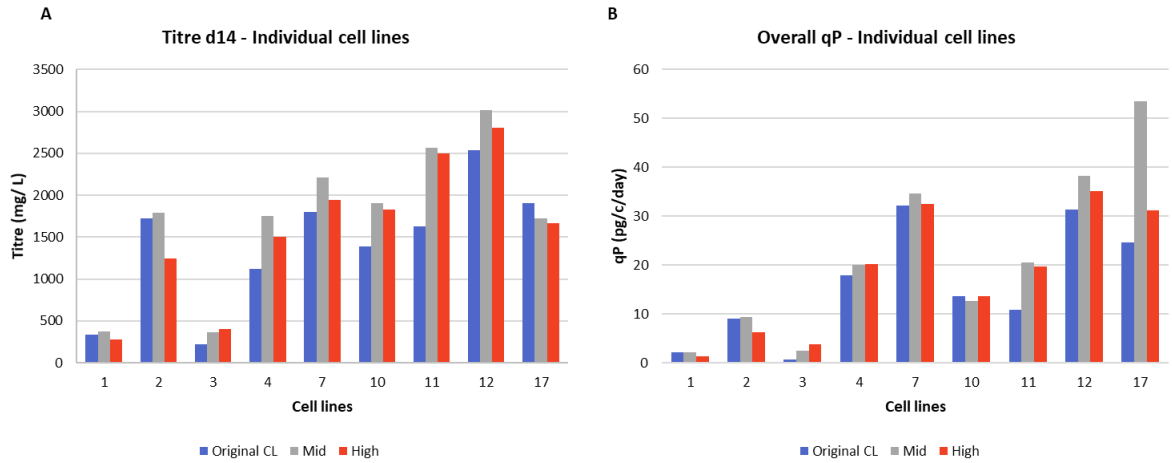

Figure 4.10 A) Final mAb titre and B) overall qP of the original cell line (blue), cells sorted based on mid (grey) and high (red) lysosome content

Lysosome content isolated pools from cell line 11 and 12 had an increase in titre and qP for the high and mid lysosome content cells. None of the pools isolated based on lysosome content from cell line 17 showed an increase in titre, although the mid lysosome content pool showed a two-fold increase in specific productivity. Many of the pools isolated from the original cell lines based on lysosome content did not have altered productivity characteristics (those isolated from cell lines 1, 2, 3, 7). Overall, pool sorting of individual cell lines based on lysosome content did not have any consistent effects on isolation of pool with altered growth or productivity characteristics.

4.2.3.2 Intracellular HC and LC content of individual mAb producing cell lines and lysosome sorted pools

Intracellular (IC) HC and LC analysis revealed that cell lines with high lysosome content generally were more homogeneous in terms of expression of HC and LC. However, analysis of IC HC and LC on cells sorted based on lysosome content for individual cell lines showed that lysosome content-based cell sorting did not have a consistent impact on the homogeneity or expression of the resulting cell pools (Fig. 4.11). No effect was observed on the distribution of the population, nor on the ratio of expressing

/ non-expressing populations for cell lines 1, 3 and 4, which had a mixed population. This result is different than what was observed for the Mix experiment described previously.

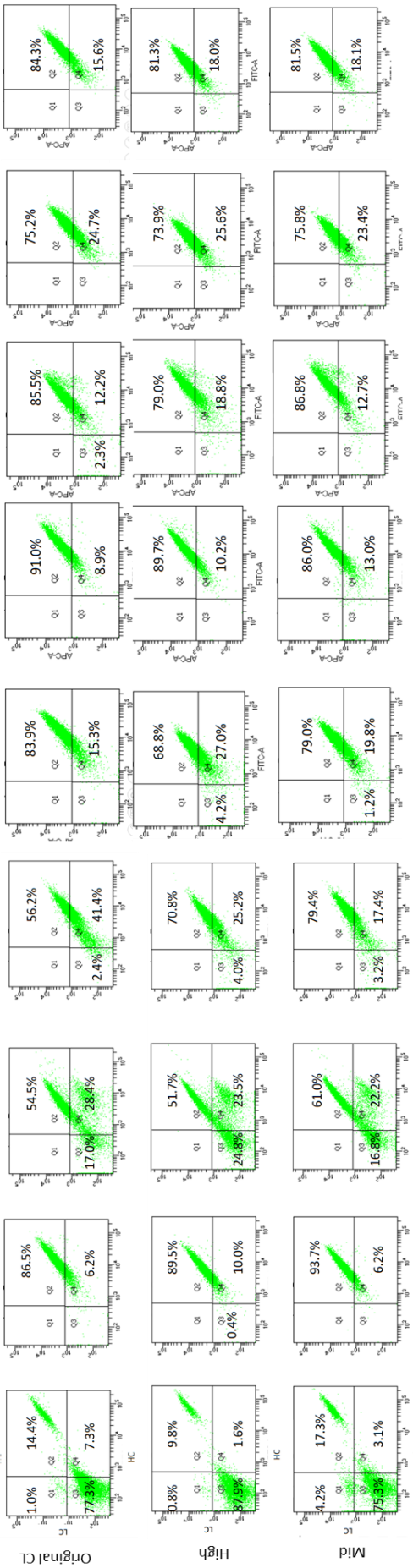

Figure 4.11 Intracellular HC and LC protein distribution of the original cell lines (top row), high lysosome content sorted cells (middle), and mid lysosome content sorted cells (bottom row), analysed by flow cytometry.

4.2.3.3 Lysosome content of individual sorted original cell lines

Lysosome content was measured by flow cytometry in live cells, on day 3. 7 and 10 of the FBOG. In lysosome content sorted cell lines, the lysosome content on day 3 (Fig 4.12 A) or 6 (Fig 4.12 B) did not show any difference between the lysosome sorted pools (high, mid) or original cell line. Differences in lysosome content were observed on day 10 (Fig 4.12 C), however there was no general trend of lysosome content with day of culture. Interestingly, the high lysosome content sorted cells did not have the highest lysosome content at any timepoints (Figure 4.12).

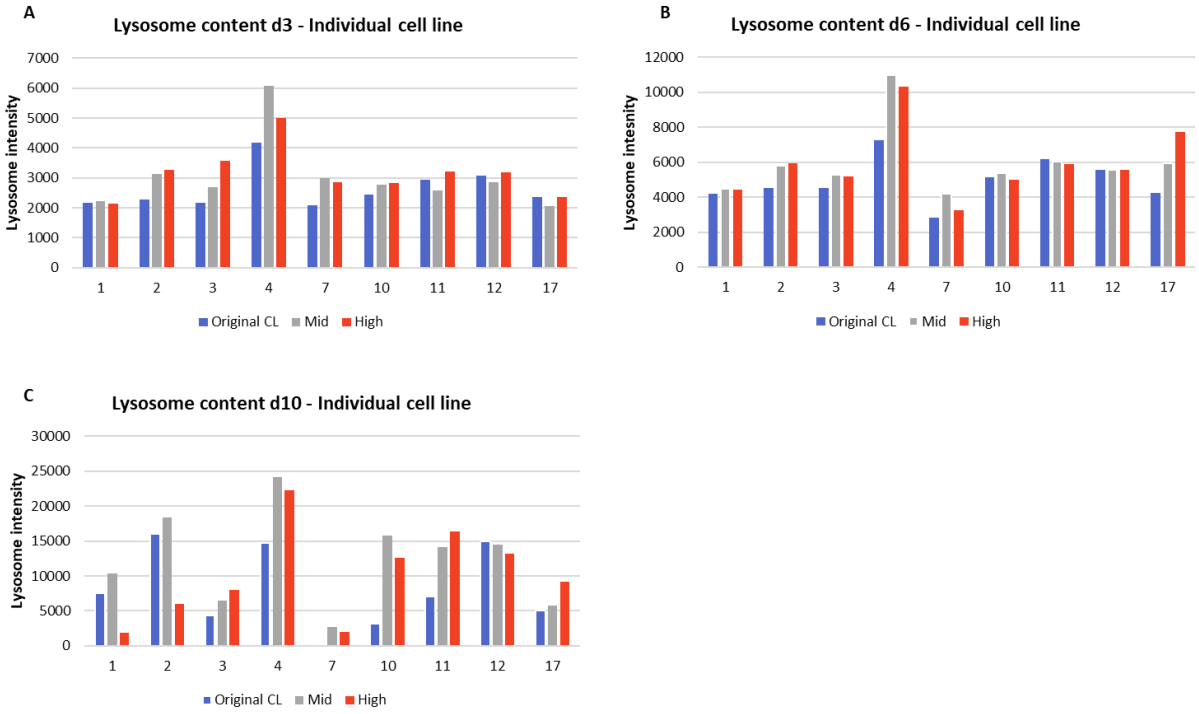

Figure 4.12 Lysosome content on A) day 3, B) day 6 and C) day 10 comparing the original cell line (blue), the high lysosome content sorted cells (red) and the mid lysosome content cells (grey).

4.2.4 Bispecific mAb: pool sorting based on lysosome content

4.2.4.1 Lysosome content sorting of bispecific mAb expressing cell lines

Two cell lines expressing a difficult to express (DTE) bispecific mAb, with different productivities (bispecific 9 = 316 mg/L and bispecific 13 = 852 mg/L), were mixed together, stained with Lyso-ID and duplicate pools were sorted based on high and mid lysosome content. The control sorted pool was generated from sorting without gating. The original cell lines used to create the mix, bispecific cell lines 9 and 13, were also compared to the sorted pools. High and mid lysosome sorted pools, and the control cell line pool sorted without gating, had similar growth profiles to each other and achieved higher cell concentrations than the original bispecific 9 or 13 cell lines (Fig. 4.13A). Culture viabilities

were maintained in all cell lines and sorted pools until day 10, at which point these rapidly decreased, despite sufficient glucose supply (Fig. 4.13B). High lysosome sorted pools culture viability was marginally increased compared to other cell lines and pools on day 12 but decreased significantly by day 14. The control sorted pool and mid lysosome content sorted pool had similar final titre and qP (Fig. 4.13 C, D). The high lysosome sorted pools had an increase in titre and qP, approximately 30% compared to the control pool (p =0.084 for titre, and p=0.19 for qP).

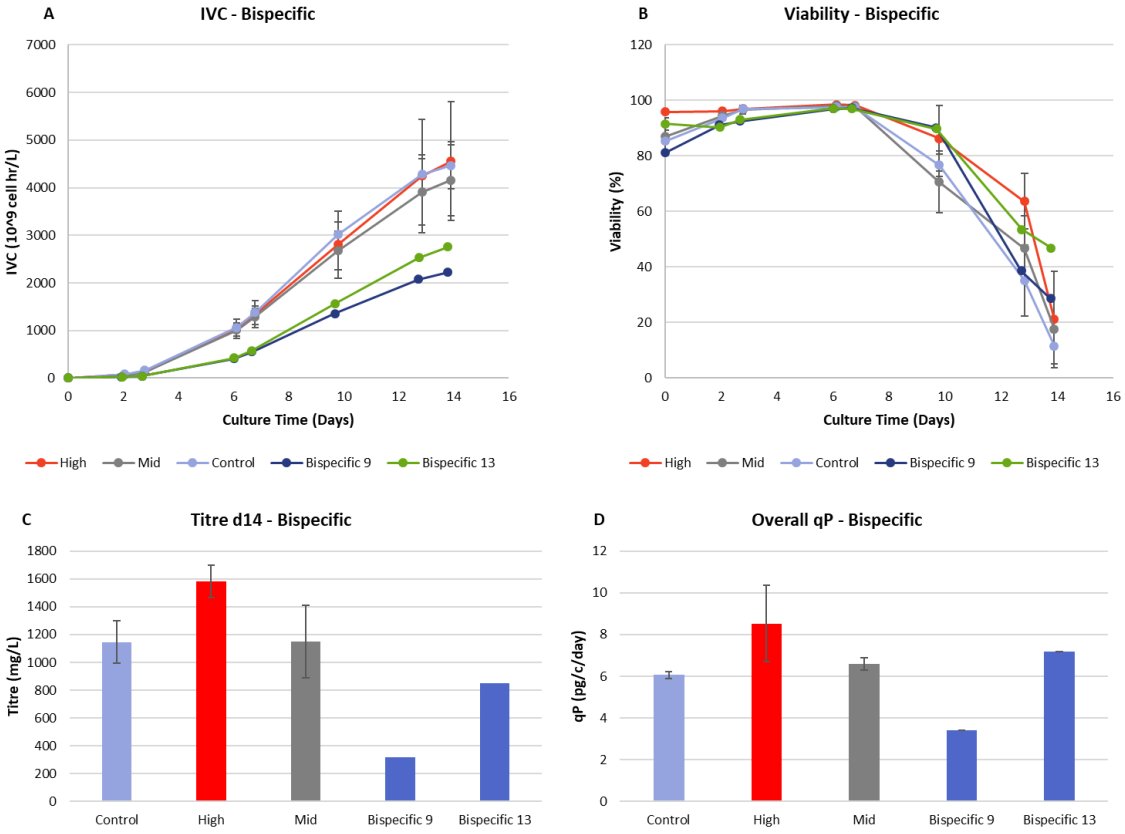

Figure 4.13 Bispecific mAb cell culture results. A) IVC, B) culture viability, C) bispecific mAb titre and D) qP of the lysosome sorted cell pools expressing a bispecific (red for high lysosome content, grey for mid lysosome content), the control cell sorted pool (light blue) and the two original bispecific cell lines (blue).

Bispecific cell lines 9 and 13 had one homogeneous single population expressing intracellular HC and LC protein, and there was no difference between the intracellular HC and LC distribution expression profiles of the sorted cell lines (Fig. 4.14).

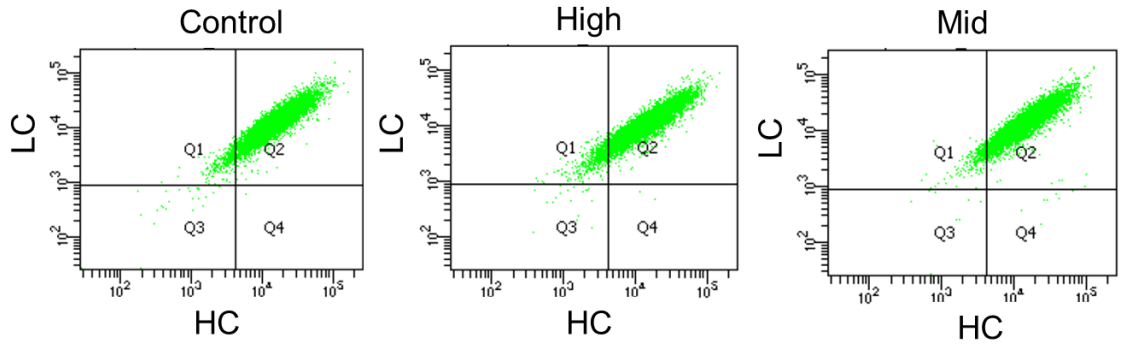

Figure 4.14 IC HC and LC protein of the bispecific control and lysosome-sorted cell lines by flow cytometry.

4.2.4.2 Lysosome content of the bispecific mAb cell pools isolated based on lysosome content

Lysosome content was measured during the FBOG culture in the bispecific expressing original cell lines, control sorted pool and those isolated on the basis of having high or mid lysosome content (Fig. 4.15). Lysosome content was quantified by imaging flow cytometry on live cells, on day 3, 7 and 10. No differences were observed between the different sorted pools and original cell lines on day 3 or 6 of culture. On day 10 of culture, the high lysosome content pool had an elevated lysosome content compared to the control pool and bispecific 13 original cell line, but this was similar to that observed in the mid lysosome content pool and original bispecific 9 cell line.

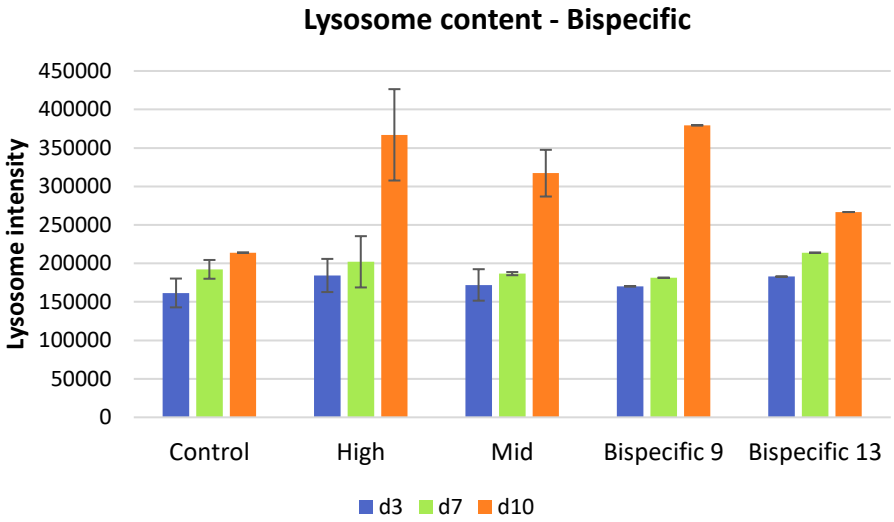

Figure 4.15 Lysosome content of the bispecific cell lines throughout the FBOG for control, high and mid lysosome sorted pools, and the original cell lines bispecific 9 and 13 on day 3 (blue), day 7 (green), and day 10 (orange) of FBOG.

4.2.5 Characterisation of lysosome sorted pools expressing an ETE mAb by western blotting

As the biggest difference in any parameters measured (titre, growth, lysosome content) from the lysosome-based cell sorting were observed in the high lysosome content cells isolated from the mixed pool of the ETE mAb, western blotting was performed comparing the high lysosome content pool and the mixed pool (control) expressing the ETE mAb. Cell pellets from day 7 of culture were studied to investigate the expression of key proteins related to lysosome expression and culture viability that might reveal some of the potential mechanisms underlying the increase in culture viability and productivity of high lysosome sorted cells compared to the control. Day 7 of culture was chosen as it was the last recorded day on which culture viabilities were similar for high lysosome sorted cell pools and the control. Autophagy (Atg12, Lamp1, LC3B, p62 and Lamp2A), apoptosis (caspase 3, cleaved caspase 3 and Bcl-xL), and mTOR pathway (Lamtor1, phosphorylated 4EBP1 (Thr37/46), phosphorylated p70 (Thr389) and phosphorylated mTOR (Ser2448)) markers were investigated.

4.2.5.1 Autophagy markers

Autophagy, the intracellular recycling required for cellular homeostasis, relies on lysosomes for the degradation of intracellular waste. Nutrient depletion or environmental stress sensed by mTORC1 leads to mTORC1 downregulation and initiation of autophagy [132]. Expression of proteins involved in different stages of autophagy progress were therefore investigated: p62, Atg5-12, LC3B, Lamp1 and Lamp2A. The p62 protein is associated with early autophagic factors such as ULK1, localises to autophagosomes in the process of nucleation and formation, and its degradation can be used as a marker of early-stage autophagy; p62 binds to LC3 and is selectively degraded by autophagy [152] [269]. Atg5-12 and LC3B are linked to phagophores and mature autophagosomes [143], and are reporters of autophagy. LC3B is converted to the 18 kDa cytosolic LC3B-I, which is subsequently converted to the 16 kDa LC3B-II during autophagy [270]. LC3B-I levels decrease during starvation, while LC3B-II levels increase. However, anti-LC3 antibodies have been shown to be more sensitive for LC3B-II detection. It is thus common practice to use LC3B-II or the ratio of LC3B-I to LC3B-II for autophagy monitoring [270]. Moreover, monitoring LC3B-II results on its own can be inconclusive with regard to autophagy, as an increase in LC3B-II can be caused by enhanced autophagosome synthesis, or a blockage of autophagic degradation causing autophagosome accumulation [271]. Atg5-Atg12 complex formation is necessary for LC3B conjugation and autophagosome membrane expansion, whereas free Atg12 has been linked to induction mitochondrial apoptosis [272]. Lamp1 and Lamp2A are lysosomal membrane protein required for the autophagosome fusion with lysosomes and are used as late-stage autophagy markers [273]. Function of these proteins, which were selected for monitoring the autophagic flux, are summarized in the table below (Table 4.1).

Table 4.1 Summary of the autophagy proteins based on their function and at which stage of autophagy they are involved

Autophagy protein	**Stage of autophagy**	**Function**
p62	Early	Autophagosome nucleation and formation
LC3B	Middle	Enhanced autophagosome synthesis or blockage of autophagic degradation
Atg 5-12	Middle	Necessary for LC3B conjugation and autophagosome membrane expansion
Lamp1	Late	Autophagosome fusion with the lysosome
Lamp2A	Late	Autophagosome fusion with the lysosome

High lysosome content exhibited a lower rate in some autophagy markers compared to control. Autophagic markers Atg12-Atg5 (Fig. 4.16A, p=0.0057) and Lamp2 (Fig. 4.16F, p=0.00040) were more than two-fold lower in expression in the high lysosomes sorted cells compared to that observed in the control sample cells. Amounts of free Atg12 (Fig. 4.16B, p=0.017), LC3BII (Fig. 4.16D, p=0.016) and p62 (Fig. 4.16E, p=0.042), were also lower in high lysosome content sorted cells to a small extent. Lamp1 expression was not significantly different between the high lysosome cells than the control (Fig. 4.16C, p=0.067).

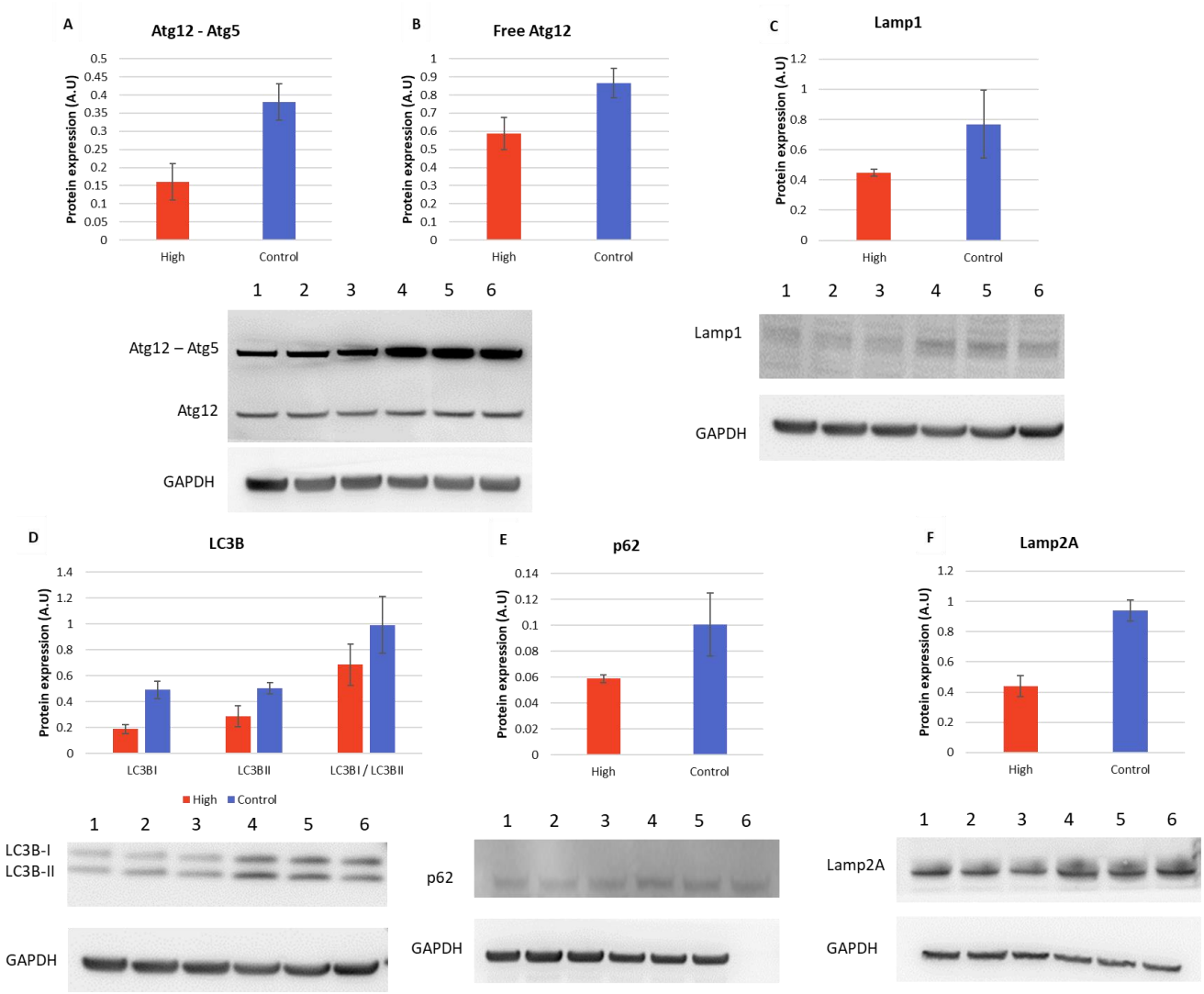

Figure 4.16 Autophagy marker analysis by western blotting in the standard mAb expressing pools. Quantification of the bands was performed by densitometry. Protein expression was normalised to GAPDH. Autophagic markers used were A) Atg12-Atg5 (p=0.0057), B) free Atg12 (p=0.017), C) Lamp1 (p=0.067), D) LC3B (p=0.016 for LC3B II), E) p62 (p=0.042) and F) Lamp2A (p=0.00040). For all samples n=3, the mean is shown with error bars = standard deviation.

4.2.5.2 mTORC1 markers

The mTORC1 pathway is involved in autophagy, cell growth, proliferation and control of protein synthesis. It acts as a sensor of nutrient availability within the cells and requires mTOR translocation to the lysosome. mTOR over-expression has been reported to increase proliferation, be more robust to sub-optimal growth factor and oxygen supply, and productivity in CHO cells [65], whereas mTOR inhibition has been showed to increase culture viability via increased autophagy [274]. The activation of mTORC1 pathway leads to the phosphorylation and inhibition of 4EBP1, leading to cap-dependent translocation [119]. mTORC1 activation also phosphorylates and activate p70 S6K protein, which

increases ribosomes and mRNA biogenesis [121]. The phosphorylated form of mTOR is a popular marker for the activation state of the PI-3 kinase pathway and the activation status of mTOR [275]. Finally, Lamtor1 (the late endosomal and lysosomal adaptor and MAPK and mTOR activator), is essential for the assembly of the mTORC1 complex components, such as the recruitment and stabilization of the Rag proteins [276, 277].

Lamtor1 expression was slightly lower in the high lysosome sorted cells compared to control (Fig. 4.17A, $p=0.012$), indicating a decrease in the recruitment of Rag proteins to form the mTORC1 complex. Phosphorylated p70 expression did not differ between high lysosome content sorted cells and the control pool (Fig. 4.17C, $p=0.48$), suggesting that both had similar initiation of the ribosome biogenesis. Levels of phosphorylated 4EBP1 (Fig. 4.17B, $p < 0.00010$) and phosphorylated mTOR (Fig. 4.17D, $p=0.028$) were significantly lower in the high lysosome content sorted pool to the control. The low levels of phosphorylated 4EBP1 in the high lysosome sorted cells indicate a down-regulation of the downstream pathway, leading to an increase in cap-dependent translation compared to control cells. The lower phosphorylated mTOR levels observed in the high lysosome content sorted cells indicates a decrease mTORC1 activity compared to control cells, although none of the other markers investigated are consistent with this observation.

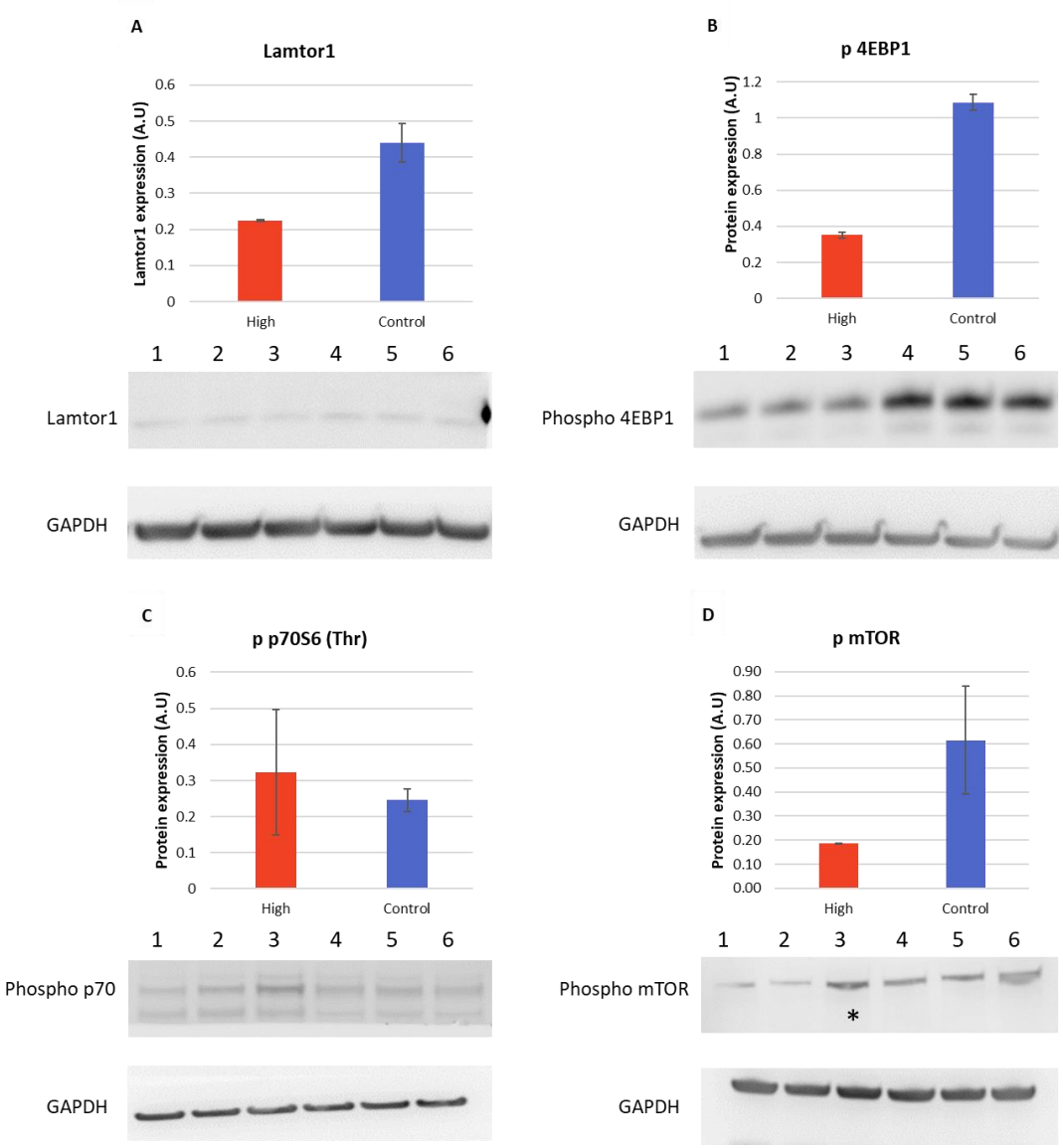

Figure 4.17 mTORC1 pathway analysis by western blotting in the standard mAb control pool and high lysosome content isolated pool. Bands were quantified by densitometry analysis. Protein expression was normalised to GAPDH. mTORC1 substrates used were A) Lamtor1 ($p=0.012$), B) phosphorylated 4EBP1 ($p < 0.00010$), C) phosphorylated p70 S6 ($p=0.48$) and D) phosphorylated mTOR ($p=0.028$). The * on D) indicates a sample that was excluded as an outlier from quantitation analysis, as when normalised to GAPDH, its value was three times higher than the other two samples (0.62 vs. 0.19 for the two duplicates). When the sample is included in the analysis, there is no significant difference in phosphorylated mTOR expression ($p=0.22$). For all other mTOR substrates, n=3 the mean is shown with error bars = standard deviation.

4.2.5.3 Apoptosis markers

Finally, apoptosis was investigated by monitoring expression of specific markers of apoptosis, caspase 3 and Bcl-xL. Caspase 3 is involved in the extrinsic apoptosis pathway, which requires activation of the cell membrane death receptors, TRAIL/Fas, leading to initiator caspases 8/9 activation, and hence

cleavage of caspase 3 and apoptosis [175]. Caspases 8/9 also trigger a cascade of signals that leads to mitochondrial damage, committing cells through both the extrinsic and mitochondrial apoptosis pathway [174]. Bcl-xL is a pro-survival protein of the Bcl-2 family, which is inhibited by the downstream cascade of events from caspases 8/9 activation, and by severe unfolded protein response, through downregulation by CHOP [155].

Levels of cleaved caspase 3, were approximately 4-fold lower in the high lysosome content sorted cells compared to control, indicating activation of the extrinsic apoptotic pathway in the control pool (Fig. 4.18A, $p < 0.00010$). Caspase 3 levels (Fig. 4.18B, $p=0.056$) and Bcl-xL (Fig. 4.18C, $p=0.15$) were not significantly different between the high lysosome content pool and the control pool. The lack of differences in the Bcl-xL expression despite the clear increase in the expression of caspase 3 could indicate that intrinsic apoptosis initiation was not activated at this stage of the culture for neither the control or the high lysosome content sorted cells.

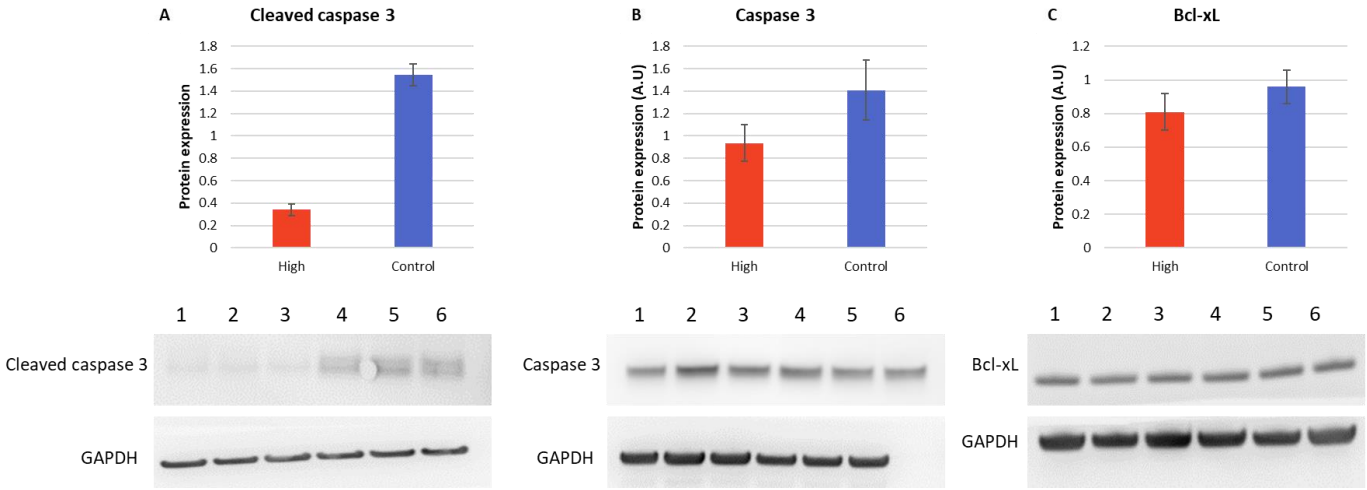

Figure 4.18 Apoptosis biomarker analysis by western blotting in the ETE mAb high lysosome content pool and control pool. Bands were quantified by densitometry analysis. The protein expression was normalised to GAPDH. Apoptosis markers used were A) cleaved caspase 3 ($p < 0.00010$), B) caspase 3 ($p=0.056$) and, C) Bcl – xL (anti-apoptotic) ($p=0.15$). For all other mTOR substrates, n=3 the mean is shown with error bars = standard deviation.

4.3 Discussion

Cell sorting by FACS is used not only as a reliable cloning method, but also as a method to enrich high producing cells based on particular cell characteristics [205, 207, 208, 210, 213, 215, 217, 253, 261, 278-280]. Methods have been reported for the isolation of cells with characteristics based on either the direct secretion of the protein of interest [204, 205, 211, 212, 242], the measure of intracellular protein [207-210] or indirect markers of productivity [213, 214, 217, 261]. All these approaches are designed to isolate high producing cell lines. Although these methods have had some success, the approaches can be time-consuming and give varying results.

In this study, lysosome content-based cell sorting was assessed as a method to isolate cells with increased productivity capacity compared to non-sorted cells. Cell sorting by FACS, despite being widely used as a cloning method, has been reported to create significant cell damage, through the hydrodynamic pressures present in the FACS nozzle [281]. Fortunately, such potential cell damage does not appear to lead to a significant increase in apoptosis or decrease in culture viability during cell sorting, as reported in a number of different studies [281] [282] [283]. To verify that there was no negative impact of FACS on the growth and productivity of the cells investigated in this study, unstained cells were sorted, while also maintaining the original shake flask in culture. No differences in cell growth or mAb productivity were observed between the sorted and non-sorted cells, indicating that the FACS process did not negatively impact the cells performance. Moreover, studies have shown that FACS sorting does not significantly alter gene expression, in mice mammary epithelial cells, based on microarray analysis of endogenous genes [284], supporting the observation that FACS sorting did not impact growth or productivity in this study.

When lysosome-based cell sorting was applied to cells producing ETE mAb, a two-fold increase in titre was observed in high lysosome content sorted cells compared to control sorted cells, and a 30% increase in titre for a bispecific mAb in high lysosome content cells compared to controls. These data suggest that cells with high lysosome content have a greater capacity for expression of secreted recombinant proteins than control cells, but that the size of the increase observed is significantly different depending on the molecule expressed. Lysosome-based cell sorting may isolate cells that are more homogenous and more resistant to apoptosis, and hence increasing titre. However, the benefits of lysosome-based cell sorting seem to be molecule-dependent, and bottleneck-dependent: cells expressing a bispecific, for which the bottleneck may be present at the protein synthesis or mAb secretion, did not increase their productivity as much as cells expressing an ETE mAb, which causes less stress to the cell. Whilst an increase in titre was observed for high lysosome content cells sorted from a mix of cell lines, no impact was observed on sorting of individual cell lines.

In a clonal cell line, the range of lysosomal protein expression should not be, and was not in our study, as wide as observed when mixing different clones together [285, 286], thus the mix of cells gives a wider range of lysosome content from which to isolate cells. Additionally, sister cells, cells derived from the same single clone, have been showed to have more similar transcriptional profiles than non-sister cells and similar transcriptional dynamics [286-288]. Within a pool of cells these can differ much more. This heterogeneity is decreased through the process of single cell cloning, at least until a cell line begins to diverge through natural accumulation of mutations. A study by Pilbrough et al. showed that FACS sorting based on high and low intensity of IC HC and LC protein resulted in both the high and low isolated populations shifting back towards the non-sorted population as soon as 5 days after cell sorting, with both low and high isolated profiles being undistinguishable from the non-sorted control by day 30 after the cell sorting. This suggests that even after cell sorting, subsequent cells 'drift' back towards a 'normal' distribution for a given cell type or product in the absence of continued selection or isolation. Such a phenomenon could explain why the lysosome content of the high lysosome content isolated cell pools does not show a large difference from the control early in the cell culture, and only show differential expression late in the culture, when more stress is present, and the lysosome content is up-regulated, hence increasing the capacity for additional lysosome content. Moreover, this suggests that despite our work being done in pools generated based on their lysosome content, and not clones, the pools originating from a mix, with their increased genetic diversity compared to clones, were still more productive than the original clonal cell lines that were mixed, despite constant population drift.

Single cell sorting based on high-lysosome content was attempted for this experiment, however there was a poor recovery of both control and high-lysosome sorted cells: not enough clones could be recovered for a statistically significant comparison of the clonal productivity. Improvements based on lysosome sorting may have been obtained for individual cell lines if the sorted cells had been single cell cloned, rather than obtaining a bulk pool.

Interestingly, the heterogeneity of the initial mix of cells prior to cell sorting appears to have a large impact on the observed improved productivity of the resultant isolated cells, potentially due to the high lysosome content cell sorting corresponding with the isolation of homogeneous and expressing cells, and low-lysosome content cells corresponding to non-expressing cells. A number of reports have noted that heterogeneity can be a significant impediment to isolating cell lines with high productivity, notably due to non-expressing cells doubling at a faster rate than producing cells, and eventually outgrowing the producing population, especially evident when a DTE molecule is expressed [198, 289]. Cloning itself does not always reduce phenotypical or genetic heterogeneity [190, 196, 290], but selection pressure, based on stable expression of a transfected surface marker transgene for example,

has been shown to improve chromosomal stability and increase population homogeneity [200, 289, 291].

In this study, lysosome content-based cell sorting of heterogeneous populations yielded cells with an increased productivity, likely through two different mechanisms: 1) increased homogeneity of the expressing population, and 2) maintained higher culture viability at later stages of FBOG cultures. To investigate the potential mechanisms underlying the improved productivity, and the effects of increased lysosome content on the cell, western blot analysis was performed. When biomarkers of the mTORC1 pathway were investigated, no major differences were observed between high lysosome content cells and control pools with regard to the expression of Lamtor1, a protein that is part of the Ragulator complex, and phosphorylated p70 S6 protein, which regulates ribosome mRNA translation and biogenesis [112]. Previous reports have associated higher expression of p70 S6 with increased productivity in cells sampled during the mid-exponential phase of cell growth [135] or cell cycle arrested cells [268]. High lysosome content cells had decreased phosphorylated 4EBP1 and phosphorylated mTOR compared to control cells. These low levels of decreased phosphorylated 4EBP1 are consistent with an increased mTOR activity, as mTOR inhibits 4EBP1. A few reports have linked increased mTOR activity with increased productivity. The increase in mTOR levels has been associated with increased productivity through decreased apoptosis initiation in studies inhibiting mTOR with rapamycin [66, 68]. This was further supported by a study by Josse et al., who showed a positive correlation between poor productivity and high levels of 4EBP1, a result of mTOR inhibition [137]. Polysome profiling is a technique used for investigating the cellular translational status, and consist of quantifying ribosome loading of each mRNA as an indication of translation efficiency [292]. Polysomes are defined as mRNAs occupied by two or more ribosomes, and monosomes consists of ribosomal subunits that have associated in the absence of mRNA [293]. Polysome profiling of rapamycin treated cells revealed mRNAs shifting from polysomes to monosomes, indicating a slowdown in translation initiation, and consequently a decrease of the growth rate when mTOR was inhibited, whereas feed supplements increased mTOR activity and productivity of the cell lines [66].

High lysosome content cells did not display an increase in overall autophagic flux. LC3B-II levels were marginally elevated in control cells compared to high lysosome content cells, but there were no differences in the LC3B-I/LC3B-II ratio, nor in p62 levels. Atg5-Atg12 complex, Lamp1 and Lamp2A were present at higher amounts in control cells than in high lysosome content cells, indicating a potential increase in late-stage autophagy. Apoptosis initiation was detected via the biomarkers in control cells, with increased amounts of cleaved caspase 3, the active form of caspase 3, but no differences between caspase 3 and Bcl-xL amounts were observed. The decreased amount of cleaved caspase 3 in high lysosome content cells indicate that they appear more resistant to apoptotic stimuli

on day 7 of FBOG culture, and thus have higher culture viabilities maintained for the following culture days. Consistent with our findings, decreased mTOR expression and decreased cell death have been associated with increased productivity, as growth rate is inversely proportional to the proportion of apoptotic cells [294], and minimal growth rate is essential for maintenance of culture viability and overall increased production [295-297].

Delaying and inhibiting apoptosis has been a widely investigated strategy to increase culture duration and cell recombinant protein productivity. NS0 pools derived from a cell line expressing a gene of interest but transfected with the neomycin gene, used as a selection marker, have recorded up-regulation of Bcl-2 compared to the original clonal cell line. Although the increase corresponded with an increased specific growth and maximum viable cell concentration, through resistance of early onset apoptosis associated with an increase in Bcl-2 expression, monoclonal antibody production rate was 70% lower than the control cell line [298]. The effect of Bcl-2 overexpression have been varied across cell lines, the antibody expressed, and culture conditions, with studies observing several fold increase in production [182, 299, 300], a modest increase of 38% in antibody titre [301], or no improvement at all [183, 302, 303]. Bcl-xL overexpression has also been associated with increased productivity [304, 305], however no increase in Bcl-xL expression was observed on day 7 in the cells investigated here. Analysis of other pro-survival members of the Bcl family could inform more on the apoptotic state of the cells. Collectively the western blot data in this study suggests that the increased productivity of the high-lysosome content sorted cells may have delayed activation of apoptosis, possibly through decreased mTOR expression compared to control cells. Moreover, there a slight increase in autophagy initiation, and late stage autophagy, as shown by the different markers investigated, on day 7 in the control cells compared to the high lysosome sorted cells.

In conclusion, cell sorting based on high-lysosome content has the potential to isolate higher producing cell lines. This increase in productivity varied depending on which molecules was expressed, probably based on what is the bottleneck for their expression. Moreover, the lysosome-based cell sorting was only successful in pre-mixed known populations, but not on the enrichment of individual clonal cell lines. Further work would need to be performed on freshly transfected pools to see if lysosome can increase productivity in a cell line development workflow. The increase in productivity ranged from 30% to 100% compared to unsorted control. The lysosome staining protocol has the advantage of being fast and easy and could be useful for the enrichment of high producing, homogeneous cell lines with increased apoptotic-resistance.

CHAPTER 5

Directed evolution of the CHO host cell line using chloroquine

5.1 Introduction

The work reported in Chapter 4 revealed that cell sorting based on increased lysosome content showed a positive impact on recombinant protein production, with an increase in final titre as a result of an increased homogeneity of the expressing pool and sustained culture viability. The increase in titre was observed for the two molecules investigated, an ETE mAb and a bispecific, but the scale of the impact was molecule-specific, with the harder to express molecule titre increasing ~30%, compared to a 100% increase in titre for the easier to express molecule. Moreover, lysosome-based cell sorting requires a flow cytometer capable of live cell sorting based on lysosome content, which are not incorporated into all cell line development platforms, as other methods such as ClonePix or single printing are also used to generate monoclonal cell lines. To determine whether manipulation of the lysosome content of CHO cells can result in isolation of cells with increased productivity, a directed evolution of the host cell line was undertaken. The aim of this approach was to increase the lysosomal content of the host cell line, and to test the hypothesis that recombinant cell lines derived from this host would also have a higher lysosome content and associated higher productivity. This novel host could then be used in a cell line development platform regardless of the cloning method, without using a FACS screen for lysosome content.

5.1.1 Directed evolution

Directed evolution is a powerful method for improving and engineering novel biological systems. Directed evolution relies on the fundamental principles of Darwinian evolution: genetic diversity manifesting as different phenotypes, and the selection, or survival, of a certain phenotype, hence strengthening and amplifying the corresponding genotype [306]. Directed evolution is described as the process of applying a selective pressure to a system and isolating those individuals in a population that 'succeed' under those conditions. This results in a population with beneficial heritable mutations or characteristics [306, 307]. Directed evolution, in cells for example, is of particular interest to the biopharmaceutical community, as the whole genome can contribute to a specific phenotype. Applying selective pressure to the cell can lead to the evolution or selection of novel complex phenotypes, that

do not only involve one gene, but potentially the entire genome [306]. Often, the selective pressure used is a mutagenic compound or stressor that can induce a higher rate of mutation in the host [308]. Other strategies involve the use of initiators or inhibitors of specific metabolic pathways, to generate novel systems with improved metabolic functions, in which the cells compensate for loss of function in one pathway by up-regulating other genes/proteins in the same, or associated, pathway [308, 309]. Addition of compounds that produce a selective pressure will screen for pre-existing diversity, or introduce diversity if the compound is mutagenic, into the system: systems that survive those conditions and those who do not. The selection and enrichment of the desired phenotype-genotype occurs naturally through differences in cell survival, or growth rate. The desired cellular phenotype can also be isolated by methods such as flow cytometry, if a fluorescent marker for the phenotype is used.

Mammalian cell lines have proven to be an intricate system for directed evolution, due to their longer doubling time and complex cellular pathway, and therefore most published works relying on directed evolution have been performed on bacterial cells. However, directed evolution in mammalian systems has been successfully reported, including in fibroblasts [310], B-cells [311, 312] and CHO cells [313]. One particular study focused on the somatic hypermutation ability of Ramos B-cells to enhance the anti-apoptosis protein Bcl-xL [311]. Ramos B-cells were subjected to repeated staurosporine treatment, an apoptosis-inducer, and allowed to recover. Cells that did not succumb to cell death developed a resistance to the staurosporine treatment, illustrated by decreased initiation of apoptosis when treated with staurosporine. Sequencing of the Bcl-xL gene identified one mutant that was found at an increased level in the staurosporine-resistant population. This Bcl-xL mutant was then over-expressed in CHO cells, and resulted in enhanced apoptosis resistance, when subjected to staurosporine treatment [311]. Another group also exploited the B-cell hypermutability, being prone to mutations, in a chicken B-cell line DT40. Cells were transfected with GFP in the IgG light chain rearrangement locus and were enriched multiple times by flow cytometry based on GFP fluorescence. This led to the isolation of cells expressing a GFP variant with superior fluorescence than the initial commercially available GFP transfected [312]. In another study, directed evolution was performed on β3 integrin to identify variants with novel transmembrane topography. This was performed in CHO cells, transfected with lentiviral plasmids encoding a library containing random mutations of the protein of interest, screened by flow cytometry and further characterised by PCR [313]. Finally, Stanley et al. generated novel lectin-resistant CHO cells, for the generation of novel glycosylation mutants, using cytotoxic plant lectins as selective pressure [314].

In the work reported in this chapter, by applying the principles of directed evolution, a new evolved host cell line was generated. This novel host cell line was treated with agents to increase the lysosome

content, as previous findings have showed increased lysosome content to correlate with improved mAb production. The chemical chosen as a selective pressure was chloroquine, a lysosomotropic agent.

5.1.2 Chloroquine

Chloroquine (CQ), N'-(7-chloroquinolin-4-yl)-N, N-diethyl pentane–1,4-diamine, is an affordable generic drug best-known for treatment of malaria and inflammatory disorders. Its lipophilic tendency allows it to permeate the lipid bilayer and enter cells [315]. As a weak base, the unprotonated-form of CQ diffuses freely and rapidly across a pH gradient into acidic subcellular compartments such as lysosomes and endosomes, where it becomes protonated (Fig. 5.1) [316]. As the lysosome's pH is ~ 4.5 and the cytoplasm's ~7.4, this pH gradient leads to the hyper-accumulation of CQ in the lysosome, up to 10,000-fold higher than its extracellular concentration via pH portioning, when a base accumulates in an acidic compartment [317]. The protonated CQ cannot pass through lipid membranes and therefore becomes trapped in acidic organelles, increasing the lysosomal volume in the cell (Fig. 5.2) [318, 319].

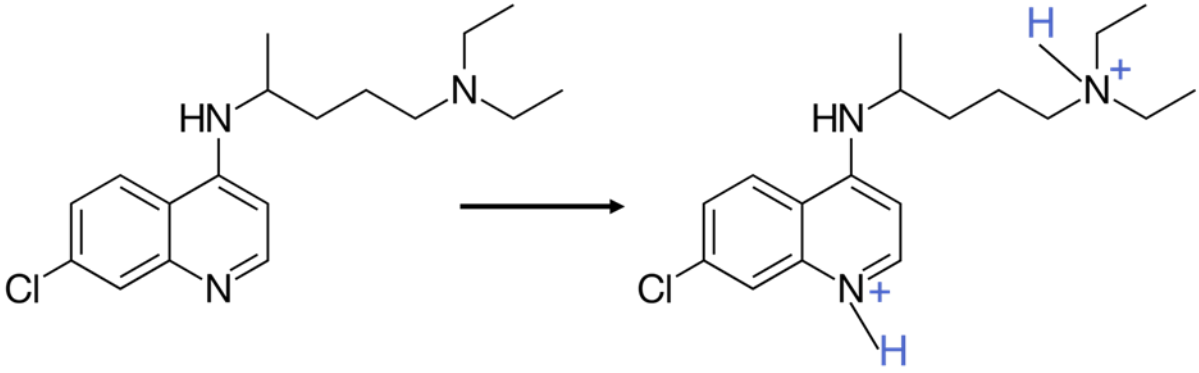

Figure 5.1 Conversion of chloroquine to its protonated form

CQ has been reported to have a wide range of effects on the cell. One of the main mechanisms of action is its lysosomotropic effect, which results in significant alterations in protein synthesis, processing and degradation, and blocking autophagy by inhibiting lysosomal proteases [320]. CQ accumulation in lysosomes inhibits the last stage of autophagy by blocking the fusion of autophagosomes with lysosomes (Fig. 5.2) [321]. As accumulation of autophagosomes is toxic to the cell, this results in apoptosis [316, 322, 323]. However, CQ has also been reported to inhibit mTORC1 activity in a Rag-dependent manner and trigger lysosomal biogenesis through activation and translocation of TFEB and TFE3 to the nucleus (Fig. 5.2)

[160, 161, 324]. This suggests that mTORC1 downregulation and the increased lysosomal stress acts as a feedback mechanism to initiate an increase in autophagic capabilities [324, 325].

Another mechanism of action of CQ is its ability to inhibit DNA polymerase at low concentrations and even block DNA synthesis at high concentrations (Fig. 5.2) [317, 326]. Its role in cancer treatment as an anti-neoplastic agent has been investigated due to its ability to trigger G0/G1 cell cycle arrest and delay cell growth [327, 328] and its genotoxic effect leading to DNA damage and induction of apoptosis [328]. Moreover, it was found that CQ treatment of liver cancer cells led to a significant upregulation of the pro-apoptotic protein Bim, loss of mitochondrial potential leading to cytochrome c release from the mitochondria and caspase 9 activation [328]. CQ has also been found to induce p53 and p21 proteins leading to apoptosis, as well as necrosis in some cases [316]. Additionally, accumulation of CQ can lead to inhibition of the enzymes phospholipase A2, lysophospholipid acylhydrolase and monoacylglycerol lipase, interfering with the proteolytic process and the formation of new glycolipids, and altering many signalling pathways [316].

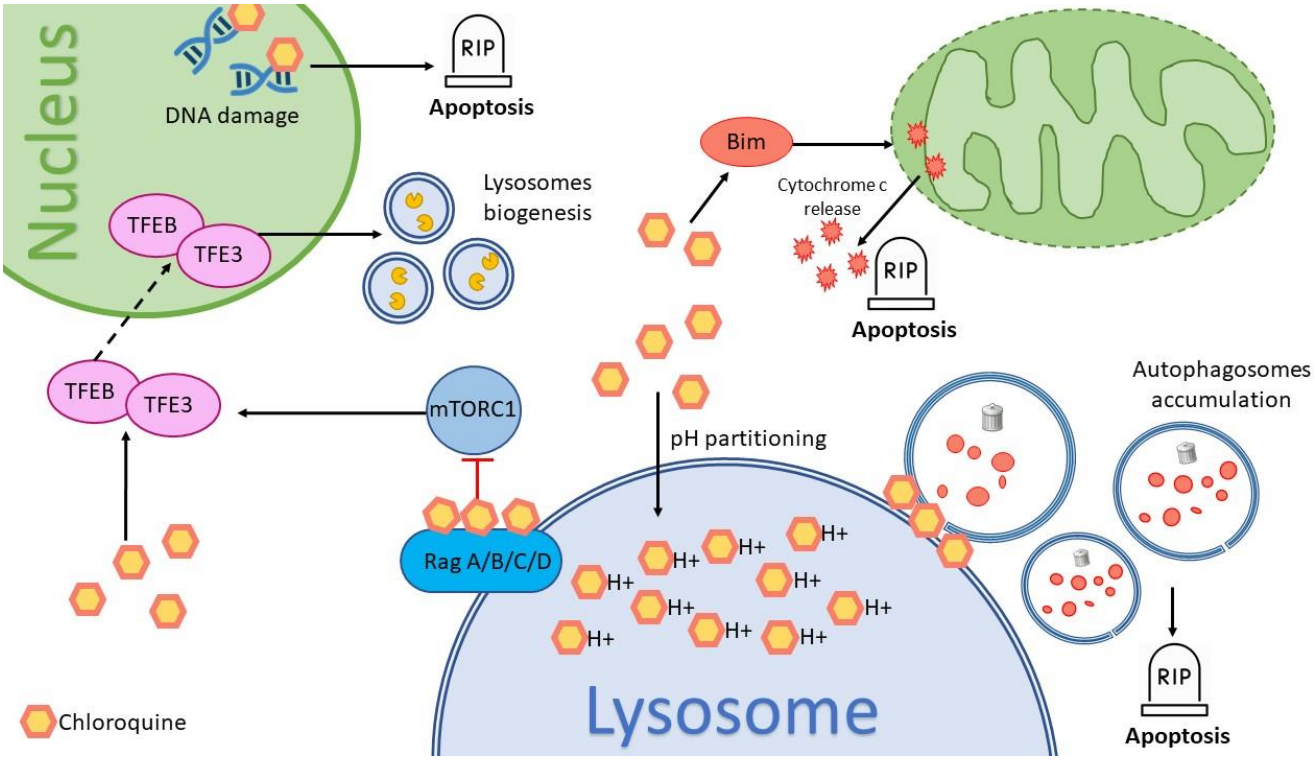

Figure 5.2 CQ mechanism of action. Due to a pH gradient, CQ accumulates in the lysosome, where it gets protonated and cannot escape. CQ inhibits mTORC1, by preventing it binding to Rag A/B/C/D, which stimulates TFEB/TFE3 translocation to the nucleus, initiating lysosome biogenesis. CQ also prevents fusion of the autophagosome with the lysosomes, leading to their accumulation which causes apoptosis. Apoptosis can also be initiated by severe DNA damage with high CQ concentrations, or through Bim activation, which leads to cytochrome c release from the mitochondria.

5.1.3 Directed evolution of the host cell line using chloroquine

The generation of a novel CHO cell host through chemical directed evolution using CQ as a selection agent was investigated. The standard host cell line (not transfected) was treated with CQ over a period of time, until it behaved similarly in terms of growth and culture viability to the non-treated control host. Once the CQ-evolved host was established, it was transfected with three different molecules: the standard ETE mAb used in the previous chapter, a DTE mAb, and the bispecific mAb used in the previous chapter. Transfected CQ-evolved host cells were assessed under FBOG conditions, alongside the transfected standard host as a control, to determine if the novel host had increased productivity or maintained culture viability longer. To assess the underlying differences between the CQ-evolved host and control host, and determine the mechanism behind any differences, transcriptomics and western blotting analysis was undertaken to identify changes at the transcript and protein level respectively.

5.2 Results

5.2.1 Development of a novel host via directed evolution using chloroquine

CQ was chosen as a lysosomotropic agent to drive and increase cellular lysosomal content, with the aim of increasing recombinant protein production. As discussed, CQ accumulates inside the lysosomes and prevents the fusion of autophagosomes with lysosomes. This in turn activates the CLEAR pathway for lysosome biogenesis [160]. However, as the effect of CQ is concentration and time-dependent, high CQ concentrations or prolonged treatment can be harmful to cells, blocking DNA synthesis [326], and even triggering apoptosis [316]. It was thus essential to identify appropriate CQ concentrations to use for directed evolution.

5.2.1.1 Initial CQ concentration screening

Initially, five concentrations of CQ were investigated on the untransfected host: 10, 50, 100, 300 and 500 µM (Fig.5.3). Cells were inoculated at $0.3x10^6$ viable cells/mL, treated with CQ and monitored everyday over a 72-hour period. Initial concentration screening revealed a drastic decrease in culture viability and cell growth (Fig. 5.3A and B), to below 20% within 72 hours for concentrations above 100 µM. Cells treated with 50 µM CQ had a culture viability of 70% after 72 hours (Fig. 5.3B, light blue), and appeared to have entered cell cycle arrest (Fig. 5.3A, light blue). Cells exposed to CQ treatment at 10 µM had growth and culture viabilities similar to the control (Fig. 5.3 A, B, red and blue).

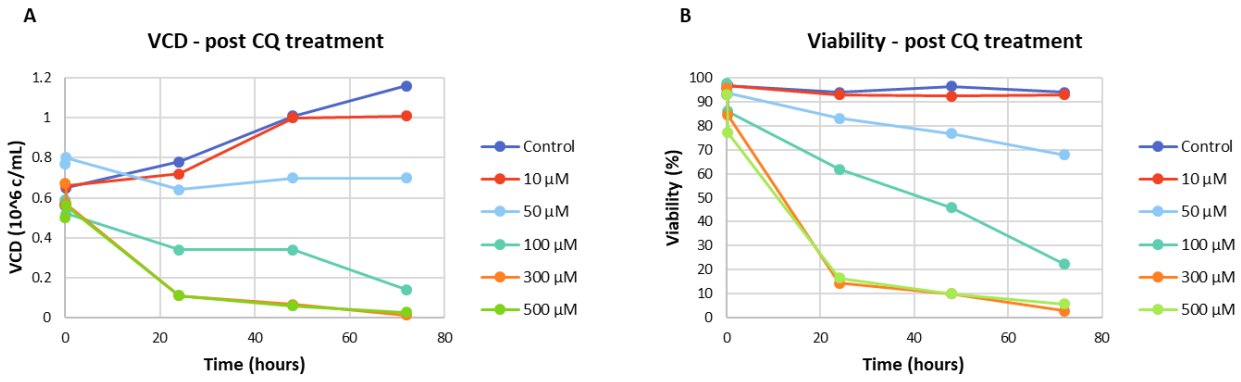

Figure 5.3 Screening of a range concentrations of CQ for directed evolution. CHO cells were treated with a range of CQ concentrations for 72 hours. A) Viable cell concentration of the cells following the CQ treatment, and B) the culture viability. Control corresponds to untreated cells. N=1 for each point.

5.2.1.2 Long-term CQ treatment of CHO cells

Cell cultures that maintained a sufficient viability (Control, 10 µM and 50 µM) were passaged after initial treatment, and CQ treatment was then added following each passage at the same concentration. Cells were first passaged on Monday/Wednesday/Friday, and from day 20 onward, only on Monday/Friday, allowing a longer recovery time between each CQ treatment. Cell counts were taken before and after each passage. CQ treatment was performed over a 41-day period, 15 passages, until treatment no longer impacted culture viability or growth compared to the control.

Treatment with 50 µM CQ led to decreased culture viability, below 50% within 3 passages (Fig. 5.4 B, light blue), and was thus not used for further culturing. From passage 12, cells treated with 10 µM CQ showed a similar growth (Fig. 5.4 A, blue) and culture viability (Fig. 5.4 B, blue) to the control cells. Cells were passaged three more times to ensure that the growth and culture viability were maintained, and cell stocks banked, for both the CQ-evolved and control cells.

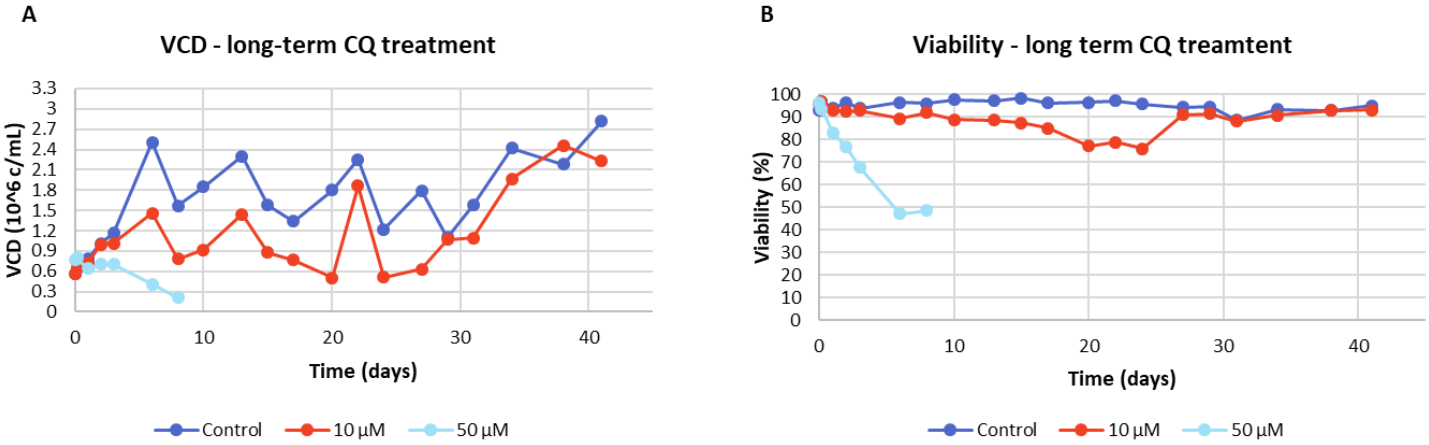

Figure 5.4 Long term CQ treatment of untransfected cells. Control (blue) and cells treated with 10 µM CQ were cultured over 15 passages, with CQ added at each passage. A) VCD and B) culture viability were monitored before each passage. Passage schedule switched from Monday/Wednesday/Friday to Monday/Friday on day 20. N=1 for each point.

5.2.1.3 Chloroquine removal and re-introduction

To assess whether the cells had developed a robust CQ resistance, CQ-treated cells (Fig. 5.5, red) had their treatment removed for 4 passages (Fig. 5.5, green) and then re-introduced (Fig. 5.5, maroon). The untreated control cell line (Fig. 5.5, blue) was cultured alongside. Cell counts and culture viability measurements were taken at each passage. Culture viability (Fig. 5.5 A) remained >94% for all conditions. Following removal of CQ treatment, culture viability increased to a small degree (Fig 5.5A,

green line 94.8% for the treated cells vs. 97.5% on day 11), and growth was marginally higher (Fig. 5.5B, green). CQ was reintroduced on day 18, with the first assessment of these cells on day 21, and the final time point on day 28. Culture viability was not affected (Fig. 5.5A, maroon line) by the CQ reintroduction. Growth was lower on day 25 ($2.83x10^6$ c/mL vs. $5.18x10^6$ c/mL), but no differences were observed on day 28. CQ treatment of the control host cell line was not performed.

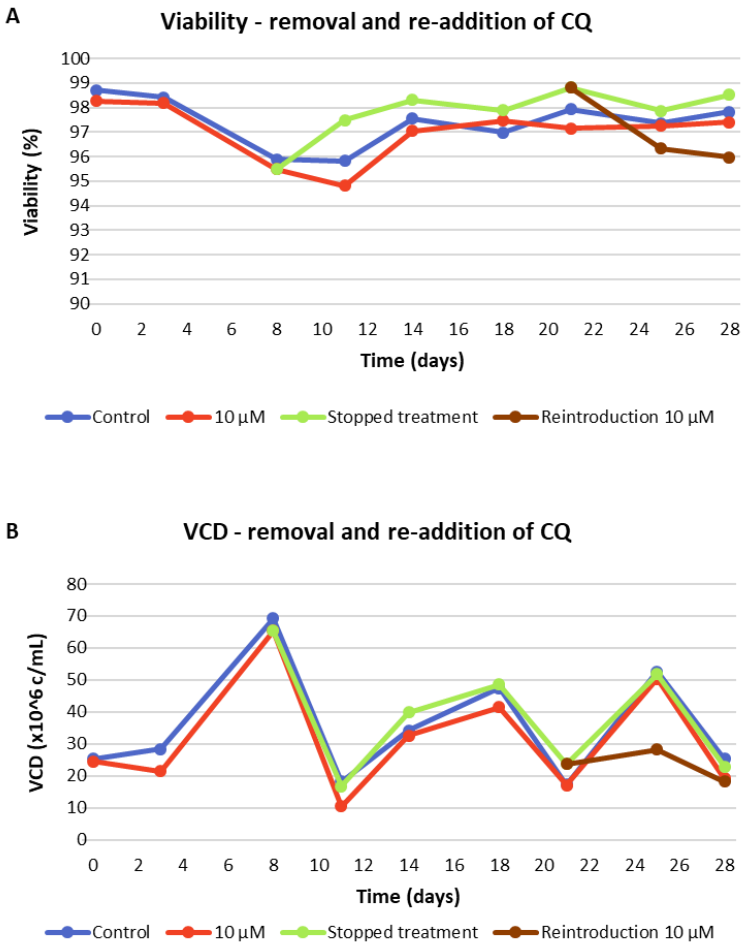

Figure 5.5 Removal of CQ treatment and re-introduction. A) Culture viability, ranging from 90 to 100% and B) VCD of the control (blue), the CQ-treated cells (red), the cells for which CQ treatment was stopped (green) and then reintroduced (maroon). N=1 for each point.

5.2.2 Strategies for chloroquine treatment of the chloroquine-evolved host post-transfection

Having developed a novel and robust CQ-evolved CHO cell host, its performance in terms of recombinant protein production was assessed. To do this, the evolved and standard non-evolved host were transfected with two different molecules: the ETE mAb (used in Chapters 3 and 4) and a DTE mAb. Initially, a single pool was generated for each molecule and each host. The standard non-evolved host used was the control cultured and banked down at the same time as the CQ-evolved cells, to ensure all cell lines had undergone the same number of passages.

Thawed cells were treated with 10 µM CQ on the second passage after thawing, until transfection. Following recovery from transfection, different CQ treatment strategies were investigated (Fig. 5.6): no CQ treatment, treatment with 10 µM CQ until the last passage before the start of the FBOG, CQ additions until day 0 of the FBOG, addition on day 0 and 3, or on day 0, 3 and 7 of the FBOG. The initial assessment of the different strategies for CQ-addition were tested for the ETE and DTE mAb, without replicates. Cells were evaluated in a 14-day FBOG process with data recorded for growth (Fig.5.7), productivity (Fig.5.8) and lysosome content (Fig.5.9).

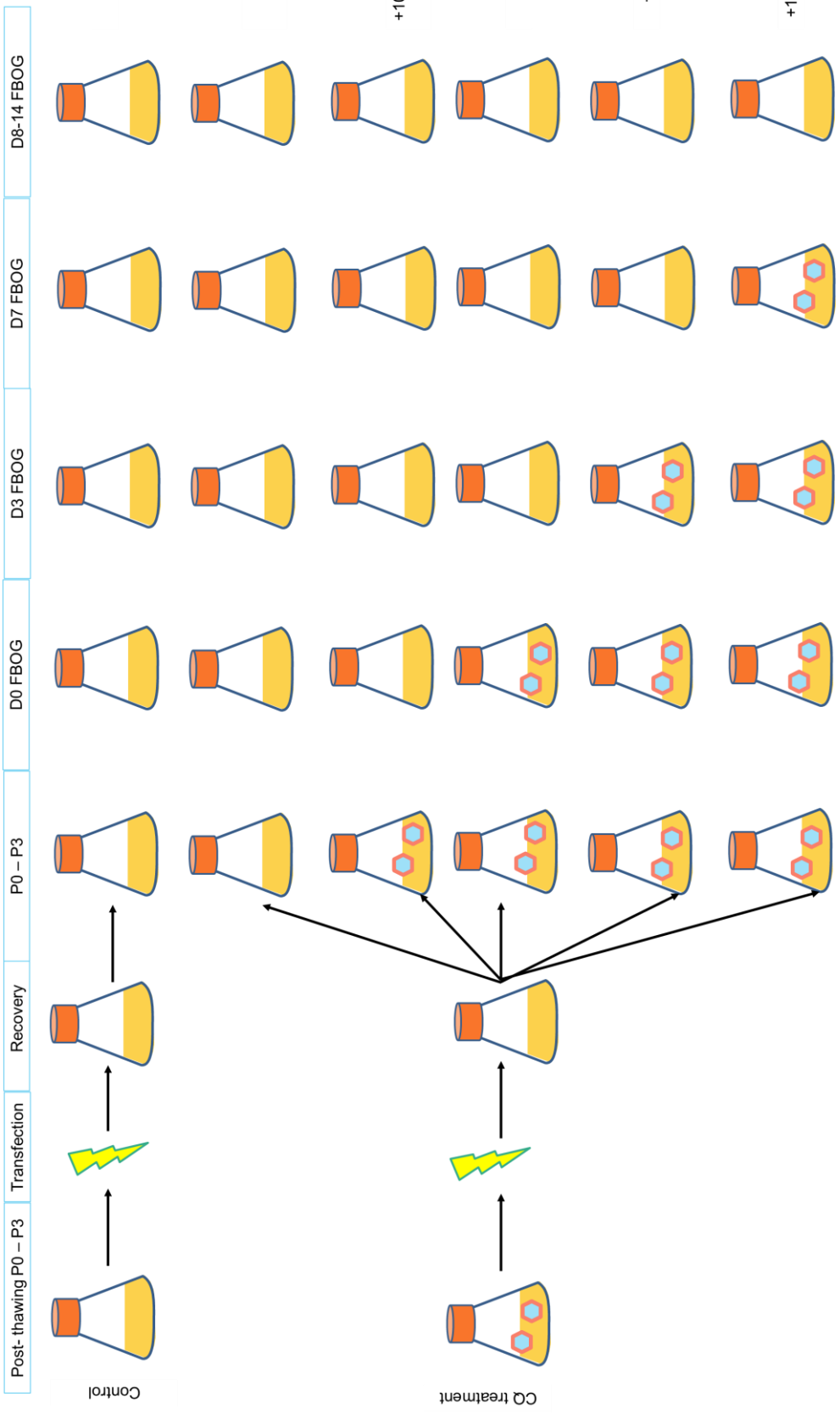

Figure 5.6 Chloroquine treatment strategies following transfection. The top row is the control cell line, that was not treated with CQ. All CQ-treated conditions originate from the same shake flask, that was treated with CQ until transfection. Following transfections, cells were either not subjected to CQ-treatment, or CQ-treatment was stopped at various stages, up to day 7 of the FBOG.

5.2.2.1 Growth profiles of CQ-treated recombinant protein expressing pools

Growth analysis of the ETE mAb pools revealed two conditions that reached a higher IVC than the control cell line (Fig.5.7A, final IVC 3470 $x10^9$ cell hr/L): the strategy that did not have CQ treatment following transfection (4643 $x10^9$ cell hr/L), and the strategy for which CQ treatment stopped at the last passage prior to commencing the FBOG (4247 $x10^9$ cell hr/L). The other CQ-treatment conditions obtained lower IVCs than the control (ranging from 1559 $x10^9$ cell hr/L to 2550 $x10^9$ cell hr/L). For the DTE mAb pools, the same two conditions; CQ treatment removed at passage pre-FBOG (Fig.5.7B; 3404 $x10^9$ cell hr/L) and CQ treatment stopped post-transfection (2751 $x10^9$ cell hr/L) reached a higher IVC than control (1871 $x10^9$ cell hr/L), as well removing CQ treatment on day 0 (2184 $x10^9$ cell hr/L) or day 3 (1984 $x10^9$ cell hr/L). Continuous CQ treatment throughout the FBOG seemed to have a negative impact only for the ETE mAb, with the growth for the DTE mAb being less affected. Moreover, for both conditions, allowing time for recovery either by removing CQ treatment after transfection or after the last passage prior to fed batch led to increases in IVC compared to the control.

For both molecules, all CQ treatment resulted in culture viability being maintained for longer and higher than the control (Fig.5.7 C, D) except for the continuous CQ treatment up to day 7 for the ETE mAb where culture viability started to decrease on day 7 for both molecules. On day 10 for the ETE mAb pool, the culture viability of the control cell line had decreased to 67.6%, whereas the other CQ-treated conditions ranged from 82.4 and 93.1% viability (Fig.5.7 C; except for the +10 CQ on day 0, 3 and 7). For the DTE mAb, culture viability on day 10 had dropped to 19.3% for control cells, while the other conditions maintained viabilities ranging from 42.7 to 71.2% (Fig.5.7 D). For both mAbs, stopping the CQ-treatment after transfection resulted in the highest maintained culture viability.

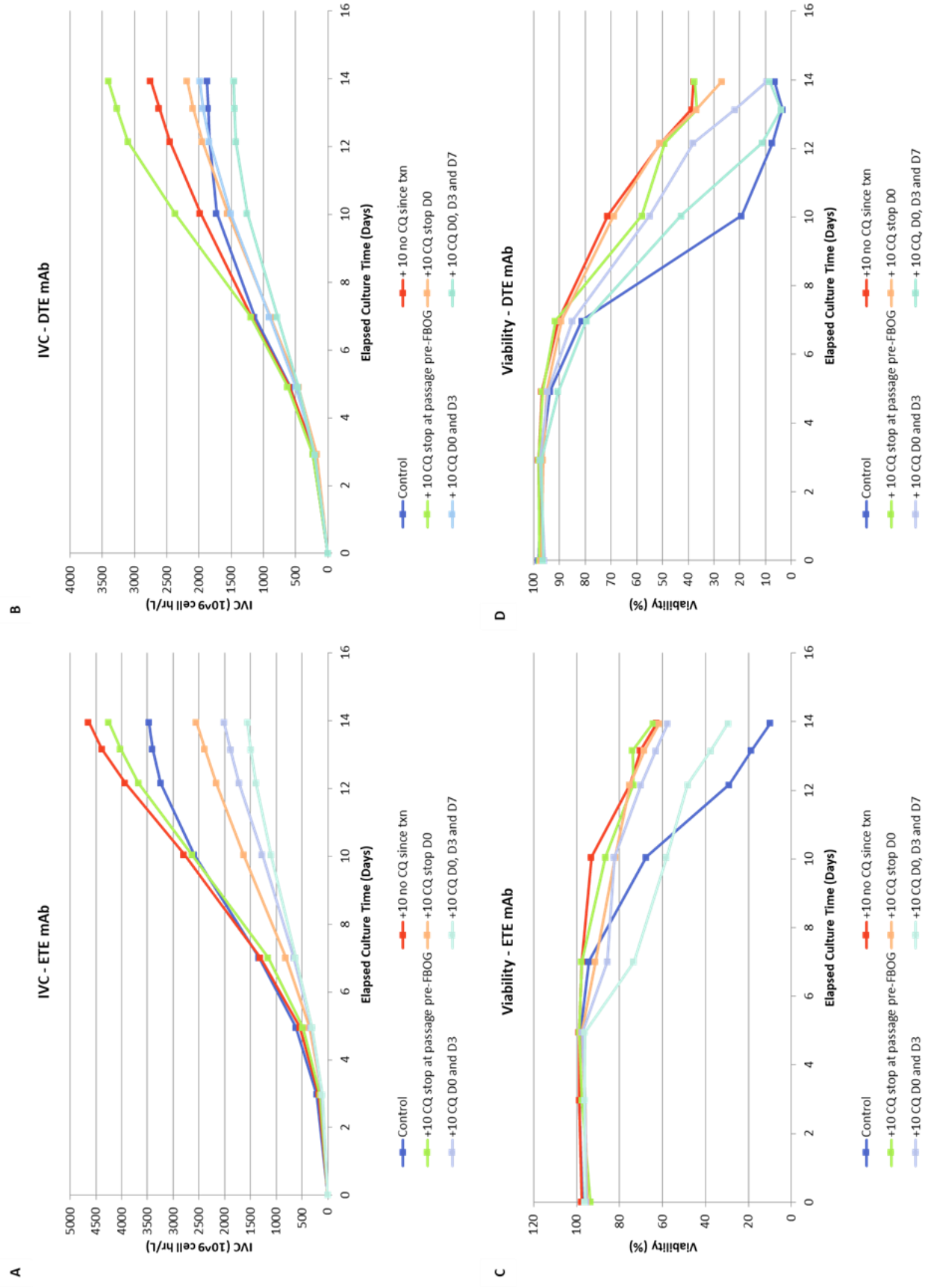

Figure 5.7 IVCs for the A) ETE mAb and the B) DTE mAb, as well as culture viability for the C) ETE mAb and D) DTE mAb. Control cell line (no CQ treatment) is in blue, and the other conditions represent different CQ-treatment strategies following transfection with the ETE or DTE mAb. N=1 for each point.

5.2.2.2 mAb productivity of CQ-evolved cells

mAb productivity was increased in the CQ-treated cells compared to the control (Fig.5.8). For the ETE mAb, the control had an overall qP of 9.0 pg/cell/day, while the CQ-treated cells achieved qPs ranging from 12.5 to 29.7 pg/cell/day (Fig.5.8 A). Similar increases were observed for the DTE molecule, for which the control qP was 3.53 pg/cell/day, while the CQ-treated cells qPs ranged from 10.7 to 18.9 pg/cell/day (Fig.5.8 B). Overall titre was also drastically improved for both molecules under some of the conditions. For the ETE mAb (Fig.5.8 C), the control produced a maximum titre of 1646 mg/L. Some CQ-conditions had a similar titre (1846 mg/L for the CQ-treatment on day 0 and day 3), or lower (885 mg/L for the CQ-treatment on days 0, 3 and 7). The condition where CQ-treatment was stopped on day 0 of the FBOG had a minor increase in titre (2159 mg/L) compared to the control cell line, whereas conditions where CQ treatment was stopped post-transfection or at the passage before FBOG had a large titre increase compared to control cells (4834 mg/L when stopping CQ treatment after transfection, and 4192 mg/L where stopping the treatment at the passage prior to the FBOG). For the DTE mAb, control cells reached a titre of 205 mg/L, whereas the titre from the various CQ conditions ranged from 507 to 1545 mg/L (Fig. 5.8 D).

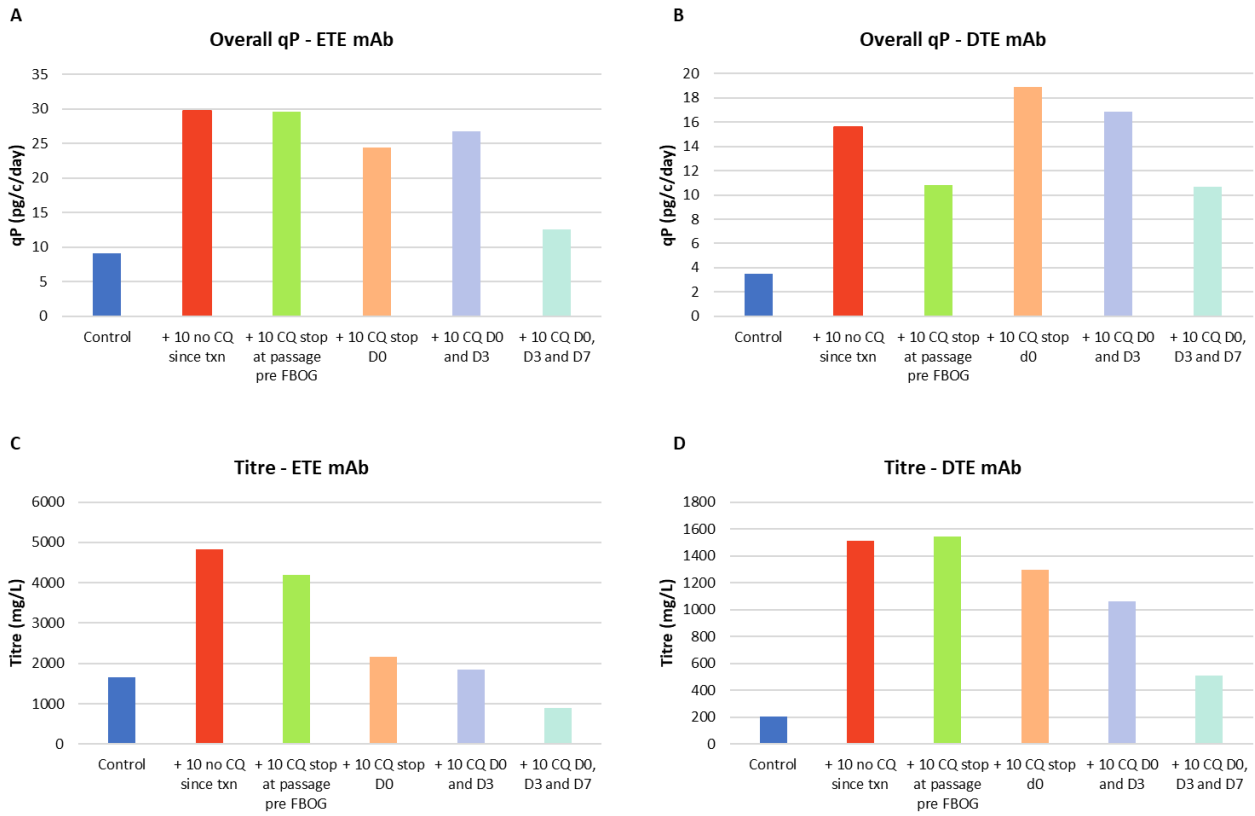

Figure 5.8 qP for the A) ETE mAb and B) DTE mAb, and final titre for the C) ETE mAb and D) DTE mAb in control and CQ-evolved and treated cells. The control corresponds to the cell line without any CQ-treatment. The other conditions are for the different strategies of CQ-treatment following recovery after transfection. N=1 for each bar.

5.2.2.3 Analysis of the lysosome content in CQ-evolved and control cells

Lysosome content was measured prior to the start of the FBOG (day 3 post passage 3) and during FBOG on days 3 and 7 for the control and CQ-evolved pools. Control cells and cells that had not been treated with CQ since transfection had a similar lysosome content on day 3 of the 3rd passage, whereas cells that were still being treated with CQ had ~5-fold higher lysosomal content for both the ETE (Fig.5.9A) and DTE mAb (Fig.5.9B), consistent with the lysosomotropic effects of CQ.

On day 3 of the FBOG, control cells and evolved cells that had not been treated with CQ still had the same lysosome content as prior to the FBOG, while cells for which the CQ-treatment was stopped at the last passage prior to the start of the FBOG showed a ~4-fold increase in lysosome content for the ETE mAb (Fig.5.9 C) and a 2-fold increase for the DTE mAb (Fig.5.9 D). Cells where CQ treatment was added on day 0 of the FBOG still showed an elevated amount of lysosome compared to the control, a ~9-fold increase for the ETE mAb (Fig.5.9 C) and a ~5-fold increase for the DTE mAb (Fig.5.9 D). Thus, 3 days after stopping CQ-treatment, cells were still affected by the previous exposure to CQ, although the effects were reduced. Continuous treatment with CQ maintained a large increase in lysosome content within the cells. As CQ blocks the fusion of autophagosomes and lysosomes, lysosome biogenesis is triggered to increase lysosome content for autophagosome processing. On day 7 of the FBOG, control cells and cells that had not been treated with CQ since transfection had similar levels of lysosome content for the ETE mAb (Fig.5.9 E) but not for the DTE mAb (Fig.5.9 F), for which the control was lower by ~2-fold. The other CQ-treated conditions had increased levels of lysosomes, although the levels decreased as time since the last CQ treatment increased.

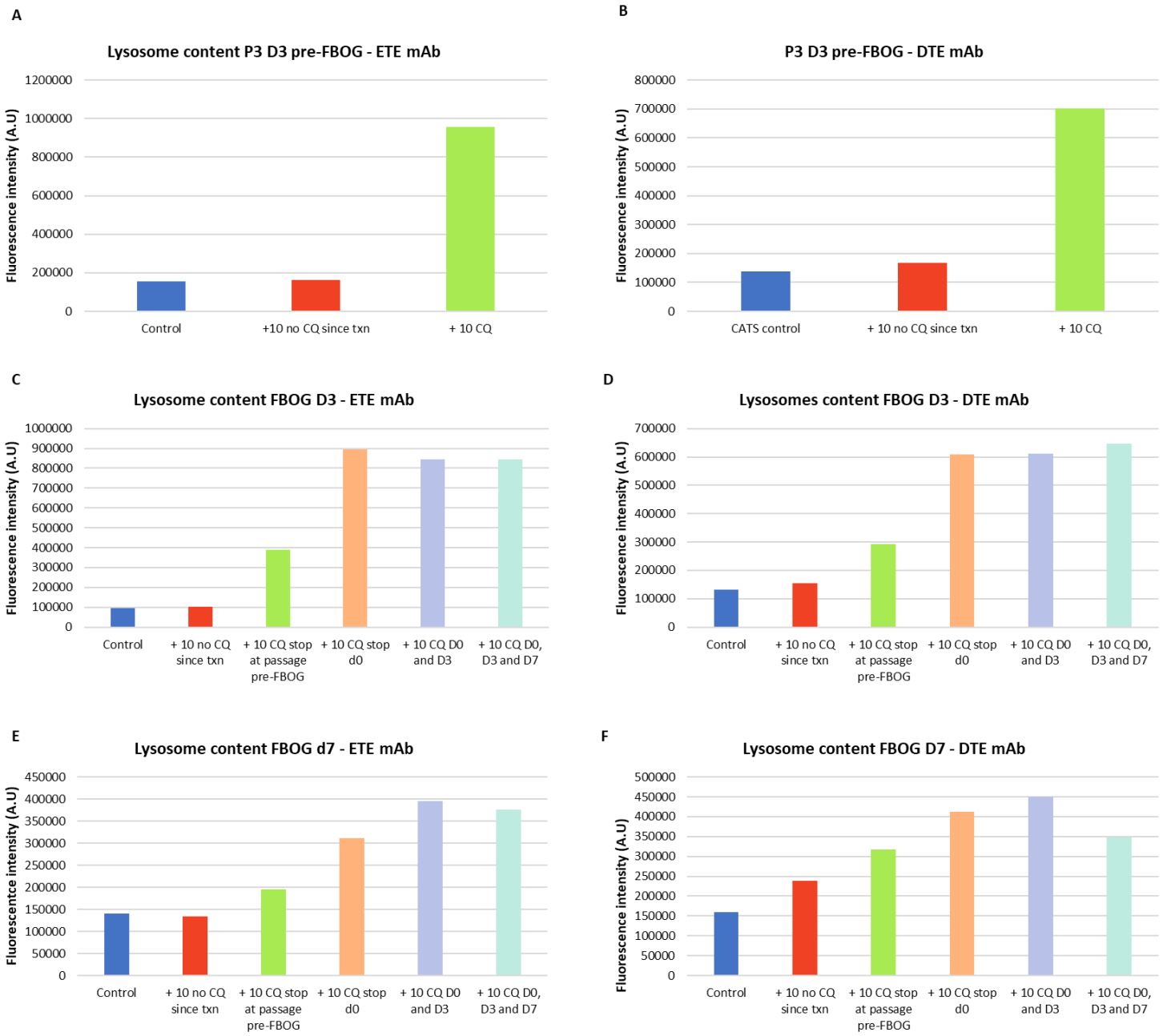

Figure 5.9 Lysosome content on day 3 of the FBOG for the control cells and CQ-evolved cells and the A) ETE mAb and B) DTE mAb. Lysosome content on day 7 of the FBOG for the C) ETE mAb and D) DTE mAb. The control corresponds to the cell line without any CQ-treatment. The other conditions are the different strategies of CQ-treatment following recovery after transfection. N=1 for each bar.

As the no CQ treatment following transfection gave the best results in terms of titre, and was the shortest treatment length, it was the chosen condition for further work. The no CQ treatment following transfection is thus hence referred to as CQ-treated cells, CQ-evolved, or 10 CQ onwards. New triplicate pools were generated, using three different molecules: the ETE mAb, the DTE mAb and a bispecific mAb (used in Chapter 4). Both the CQ-treated and control triplicates pools were further characterised in FBOG conditions.

5.2.3 Evaluation of the chloroquine evolved host expressing an ETE mAb

5.2.3.1 Culturing of chloroquine – evolved host expressing an ETE mAb

The standard control host and the CQ-evolved host were transfected with an ETE mAb and assessed under FBOG conditions. The CQ-evolved host had a higher IVC than the control (Fig 5.10 A) and maintained a higher culture viability for longer (Fig. 5.10 B). Control cells culture viability declined after day 7, with 79% culture viability on day 10 (vs. 89 for CQ-evolved), and 50% on day 12. CQ-evolved cells had a two-fold increase in final titre compared to control cells (Fig. 5.10 C; 2393 vs. 4957 mg/L, p=0.00010), and an overall qP approximately twice that of the control (Fig. 5.10 D; 12.4 vs. 24.0 pg/cell/day, p=0.00020). The CQ-evolved cells reached a higher cell concentration and had delayed cell death, explaining some of the increase in titre compared to the control.

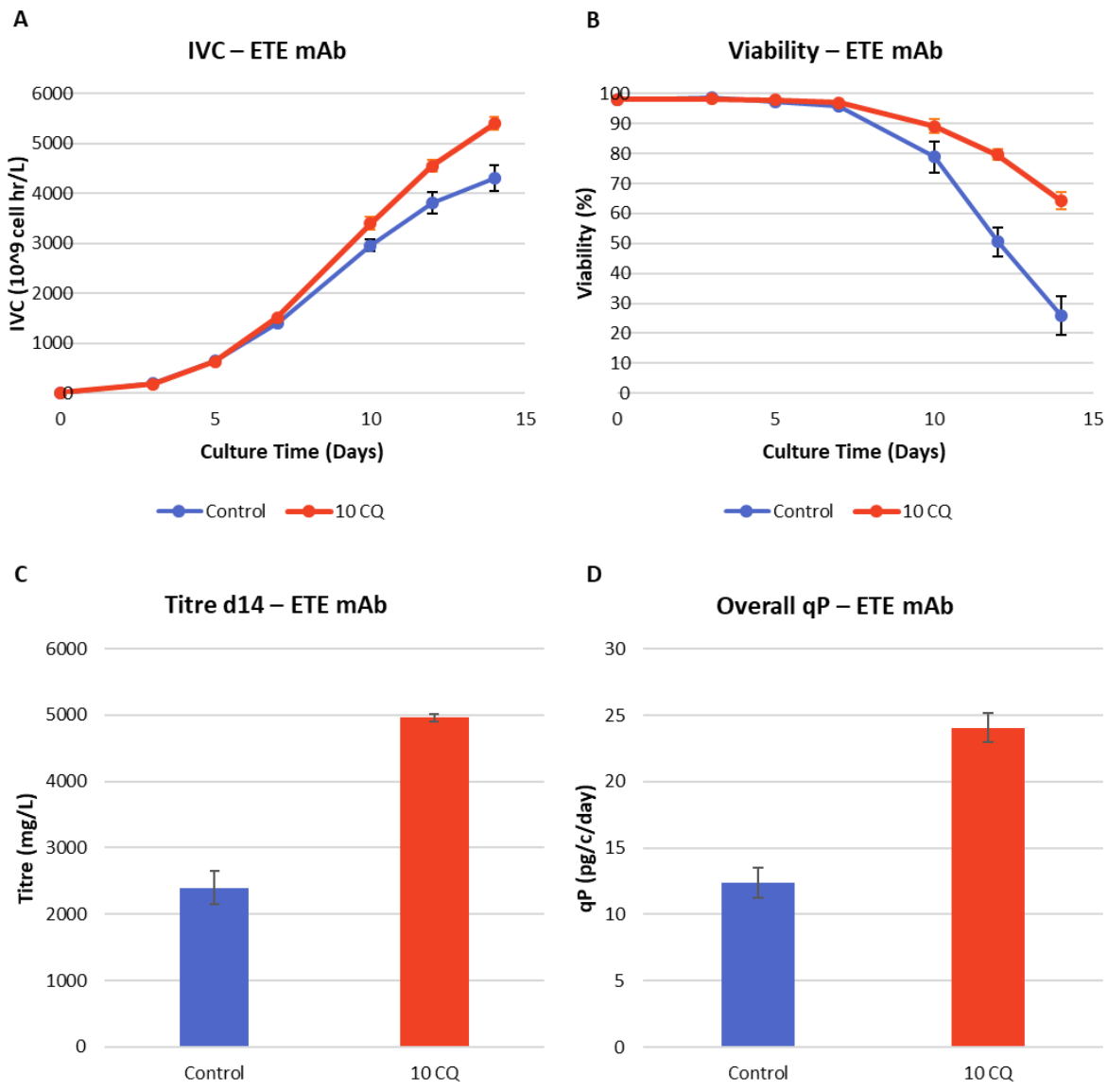

Figure 5.10 FBOG cell culture data comparing the control (blue) and CQ-evolved (10 CQ) pools, expressing an ETE mAb in terms of A) IVC, B) culture viability, C) mAb final titre (p=0.00010) and E) overall qP (p=00020). N=3, the mean is shown and error bars = standard deviation.

5.2.3.2 Analysis of intracellular HC and LC content of the chloroquine evolved host expressing an ETE mAb

Intracellular HC and LC protein were quantified by flow cytometry on day 3 for the control and CQ-evolved cells expressing an ETE mAb. The analysis revealed a heterogeneity in HC and LC protein expressing populations for both hosts (Fig. 5.11), with 84.0±0.9% cells positively expressing both HC and LC for the control (Fig.5.11, Q2) and 88.8±1.4% for the evolved host. Therefore, the differences in productivity observed are not due to different ratios of expressing populations.

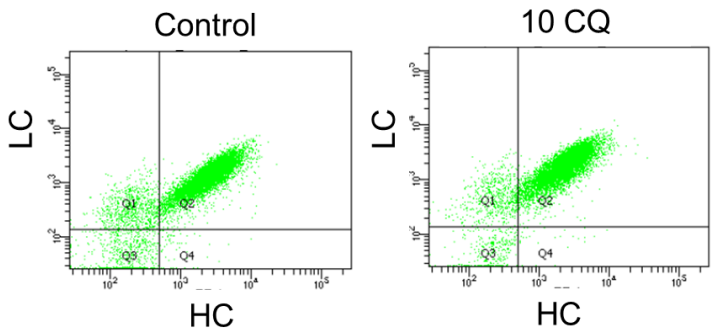

Figure 5.11 Intracellular HC and LC protein for the ETE mAb in the control and CQ-evolved cells showing the existence of homogenous expressing populations. Images are representative of the triplicate samples.

5.2.3.3 Product quality analysis of ETE mAb expressed from the different hosts

Post-translation modifications of therapeutic mAbs can impact important parameters such as solubility, stability and half-life [329, 330]. IgG mAbs are N-glycosylated on the two HCs in the Fc-portion, and micro-heterogeneities in the glycan structure, such as the absence of certain sugar residues, can affect the activity of the mAb and the antibody-dependent cellular cytotoxicity [330]. Glycan profiles can be affected by a number of parameters, with the host cell line being one of the most important [331]. Usually, there are three major peaks observed in the electropherogram of N-glycans: G0F, G1F and G2F, which are typical of mAbs produced in CHO cells (Table 5.1). Additional glycan peaks can also be observed but at reduced amounts, including Man5 (mannose 5), G0, G2FS1, and G2FS2 [196].

Table 5.1 Overview of the detected N-glycan structures of a monoclonal antibody (source: Agilent Application Note (N-Glycan analysis of monoclonal antibodies and other glycoproteins using UHPLC with fluorescence detection). In the analysis in this work, the two G1F peaks were combined (1,3 and 1,6).

Name	Calculated mass	Mass + AB	Monosaccharide composition	Structure
G0	1317.5	1437.6	$GlcNAc_2Man_3GlcNAc_2$	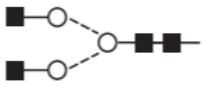
G0F	1463.6	1583.6	$GlcNAc_2Man_3GlcNAc_2Fuc$	
Man5	1235.4	1355.5	$Man_5GlcNAc_2$	
(1,6)G1F	1625.6	1745.7	$GalGlcNAc_2Man_3GlcNAc_2Fuc$	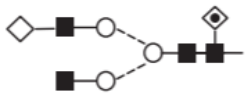
(1,3)G1F	1625.6	1745.7	$GalGlcNAc_2Man_3GlcNAc_2Fuc$	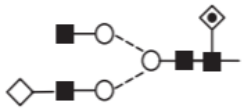
G2F	1787.6	1907.7	$GalGlcNAc_2Man_3GlcNAc_2Fuc$	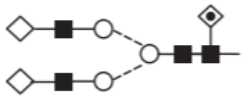
G2FS1	2077.8	2197.8	$NeuNAcGal_2GlcNAc_2Man_3GlcNAc_2Fuc$	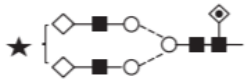
G2FS2	2368.9	2488.9	$NeuNAc_2Gal_2GlcNAc_2Man_3GlcNAc_2Fuc$	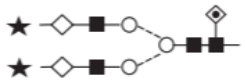

N-glycan profiles of the ETE mAb from control and CQ-evolved host were generated using mass spectrometry. Glycans present at less than 5% of the total were considered to not be significant. There were no major differences observed in the profiles of the N-linked glycans between control and the CQ-evolved hosts (Fig 5.12). G0F glycan comprised ~75% of the glycans present for both hosts, with G1F levels reaching 15 and 19% for control and CQ-evolved host respectively. This indicates that there were no major differences in the product quality of ETE mAb based on N-glycan profiling.

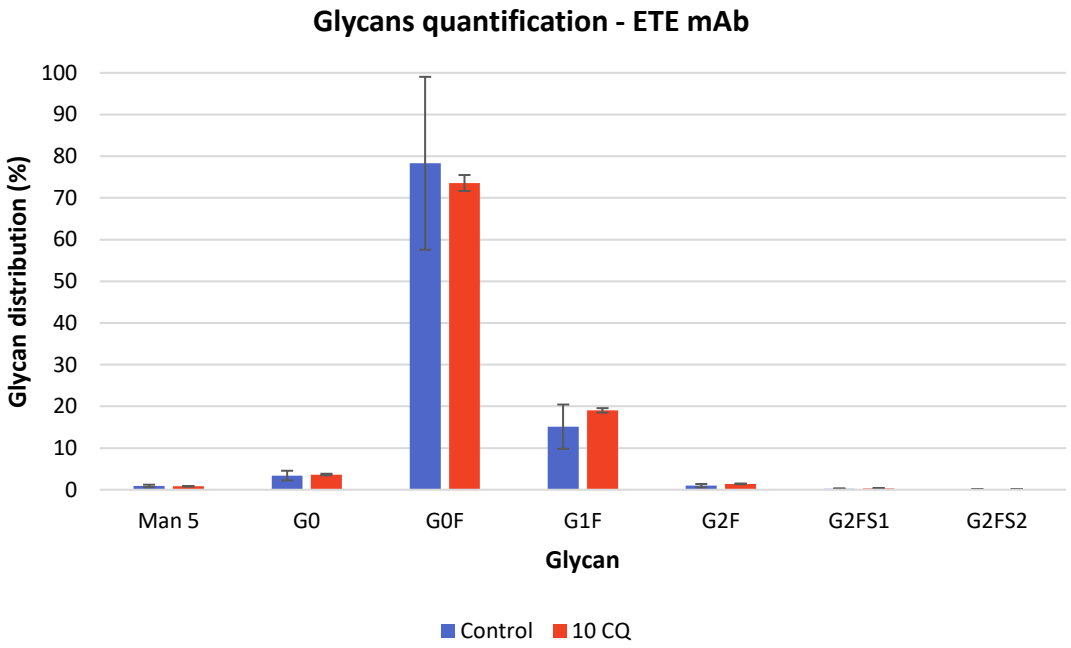

Figure 5.12 N-linked glycan profiles of an ETE mAb from control (blue) and CQ-evolved (red) CHO cells. N=3, mean is shown and error bar = standard deviation.

5.2.3.4 Analysis of lysosome content of the chloroquine evolved host expressing an ETE mAb

Lysosome content was determined during FBOG on days 3, 7 and 10 for the control and CQ-evolved pools (Fig.5.13). Lysosome content increased with culture time in cell lines derived from both hosts, but there was no difference between the control and CQ-evolved host (p=0.071 on day 3, p=0.15 on day 7, and p=0.055 on day 10).

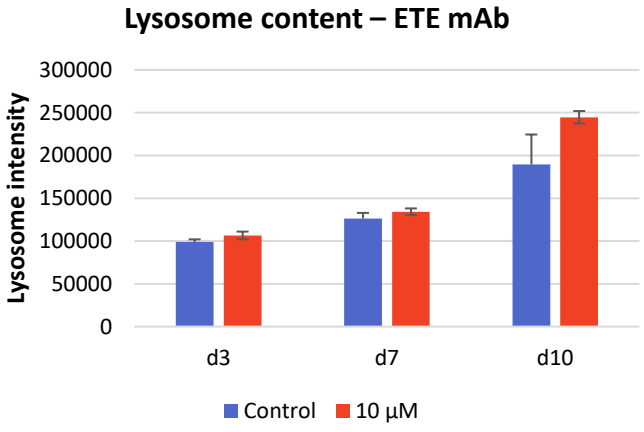

Figure 5.13 Lysosome content of control (blue) and CQ-evolved (red) CHO cells expressing an ETE mAb on day 3, 7 and 10 of the FBOG. N=3, mean is shown and error bar = standard deviation.

5.2.4 Analysis of the CHO cell chloroquine evolved host expressing a DTE mAb

5.2.4.1 Culturing of the control and chloroquine evolved host expressing a DTE mAb

Like the trends observed for the ETE mAb, the CQ-evolved host obtained a higher IVC (Fig. 5.14 A) than the control cells. Culture viability started dropping from day 7 onwards for both cell lines (Fig. 5.14 B), although the decline was faster for the control (70.4% vs. 48.3% on day 10). Final culture viability on day 14 was nearing 0% for the control while for the CQ-evolved cells culture viability remained around 30%. A three-fold increase in titre was observed in CQ-evolved cells compared to control cells (Fig. 5.14 C; 1881 vs. 606 mg/L, p=0.0038). Overall, qP was increased by 1.8-fold in the CQ-evolved host (Fig. 5.14 D; 18.09 vs. 9.78 pg/cell/day, p=0.022), a similar increase to that observed for the ETE mAb. The higher cell concentration reached and maintenance of culture viability for longer, like the ETE mAb culture, again explains some of the improved productivity achieved by the CQ-evolved host compared to control cells.

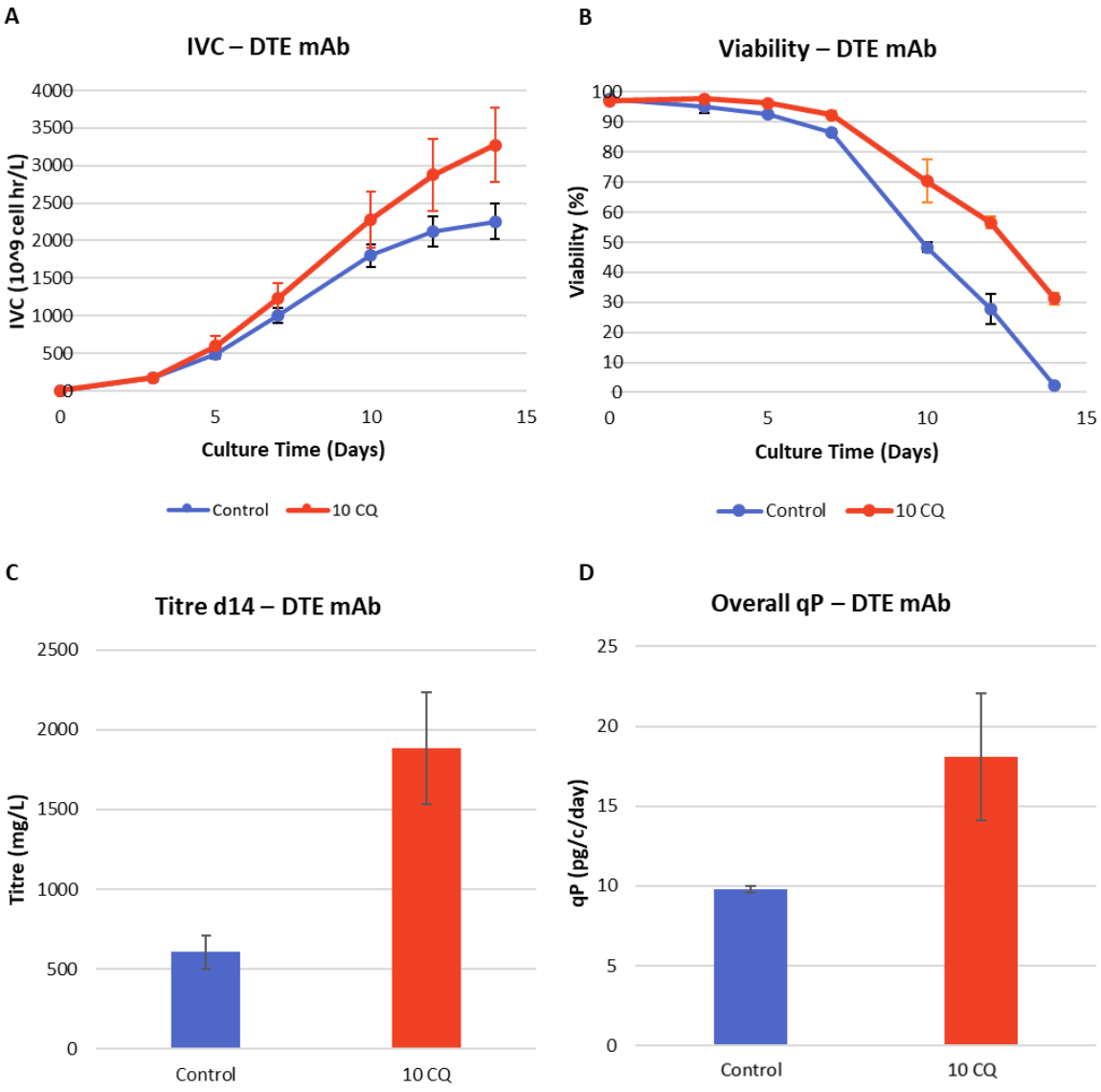

Figure 5.14 Cell culture data comparing control (blue) and CQ-evolved (10 CQ) pools, expressing a DTE mAb, in terms of A) IVC, B) culture viability, C) mAb final titre (p=0.0038) and E) overall qP (p=0.022). N=3, mean is showed and error bar = standard deviation.

5.2.4.2 Analysis of intracellular HC and LC content of chloroquine evolved host expressing a DTE mAb

Intracellular HC and LC protein were quantified by flow cytometry on day 3 of the FBOG for control and CQ-evolved cells expressing a DTE mAb. The analysis revealed homogenous HC and LC protein expressing populations for both hosts (Fig. 5.15), with 92.8±6% cells positively expressing both HC and LC for the control (Fig.5.15, Q2), and 97.1±2.4% for the evolved host. Thus, productivity differences do not arise from the presence of a non-expressing population.

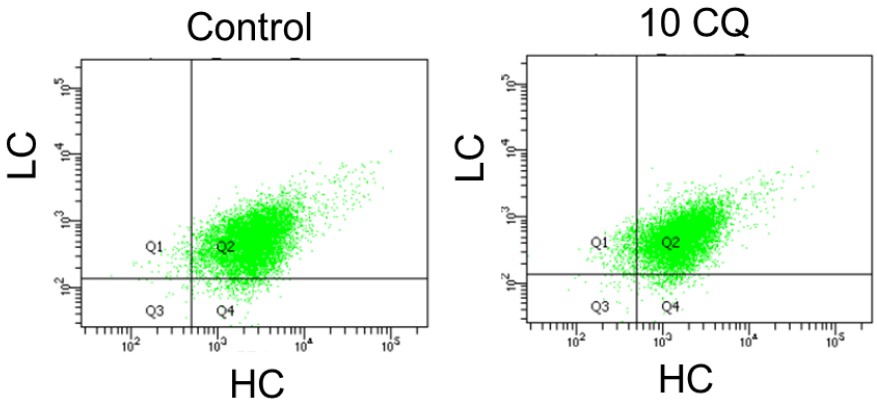

Figure 5.15 Intracellular HC and LC protein for the DTE mAb. Both control and CQ-evolved cells had homogenous expressing populations. Images show representative data from triplicate analyses.

5.2.4.3 Product quality analysis of DTE mAb

N-glycan profiles of the DTE mAb produced from the control and CQ-evolved host were investigated by mass spectrometry. There were no major differences in the levels of the N-glycans (those with a distribution above 5%) between the control and CQ-evolved hosts (Fig. 5.16). G0F levels were ~75% for both host cell lines, while G1F levels were ~20%. Consistent with what was observed for the ETE mAb, based on N-glycans profiling, the CQ-evolved host does not impact on the observed glycan profile.

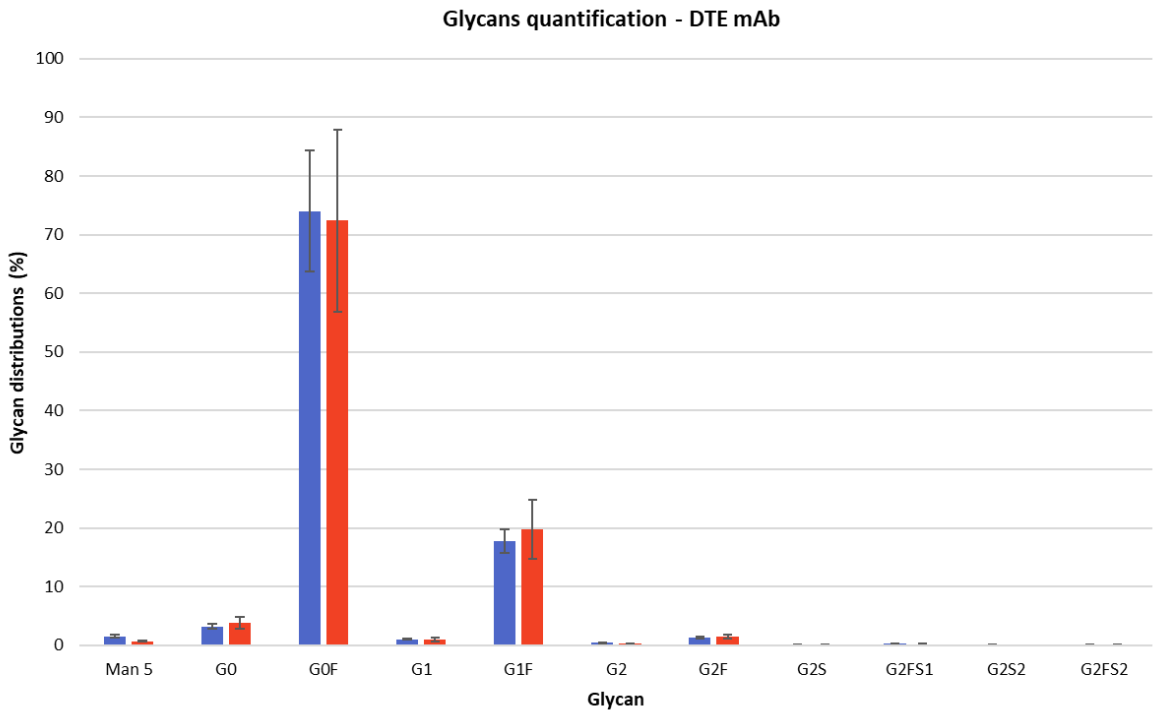

Figure 5.16 N-linked glycan profiles of DTE mAb from Control (blue) and CQ-evolved (red) cells. N=3, mean is shown and error bar = standard deviation.

5.2.4.4 Analysis of lysosome content of the chloroquine evolved host expressing a DTE mAb

Lysosome content was measured during FBOG on days 3, 7 and 10 for the control and CQ-evolved pools (Fig. 5.17). Lysosome content was similar on day 3 between control and CQ-evolved but was elevated for the CQ-evolved cells on both day 7 (1.5-fold increase, p=0.0030) and day 10 (4-fold increase, p=0.0017).

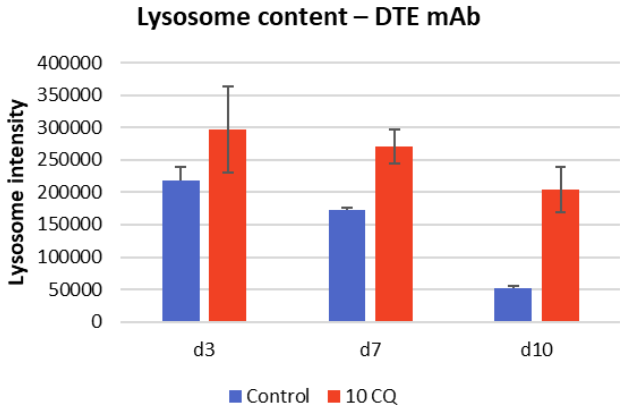

Figure 5.17 Lysosome content of control (blue) and CQ-evolved (red) cells expressing a DTE mAb on day 3, 7 and 10 of the FBOG. N=3, mean is shown and error bar = standard deviation.

5.2.5 Evaluation of the chloroquine evolved host expressing a bispecific mAb

5.2.5.1 Culturing of chloroquine evolved host expressing a bispecific mAb

The control host and CQ-evolved host were transfected with a bispecific mAb and cultured in FBOG for 12 days. IVC profiles were similar for both control and CQ-evolved hosts until day 7 (Fig. 5.18 A). From day 7 onwards, CQ-evolved cells reached a higher IVC than the control, due to a drastic drop in culture viability of the control cell line where the culture viability dropped to 20% by day 10, compared to 73% for CQ-evolved cells (Fig. 5.18 B). This was despite glucose availability for the control but not for the CQ-evolved cell. The CQ-evolved cells had a 5.7-fold increase in titre compared to control (Fig. 5.18 C; 524 vs. 92 mg/L, $p=0.0014$) as well as a 2.9-fold increase in qP (Fig. 5.18 D; 3.44 vs. 1.19 pg/cell/day, $p=0.0068$).

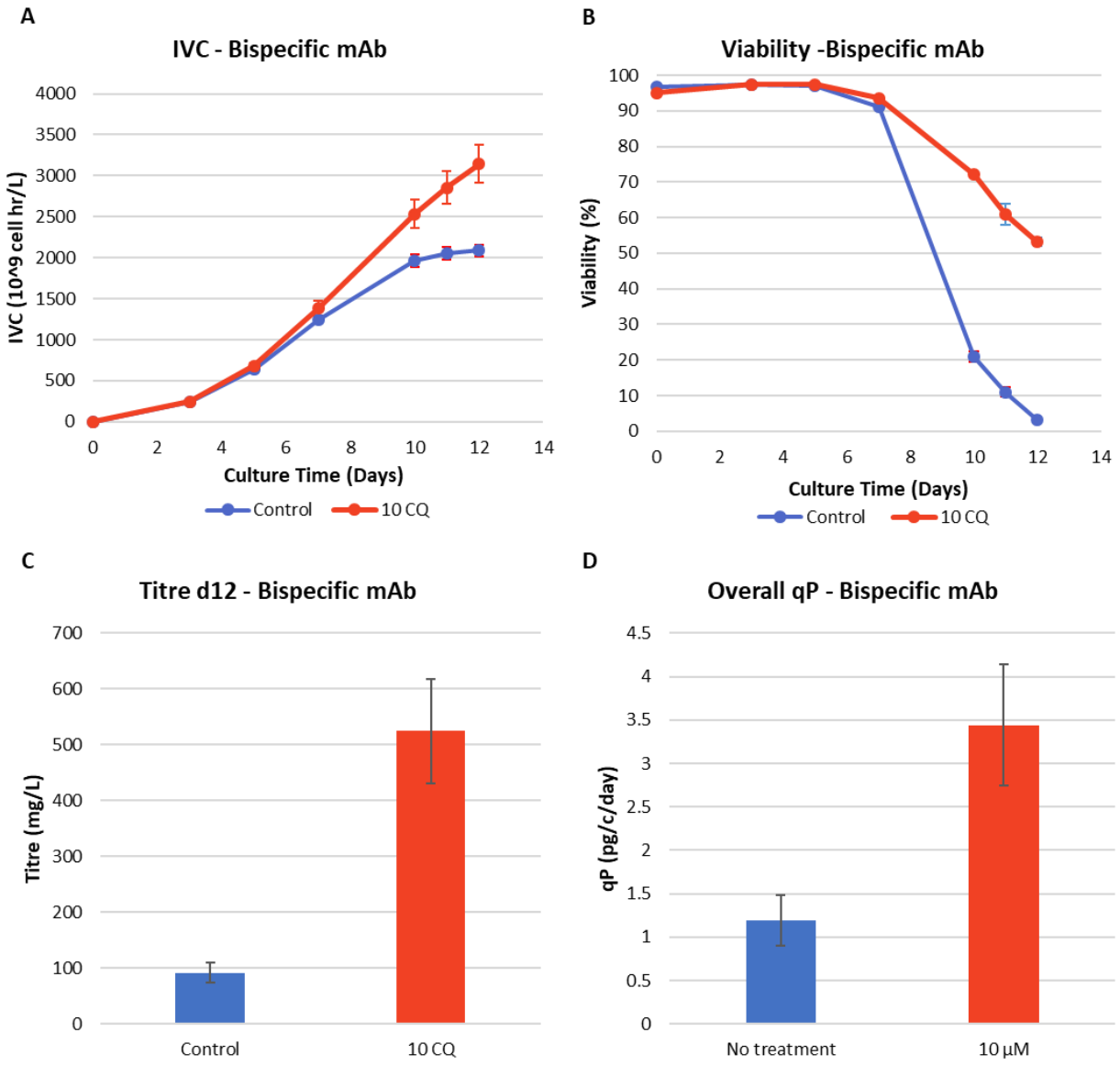

Figure 5.18 FBOG cell culture data comparing Control (blue) and CQ-evolved (10 CQ, red) CHO cell pools, expressing a bispecific mAb in terms of A) IVC, B) culture viability, C) mAb final titre (p=0.0014) and E) overall qP (p=0.0068). N=3, mean is shown and error bar = standard deviation.

5.2.5.2 Analysis of intracellular HC and LC content of control and chloroquine evolved host expressing a bispecific mAb

Intracellular HC and LC protein content were investigated prior to the FBOG (second passage after the recovery following transfection) and on day 3 of the FBOG (Fig. 5.19). Despite identical transfection methods, the control host had a significantly smaller population of cells expressing HC and LC protein compared to the CQ-evolved host (57.2 vs. 74.8%, p=0.0013) prior to the FBOG, and the double positive population of the control continue to significantly decrease with culture time, dropping from 57.2% to 44.9% (p=0.0036). The CQ-evolved cells maintained their expressing population of cells. The difference in the ratio of expressing to non-expressing cells may partly explain the increased titre observed in the CQ-evolved cells.

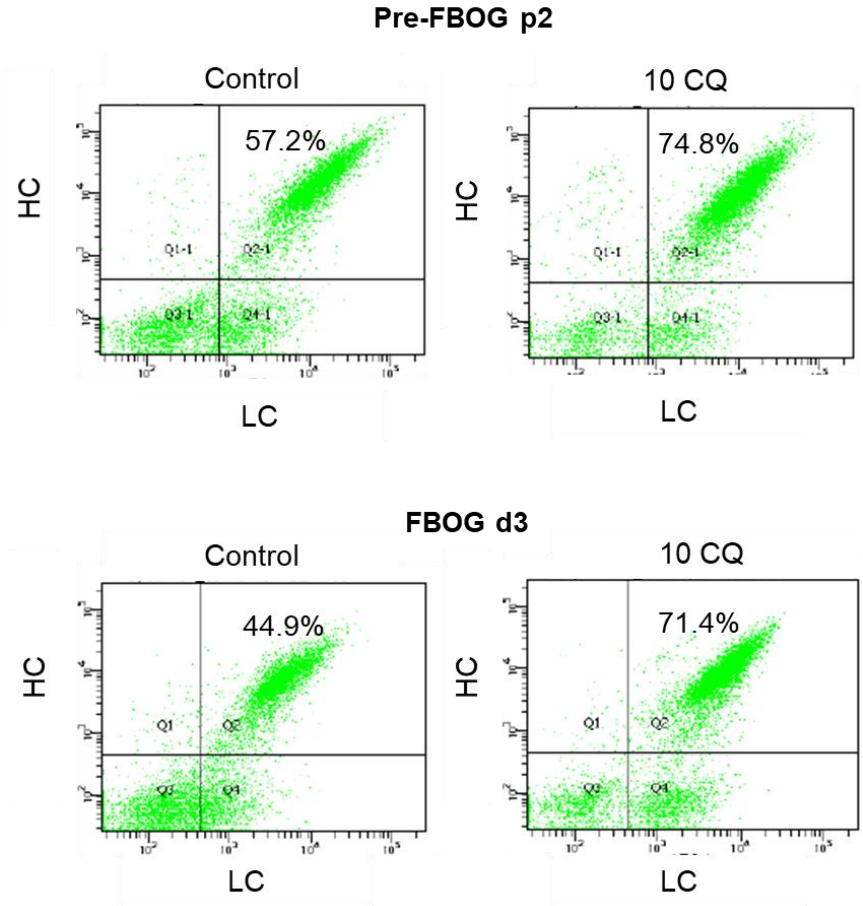

Figure 5.19 Intracellular HC and LC protein for the bispecific mAb, on the second passage pre FBOG (top) and on day 3 of the FBOG (bottom). The number in Q2 indicate the proportion of cells expressing both HC and LC protein.

5.2.5.3 Analysis of lysosome content of the CQ-evolved host expressing a bispecific mAb

Lysosome content was measured during the FBOG on days 3 and 7 only, due to the low culture viabilities on day 10 (Fig. 5.20). Lysosome content was similar on day 3 and 7 between both control and the CQ-evolved host (Fig. 5.20).

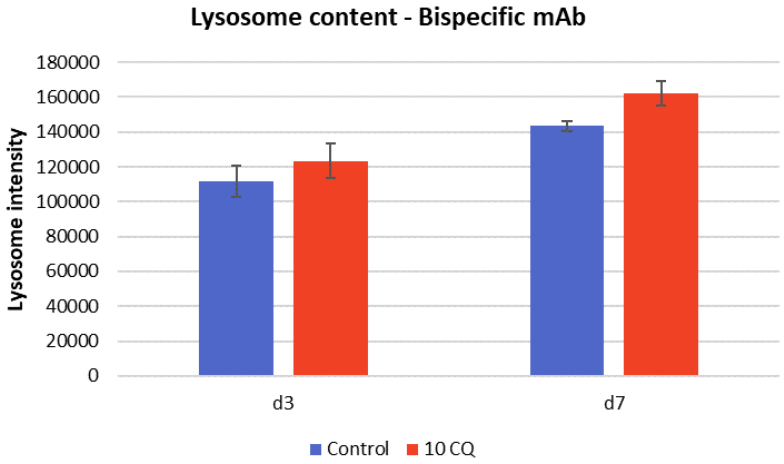

Figure 5.20 Lysosome content of control (blue) and CQ-evolved (red) cells expressing a bispecific mAb on day 3 and 7 of the FBOG. N=3, mean is shown and error bar = standard deviation.

5.2.5.4 Product quality analysis of the bispecific mAb

The bispecific used in this study was known to be prone to aggregation. Therefore, aggregate analysis was performed on cell culture supernatant samples collected on day 12 of the FBOG using an automated western blot. The data can be visualised in multiple views, such as a western blot view (Fig. 5.21 A) or chromatogram view (Fig. 5.21 C, D). Quantification of the aggregation amounts was performed on the chromatograms, integrating the area below the curve between ~106 and 280 kDa. A visible decrease in aggregation was observed in the higher molecular weight areas of the gel, between 125 and 240 kDa (Fig. 5.21 A) for the CQ-evolved host, and quantification showed this decrease to be statistically significant (Fig. 5.21 B, p=0.0022). Moreover, the chromatogram view revealed two distinct peaks for the CQ-evolved cells, one at ~116 kDa representing the mAb monomer, and a second peak at ~200 kDa corresponding to the aggregate. The lack of distinction between the two peaks for control samples 1 and 3 reflect high levels of heterogenous aggregate species.

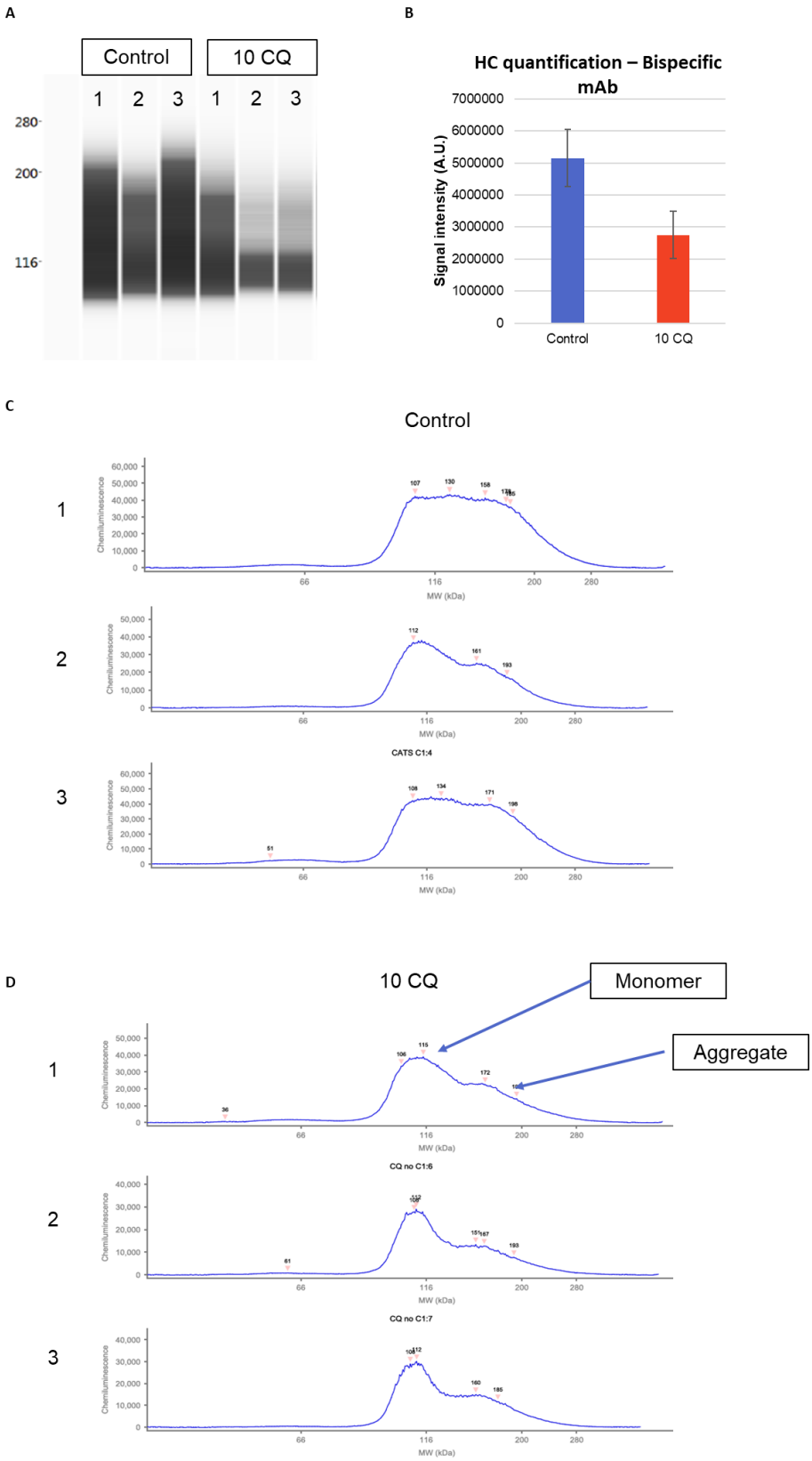

Figure 5.21 Non-reduced HC automated western of supernatant harvested on day 12, showing product aggregates. A) Gel view of the non-reduced HC protein, the first three samples are from control and the last three from the CQ-evolved cells. B) Non-reduced quantification of HC aggregates species of the western. Chromatogram view of the C) Control and D) CQ-evolved non-reduced HC supernatant analysis. For B) N=3, mean is shown and error bar = standard deviation.

5.2.6 Overall summary of results from the CQ-evolved host

The novel CQ-evolved host was assessed under FBOG conditions for expression of three different molecules. The CQ-evolved host displayed increased titre compared to the control host for all three molecules investigated. This host had delayed cell death and maintained a higher culture viability throughout the later stages of the culture, which resulted in significant increases in both titre and specific productivity. The CQ-evolved host showed a greater proportion of cells expressing both HC and LC compared to the control host for all three molecules tested. This was especially evident for the bispecific mAb during the FBOG. For the bispecific mAb, the CQ-evolved host displayed an increased stability, in terms of the maintenance of HC and LC expressing populations, during the FBOG compared to the control host.

The glycan profiles of the secreted molecules were assessed by mass spectrometry for the ETE and DTE mAbs. N-glycan profiles were similar between the CQ-evolved host and control, showing that the CQ-evolved host did not impact the N-glycan product quality. For the bispecific mAb, the molecule was known historically to have aggregation issues, therefore aggregation was assessed using an automated western system of the harvested culture supernatant. The CQ-host showed a decreased amount of aggregate species in the non-reduced HC sample. The sample used for product quality analysis was crude supernatant, and it is important to note that if the product had been purified, these differences in aggregation may have not been observed.

Overall, the CQ-evolved host shows promise as a host that has the potential of increasing the production of recombinant protein, without affecting product quality, and even potentially reducing aggregation for specific molecules.

5.2.7 Investigating the mechanisms underlying the improved recombinant protein production and prolonged culture viability of the CQ-evolved host

5.2.7.1 RNA sequencing of the CQ-evolved host and standard host expressing an ETE or DTE mAb

To investigate the mechanisms underlying the differences between the control and CQ-evolved host, transcriptomics analysis, by RNA-sequencing, was performed on day 7 FBOG samples from pools expressing the ETE or DTE mAb. Day 7 was chosen as the cells are no longer in the growth phase whilst culture viability remained high for both control and CQ-evolved cells. Cultures were over 95% viable for the ETE, and over 85% viable for the DTE mAb, with no significant differences in viability between

control and CQ-evolved cells. For data analysis, control cells expressing the ETE and DTE mAb were grouped together and analysed against CQ-evolved cells expressing the ETE or DTE mAb. Performing the analysis in this manner allowed identification of genes with differential expression caused by the CQ treatment, rather than by the differences in molecule expressed.

5.2.7.2 PCA analysis of transcript expression and identification of differentially expressed genes

Differentially expressed genes between all cell lines and conditions were analysed using PCA (Fig. 5.22). PCA analysis uses linear combinations of gene expression to define a new set of unrelated variables, the principal components, allowing the visualisation of subgroups. The first and second principal components (PC1 v PC2) explained 52% of the variation between the different samples. Biological replicates of each host cell lines and molecule were found to cluster (as expected) and separate from the other cell lines. PC1 distinguishes between the molecule expressed, DTE or ETE, and PC2 separated the host cells used, control or CQ, proving that CQ-treatment had a distinguishable effect at the transcriptome level.

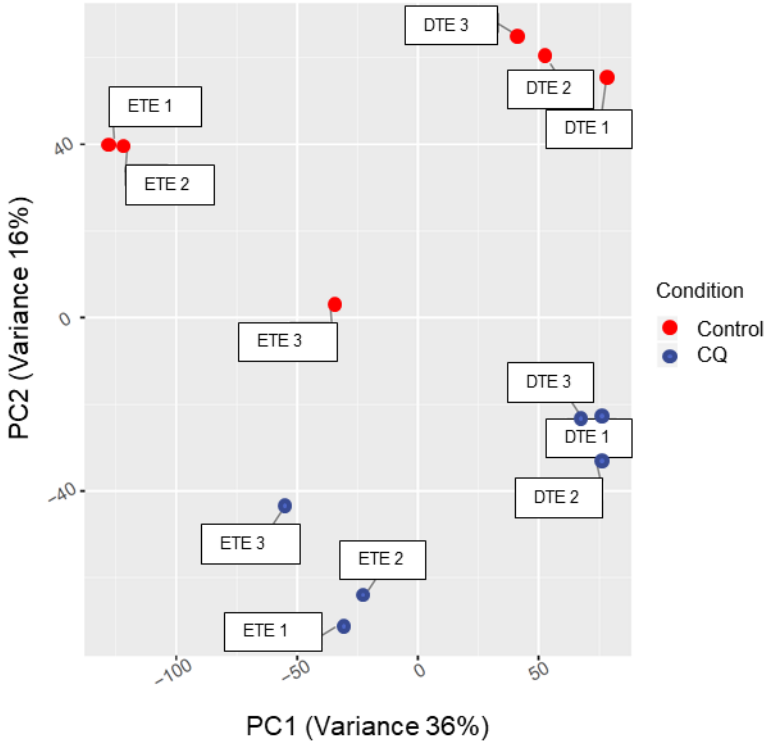

Figure 5.22 PCA analysis of RNA-seq transcriptomic gene expression data comparing all the samples from control (red) and CQ (blue) expressing either the ETE or DTE mAb.

Considering an adjusted p-value of 0.05 and a fold change threshold of 1.5-fold change, 412 genes were differentially expressed, with 318 genes up-regulated in the control compared to the CQ-evolved host (App. C Table 1), and 94 genes down-regulated in the control (App. C Table 5.2). Increasing the fold change threshold to 2-fold decreased the number of differentially expressed genes to 172 genes, with 134 genes being up-regulated in the control compared to CQ-evolved host, and 38 genes downregulated in the control. Heatmaps of the differentially expressed genes shows this pictorially with more genes being down-regulated in the CQ-evolved cells than in the control (Fig. 5.23 A). This is also visible on the MA-plot, with M corresponding to the log2 fold change, and A to the mean (Fig. 5.23 B).

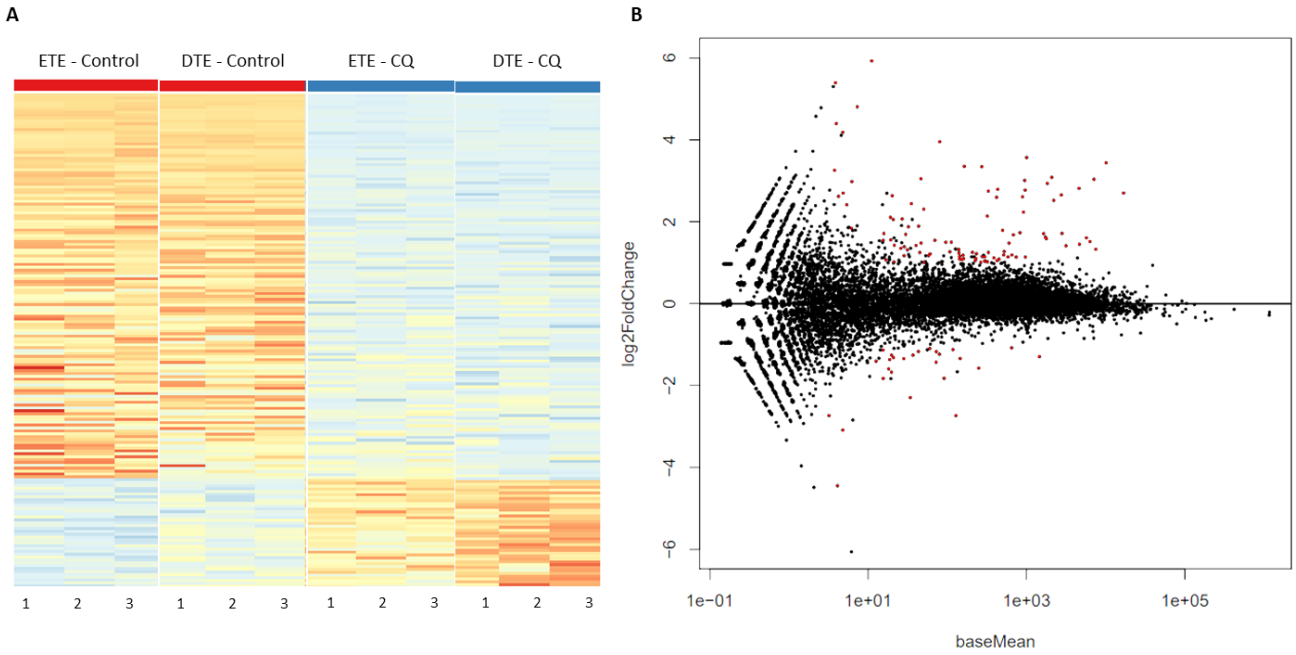

Figure 5.23 A) Heatmap comparing the differentially expressed genes of the control (red) and the CQ-evolved cells (blue) expressing an ETE or DTE mAb. Red colour on the map indicates up-regulation and blue down-regulation. The number at the bottom of the map is the different replicates. B) MA-plot showing all genes (black dots) and genes that are differentially expressed between the two hosts (red dots).

5.2.7.3 Gene ontology analysis

Gene ontology (GO) analysis, in which genes are organised by their molecular functions, cellular component or biological process, was performed using the online software Fidea [237]. Fidea analysis requires the gene name, fold change and p-value of the fold change. A threshold of 1.5-fold change and 0.05 for the adj. p-value were set for the gene list analysed. The different GO analyses performed included biological processes, molecular function and cellular component.

GO biological process analysis using Fidea identified 46 pathways to be significantly enriched in CQ-evolved cells ($p < 0.05$), 38 of which were down-regulated in CQ-evolved cells, and 8 which were up-regulated (Table 5.2). The top three biological processes with the highest number of differentially expressed (DE) genes in their pathways included 'development process' (80 genes, 1.53-fold enrichment, down-regulated in CQ-evolved cells), 'positive regulation of biological process' (79 genes, 1.69-fold enrichment, down-regulated in CQ-evolved cells), and 'positive regulation of cellular process' (77 genes, 1.82-fold enrichment, down-regulated in CQ-evolved cells). Most identified biological processes were general and non-specific. Of potential interest, 'differentiation of cell differentiation' was down-regulated in CQ-evolved cells (2.15-fold change), as well as 'positive regulation of cellular component organization' (2.96-fold change). Both 'extracellular matrix organisation' (9.33-fold change), and 'extracellular structure organization' (9.27-fold change) were found to be up-regulated in CQ-evolved cells. This implies that CQ-treatment had an overall effect of decreasing the activity of many biological processes related to cell differentiation or general cellular processes but increased the activity of processes related to extracellular organization.

GO molecular function analysis did not identify any significantly enriched pathway when considering up-regulated and down-regulated genes in separate groups, even when increasing the p-value threshold to 0.10. Grouping the differentially expressed genes (regardless of up or down-regulation) together however identified 'protein binding' (1.3-fold enrichment, 145 genes, p-value=0.024) and 'SMAD binding' (6.71-fold enrichment, 8 genes, p-value=0.024) as being significantly enriched in the differentially expressed genes.

Table 5.2 Biological processes identified as being enriched by the GO analysis. The 'Sign' column refers to the gene expression in the control.

SIGN	GO ID	Biological Proces	Adj. p-value	Fold Enrichme	# genes
UP-reg	GO:0048522	positive regulation of cellular process	1.75E-04	1.82	77
UP-reg	GO:0048518	positive regulation of biological process	1.55E-03	1.69	79
UP-reg	GO:0050793	regulation of developmental process	2.67E-03	2.15	44
UP-reg	GO:0009966	regulation of signal transduction	2.67E-03	2.06	47
UP-reg	GO:0010646	regulation of cell communication	5.23E-03	1.89	50
UP-reg	GO:0023051	regulation of signaling	5.23E-03	1.9	50
UP-reg	GO:0071675	regulation of mononuclear cell migration	5.23E-03	30.42	4
UP-reg	GO:0048731	system development	5.23E-03	1.69	67
UP-reg	GO:2000026	regulation of multicellular organismal development	5.23E-03	2.2	36
UP-reg	GO:0010759	positive regulation of macrophage chemotaxis	5.23E-03	34.23	4
UP-reg	GO:0051239	regulation of multicellular organismal process	5.23E-03	1.91	50
UP-reg	GO:0051130	positive regulation of cellular component organization	5.23E-03	2.96	22
UP-reg	GO:0048583	regulation of response to stimulus	6.05E-03	1.82	53
UP-reg	GO:0010758	regulation of macrophage chemotaxis	6.56E-03	27.38	4
UP-reg	GO:0071622	regulation of granulocyte chemotaxis	6.56E-03	27.38	4
UP-reg	GO:0048856	anatomical structure development	6.81E-03	1.59	73
UP-reg	GO:0023056	positive regulation of signaling	6.99E-03	2.5	27
UP-reg	GO:0032502	developmental process	7.83E-03	1.53	80
UP-reg	GO:0031346	positive regulation of cell projection organization	1.22E-02	4.77	11
UP-reg	GO:0009967	positive regulation of signal transduction	1.26E-02	2.5	25
UP-reg	GO:0007275	multicellular organismal development	1.50E-02	1.55	73
UP-reg	GO:0015793	glycerol transport	1.50E-02	41.07	3
UP-reg	GO:0010647	positive regulation of cell communication	1.50E-02	2.4	26
UP-reg	GO:0048585	negative regulation of response to stimulus	1.62E-02	2.44	25
UP-reg	GO:0006884	cell volume homeostasis	1.79E-02	19.56	4
UP-reg	GO:0045595	regulation of cell differentiation	1.81E-02	2.15	31
UP-reg	GO:0009968	negative regulation of signal transduction	2.08E-02	2.64	21
UP-reg	GO:0006833	water transport	2.16E-02	18.25	4
UP-reg	GO:0015840	urea transport	2.33E-02	34.23	3
UP-reg	GO:0007167	enzyme linked receptor protein signaling pathway	4.39E-02	2.94	16
UP-reg	GO:0023057	negative regulation of signaling	4.60E-02	2.46	21
UP-reg	GO:0030335	positive regulation of cell migration	4.60E-02	3.6	12
UP-reg	GO:0048584	positive regulation of response to stimulus	4.60E-02	2.09	29
UP-reg	GO:0042044	fluid transport	4.68E-02	14.41	4
UP-reg	GO:0010648	negative regulation of cell communication	4.68E-02	2.45	21
UP-reg	GO:2000147	positive regulation of cell motility	4.89E-02	3.53	12
UP-reg	GO:0010642	negative regulation of platelet-derived growth factor receptor signaling pathway	4.89E-02	25.67	3
UP-reg	GO:0015791	polyol transport	4.89E-02	25.67	3
DOWN-reg	GO:0072166	posterior mesonephric tubule development	2.72E-02	222.47	2
DOWN-reg	GO:0072358	cardiovascular system development	2.72E-02	4.36	12
DOWN-reg	GO:0072359	circulatory system development	2.72E-02	4.36	12
DOWN-reg	GO:0030198	extracellular matrix organization	3.28E-02	9.33	6
DOWN-reg	GO:0043062	extracellular structure organization	3.28E-02	9.27	6
DOWN-reg	GO:0001568	blood vessel development	3.28E-02	5.26	9
DOWN-reg	GO:0001944	vasculature development	4.01E-02	5.02	9
DOWN-reg	GO:0072210	metanephric nephron development	4.79E-02	33.37	3

Finally GO cellular component analysis identified 7 cell components to be significantly enriched ($p<0.05$), all up-regulated in CQ-evolved cells (Table 5.3). All cellular components refer to extracellular functions, such as 'extracellular region part', 'extracellular matrix', 'extracellular space' and 'filopodium membrane'.

Table 5.3 Cellular components identified as being enriched by the GO analysis. The 'Sign' column refers to the gene expression in the control

SIGN	GO ID	Cellular component	Adj. p-value	Fold Enrichment	# genes
DOWN-reg	GO:0044421	extracellular region part	2.61E-04	4	17
DOWN-reg	GO:0005578	proteinaceous extracellular matrix	2.93E-04	7.02	10
DOWN-reg	GO:0031012	extracellular matrix	5.50E-04	6.26	10
DOWN-reg	GO:0005615	extracellular space	1.29E-03	4.12	13
DOWN-reg	GO:0005576	extracellular region	7.96E-03	2.53	19
DOWN-reg	GO:0044420	extracellular matrix part	1.02E-02	7.51	6
DOWN-reg	GO:0031527	filopodium membrane	3.78E-02	52.28	2

5.2.7.4 KEGG pathway analysis

KEGG pathway analysis, another database for genes (organised based on pathways of genes involved in the same biological process), was also performed using the online software Fidea, with the same threshold for fold change and p-values as for the GO analysis. KEGG pathway analysis only identified two pathways as being significantly enriched, when looking at up-regulated and down-regulated genes separately. 'Transcriptional mis-regulation' (3.89-fold change, 11 genes, p=0.00011) was down-regulated in CQ-evolved cells, and 'ECM-receptor interaction' (10.74-fold change, 4 genes, p=0.00047) was up-regulated in CQ-evolved cells. Combining both down-regulated and up-regulated genes also revealed 'sphingolipid metabolism' (6.15-fold change, 6 genes, p=0.050) pathway as being enriched for both the ETE and DTE mAb.

5.2.7.5 Manual analysis of differentially expressed genes

As neither the GO or KEGG pathway analysis identified pathways relevant to bioprocessing or specific cellular metabolism, or linked to lysosomes, manual analysis of the differentially expressed genes were performed. Of interest, several genes related to glutathione metabolism were differentially expressed. The genes *Gtm7*, *Gpx3* and *Gstm3* were all down-regulated in control compared to CQ-evolved cells (Table 5.4).

Table 5.4 Differentially expressed genes involved in the glutathione pathway

Gene name	Fold change	Adj. p-value	Complete gene name
Gstp3	1.48	4.26E-05	Glutathione S-transferase pi 3
Gstm7	-0.85	2.85E-43	Glutathione S-transferase Mu 7
Gpx3	-1.68	4.42E-04	Glutathione peroxidase 3
Gstm3	-1.59	4.09E-05	Glutathione S-Transferase Mu 3

Both glutathione S-transferases and glutathione peroxidases are the catalysts to the detoxification of various compounds, particularly related to oxidative stress [332]. Glutathione S-transferase has a number of isoforms, such as pi (*Gstp3*) which was down-regulated in CQ-evolved cells, and the mu isoform, which was up-regulated in CQ-evolved cells (*Gstm7* and *Gstm3*). Glutathione peroxidase 3 (*Gpx3*) was also found to be up-regulated in CQ-evolved cells. The increased expression of these enzymes in the CQ-evolved cells compared to control could suggest a better capacity to cope with reactive oxygen species (ROS).

5.2.7.6 Summary of transcriptomic analyses

Transcriptomic analysis of the control and CQ-evolved cells expressing an ETE or DTE mAb was performed on samples from day 7 of the FBOG. The analysis revealed only a few genes that were differentially expressed, 412 genes when setting a threshold of 1.5-fold change, with most of those genes being down-regulated in the CQ-evolved cells. Furthermore, GO analysis and KEGG pathway analysis did not reveal any specific or biologically-relevant pathway affected. Manual inspections of the genes identified several genes related to glutathione biosynthesis, which is involved in oxidative stress, that were up-regulated in the CQ-evolved host. Overall, this could mean that the impact of CQ treatment is a wide-spread decreased activity of many genes, without impacting specific cellular processes, at least for the timepoint studied in this transcriptomic analysis. As shown by the cell culture data, the control and CQ-evolved host behaved similarly up to day 7 of the FBOG, with significant differences arising later in the culture. Transcriptomic analysis of later timepoints may have revealed more significant differences in gene expression.

5.2.8 Oxidative stress analysis of chloroquine-evolved host and control host expressing an ETE or DTE mAb

Glutathione biosynthesis genes were identified as being up-regulated in the CQ-host from the transcriptomic analysis. Therefore, glutathione protein levels were investigated using a luminescence cell-based assay. Moreover, as glutathione is involved in oxidative stress, a flow cytometry assay was used to measure oxidative stress of the cells under FBOG conditions to identify any differences between the two host cell lines.

5.2.8.1 Glutathione quantification

Reduced glutathione (GSH) is an intracellular and extracellular protective antioxidant, which is found both freely in the cell and bound to proteins. Upon oxidative stress, such as the accumulation of reactive oxygen species, the enzyme glutathione reductase is activated, and free glutathione is converted to its oxidised form (GSSG) (Fig. 5.24) [332, 333]. The ratio of GSH:GSSG is typically used as a marker of cellular toxicity, with oxidative stress corresponding to a low ratio of GSH:GSSG [332, 333].

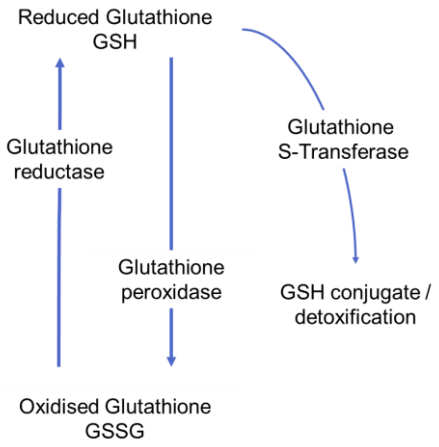

Figure 5.24 Schematic outlining the conversion of reduced glutathione to oxidised glutathione and key enzymes involved in that conversion.

Total glutathione (GSH) and oxidised glutathione levels were quantified using a cell-based luminescence assay (Fig. 5.25) on days 3 and 7 of the FBOG cultures. A non-evolved cell line transfected with an empty vector was used as a control, as these cells are not subjected to the additional stress of mAb production. GSH levels were statistically lower in the CQ-evolved host for ETE and DTE expressing cells on day 3 (Fig. 5.25 A, blue; p=0.020 for ETE mAb and p=0.010 for DTE mAb).

GSH levels were also lower in the CQ-evolved host on day 7, but the difference in GSH expression was only significant for the DTE mAb (Fig. 5.25 A, green; p=0.056 for ETE mAb and p=0.011 for DTE mAb). Both the null vector cell line and the control expressing the ETE or DTE mAb had more-or-less the same levels of total glutathione. For all samples, total GSH levels were higher on day 7 than day 4.

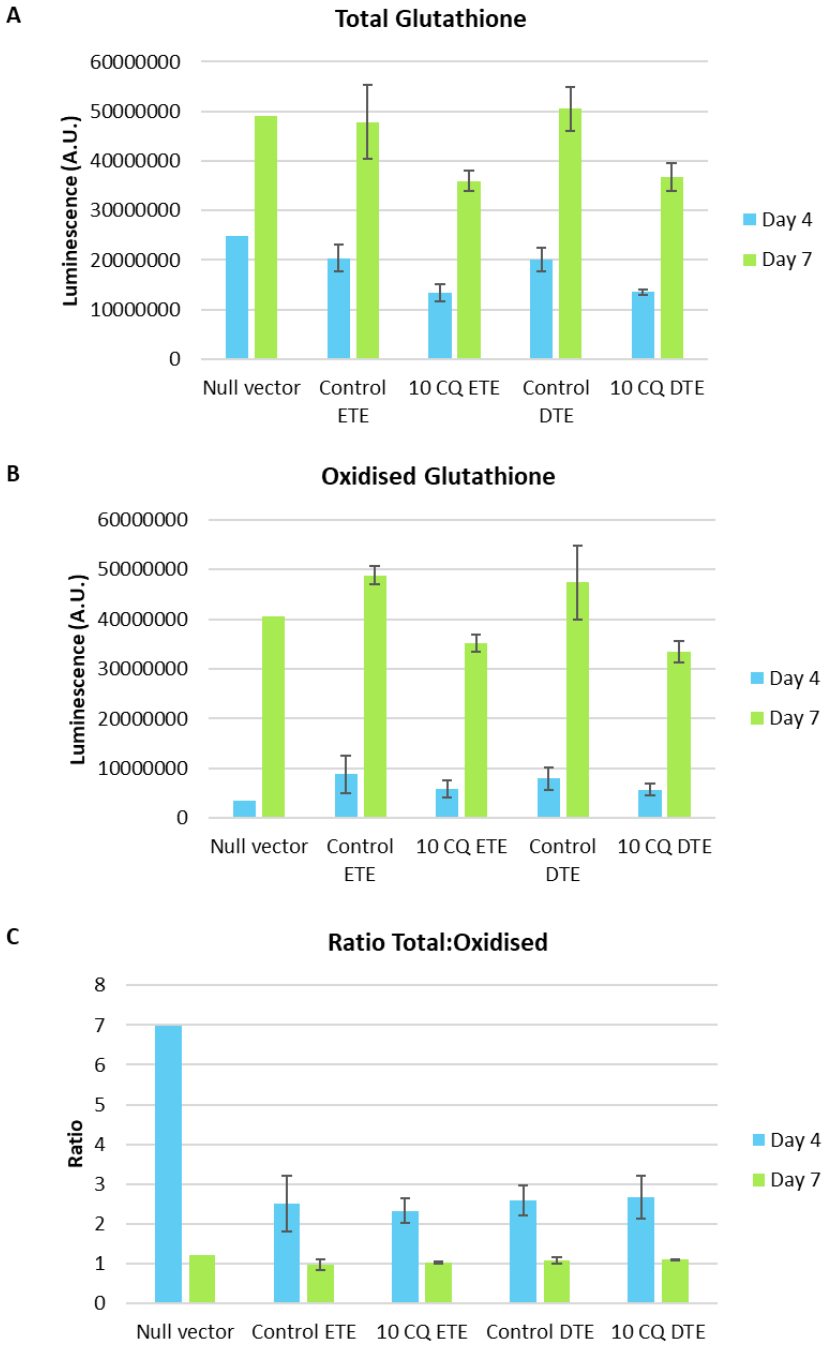

Figure 5.25 A) Total glutathione, B) oxidised glutathione, and C) ratio of total: oxidised on day 4 (blue) and day 7 (green) of the FBOG. N=3, mean is shown and error bar = standard deviation.

Oxidised glutathione (GSSG) levels were also higher on day 7 compared to day 4 (Fig. 5.25 B). On day 4, GSSG levels for the CQ-evolved host were much the same as the control (Fig. 5.25 B, blue). However, the CQ-evolved host had significantly lower levels of GSSG for cell lines expressing either the ETE or DTE mAbs (Fig. 5.25 B, green; p=0.00060 for ETE mAb and p=0.036 for DTE mAb). The ratio of GSH:GSSG was not significantly different on day 4 nor on day 7 between the two hosts (Fig. 5.25 C). The null vector control had a higher GSH:GSSG ratio on day 4 than the other cell lines studied, likely due to the lack of stress present early in the culture. Overall, the lack of differences in the GSH:GSSG ratio between CQ-evolved cells and control cells appears to indicate that the oxidative stress experienced by the cells is similar between the two hosts. The DTE molecule did not have an additional impact on cellular stress, at least on the days tested. Interestingly, despite no differences in the GSH:GSSG ratio, CQ-evolved cells had decreased expression of both total and oxidised glutathione.

5.2.8.2 Flow cytometry analysis of oxidative stress

To measure oxidative stress levels in the cells, a flow cytometry assay, CellROX, was used during the FBOG on days 4, 7 and 10 for the ETE mAb, and on days 4 and 7 for the DTE mAb, due to a decrease in culture viability by day 10. CellROX is a commercially available DNA dye, which upon oxidation binds to DNA, and increases its fluorescence. For a positive control, cells in culture from the control expressing the ETE or DTE mAb, were treated for one hour with tert-Butyl hydroperoxide (TBHP), an inducer of ROS, prior to staining with CellROX. For cells expressing the ETE mAb (Fig. 5.26 A, C), no significant differences were observed on any of the days between the oxidative stress levels of the control and CQ-evolved cells. Increased levels of oxidative stress were indicated on days 4 and 7 for the CQ-evolved cells compared to the controls (Fig. 5.26 B; p=0.0085 for day 4 and p=0.033), however, these levels were not significantly higher than the oxidative stress induced by TBHP.

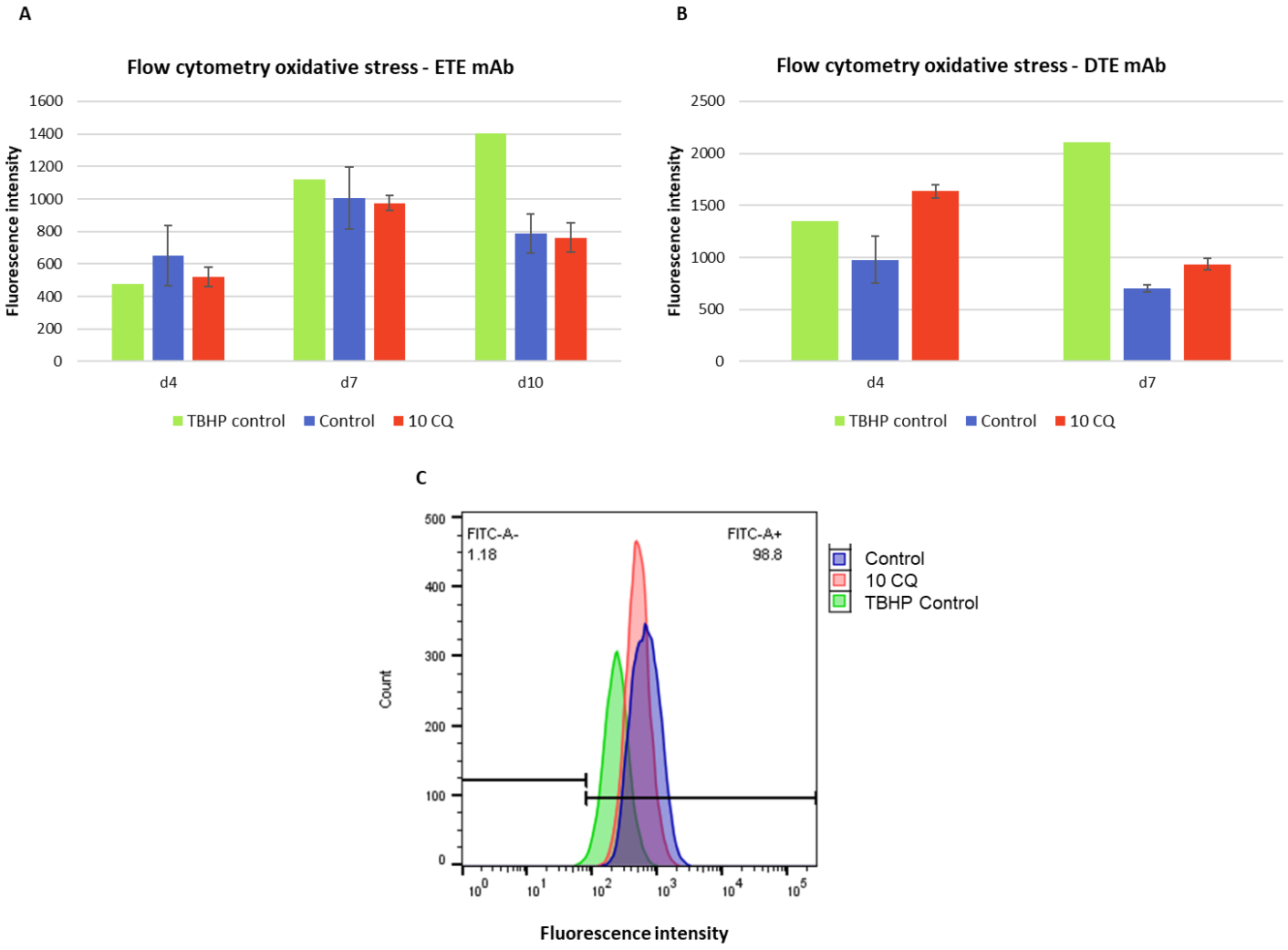

Figure 5.26 Median fluorescence intensity of CellROX dye for the TBHP-treated cells (green), control (blue) and CQ-evolved (red) for the A) ETE mAb and B) DTE mAb in a FBOG, with samples taken on day 4, 7 and 10. N=3, mean is shown and error bar = standard deviation. C) Example of flow plots for the ETE mAb on day 4 of the FBOG.

5.2.9 Western blot analysis of specific intracellular proteins in the chloroquine evolved host and standard host expressing an ETE or DTE mAb

Western blotting was performed to compare the CQ-evolved and control cells on day 7 of the FBOG. Despite the transcriptomic analysis not identifying any enriched pathways, autophagy (Atg12, LC3B, p62 and Lamp2A), mTORC1 pathway (Lamtor1, phosphorylated 4EBP1 (Thr37/46), phosphorylated p70 (Thr389) and phosphorylated mTOR (Ser2448)) and apoptosis marker levels (caspase 3, cleaved caspase 3 and Bcl-xL) were investigated, as these pathways have been reported to be affected by CQ. This analysis was aimed at deepening our understanding of the mechanisms underlying the increased productivity and delayed apoptosis observed in the CQ-evolved cells compared to control.

As previously mentioned, the different markers of autophagy are used to inform on the activity of the different stages of autophagy. Autophagy initiation and early autophagosomes formation is associated with p62 expression. Atg5-Atg12 and LC3 are markers associated with mature autophagosomes, whereas Lamp2A is a lysosomal membrane protein that is required for the fusion of autophagosomes with lysosomes and is thus a marker of later stage autophagy. mTORC1 can also be involved in autophagy, but also directly affects cell growth and proliferation, as well as protein synthesis. All western protein quantification was performed by densitometry analysis.

5.2.9.1 Analysis of autophagy markers in the ETE mAb expressing cells

Half of the autophagy markers investigated did not show any differences in protein expression between CQ-evolved cells and control: Atg12-Atg5 (Fig. 5.27 A, p=0.26), free Atg12 (Fig. 5.27 B, p=0.74) and p62 (Fig. 5.27 D, p=0.31). This suggests that there are no differences in the autophagy initiation between the two hosts. The only markers that showed differences in the autophagic flux were (i) LC3BII (Fig. 5.27 C, p=0.0018), in which expression was decreased ~2-fold in the CQ-evolved cells compared to control, (ii) the LC3BI/LC3BII ratio, which was 2-fold higher in CQ-evolved cells compared to control (Fig. 5.27 C, p=0.0093), and (iii) Lamp2A (Fig. 5.27 E, p=0.016) where levels were decreased in the CQ-evolved cells. An LC3BII increase without an increase in the LC3BI/LC3BII ratio can be indicative of either increased autophagosome synthesis or accumulation of non-degraded autophagosomes. The increase in Lamp2A protein, essential for autophagosomes fusion to the lysosomes, suggests that the LC3BII increase is more likely due to an accumulation of autophagosomes, and that the cell is attempting to cope with this accumulation by increasing Lamp2A expression. This would indicate a decrease in late-stage autophagy for the CQ-evolved cells.

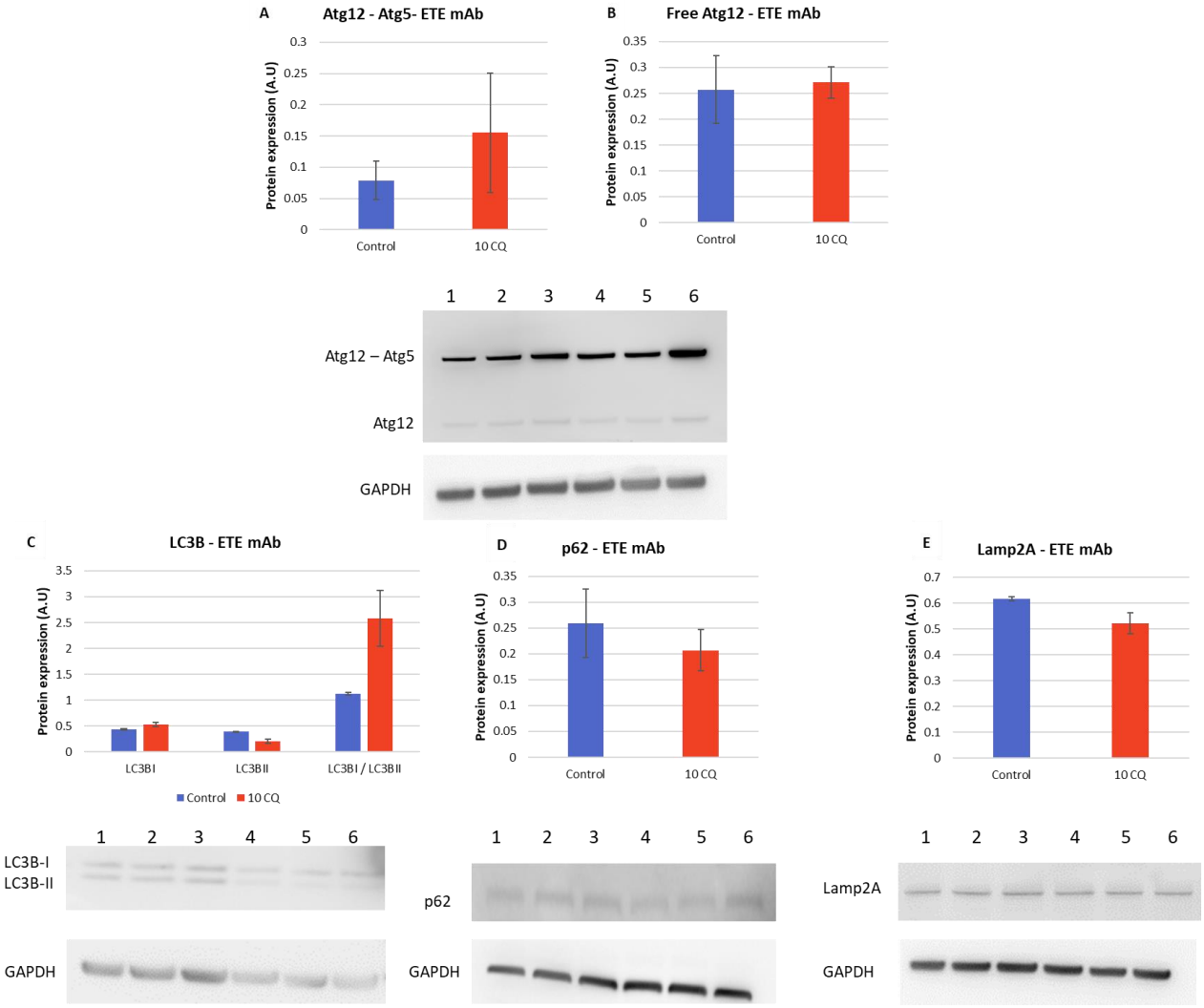

Figure 5.27 Autophagy marker analysis by western blotting for the ETE mAb pools. For each blot, samples 1-3 are from control and 4-6 from the CQ-evolved cells. Densitometry analysis was performed for quantification. Protein expression was normalised to GAPDH. Autophagic markers used were A) Atg12-Atg5 (p=0.26), B) free Atg12 (p=0.74), C) LC3B (p=0.0018 for LC3B II, and p=0.0093 for LC3BI / LC3BII), D) p62 (p=0.31) and E) Lamp2A (p=0.016). N=3, mean is shown and error bar = standard deviation.

5.2.9.2 Assessment of autophagy marker expression in DTE mAb Expressing Cells

Autophagy flux was increased in CQ-evolved cells compared to control as determined from the expression of markers of autophagy activity. Atg12-Atg5 (Fig. 5.28 A, p=0.031), LC3BI/LC3BII (Fig. 5.28 C, p=0.0047) and Lamp2A (Fig. 5.28 E, p=0.049) were all expressed at higher amounts in CQ-evolved cells compared to control cells, indicating an increase in on-going autophagy as well as late-stage autophagy. There were no differences in the expression of free Atg12 (Fig. 5.28 B, p=1.00), LCB3II (Fig 5.28 C, p=0.15) and p62 (Fig. 5.28 D, p=0.19). These data indicate that on day 7 there was no difference in autophagy initiation between control and CQ-evolved cells, but that previous initiation rates may have been different to account for the increased autophagic flux in CQ-evolved cells.

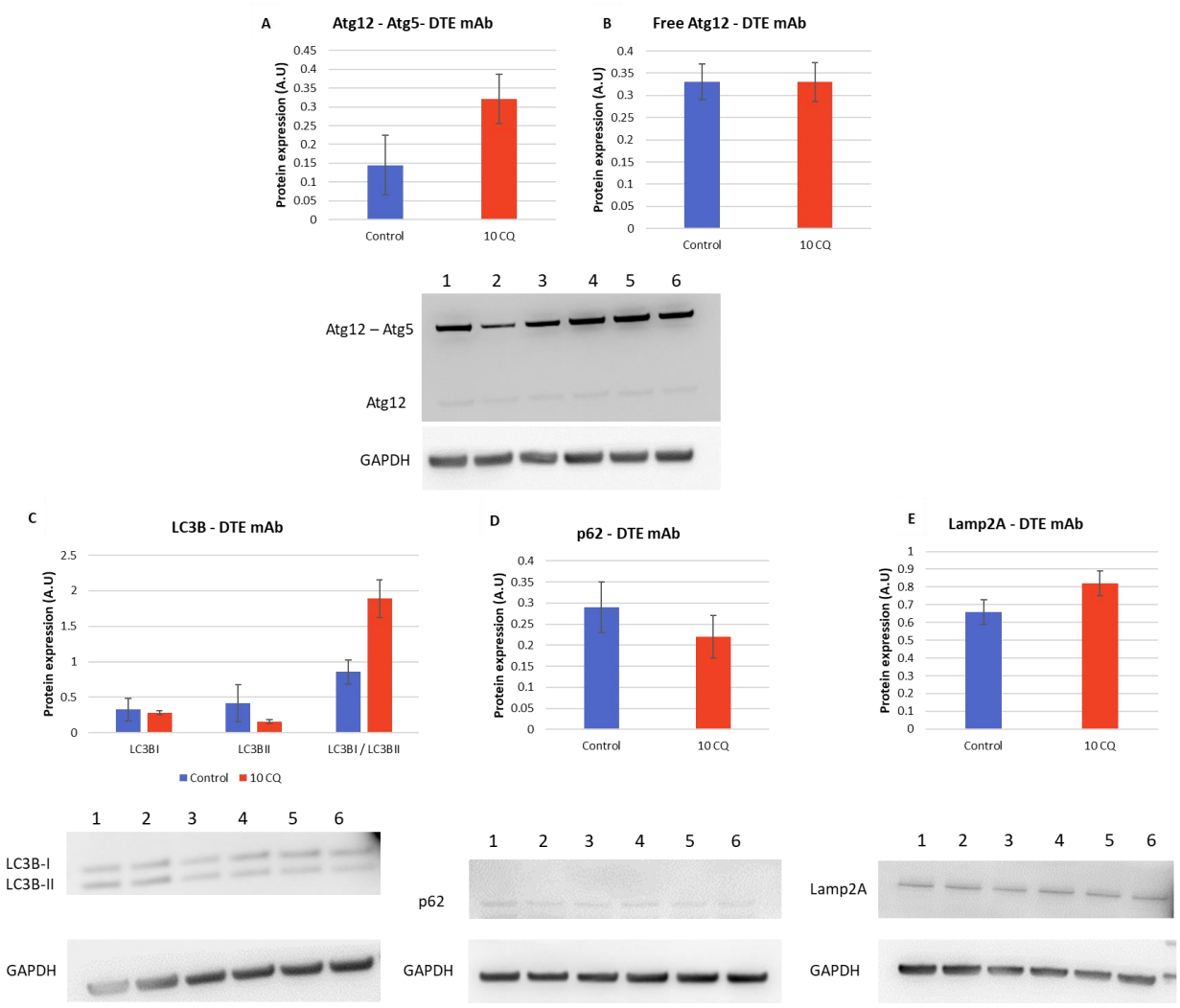

Figure 5.28 Autophagy marker analysis by western blot in the control and CQ-evolved CHO cell DTE mAb pools. For each blot, samples 1-3 are from control and 4-6 from the CQ-evolved cells. Protein expression was normalised to GAPDH. Autophagic markers used were A) Atg12-Atg5 (p=0.038), B) free Atg12 (p=1.00), C) LC3B (p=0.0047 for the ratio), D) p62 (p=0.19) and Lamp2A (p=0.049). N=3, mean is shown and error bar = standard deviation.

5.2.9.3 Analysis of mTORC1 markers in ETE mAb expressing cells

A number of mTORC1 pathway markers were also analysed in the control and CQ-evolved cells expressing the ETE mAb. Lamtor1 expression was more than 3-fold decreased in CQ-evolved cells samples compared to control samples (Fig. 5.29 A, p=0.0021). However, the other markers investigated, including phosphorylated 4EBP1 (Fig. 5.29 B, p=0.76), phosphorylated p70 (Fig. 5.29 C, p=0.51) and phosphorylated mTOR (Fig.5.29), did not show any differences in expression. The increase in Lamtor1 could suggest an increase in mTORC1 pathway signalling and formation of the Rag complex, however, other proteins from the Rag complex would need to be quantified to confirm this hypothesis.

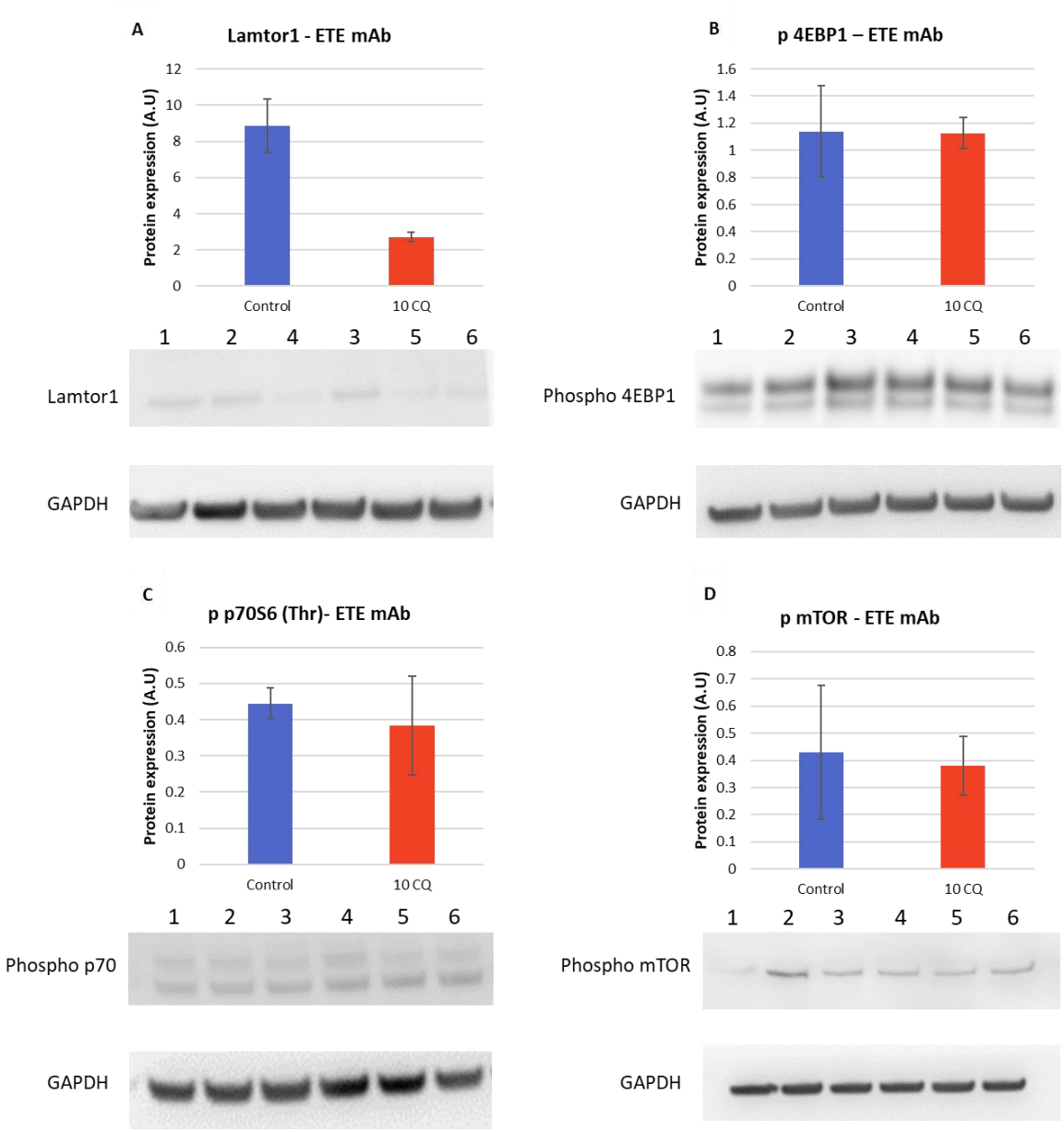

Figure 5.29 mTORC1 pathway analysis by western blot in the ETE mAb control and CQ-evolved cells. For each blot, samples 1-3 are from control and 4-6 from the CQ-evolved cells. The protein expression was normalised to GAPDH. A) Lamtor1 (p=0.0021), B) phosphorylated 4EBP1 (p=0.92), C) phosphorylated p70 S6 (p=0.51) and D) phosphorylated mTOR (p=0.76). For Lamtor1, the sample order is 1, 2, 4, 3, 5. Samples 3 and 4 were mixed. N=3, mean is shown and error bar = standard deviation.

5.2.9.4 Analysis of mTORC1 markers in DTE expressing cells

As in the analysis of cells expressing the ETE mAb, Lamtor1 expression was ~3 times lower in CQ-evolved cells than control cells (Fig 5.30 A, p=0.035), with none of the other mTORC1 markers showing any differences in expression (Fig. 5.30 B, D; p=0.20 for phosphorylated 4EBP1, and p=0.81 for phosphorylated mTOR). The phosphorylated p70 signal was too faint to be accurately quantified (Fig. 5.30 C).

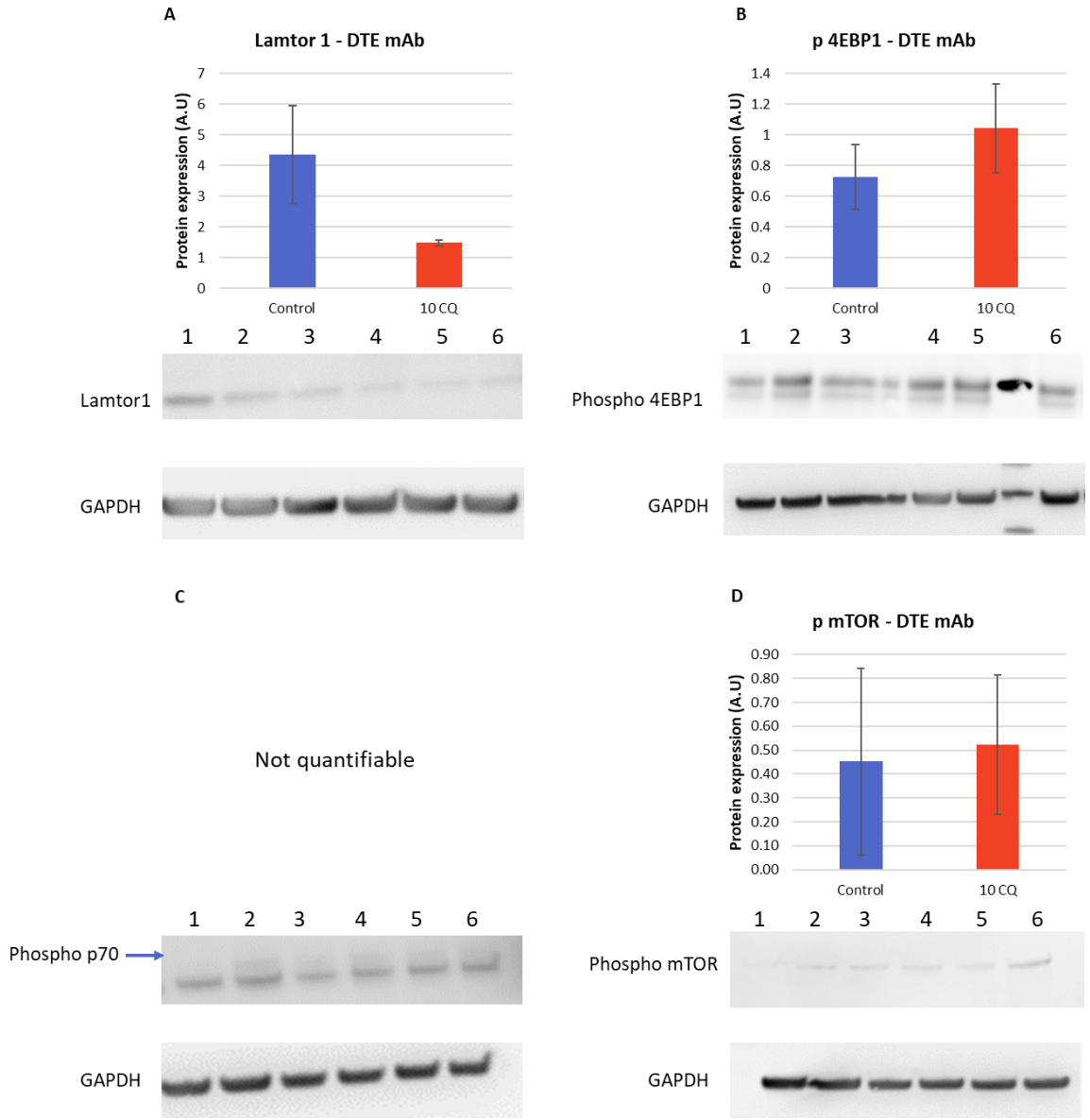

Figure 5.30 mTORC1 pathway analysis by western blot for the DTE mAb control and CQ-evolved cells. For each blot, samples 1-3 are from control and 4-6 from the CQ-evolved cells. The protein expression was normalised to GAPDH. mTORC1 substrates used were A) Lamtor1 (p=0.035), B) phosphorylated 4EBP1 (p=0.20), C) phosphorylated p70 S6 was run, but not quantifiable (arrow to top band on the membrane, very faint signal), and D) phosphorylated mTOR (p=0.81). For Lamtor1, the sample order is 1, 2, 4, 3, 5. Samples 3 and 4 were mixed. N=3, mean is shown and error bar = standard deviation. Lane 3 for phosphor 4EBP1 was not used.

5.2.9.5 Apoptosis markers in the control and CQ-evolved host cells expressing an ETE mAb

Analysis of the apoptotic markers; cleaved caspase 3 (Fig. 5.31 A), caspase3 (Fig. 5.31 B) and anti-apoptotic marker Bcl-xL (Fig. 5.31 C) revealed that their protein expression did not differ between the control and CQ-evolved cells. This would suggest that neither the extrinsic or intrinsic apoptotic pathways are differentially activated between the control and CQ-evolved cells at the time of the FBOG that samples were taken for analysis.

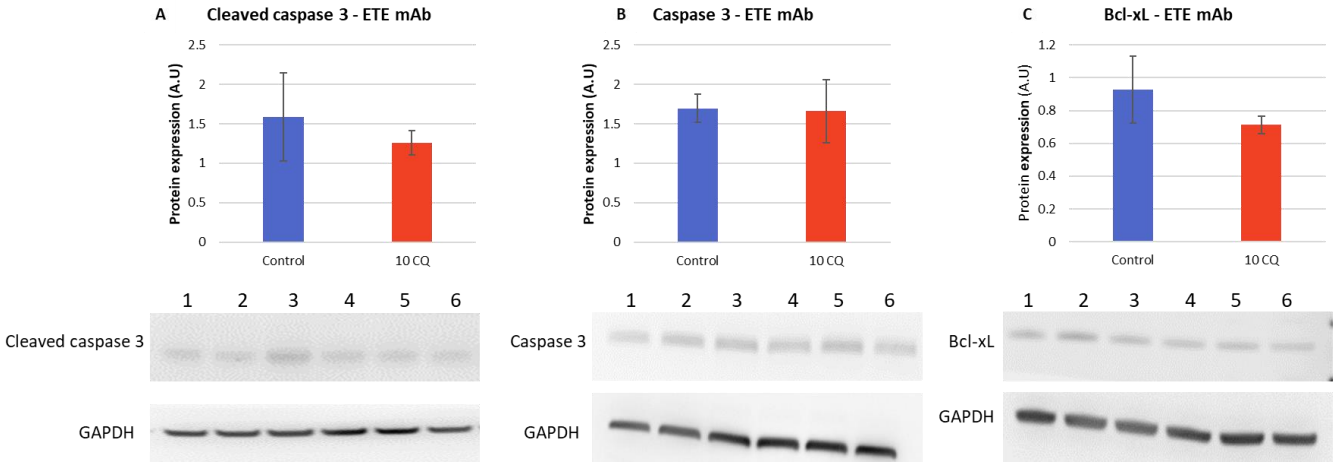

Figure 5.31 Apoptosis markers analysis by western blotting of the ETE mAb. For each blot, samples 1-3 are from control and 4-6 from the CQ-evolved cells. Protein expression was normalised to GAPDH. Apoptotic markers were A) cleaved caspase 3 (p=0.42), B) caspase 3 (p=0.89) and C) Bcl-xL (p=0.17). N=3, mean is shown and error bar = standard deviation.

5.2.9.6 Apoptosis markers in the control and CQ-evolved host cells expressing a DTE mAb

A significant decrease in cleaved caspase 3 activity was observed in the CQ-evolved cells compared to control expressing the DTE mAb, with protein expression ~5-fold lower in the CQ-evolved cells (Fig. 5.32 A, p=0.0099). This indicates a stronger apoptosis initiation from the extrinsic, and also potentially the intrinsic pathway, in the control cells compared to the CQ-evolved cells. Further, the culture viability was lower in the control cell pool samples compared to the CQ-evolved cells (86.7% for control vs. 92.4% for CQ-evolved cells). The expression of the pro-survival marker Bcl-xL (Fig. 5.32 C, p=0.16) was not significantly different between the control and CQ-evolved cells.

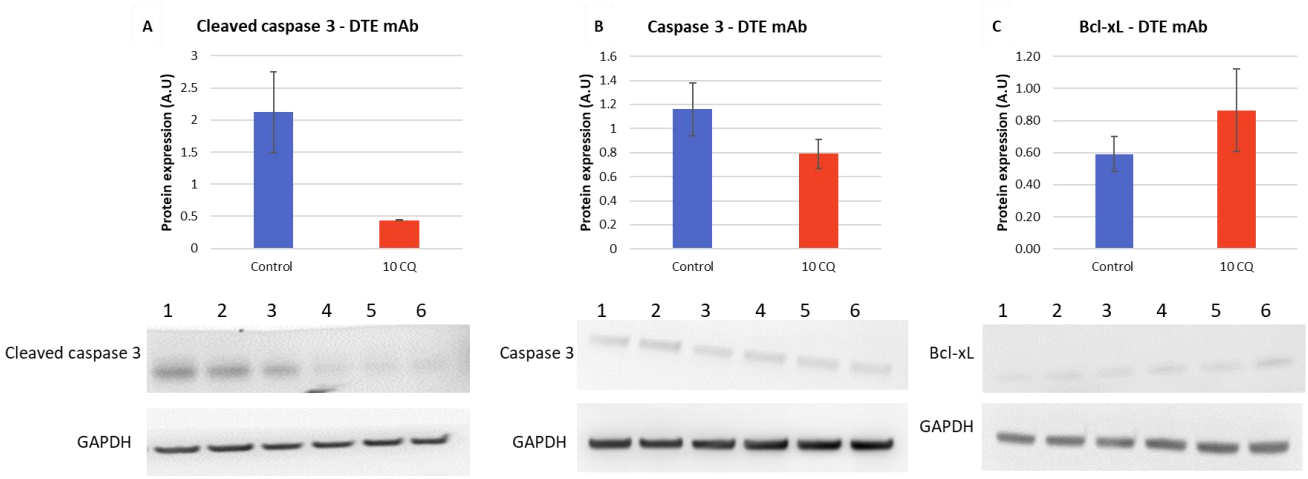

Figure 5.29 Apoptosis markers analysis by western blot of samples from control and CQ-evolved cells expressing the DTE mAb molecule. For each blot, samples 1-3 are from control and 4-6 from the CQ-evolved cells. Protein expression was normalised to GAPDH. Apoptotic markers were A) cleaved caspase 3 (p=0.0099), B) caspase 3 (p=0.06) and C) Bcl-xL (p=0.16). N=3, mean is shown and error bar = standard deviation.

5.3 Discussion

CHO cells are considered to have an unstable, plastic genome, susceptible to mutations and hence relatively easy to evolve for a mammalian system compared to other cell types. Thus, in this chapter, a novel CHO host cell pool was generated by chemical directed evolution using CQ. The aim was to develop a novel host cell line pool with increased lysosomal content, and to subsequently determine if this would result in a host cell pool with the same attributes as those obtained using cell sorting based on high lysosome content described in previous chapters, these being delayed apoptosis onset and increased homogeneity for intracellular HC/LC staining, leading to a significant improvement of mAb titre. It is also possible that directed evolution of the initial CHO host cell line could generate cell pools with a great range of specific characteristics, such as enhanced productivity.

The current AstraZeneca host cell line, in its heterogenous state, used for CLD was therefore subjected to multiple rounds of treatment with CQ, added directly into the culture media at every passage. Due to the decreased growth as a result of CQ-treatment, routine passaging was changed from 3 times a week to twice a week. As CQ-effects are concentration and time-dependent, the increased time between each addition of CQ allowed the cells more time to recover for being subjected to the compound. A range of CQ concentrations were initially assessed, and a concentration of 10 µM selected for continued CQ-treatment to evolve the cells. Higher concentrations resulted in cell death or cell growth arrest, consequences consistent with the DNA damage concentration-dependent effects of CQ [328, 334]. As it was not possible to perform genome analysis of the novel CQ-evolved host pool to determine any mutations present in the CQ-evolved host compared to the control, CQ-treatment was then withdrawn for a number of passages and then re-introduced to ensure that (i) the cells had acquired a robust CQ-resistance, and (ii) that the changes caused by CQ are a heritable trait. Re-introduction of the CQ treatment did not have a negative impact on the cells, suggesting that the cells did acquire a resistance to CQ and that this was heritable.

Once this new evolved host cell pool was evolved, different strategies for CQ-treatment post transfection were assessed. This involved removing CQ treatment at different stages prior to, or during, subsequent FBOG culturing of mAb transfected and selected cell pools. Monitoring of the lysosome content prior to, and during, FBOG culture revealed the CQ effect on lysosomes was not sustained in the absence of CQ, as lysosome content decreased as soon as CQ-treatment was removed although it did still remain higher than in the original control cells.

The CQ-evolved host cell pool performance was then assessed in terms of its ability to produce three different mAbs: one considered an ETE mAb, one considered to be a DTE mAb and a bispecific mAb. For all three molecules, the CQ-evolved host showed an increase in titre and qP compared to the

control host, ranging from a 2-fold to a 5.7-fold increase in titre depending on the molecule. A recent study investigated the effects of treating CHO cell lines expressing a mAb with different autophagy inhibitors, including CQ [267]. In this study, cells were treated with 50 µM CQ on day 4 of a FBOG culture and the authors did not observe any effect of the CQ treatment on culture viability, mAb titre or qP [267]. Another late-stage autophagy inhibitor, bafilomycin A1, also did not have any impact on productivity. The differences in the result of that study compared to the results reported here is likely due to the nature of the CQ treatment. One-time CQ addition is unlikely to have the same effect on the cells that the prolonged CQ-treatment, and the accompanied acquired resistance to CQ developed in this study, and the subsequent removal of CQ during the FBOG culture. These data suggest that the selective pressure of CQ and resistant developed to this is essential to evolve cells with a benefit in mAb productivity and prolonged culture viability.

Interestingly, there were differences observed between the ETE and DTE mAb-expressing cell pools. The culture viability of the control pools expressing the DTE mAb dropped significantly more than for the control expressing the ETE mAb. Cleaved caspase-3 levels were elevated on day 7 in the control expressing the DTE mAb, suggesting that apoptosis was already initiated at this stage of culture. Further, lysosome levels on day 10 were elevated in the CQ-evolved host expressing the DTE (compared to its control) but not for the ETE mAb. IC HC and LC protein expression were also found to be less homogenous for the cells expressing the DTE mAb compared to the ETE mAb. Taken together these observations suggest that there is an additional cellular burden placed on the cells by the DTE mAb, but the CQ-evolved host cells are able to better 'deal with;' the expression of the DTE mAb and had higher titres. As the CQ-evolved host had already been subjected to the CQ-treatment stress, it is possible that these cells have evolved to better manage different types of cellular stress explaining why the CQ-evolved cells are more robust to apoptosis for example, compared to control. However, subsequent transcriptomic analysis did not necessarily support modification of specific pathways. Rather a reduction in general gene expression as discussed below.

The CQ-evolved host cells gave the greatest increase in titre compared to that from the controls for the bispecific mAb, a 5.8-fold increase. This was largely due to the CQ-evolved host maintaining HC and LC protein expression whilst this was not the case for the control cells. Indeed, during the FBOG cultures the control host had a declining number of cells that were double positive for HC/LC protein, whereas the CQ host maintained the same ratio of expressing to non-expressing cells throughout. It is not clear why this would be the case or how the CQ-evolved cells maintain expression whilst it was lost in the control cells. However, there was no differences in the percentage of double positive HC/LC cells, or changes during the fed batch process, observed for the ETE and DTE mAb pools, potentially because these standard mAb formats are less likely to lose gene copies. On-the-other-hand, the

bispecific mAb subjects the cells to an additional burden, so cells with low mAb expression may be in higher proportions. Large increases in titres were also observed for the ETE and DTE mAb, a 2 and 3-fold increase in titre respectively, suggesting that the CQ-evolved host pool can provide increased production of different molecules. Finally, as the work used pools, and no clonal cell lines were generated, it would be of interest to combine the CQ-evolved host with cloning methods and clonal screening, to assess whether individual clones show the same titre increase or further increases compared to those isolated from the control host.

As previously described, CQ can interact with DNA and alter its structure [335], inhibit DNA polymerases at low concentrations [326], and result in defects in DNA synthesis and repair [316]. All these can potentially change the cellular makeup which could impact upon the cells' ability to synthesise, fold, assemble and apply post-translational modifications to a recombinant mAb. Thus, the product quality of the mAbs was assessed for the different hosts. For the ETE and DTE mAb, the *N*-glycan profiles were generated by mass spectrometry and did not show any differences in the relative distribution of the different glycan species present between the CQ-evolved cell pool and the control cell pool. A potential limitation of this study was that no other aspects of product quality were assessed, such as fragments, aggregates, sequence variants and glycan profiles for the bispecific mAb. Host cell protein (HCP) profiles were also not investigated. Despite most HCPs in cell culture supernatants being removed by the purification process, some HCPs can remain in the product, and impact product quality and stability [336, 337]. This could be of particular interest as some HCPs are lysosomal proteins, such cathepsins, and it would be interesting to verify that CQ manipulation of lysosomes does not increase the proportion of adverse HCPs.

For the bispecific mAb, aggregation analysis of the harvest was performed using an automated western system. A significant decrease in aggregation was observed when looking at the HC non-reduced western in the mAb derived from the CQ-evolved cells compared to that derived from the control host. However, the analysis was performed on non-purified crude cell culture supernatant samples, and it is thus possible that further purification of the product by the appropriate downstream methods would not yield any differences in aggregation profiles between the two hosts.

In order to try and begin unravelling the cellular changes that CQ evolution had on the CHO cell host pool, transcriptomic analysis was performed to compare the control and CQ-evolved cells expressing either the ETE mAb or the DTE mAb. Samples from biological triplicates were taken on day 7 of the FBOG to minimize the impact of genes differentially expressed due to the growth requirements of the cells in the early stage of the culture, or from apoptosis onset, as culture viability dropped for control cells from day 10 onwards. Subsequent PCA analysis of the transcriptomic data showed that for each

molecule and host, the biological triplicates grouped together as expected. Along the first PCA axis, cells were grouped based on the molecule they expressed, whereas CQ vs. standard host cells were differentiated along the second axis. This highlights that most differences in expression were first attributed to the molecule expressed: ETE vs. DTE, but clear differences were also present based on which host was use: control vs. CQ-evolved. For further data analysis, controls expressing the ETE or DTE mAbs were pooled together for data analysis, as were the CQ-evolved cells. This grouping allows the minimization of differences arising from different molecules expressed and to focus on the differences that arise from the CQ treatment.

Traditional gene ontology analysis or KEGG pathway analysis did not highlight any particularly relevant, actionable or specific cellular pathway(s) that that were up or down-regulated in the CQ-evolved host compared to the control. The transcriptomic analysis did exclude a number of pathways that we hypothesized as being involved in the observed increased productivity and culture viability, such as genes related to lysosomes and their biogenesis, mTORC1, pathways related to the ER and increased protein processing, or even autophagy and apoptosis. This was somewhat surprising and suggest that the observed changes in productivity and culture viability were underpinned by a large number of small changes in gene expression, by unexpected pathway regulation or via the change in expression of multiple genes from different pathways but not by whole pathway regulation. Considering that growth and productivity data was similar for the control and CQ-evolved host up to day 7, transcriptomics analysis on later stages of the culture may have revealed more significant differences between the two hosts.

It is noted that CQ is a widely used anti-malarial drug, and as such, transcriptomic analysis has been performed on *Plasmodium falciparum* (*P. falciparum*), the unicellular protozoan parasite that causes malaria in humans, treated with CQ compared to untreated. CQ treatment works by the CQ accumulation inside the acidic food vacuoles of the plasmodium, preventing the polymerization of toxic heme released during haemoglobin degradation [338, 339]. Transcriptome analysis of *P. falciparum* treated with CQ did not yield conclusive changes in gene expression pathways. In a study comparing the transcriptomic profiles of CQ-sensitive and CQ-resistant strains of *P. falciparum*, only a very few genes were identified that were differentially expressed between the two conditions. These results agree with those presented in this chapter, the authors of the study observing a similar large proportion of genes down-regulated in the CQ-treated cells compared to control (409 down-regulated genes out of 454 differentially expressed genes) [340]. GO enrichment also identified pathways linked to cell adhesion binding, host cell surface binding, receptor binding, heparin binding and lipid metabolism as being down-regulated in the CQ-treated samples [340], consistent with the analysis in this study.

In another transcriptomic study, the treatment of *P. falciparum* with CQ also reportedly resulted in only in a small number of genes being differentially expressed [341, 342]. Gunasekera et al. recorded the up-regulation of a number of antioxidant and heat shock protein genes, and the down-regulation of some mitochondrial protein genes [341, 342]. This suggests that treatment with CQ induces oxidative stress, leading to the up-regulation of antioxidant defences in the cell, [341, 342]. After CQ-treatment, the most upregulated genes were superoxide dismutase, glutathione peroxidase and glucose-6-phosphate dehydrogenase [341, 342]. Superoxide dismutase and glucose-6-phosphate dehydrogenase were not differentially expressed in the CHO CQ-evolved host pool compared to the control host, but glutathione peroxidase, along with other genes involved in glutathione metabolism were found to be upregulated in the CHO CQ-evolved cells from the RNA-seq studies.

Oxidised glutathione in the ER is involved in the formation of disulphide bonds in proteins [343], while glutathione has been reported to result in the reduction of antibody interchain disulphide bonds [344, 345]. Glutathione has also been shown to be crucial in the detoxification and protection against both hydrogen peroxide [346, 347] and nitric oxide [348]. Further, when intracellular glutathione concentrations were modulated by diethylmaleate treatment, this had a protective effect against hyperthermic treatment of cells at 43 or 45°C [349]. As (a) higher levels of glutathione have been observed in high-producing CHO cell lines [350], (b) overexpression of the glutamate-cysteine ligase catalytic subunit improves CHO cells productivity and titre [351], (c) supplementation with serum during culture results in less cellular stress and consequently a down-regulation of glutathione metabolism [352], and (d) during late exponential and stationary phase, where increased oxidative metabolism is a source of increased reactive oxygen species, glutathione level increases counteract the increased stress [353], glutathione and oxidative stress was investigated in the CQ-evolved cells here.

Using a luminescence assay, total and oxidised glutathione was measured on days 4 and 7 of a FBOG culture. CQ-evolved cells had lower levels of both total and oxidised glutathione, despite some of the glutathione genes being up-regulated. Changes and regulation at the protein level, which can be regulated post-translationally, may not be captured by transcriptomic analysis. It is also possible that there is a delay between gene expression and protein metabolism. Thus, although the effects of the increased gene expression on day 7 are not observed at the protein level on day 7, if the increased transcript levels are maintained later in culture, the levels of glutathione protein may be elevated in the later days of the FBOG. A flow cytometry assay was also used to assess the oxidative stress of the cell lines throughout the FBOG culture. This assay did not show any differences between the control and CQ-evolved cells, except for cells expressing the DTE mAb on day 4, for which the CQ-evolved cells showed a slight increase in oxidative stress compare to control.

Glutathione metabolism can also modulate autophagy and apoptosis initiation and activity. In *C. elegans*, it was observed that loss of glutathione function by knockout resulted in aggregation-prone protein, while glutathione reductase had a key role in the clearance of protein aggregation by autophagy through TFEB translocation to the nucleus and activation of p62 [354]. In three different carcinoma cell lines, nutrient deprivation was also associated with a decrease in glutathione levels and autophagy initiation [355] Moreover, glutathione and Bcl-2 have been shown to block apoptosis, by promoting GSH translocation into the nucleus, altering the nuclear redox state and inhibiting caspase activity [356-358]. To investigate whether the up-regulation of glutathione genes influenced autophagy or apoptosis at the protein level in the CQ-evolved CHO cell pools, western blot analysis was performed.

Western blot analysis of autophagy, mTORC1 and apoptosis pathway markers revealed different trends between the ETE and DTE mAb. Cells expressing the ETE-mAb displayed an increase in late stage autophagy in the CQ-evolved cells compared to control, whereas the cells expressing the DTE mAb did not show any differences in expression of the studied proteins. On the other hand, apoptosis was clearly initiated in the control cell pools expressing the DTE mAb, as seen by the increased amount of cleaved caspase 3 compared to CQ-evolved cells (although difference in culture viability between the two hosts was small, 86.7 vs. 92.4% for the control and CQ-evolved cells, respectively), but no such activation was observed in the cells expressing the ETE mAb. This suggests the effect of autophagy pathway activation is different depending on the molecule being expressed. In a study by Baek et al., two DG44 CHO cell lines expressing either an Fc fusion protein or a mAb were treated with different manipulators of autophagy [267]. Specific productivity of the Fc-fusion protein producing cell line was increased by multiple compounds (3-methyl adenine (3-MA), dorsomorphin and SP600125), all described as inhibitors of autophagy, although the authors observed that the cell lines instead exhibited an increased autophagic flux. The cell line expressing the mAb was only affected by 3-MA, which increased autophagy [267]. The differences in the effect of the autophagy inhibitors suggest that autophagy pathways may be affected by the molecule-expressed and by culture conditions, as 3-MA has been reported to increase qP both in batch and fed-batch conditions [75, 267]. A further study using 3-MA treatment also reported that the increase in productivity was CHO cell clone-dependent [359]. This suggests that depending on the molecule expressed, and variation between cell lines/pools, the autophagic flux and activation may differ.

Analysis of the mTORC1 pathway revealed over-expression of only the Lamtor1 protein in control compared to the CQ-evolved cells, for both the ETE and DTE mAb. Lamtor1 is essential for the formation of the Ragulator-Rag complex and activation of mTORC1 [360]. The levels of the *lamtor1* gene was also up-regulated at the mRNA level in control cells, with a 2.2-fold change compared to CQ-

evolved cells. Lamtor1 depletion, in a human neuroblastoma cell line (SHEP), has been associated with increased lysosomal activation and catabolism, generating many reactive oxygen species and eventually leading to p53 dependent apoptosis [361]. In T-cells, Lamtor1-deficient cells showed decreased cell proliferation and mTORC1 activity, [362], which was not observed in the CQ-evolved CHO cell pools. As no other lysosomal genes or mTORC1 related genes were differentially expressed in the CQ-evolved cell pools, it is difficult to explain any impact of the increased Lamtor1 expression. There could be a delay between increased Lamtor1 expression and increased activation of the mTORC1 pathway, however there was no data to support this hypothesis.

Overall, the exact pathways underpinning the increased productivity of the CQ-evolved host remain unclear. As reported with CQ-transcriptomics of other organisms, the CQ effect is broad but low in intensity, and can affect many different pathways. Many genes were found to be down-regulated in the CQ-evolved cells compared to control cells, consistent with other transcriptomic studies. Our transcriptomic data did not identify any lysosome related pathways, autophagy or mTORC1 pathway to be differentially activated, and protein analysis confirmed those observations. Several genes related to glutathione metabolism were up-regulated in CQ-evolved cells compared to control cells, but the protein levels of glutathione, total and oxidised, on day 7 of the FBOG culture did not show any increase in glutathione levels compared to the control. Further work at the protein level and on different days would need to be performed to further elucidate the specific mechanism(s) underpinning the increased productivity of the CQ-evolved host.

In conclusion, a novel CQ-evolved host cell pool has been developed and shown to deliver increased productivity compared to the control cell pool. Increases in titre were shown for three different molecules, ranging from a 2-fold to a 5.8-fold increase in productivity, without affecting product quality. Transcriptomic and protein analysis of the control and the CQ-evolved host did not reveal a clear mechanism by which productivity was improved, and it is thus possible that the CQ-treatment has impacted many different cellular pathways. Analysis of samples obtained at different stages of a FBOG culture may reveal more differences between the two hosts. The CQ-evolved host has the advantage of improving titre and sustaining culture viability and can be combined with different cloning methods in a cell line development campaign for the generation of more productive clonal cell lines.

CHAPTER 6

Discussion

6.1 Overall discussion

When considering the biopharmaceutical markets, IgG products have shown success over the past decades, as they are easy to develop and manufacture in large quantity. However, saturation of the biopharmaceutical market has meant that the new drugs developed need to have a more advanced mode of action with a better efficacy than the already approved drug products, hence resulting in novel molecule formats, such as molecules that can have two targets and hence a combinational effect. Analysis of the biopharmaceutical products approved globally between 2014 and 2018 shows that only 52% (of 155 individual products) were novel, with the other 48% consisting of biosimilars or products previously approved in a different geographical region, as it is cheaper to copy previously validated molecules, compared to the research and development of novel molecules, which comprise the cost of many failed molecules [4]. Production capacities have soared since the first biological approval in the mid-1980's, with current productivities for IgGs, reaching titres up to 1,000-fold higher [18]. However, novel modalities and drug formats, such as bispecific mAbs, are becoming increasingly more common in development pipelines, and bring their own development challenges. In particular, such 'non-natural' molecules are more challenging for the current mammalian host cell lines to correctly synthesise, assemble and secrete and as such the yields and product quality are much inferior to those obtained for standard mAb products.

Improvement of the cell line development process, using selection markers during FACS cloning or via engineering of different cellular pathways of the host cell line, has proven a successful strategy to isolate or develop host cells with increased capacity for biotherapeutic productivity or product quality. However, as described above, these hosts can struggle to deliver such product titres and quality when novel format molecules are expressed. There is a need to develop new hosts that are able to 'handle' the requirements of such molecules. In the work reported here, development of a novel screening strategy during FACS cloning based upon the investigation of cellular attributes, in particular organelle content, and the relationship with productivity and/or growth, was first investigated using IFC (Chapter 3). Having identified lysosome content as having a positive correlation with mAb productivity, the work then focused upon investigating whether lysosome content could be used as a

screening tool for cell sorting by FACS (Chapter 4), and finally, whether through the directed evolution of CHO cells by applying chloroquine selection, the lysosome content of the host cell could be enhanced and lead to isolation of a more productive host cell pool (Chapter 5).

Initially, a panel of 19 cell lines expressing what was considered to be an ETE mAb was characterised throughout a FBOG culture based on their organelle content by IFC. All dyes to analyse organelle content were commercially available and could be used in live cell imaging, thus could potentially be easily incorporated into the cell line development platform. IFC is a powerful tool for cellular analysis, and assays are fully transferable to a standard flow cytometer, yet its use in cell line development remains limited. The lack of capabilities for cell sorting, based on simple fluorescence intensity or more complex features such as sub-cellular localization of proteins for example, currently limits IFC to be a screening tool. However, imaging cell sorters may be commercially available in the next few years as researchers have been working towards their development for just such purposes [251]. This is likely to result in the application of such technology for novel strategies for cell line development based on intracellular staining localisation and morphological features.

In the study here, organelles including the ER and Golgi apparatus were investigated as cellular markers of productivity due to their role in protein folding and overall protein production. Consistent with other reports, no correlations were found between the ER and Golgi apparatus content of mAb expressing clones and their cellular productivity [50, 252]. Mitochondria content was also investigated, considering its role in cellular energy production, but again this revealed no correlation with productivity although it is noted that mitochondrial membrane potential is a better marker of cellular metabolism than the number of mitochondria in a cell [260]. The lysosome content was investigated, as it is the main organelle related to autophagy, and is also essential for mTORC1 activation. Of all the organelles studied, only the lysosome content of the cell showed a positive correlation with mAb specific productivity (Chapter 3). As the lysosome is involved in autophagy, the initial hypothesis was that cells with a higher lysosome content might be capable of handling larger volumes of autophagic material, and hence can be more resistant to cellular stress. To the best of the author' knowledge, this is the first report suggesting that the lysosome content itself is indicative of mAb productivity. It is noted that the work presented in Chapter 3 was applied only to cell lines expressing one ETE mAb, however the toolbox of assays developed can easily be applied to cells expressing different molecules to determine which, if any, organelle content correlates with productivity. Investigation of different recombinant biopharmaceutical molecules with the IFC assays could be an effective platform to better characterise and understand the factors underpinning secretory recombinant protein production on a molecule-to-molecule basis, and subsequently

develop cell sorting strategies to isolate cells with increased capacity to synthesise and secrete such molecules.

To further investigate the finding that lysosome content has a positive correlation with productivity, cell sorting based on lysosome-content was undertaken (Chapter 4). The results of the cell sorting were mixed, cells with high lysosome content showed increased titres between 30-100% depending on the molecule expressed (bispecific mAb or ETE mAb). Importantly, we only investigated sorting from a pool produced from mixing clonal cell lines with different productivities together. Further work on cell lines expressing different molecules and generating clonal cell lines from transfection pools (rather than a mix of clonal cell lines) with the high-lysosome content screening step would help inform as to whether the lysosome content-based cell sorting could be a useful screening tool to incorporate into the cell line development process. If higher producing cells were isolated, this could have the benefit of decreasing the number of clonal cell lines that need to be screened, as well as decreasing the resources needed to identify high expressing and stable clonal cell lines.

Published strategies for improving titre based on cell sorting by FACS have also showed a range of success. Cell sorting based on extracellular cell surface staining of secreted mAb did not show any improvement in productivity [214]. However, combining the staining of antibody bound to the cell membrane, with cold capture, has shown great success, ranging from up to 3-fold increase in productivity [216], to up to 20-fold increase in specific productivity when using three rounds of FACS cloning, and enriching the desired population [215]. The use of a surface affinity matrix, which also relies on capturing secreted proteins onto the cell surface, using biotin-avidin bridge, has also been successful, with up to 5-fold increase in specific productivity [205]. The use of co-expression methods to generate surface displayed mAbs has also been reported in the literature. The antibody-membrane switch, as described by Yu et al. [211], managed to isolate cell lines with specific productivity reaching 40-60 pg/cell/day, with final titres of 2-4 g/L in 10-day batch culture. Another antibody cell surface capture method, described by Land et al., achieved an 8-fold increase in productivity compared to limiting dilution or cold capture [212]. Finally, Chakrabarti et al., through the use of an amber stop codon combined with a non-natural amino acid achieved a 2-fold increase in productivity [213]. Co-expression of the recombinant protein and GFP has also been a commonly used method. A 6-fold increase in specific productivity was achieved by Meng et al., by transfecting cells with GFPI on a different vector than the protein of interest [210]. By using split GFP, half of the GFP on the HC and the other half on the LC, Kim et al. isolated clones after two FACS cloning rounds with titres increased by 2-10 fold compared to unsorted cells [207]. Finally, one FACS cloning method based solely on gating on forward and side scatter has led to 3.4-4.7-fold increase in final titre [214]. Compared to the methods described above, the lysosome-based cell sorting described in this thesis, which has showed

increase in titres ranging from 30-100% based on the molecule, is a novel and promising method, easy to implement, that could significantly improve the production of biopharmaceutical products. Moreover, as the lysosome content-based cell sorting relies on the use of a fluorescent dye, it could be used in combination with other cell sorting methods.

Manipulation of lysosome content was also investigated by the development of a novel host cell pool via a directed evolution approach. For this purpose, CQ was used as a chemical selective pressure, increasing lysosome content in our cells. The directed evolution cell pool was then used to generate recombinant mAb expressing cell pools. Following transfection, CQ treatment was stopped and lysosome content was shown to be similar compared to the original control cell line. However, CQ-treated cells showed a significant increase in titre for three different molecules (an ETE and DTE mAb, and a bispecific mAb). This novel host pool provides a new host with different attributes to the original host for the development process. The host cell selection is crucial when starting a cell line development campaign, and the addition of a novel host with different attributes may provide the opportunity to explore this as a host for the production requirements of specific molecules when other hosts cannot provide the required titre or product quality. Moreover, as CQ is an inexpensive reagent and can be easily added to cultures, the development of CQ-evolved hosts or cell line development processes is achievable not only for the industry, but also academic labs. The study reported here has only focused on the development of a CQ-evolved host based on the proprietary standard host of AstraZeneca, but it would be interesting to investigate whether other host cell lines, with their different lineages and attributes, would benefit from CQ directed evolution with respect to the expression of biopharmaceuticals.

Both strategies of the high-lysosome content sorted cells and the CQ-evolved cells, despite having the end goal of increasing baseline lysosome content, did not produce cells that maintained the phenotype of increased lysosome content in the early stages of a FBOG culture compared to their respective controls. However, these strategies did deliver an increased product titre overall. Lysosome content throughout the recovery post cell sorting or post transfection for the CQ-evolved host was not monitored, and it is thus unknown when the decrease in lysosome content occurred. It appears that in both cases, the cells with increased lysosome content reverted towards a lysosome content which was an average of non-sorted (or control) cells. However, differences in lysosome content was observed in later stages of the FBOG culture, although to varying amounts, when cellular and culture stress are higher than in the earlier stages of the FBOG culture. This suggests that cell sorting based on lysosome content or CQ-selection pressure does not generate a new host cell pool with a constantly enhanced lysosome content, but rather cells with an enhanced capacity to increase

their lysosome content. Thus, such cells might have an increased ability for lysosome biogenesis, increasing the lysosomes capacity and lysosomes number in response to stress.

CQ-evolution was performed as an alternative to the lysosome content cell sorting. Both the CQ-evolved cells and the high lysosome content cells resulted in increased titres as well as delayed apoptosis. The high lysosome content sorted cells also had an increase in homogeneity of IC HC/LC expressing cells for the ETE mAb. The CQ-evolved cells also showed an increase in the ratio of double positive LC/HC expressing to non-expressing cells and did not lose expression of HC/LC during a FBOG for a bispecific mAb, but no differences in expressing populations were observed for the ETE or DTE mAb. The strategy to improve cells' productivity might vary for each biotherapeutic, as for the ETE mAb cell sorting based on high lysosome content was most beneficial, whereas for the DTE mAb, the CQ-evolved host gave the largest increase in productivity compared to the control cell line. Despite the increased titre of both the lysosome content cell sorted pools and the CQ-evolved host, transcriptomic and proteomic analysis suggests potentially different mechanisms underlying the observed increased productivity, as no lysosome-related genes were found to be differentially expressed.

The role of mTORC1 pathway was investigated, as mTORC1 is essential for cell growth and protein production and requires translocation to the lysosome membrane for its activation. When considering the activity of the mTORC1 signalling pathway in these cells, there were very few proteins that had significant differences in their level of expression, suggesting that mTORC1 activity is similar between the high lysosome content sorted, CQ-evolved cells and their respective controls. High lysosome content cells had decreased levels of phosphorylated 4EBP1 compared to controls, but this was not apparent in the CQ-evolved cells for either of the mAbs investigated. Increased levels of phosphorylated 4EBP1 are indicative of inhibition / decreased activity of the mTORC1 pathway, which leads to reduced protein synthesis and autophagy activation. It is interesting to note that cell lines with low levels of 4EBP1 have been associated with higher productivity previously [137]. This suggests that mTORC1 activity on day 7 of the FBOG cultures was different between the high lysosome content sorted cells and the CQ-evolved cells.

Autophagic flux was also different between the high lysosome content sorted cells and the CQ-evolved cells. Late stage autophagy was decreased in both CQ-evolved cells expressing the ETE mAb compared to control, as well as the high lysosome content sorted cells. However, the overall autophagic flux was similar between control and CQ-evolved cells, but for the high lysosome content sorted cells, their autophagic flux was increased compared to their respective control. The differences in the autophagy flux between the two strategies suggest that different cellular mechanisms are at play. This is also

supported by the fact that for the high lysosome content sorted cells, an increase in lysosome content was observed on day 10 of the culture, but this increase in lysosome content was not observed for the CQ-evolved cells. Overall autophagic flux of the CQ-evolved cells expressing the DTE mAb was up-regulated compared to control. This highlights how autophagy flux can be molecule-dependent, and that the cellular stresses associated with expression of different molecules have different impact on cellular processes. Apoptosis initiation was decreased in both the high lysosome content sorted cells expressing an ETE mAb, and the CQ-evolved host expressing the DTE mAb, compared to their respective controls. No differences in apoptosis initiation were observed for the CQ-evolved host expressing the ETE mAb and its control, despite the culture viability of the control dropping to 80% on day 10. For the CQ-evolved cells, cells expressing the DTE mAb showed both an increase in autophagy and a decrease in apoptosis compared to their control, which was not observed for the ETE mAb. This could be because the DTE mAb expression is more challenging, and the cells have more stress to handle compared to the expression of the ETE mAb.

Collectively these data suggest that the high lysosome content sorted cells and the CQ-evolved host have different cellular properties, and sense and respond to cellular and culture stress associated with the production of mAbs in diverse manners. The data suggest that different pathways may underpin the observed impact on productivity of these two different approaches. Cell sorting only focused on isolating cells based upon high lysosome content, whereas CQ effects are not limited to its action on lysosomes. As the impact of CQ is wider at the cellular level, it is likely that the mechanisms underlying the increase in titre observed in the CQ-evolved host are different than those involved in the cell sorted based on high lysosome content alone.

In this study, CQ-treatment has been shown to increase cell productivity and prolong culture viability, while maintaining product quality, and in the case of a bispecific mAb, potentially reducing aggregation. To inform on future targets for cell line engineering strategies, transcriptomic analysis of the CQ-evolved and the control hosts, expressing the ETE and DTE mAb, was performed. Interestingly, but consistent with transcriptomics studies of *P. falciparum* [340, 341], GO and KEGG analysis did not identify any specific pathway or molecular functions as being enriched in the CQ-evolved host recombinant producing pools compared to controls. Out of the differentially expressed genes identified, most (77%) were down-regulated in the CQ-evolved host compared to control. Of particular interest, genes related to glutathione metabolism were up-regulated (as identified by manual analysis of the differentially expressed genes) in CQ-evolved cells, and reports of increased glutathione levels have been associated with increased CHO cell productivity [350, 351]. However, the increased glutathione gene expression did not appear to be translated at the protein level, potentially due to an

increased degradation of the protein, with the ratio of total to oxidised glutathione being similar between the CQ-evolved cells and the control, on days 4 and 7 of the FBOG.

As illustrated by this work, the solutions identified to increase recombinant protein productivity, either through high lysosome content cell sorting or the use of a novel CQ-evolved host, remain molecule-specific. High lysosome content cell sorting had a greater impact on the expression of an ETE mAb, whereas the CQ-evolved host pool significantly increased the productivity of more DTE molecules over that from the control. Thus, characterisation of the organelle content of host and recombinant cells on a product-by-product-basis could be used to determine the cell content of organelles that can be used as a predictive tool of final titre. As well as the application of the CQ-evolved cell pool or use of CQ in cell line development to deliver recombinant cell lines with product specific enhanced titre and product quality.

6.2 Future work

From the results presented in this thesis, the direction of future work could follow different paths. One limitation of this study is that the organelle characterisation was only performed on a panel of cell lines expressing what was considered an ETE mAb. However, as cellular bottlenecks can be product-specific, it is likely that organelles other than the lysosome content may be identified as predictors of productivity for different molecules. An interesting experiment would be to characterise the organelle content of a panel of cell lines expressing different antibodies or recombinant products and determine whether any correlations with productivity are present. A further limitation of the work was that it did not reflect the complete and optimal cell line development process. All the work presented in this thesis was performed with pools and sorted from a mixture of different clonal cell lines. It would be valuable to perform a cell line development campaign, starting by transfection of the host cell line with different molecules of interest, and perform single cell cloning by FACS based on high lysosome content, and as a control, random FACS cloning regardless of lysosome content. Additional controls based on other cloning methods (ClonePix or single cell printing) could be included as well to assess whether cell sorting based on lysosome content offers a benefit in the cell line development platform in terms of isolating high producing clonal cell lines.

From the high lysosome content cell sorting study, we observed that the more heterogenous the original cell mix was in its IC HC and LC expression, and the wider the range of lysosome content was, the more effective the screen was at isolating homogenous high expressing cells. Pre-screening a transfected pool of cells for lysosome content to check if it was heterogeneous enough for the high

lysosome cell sorting to work would be essential. Moreover, only two molecules were investigated in this work, an ETE and a bispecific mAb. The increase in titre of the ETE mAb was 200% whereas the bispecific mAb titre only increased by 30%. As cell sorting based on high lysosome content appears to be product-specific, investigating the impact of this method on different molecules would be valuable to identify which product-formats would benefit most from this cell sorting strategy. From the two molecules investigated here, it appears that cell sorting based on high lysosome content is more successful for ETE standard mAbs, whereas the impact on more difficult formats such as bispecifics was more modest. This likely reflects the challenge of expressing bispecific formats to the cell, and due to the low expression levels a 30% increase in bispecific mAb expression, if consistent across different bispecifics, may still be sufficient to generate a real advancement in expression and cost benefit.

Another commonly used strategy used within industry is repeated enrichment by FACS through multiple rounds of cell cloning based on the desired product attribute, or a more stringent selection parameter [200]. By enriching cells with high lysosome content through multiple cloning rounds, the probability of isolating rare cells with heritable phenotypes would be increased. This strategy could isolate cells with a stable and higher level of lysosome content, something not observed with the pool sorting based on one round of high lysosome content cell sorting in this work.

Building on the development of the CQ-evolved host, it would be interesting to generate clonal cell lines from the CQ pool and investigate whether the titre increase seen with sorted pools could be further increased from generating clonal cell lines. Combining the high lysosome cell sorting with the CQ-evolved host would allow the investigation of whether the two strategies could be synergistic in producing cell lines with increased titres. Another strategy that could be combined with the CQ-evolved host is the use of a temperature shift to further improve protein production [363]. The lower temperature not only initiate the growth arrest phase, but also leads to a decrease in apoptosis, hence an extended production phase, yielding a higher final titre [363, 364]. Finally, the CQ-evolved host has also showed the ability to decrease aggregation in the bispecific mAb. Further work could investigate the impact of using the CQ-evolved host transfected with different mAbs prone to aggregation. If the CQ-evolved host was able to consistently decrease protein aggregation, this could have a positive impact on the downstream process, reducing resources needed and costs.

Finally, the mechanisms underlying the observed increased productivity of the CQ-evolved host have not been fully unravelled. It remains unclear at present which genes and proteins, played a key role in improving culture viability and productivity. This requires further investigation, by monitoring the genes and proteins expression on different days of the FBOG, to deepen our understanding of the

Nevertheless, the increased product titre delivered by the CQ-evolved cell pool offers an exciting novel host to enhance biopharmaceutical production of a range of different molecule formats from CHO cells.

In summary, the work described in this thesis has delivered:

- Development of IFC assays for organelle quantification and application of these to a panel of cell lines to identify lysosome content as a positive marker of mAb productivity
- Application of lysosome content-based cell sorting to cell lines expressing two different molecules, which generated more productive pools.
- Development of a novel host cell pool through directed evolution using chloroquine
- Demonstration that the chloroquine-evolved host, when assessed in FBOG culture for expression of different recombinant molecules, delivers a significant increase in productivity compared to the standard host cell line, although the exact molecular mechanism underlying this increased productivity remain unknown.

References

1. Walsh, G., *Biopharmaceutical benchmarks 2014.* Nature biotechnology, 2014. **32**(10): p. 992-1000.
2. Ecker, D.M., S.D. Jones, and H.L. Levine, *The therapeutic monoclonal antibody market.* MAbs, 2015. **7**(1): p. 9-14.
3. Gaughan, C.L., *The present state of the art in expression, production and characterization of monoclonal antibodies.* Molecular diversity, 2015.
4. Walsh, G., *Biopharmaceutical benchmarks 2018.* Nat Biotechnol, 2018. **36**(12): p. 1136-1145.
5. Sven Sommerfeld, J.S., *Challenges in biotechnology production—generic processes and process optimization for monoclonal antibodies.* Chemical Engineering and Processing: Process Intensification, 2005. **44**(10): p. 1123-1137.
6. Liu, J.K., *The history of monoclonal antibody development - Progress, remaining challenges and future innovations.* Annals of medicine and surgery (2012), 2014. **3**(4): p. 113-116.
7. Scott, C.T., *Mice with a human touch.* Nature biotechnology, 2007. **25**: p. 1075.
8. Weinberg, W.C., et al., *Development and regulation of monoclonal antibody products: challenges and opportunities.* Cancer metastasis reviews, 2005. **24**(4): p. 569-584.
9. Diamantis, N. and U. Banerji, *Antibody-drug conjugates--an emerging class of cancer treatment.* Br J Cancer, 2016. **114**(4): p. 362-7.
10. Zhu, J., *Mammalian cell protein expression for biopharmaceutical production.* Biotechnol Adv, 2012. **30**(5): p. 1158-70.
11. Ghaderi, D., et al., *Implications of the presence of N-glycolylneuraminic acid in recombinant therapeutic glycoproteins.* Nat Biotechnol, 2010. **28**(8): p. 863-7.
12. Jager, V., et al., *High level transient production of recombinant antibodies and antibody fusion proteins in HEK293 cells.* BMC Biotechnol, 2013. **13**: p. 52.
13. Kuczewski, M., et al., *A single-use purification process for the production of a monoclonal antibody produced in a PER.C6 human cell line.* Biotechnol J, 2011. **6**(1): p. 56-65.
14. Spens, E. and L. Haggstrom, *Defined protein and animal component-free NS0 fed-batch culture.* Biotechnol Bioeng, 2007. **98**(6): p. 1183-94.
15. Dumont, J., et al., *Human cell lines for biopharmaceutical manufacturing: history, status, and future perspectives.* Crit Rev Biotechnol, 2016. **36**(6): p. 1110-1122.
16. Kunert, R. and D. Reinhart, *Advances in recombinant antibody manufacturing.* Appl Microbiol Biotechnol, 2016. **100**(8): p. 3451-61.
17. Butler, M. and M. Spearman, *The choice of mammalian cell host and possibilities for glycosylation engineering.* Curr Opin Biotechnol, 2014. **30**: p. 107-12.
18. Wurm, F.M., *Production of recombinant protein therapeutics in cultivated mammalian cells.* Nature biotechnology, 2004. **22**(11): p. 1393-1398.
19. Li, F., et al., *Cell culture processes for monoclonal antibody production.* mAbs, 2010. **2**(5): p. 466-479.
20. Kim, J.Y., Y.G. Kim, and G.M. Lee, *CHO cells in biotechnology for production of recombinant proteins: current state and further potential.* Appl Microbiol Biotechnol, 2012. **93**(3): p. 917-30.
21. Wurm, F. and A. Bernard, *Large-scale transient expression in mammalian cells for recombinant protein production.* Curr Opin Biotechnol, 1999. **10**(2): p. 156-9.
22. Chu, G., H. Hayakawa, and P. Berg, *Electroporation for the efficient transfection of mammalian cells with DNA.* Nucleic Acids Res, 1987. **15**(3): p. 1311-26.
23. Brown, M.E., et al., *Process development for the production of recombinant antibodies using the glutamine synthetase (GS) system.* Cytotechnology, 1992. **9**(1-3): p. 231-6.
24. Flintoff, W.F., et al., *Moderate-level gene amplification in methotrexate-resistant Chinese hamster ovary cells is accompanied by chromosomal translocations at or near the site of the amplified DHFR gene.* Mol Cell Biol, 1984. **4**(1): p. 69-76.
25. Yoshikawa, T., et al., *Evaluation of stable and highly productive gene amplified CHO cell line based on the location of amplified genes.* Cytotechnology, 2000. **33**(1-3): p. 37-46.
26. ICH, *Preclinical safety evaluation of biotechnology-derived pharmaceuticals. ICH Guideline S6 (R1)*, I.C.o.H.o.T.R.f.R.o.P.f.H. Use, Editor. 2011: Geneva.

27. Dharshanan, S., et al., *Rapid automated selection of mammalian cell line secreting high level of humanized monoclonal antibody using Clone Pix FL system and the correlation between exterior median intensity and antibody productivity.* Electronic Journal of Biotechnology, 2011. **14**(2).
28. Newman, E.N.C. and D. Whitney, *Rapid automated selection of mammalian cell colonies by cell surface protein expression.* Nature Methods, 2007. **4**: p. 462.
29. Coller, H.A. and B.S. Coller, *Poisson statistical analysis of repetitive subcloning by the limiting dilution technique as a way of assessing hybridoma monoclonality.* Methods Enzymol, 1986. **121**: p. 412-7.
30. Nakamura, T. and T. Omasa, *Optimization of cell line development in the GS-CHO expression system using a high-throughput, single cell-based clone selection system.* Journal of bioscience and bioengineering, 2015. **120**(3): p. 323-329.
31. Roy, G., et al., *Sequential screening by ClonePix FL and intracellular staining facilitate isolation of high producer cell lines for monoclonal antibody manufacturing.* J Immunol Methods, 2017. **451**: p. 100-110.
32. Molecular Devices, L., *Method of selecting monoclonal cell colony*. 2013, Molecular Devices, Inc.
33. Rameez, S., et al., *High-throughput miniaturized bioreactors for cell culture process development: reproducibility, scalability, and control.* Biotechnol.Prog., 2014. **30**(3): p. 718.
34. Wurm, F., *CHO Quasispecies—Implications for Manufacturing Processes.* Processes, 2013. **1**(3): p. 296-311.
35. Puck, T.T., S.J. Cieciura, and A. Robinson, *Genetics of somatic mammalian cells. III. Long-term cultivation of euploid cells from human and animal subjects.* J Exp Med, 1958. **108**(6): p. 945-56.
36. Jayapal , W., Hu *Recombinant Protein Therapeutics from CHO cells -*

20 years and counting., in *CHO Consortium*. 2007. p. 40-47.
37. Hayflick, L. and P.S. Moorhead, *The serial cultivation of human diploid cell strains.* Exp Cell Res, 1961. **25**: p. 585-621.
38. Puck, T.T. and F.T. Kao, *Genetics of somatic mammalian cells, VI, use of an antimetabolite in analysis of gene multiplicity.* Proc Natl Acad Sci U S A, 1968. **60**(2): p. 561-8.
39. Wurm, F., H. Hauser, and R. Wagner, *CHO History, CHO Evolution and CHO Genomics - an unsolvable Enigma?*, in *Animal Cell Biotechnology: In biologics production*. 2015, De Gruyter: Germany.
40. Kao, F.T. and T.T. Puck, *Genetics of somatic mammalian cells. IV. Properties of Chinese hamster cell mutants with respect to the requirement for proline.* Genetics, 1967. **55**(3): p. 513-24.
41. Graf, L.H., Jr. and L.A. Chasin, *Direct demonstration of genetic alterations at the dihydrofolate reductase locus after gamma irradiation.* Mol Cell Biol, 1982. **2**(1): p. 93-6.
42. Thompson, L.H., S. Fong, and K. Brookman, *Validation of conditions for efficient detection of HPRT and APRT mutations in suspension-cultured Chinese hamster ovary cells.* Mutat Res, 1980. **74**(1): p. 21-36.
43. Urlaub, G., et al., *Deletion of the diploid dihydrofolate reductase locus from cultured mammalian cells.* Cell, 1983. **33**(2): p. 405-12.
44. Xu, N., et al., *Comparative Proteomic Analysis of Three Chinese Hamster Ovary (CHO) Host Cells.* Biochem Eng J, 2017. **124**: p. 122-129.
45. Worton, R.G., C.C. Ho, and C. Duff, *Chromosome stability in CHO cells.* Somatic Cell Genet, 1977. **3**(1): p. 27-45.
46. Cao, Y., et al., *Construction of BAC-based physical map and analysis of chromosome rearrangement in Chinese hamster ovary cell lines.* Biotechnol Bioeng, 2012. **109**(6): p. 1357-67.
47. Urlaub, G. and L.A. Chasin, *Isolation of Chinese hamster cell mutants deficient in dihydrofolate reductase activity.* Proc Natl Acad Sci U S A, 1980. **77**(7): p. 4216-20.
48. Kaufman, R.J., et al., *Coamplification and coexpression of human tissue-type plasminogen activator and murine dihydrofolate reductase sequences in Chinese hamster ovary cells.* Mol Cell Biol, 1985. **5**(7): p. 1750-9.
49. Carlsen, S.A., *Stimulation of plasminogen activator production by dimethyl sulfoxide in Chinese hamster ovary cells.* Biochem Cell Biol, 1987. **65**(8): p. 710-6.
50. Reinhart, D., et al., *Benchmarking of commercially available CHO cell culture media for antibody production.* Applied Microbiology and Biotechnology, 2015. **99**(11): p. 4645-4657.
51. Berting, A., M.R. Farcet, and T.R. Kreil, *Virus susceptibility of Chinese hamster ovary (CHO) cells and detection of viral contaminations by adventitious agent testing.* Biotechnol Bioeng, 2010. **106**(4): p. 598-607.
52. Kelley, B., *Industrialization of mAb production technology: the bioprocessing industry at a crossroads.* MAbs, 2009. **1**(5): p. 443-52.

53. van Berkel, P.H., et al., *N-linked glycosylation is an important parameter for optimal selection of cell lines producing biopharmaceutical human IgG.* Biotechnol Prog, 2009. **25**(1): p. 244-51.
54. Vidarsson, G., G. Dekkers, and T. Rispens, *IgG subclasses and allotypes: from structure to effector functions.* Front Immunol, 2014. **5**: p. 520.
55. Liu, H. and K. May, *Disulfide bond structures of IgG molecules: structural variations, chemical modifications and possible impacts to stability and biological function.* MAbs, 2012. **4**(1): p. 17-23.
56. Torres, M., et al., *The immunoglobulin heavy chain constant region affects kinetic and thermodynamic parameters of antibody variable region interactions with antigen.* The Journal of biological chemistry, 2007. **282**(18): p. 13917-13927.
57. Jefferis, R., *Posttranslational Modifications and the Immunogenicity of Biotherapeutics.* J Immunol Res, 2016. **2016**: p. 5358272.
58. Huber, R., et al., *Crystallographic structure studies of an IgG molecule and an Fc fragment.* Nature, 1976. **264**(5585): p. 415-20.
59. Suzuki, M., C. Kato, and A. Kato, *Therapeutic antibodies: their mechanisms of action and the pathological findings they induce in toxicity studies.* J Toxicol Pathol, 2015. **28**(3): p. 133-9.
60. Le Fourn, V., et al., *CHO cell engineering to prevent polypeptide aggregation and improve therapeutic protein secretion.* Metab Eng, 2014. **21**: p. 91-102.
61. Mead, E.J., et al., *Biological insights into the expression of translation initiation factors from recombinant CHOK1SV cell lines and their relationship to enhanced productivity.* The Biochemical journal, 2015. **472**(3): p. 261-273.
62. Carpentier, E., et al., *Limiting factors governing protein expression following polyethylenimine-mediated gene transfer in HEK293-EBNA1 cells.* J Biotechnol, 2007. **128**(2): p. 268-80.
63. Mead, E.J., et al., *Identification of the limitations on recombinant gene expression in CHO cell lines with varying luciferase production rates.* Biotechnol Bioeng, 2009. **102**(6): p. 1593-602.
64. Mead, E.J., et al., *Experimental and in silico modelling analyses of the gene expression pathway for recombinant antibody and by-product production in NS0 cell lines.* PloS one, 2012. **7**(10): p. e47422.
65. Dreesen, I.A. and M. Fussenegger, *Ectopic expression of human mTOR increases viability, robustness, cell size, proliferation, and antibody production of chinese hamster ovary cells.* Biotechnol Bioeng, 2011. **108**(4): p. 853-66.
66. Courtes, F.C., et al., *Understanding translational control mechanisms of the mTOR pathway in CHO cells by polysome profiling.* N Biotechnol, 2014. **31**(5): p. 514-23.
67. Yun, C.Y., et al., *Specific inhibition of caspase-8 and -9 in CHO cells enhances cell viability in batch and fed-batch cultures.* Metab Eng, 2007. **9**(5-6): p. 406-18.
68. Lee, J.S. and G.M. Lee, *Rapamycin treatment inhibits CHO cell death in a serum-free suspension culture by autophagy induction.* Biotechnol Bioeng, 2012. **109**(12): p. 3093-102.
69. Kim, Y.G., et al., *Effect of Bcl-xL overexpression on apoptosis and autophagy in recombinant Chinese hamster ovary cells under nutrient-deprived condition.* Biotechnol Bioeng, 2009. **103**(4): p. 757-66.
70. Mohan, C., et al., *Effect of doxycycline-regulated protein disulfide isomerase expression on the specific productivity of recombinant CHO cells: thrombopoietin and antibody.* Biotechnol Bioeng, 2007. **98**(3): p. 611-5.
71. Mohan, C. and G.M. Lee, *Effect of inducible co-overexpression of protein disulfide isomerase and endoplasmic reticulum oxidoreductase on the specific antibody productivity of recombinant Chinese hamster ovary cells.* Biotechnology and bioengineering, 2010. **107**(2): p. 337-346.
72. Chung, J.Y., et al., *Effect of doxycycline-regulated calnexin and calreticulin expression on specific thrombopoietin productivity of recombinant Chinese hamster ovary cells.* Biotechnol Bioeng, 2004. **85**: p. 539-546.
73. Tigges, M. and M. Fussenegger, *Xbp1-based engineering of secretory capacity enhances the productivity of Chinese hamster ovary cells.* Metabolic engineering, 2006. **8**(3): p. 264-272.
74. Pybus, L.P., et al., *Model-directed engineering of "difficult-to-express" monoclonal antibody production by Chinese hamster ovary cells.* Biotechnol Bioeng, 2014. **111**(2): p. 372-85.
75. Jardon, M.A., et al., *Inhibition of glutamine-dependent autophagy increases t-PA production in CHO cell fed-batch processes.* Biotechnol Bioeng, 2012. **109**(5): p. 1228-38.
76. Ellgaard, L., M. Molinari, and A. Helenius, *Setting the standards: quality control in the secretory pathway.* Science, 1999. **286**(5446): p. 1882-8.
77. Hammond, C., I. Braakman, and A. Helenius, *Role of N-linked oligosaccharide recognition, glucose trimming, and calnexin in glycoprotein folding and quality control.* Proc Natl Acad Sci U S A, 1994. **91**(3): p. 913-7.

78. Ellgaard, L. and A. Helenius, *Quality control in the endoplasmic reticulum.* Nat Rev Mol Cell Biol, 2003. **4**(3): p. 181-91.
79. Ellis, R.J. and S.M. van der Vies, *Molecular chaperones.* Annu Rev Biochem, 1991. **60**: p. 321-47.
80. Hellman, R., et al., *The in vivo association of BiP with newly synthesized proteins is dependent on the rate and stability of folding and not simply on the presence of sequences that can bind to BiP.* J Cell Biol, 1999. **144**(1): p. 21-30.
81. Roobol, A., et al., *p58IPK is an inhibitor of the eIF2alpha kinase GCN2 and its localization and expression underpin protein synthesis and ER processing capacity.* Biochem J, 2015. **465**(2): p. 213-25.
82. Halperin, L., J. Jung, and M. Michalak, *The many functions of the endoplasmic reticulum chaperones and folding enzymes.* IUBMB Life, 2014. **66**(5): p. 318-26.
83. Stronge, V.S., et al., *Relationship between calnexin and BiP in suppressing aggregation and promoting refolding of protein and glycoprotein substrates.* J Biol Chem, 2001. **276**(43): p. 39779-87.
84. Saito, Y., et al., *Calreticulin functions in vitro as a molecular chaperone for both glycosylated and non-glycosylated proteins.* EMBO J, 1999. **18**(23): p. 6718-29.
85. Araki, K. and K. Nagata, *Protein folding and quality control in the ER.* Cold Spring Harb Perspect Biol, 2011. **3**(11): p. a007526.
86. Melnick, J., J.L. Dul, and Y. Argon, *Sequential interaction of the chaperones BiP and GRP94 with immunoglobulin chains in the endoplasmic reticulum.* Nature, 1994. **370**(6488): p. 373-5.
87. Marzec, M., D. Eletto, and Y. Argon, *GRP94: An HSP90-like protein specialized for protein folding and quality control in the endoplasmic reticulum.* Biochim Biophys Acta, 2012. **1823**(3): p. 774-87.
88. Schroder, M., *Endoplasmic reticulum stress responses.* Cell Mol Life Sci, 2008. **65**(6): p. 862-94.
89. Du, Z., et al., *Non-invasive UPR monitoring system and its applications in CHO production cultures.* Biotechnol Bioeng, 2013. **110**(8): p. 2184-94.
90. Schwarz, D.S. and M.D. Blower, *The endoplasmic reticulum: structure, function and response to cellular signaling.* Cell Mol Life Sci, 2016. **73**(1): p. 79-94.
91. Ruggiano, A., O. Foresti, and P. Carvalho, *Quality control: ER-associated degradation: protein quality control and beyond.* J Cell Biol, 2014. **204**(6): p. 869-79.
92. Friedlander, R., et al., *A regulatory link between ER-associated protein degradation and the unfolded-protein response.* Nat Cell Biol, 2000. **2**(7): p. 379-84.
93. Chakrabarti, A., A.W. Chen, and J.D. Varner, *A review of the mammalian unfolded protein response.* Biotechnol Bioeng, 2011. **108**(12): p. 2777-93.
94. Harding, H.P., et al., *Perk is essential for translational regulation and cell survival during the unfolded protein response.* Mol Cell, 2000. **5**(5): p. 897-904.
95. Lu, P.D., H.P. Harding, and D. Ron, *Translation reinitiation at alternative open reading frames regulates gene expression in an integrated stress response.* J Cell Biol, 2004. **167**(1): p. 27-33.
96. Thuerauf, D.J., et al., *Effects of the isoform-specific characteristics of ATF6 alpha and ATF6 beta on endoplasmic reticulum stress response gene expression and cell viability.* J Biol Chem, 2007. **282**(31): p. 22865-78.
97. Senft, D. and Z.A. Ronai, *UPR, autophagy, and mitochondria crosstalk underlies the ER stress response.* Trends Biochem Sci, 2015. **40**(3): p. 141-8.
98. Tigges, M. and M. Fussenegger, *Xbp1-based engineering of secretory capacity enhances the productivity of Chinese hamster ovary cells.* Metab Eng, 2006. **8**(3): p. 264-72.
99. Yoshida, H., et al., *XBP1 mRNA is induced by ATF6 and spliced by IRE1 in response to ER stress to produce a highly active transcription factor.* Cell, 2001. **107**(7): p. 881-91.
100. Ogata, M., et al., *Autophagy is activated for cell survival after endoplasmic reticulum stress.* Mol Cell Biol, 2006. **26**(24): p. 9220-31.
101. Davis, R., et al., *Effect of PDI overexpression on recombinant protein secretion in CHO cells.* Biotechnol Prog, 2000. **16**(5): p. 736-43.
102. Borth, N., et al., *Effect of increased expression of protein disulfide isomerase and heavy chain binding protein on antibody secretion in a recombinant CHO cell line.* Biotechnol Prog, 2005. **21**(1): p. 106-11.
103. Hayes, N.V., C.M. Smales, and P. Klappa, *Protein disulfide isomerase does not control recombinant IgG4 productivity in mammalian cell lines.* Biotechnol Bioeng, 2010. **105**(4): p. 770-9.
104. Becker, E., et al., *An XBP-1 dependent bottle-neck in production of IgG subtype antibodies in chemically defined serum-free Chinese hamster ovary (CHO) fed-batch processes.* J Biotechnol, 2008. **135**: p. 217-223.

105. Ku, S.C., et al., *Effects of overexpression of X-box binding protein 1 on recombinant protein production in Chinese hamster ovary and NS0 myeloma cells.* Biotechnology and bioengineering, 2008. **99**(1): p. 155-164.
106. Mathias, S., et al., *Visualisation of intracellular production bottlenecks in suspension-adapted CHO cells producing complex biopharmaceuticals using fluorescence microscopy.* J Biotechnol, 2018. **271**: p. 47-55.
107. Vezina, C., A. Kudelski, and S.N. Sehgal, *Rapamycin (AY-22,989), a new antifungal antibiotic. I. Taxonomy of the producing streptomycete and isolation of the active principle.* J Antibiot (Tokyo), 1975. **28**(10): p. 721-6.
108. Benjamin, D., et al., *Rapamycin passes the torch: a new generation of mTOR inhibitors.* Nat Rev Drug Discov, 2011. **10**(11): p. 868-80.
109. Laplante, M. and D.M. Sabatini, *mTOR signaling at a glance.* J Cell Sci, 2009. **122**(Pt 20): p. 3589-94.
110. Dunlop, E.A. and A.R. Tee, *mTOR and autophagy: a dynamic relationship governed by nutrients and energy.* Semin Cell Dev Biol, 2014. **36**: p. 121-9.
111. Loewith, R., et al., *Two TOR complexes, only one of which is rapamycin sensitive, have distinct roles in cell growth control.* Mol Cell, 2002. **10**(3): p. 457-68.
112. Jhanwar-Uniyal, M., et al., *Distinct signaling mechanisms of mTORC1 and mTORC2 in glioblastoma multiforme: a tale of two complexes.* Adv Biol Regul, 2015. **57**: p. 64-74.
113. Kim, D.H., et al., *mTOR interacts with raptor to form a nutrient-sensitive complex that signals to the cell growth machinery.* Cell, 2002. **110**(2): p. 163-75.
114. Wang, L., et al., *PRAS40 regulates mTORC1 kinase activity by functioning as a direct inhibitor of substrate binding.* J Biol Chem, 2007. **282**(27): p. 20036-44.
115. Guertin, D.A., et al., *Ablation in mice of the mTORC components raptor, rictor, or mLST8 reveals that mTORC2 is required for signaling to Akt-FOXO and PKCalpha, but not S6K1.* Dev Cell, 2006. **11**(6): p. 859-71.
116. Kazi, A.A., et al., *Deptor knockdown enhances mTOR Activity and protein synthesis in myocytes and ameliorates disuse muscle atrophy.* Mol Med, 2011. **17**(9-10): p. 925-36.
117. Betz, C. and M.N. Hall, *Where is mTOR and what is it doing there?* J Cell Biol, 2013. **203**(4): p. 563-74.
118. Zhou, X., et al., *Dynamic Visualization of mTORC1 Activity in Living Cells.* Cell Rep, 2015.
119. Hara, K., et al., *Regulation of eIF-4E BP1 phosphorylation by mTOR.* J Biol Chem, 1997. **272**(42): p. 26457-63.
120. Xiao, L., et al., *The role of mTOR and phospho-p70S6K in pathogenesis and progression of gastric carcinomas: an immunohistochemical study on tissue microarray.* J Exp Clin Cancer Res, 2009. **28**: p. 152.
121. Volarevic, S. and G. Thomas, *Role of S6 phosphorylation and S6 kinase in cell growth.* Prog Nucleic Acid Res Mol Biol, 2001. **65**: p. 101-27.
122. Kim, E., et al., *Regulation of TORC1 by Rag GTPases in nutrient response.* Nat Cell Biol, 2008. **10**(8): p. 935-45.
123. Sancak, Y., et al., *Ragulator-Rag complex targets mTORC1 to the lysosomal surface and is necessary for its activation by amino acids.* Cell, 2010. **141**(2): p. 290-303.
124. Alers, S., et al., *Role of AMPK-mTOR-Ulk1/2 in the regulation of autophagy: cross talk, shortcuts, and feedbacks.* Mol Cell Biol, 2012. **32**(1): p. 2-11.
125. Long, X., et al., *Rheb binds and regulates the mTOR kinase.* Curr Biol, 2005. **15**(8): p. 702-13.
126. Huang, J. and B.D. Manning, *A complex interplay between Akt, TSC2 and the two mTOR complexes.* Biochem Soc Trans, 2009. **37**(Pt 1): p. 217-22.
127. Rabanal-Ruiz, Y., E.G. Otten, and V.I. Korolchuk, *mTORC1 as the main gateway to autophagy.* Essays Biochem, 2017. **61**(6): p. 565-584.
128. Inoki, K., et al., *Rheb GTPase is a direct target of TSC2 GAP activity and regulates mTOR signaling.* Genes Dev, 2003. **17**(15): p. 1829-34.
129. Jung, C.H., et al., *ULK-Atg13-FIP200 complexes mediate mTOR signaling to the autophagy machinery.* Mol Biol Cell, 2009. **20**(7): p. 1992-2003.
130. Zoncu, R., et al., *mTORC1 senses lysosomal amino acids through an inside-out mechanism that requires the vacuolar H(+)-ATPase.* Science, 2011. **334**(6056): p. 678-83.
131. Averous, J., et al., *Requirement for lysosomal localization of mTOR for its activation differs between leucine and other amino acids.* Cell Signal, 2014. **26**(9): p. 1918-27.
132. Kim, J., et al., *AMPK and mTOR regulate autophagy through direct phosphorylation of Ulk1.* Nat Cell Biol, 2011. **13**(2): p. 132-41.

133. Di Bartolomeo, S., et al., *The dynamic interaction of AMBRA1 with the dynein motor complex regulates mammalian autophagy.* J Cell Biol, 2010. **191**(1): p. 155-68.
134. Hara, T., et al., *FIP200, a ULK-interacting protein, is required for autophagosome formation in mammalian cells.* J Cell Biol, 2008. **181**(3): p. 497-510.
135. Edros, R., S. McDonnell, and M. Al-Rubeai, *The relationship between mTOR signalling pathway and recombinant antibody productivity in CHO cell lines.* BMC Biotechnol, 2014. **14**: p. 15.
136. Godfrey, C.L., et al., *Polysome profiling of mAb producing CHO cell lines links translational control of cell proliferation and recombinant mRNA loading onto ribosomes with global and recombinant protein synthesis.* Biotechnology journal, 2017. **12**(8): p. 10.1002/biot.201700177. Epub 2017 Jul 5.
137. Josse, L., et al., *mTORC1 signalling and eIF4E/4E-BP1 translation initiation factor stoichiometry influence recombinant protein productivity from GS-CHOK1 cells.* Biochem J, 2016. **473**(24): p. 4651-4664.
138. Mukhopadhyay, S., et al., *Autophagy and apoptosis: where do they meet?* Apoptosis, 2014. **19**(4): p. 555-66.
139. Levine, B., *Eating oneself and uninvited guests: autophagy-related pathways in cellular defense.* Cell, 2005. **120**(2): p. 159-162.
140. Eskelinen, E.L., et al., *Role of LAMP-2 in lysosome biogenesis and autophagy.* Mol Biol Cell, 2002. **13**(9): p. 3355-68.
141. Lu, S., et al., *Lysosomal adaptation: How cells respond to lysosomotropic compounds.* PLoS One, 2017. **12**(3): p. e0173771.
142. Glick, D., S. Barth, and K.F. Macleod, *Autophagy: cellular and molecular mechanisms.* J Pathol, 2010. **221**(1): p. 3-12.
143. Mizushima, N., T. Yoshimori, and Y. Ohsumi, *The role of Atg proteins in autophagosome formation.* Annu Rev Cell Dev Biol, 2011. **27**: p. 107-32.
144. Rogov, V., et al., *Interactions between autophagy receptors and ubiquitin-like proteins form the molecular basis for selective autophagy.* Mol Cell, 2014. **53**(2): p. 167-78.
145. Webber, J.L., A.R. Young, and S.A. Tooze, *Atg9 trafficking in Mammalian cells.* Autophagy, 2007. **3**(1): p. 54-6.
146. Geng, J., et al., *Quantitative analysis of autophagy-related protein stoichiometry by fluorescence microscopy.* J Cell Biol, 2008. **182**(1): p. 129-40.
147. Zhuang, X., et al., *ATG9 regulates autophagosome progression from the endoplasmic reticulum in Arabidopsis.* Proc Natl Acad Sci U S A, 2017. **114**(3): p. E426-E435.
148. Yu, X., Y.C. Long, and H.M. Shen, *Differential regulatory functions of three classes of phosphatidylinositol and phosphoinositide 3-kinases in autophagy.* Autophagy, 2015. **11**(10): p. 1711-28.
149. Kuma, A., et al., *Formation of the approximately 350-kDa Apg12-Apg5.Apg16 multimeric complex, mediated by Apg16 oligomerization, is essential for autophagy in yeast.* J Biol Chem, 2002. **277**(21): p. 18619-25.
150. Otomo, C., et al., *Structure of the human ATG12~ATG5 conjugate required for LC3 lipidation in autophagy.* Nat Struct Mol Biol, 2013. **20**(1): p. 59-66.
151. Pankiv, S., et al., *p62/SQSTM1 binds directly to Atg8/LC3 to facilitate degradation of ubiquitinated protein aggregates by autophagy.* J Biol Chem, 2007. **282**(33): p. 24131-45.
152. Bjorkoy, G., et al., *p62/SQSTM1 forms protein aggregates degraded by autophagy and has a protective effect on huntingtin-induced cell death.* J Cell Biol, 2005. **171**(4): p. 603-14.
153. Yang, Z., et al., *Atg22 recycles amino acids to link the degradative and recycling functions of autophagy.* Mol Biol Cell, 2006. **17**(12): p. 5094-104.
154. Verfaillie, T., et al., *Linking ER Stress to Autophagy: Potential Implications for Cancer Therapy.* Int J Cell Biol, 2010. **2010**: p. 930509.
155. Senft, D. and Z.A. Ronai, *UPR, autophagy, and mitochondria crosstalk underlies the ER stress response.* Trends in biochemical sciences, 2015. **40**(3): p. 141-148.
156. Nishikawa, S., A. Hirata, and A. Nakano, *Inhibition of endoplasmic reticulum (ER)-to-Golgi transport induces relocalization of binding protein (BiP) within the ER to form the BiP bodies.* Mol Biol Cell, 1994. **5**(10): p. 1129-43.
157. Valetti, C., et al., *Russell bodies: a general response of secretory cells to synthesis of a mutant immunoglobulin which can neither exit from, nor be degraded in, the endoplasmic reticulum.* J Cell Biol, 1991. **115**(4): p. 983-94.

158. Palmieri, M., et al., *Characterization of the CLEAR network reveals an integrated control of cellular clearance pathways.* Hum Mol Genet, 2011. **20**(19): p. 3852-66.
159. Settembre, C., et al., *TFEB links autophagy to lysosomal biogenesis.* Science, 2011. **332**(6036): p. 1429-33.
160. Martina, J.A., et al., *The nutrient-responsive transcription factor TFE3 promotes autophagy, lysosomal biogenesis, and clearance of cellular debris.* Sci Signal, 2014. **7**(309): p. ra9.
161. Roczniak-Ferguson, A., et al., *The transcription factor TFEB links mTORC1 signaling to transcriptional control of lysosome homeostasis.* Sci Signal, 2012. **5**(228): p. ra42.
162. Settembre, C., et al., *A lysosome-to-nucleus signalling mechanism senses and regulates the lysosome via mTOR and TFEB.* EMBO J, 2012. **31**(5): p. 1095-108.
163. Sardiello, M., et al., *A gene network regulating lysosomal biogenesis and function.* Science, 2009. **325**(5939): p. 473-7.
164. Leeman, D.S., et al., *Lysosome activation clears aggregates and enhances quiescent neural stem cell activation during aging.* Science, 2018. **359**(6381): p. 1277-1283.
165. Ballabio, A., *The awesome lysosome.* EMBO Mol Med, 2016. **8**(2): p. 73-6.
166. Lim, C.Y. and R. Zoncu, *The lysosome as a command-and-control center for cellular metabolism.* J Cell Biol, 2016. **214**(6): p. 653-64.
167. Hwang, S.O. and G.M. Lee, *Nutrient deprivation induces autophagy as well as apoptosis in Chinese hamster ovary cell culture.* Biotechnology and bioengineering, 2008. **99**(3): p. 678-685.
168. Han, Y.K., et al., *Autophagy and apoptosis of recombinant Chinese hamster ovary cells during fed-batch culture: effect of nutrient supplementation.* Biotechnology and bioengineering, 2011. **108**(9): p. 2182-2192.
169. Han, Y.K., et al., *Hyperosmotic stress induces autophagy and apoptosis in recombinant Chinese hamster ovary cell culture.* Biotechnology and bioengineering, 2010. **105**(6): p. 1187-1192.
170. Pattingre, S., et al., *Bcl-2 antiapoptotic proteins inhibit Beclin 1-dependent autophagy.* Cell, 2005. **122**(6): p. 927-39.
171. Lee, J.S., et al., *Anti-cell death engineering of CHO cells: co-overexpression of Bcl-2 for apoptosis inhibition, Beclin-1 for autophagy induction.* Biotechnol Bioeng, 2013. **110**(8): p. 2195-207.
172. Zustiak, M.P., et al., *Feast or famine: autophagy control and engineering in eukaryotic cell culture.* Curr Opin Biotechnol, 2008. **19**(5): p. 518-26.
173. Baehrecke, E.H., *Autophagy: dual roles in life and death?*, in *Nat Rev Mol Cell Biol*. 2005. p. 505-510.
174. Indran, I.R., et al., *Recent advances in apoptosis, mitochondria and drug resistance in cancer cells.* Biochim Biophys Acta, 2011. **1807**(6): p. 735-45.
175. Fulda, S. and K.M. Debatin, *Extrinsic versus intrinsic apoptosis pathways in anticancer chemotherapy.* Oncogene, 2006. **25**(34): p. 4798-811.
176. Garcia-Saez, A.J., *The secrets of the Bcl-2 family.* Cell Death Differ, 2012. **19**(11): p. 1733-40.
177. Reynolds, J.E., et al., *BCL-2 and MCL-1 expression in Chinese hamster ovary cells inhibits intracellular acidification and apoptosis induced by staurosporine.* Exp Cell Res, 1996. **225**(2): p. 430-6.
178. O'Connor, L., et al., *Bim: a novel member of the Bcl-2 family that promotes apoptosis.* EMBO J, 1998. **17**(2): p. 384-95.
179. Han, Y.K., et al., *Bcl-x(L) overexpression delays the onset of autophagy and apoptosis in hyperosmotic recombinant Chinese hamster ovary cell cultures.* Journal of Biotechnology, 2011. **156**(1): p. 52-55.
180. Templeton, N., et al., *The impact of anti-apoptotic gene Bcl-2 expression on CHO central metabolism.* Metab Eng, 2014. **25**: p. 92-102.
181. Dorai, H., et al., *Combining high-throughput screening of caspase activity with anti-apoptosis genes for development of robust CHO production cell lines.* Biotechnol Prog, 2010. **26**(5): p. 1367-81.
182. Kim, N.S. and G.M. Lee, *Response of recombinant Chinese hamster ovary cells to hyperosmotic pressure: effect of Bcl-2 overexpression.* J Biotechnol, 2002. **95**(3): p. 237-48.
183. Tey, B.T., et al., *Influence of bcl-2 on cell death during the cultivation of a Chinese hamster ovary cell line expressing a chimeric antibody.* Biotechnol Bioeng, 2000. **68**(1): p. 31-43.
184. Sung, Y.H., et al., *Influence of co-down-regulation of caspase-3 and caspase-7 by siRNAs on sodium butyrate-induced apoptotic cell death of Chinese hamster ovary cells producing thrombopoietin.* Metab Eng, 2007. **9**(5-6): p. 452-64.
185. Crea, F., et al., *Over-expression of hTERT in CHO K1 results in decreased apoptosis and reduced serum dependency.* J Biotechnol, 2006. **121**(2): p. 109-23.

186. U.S. Department of Health and Human Services, F.a.D.A., Center for Biologics Evaluation and Research, *Points to Consider in the Manufacture and Testing of Monoclonal Antibody Products for Human Use*. 1997.
187. Q5D *ICH HARMONISED TRIPARTITE GUIDELINE DERIVATION AND CHARACTERISATION OF CELL SUBSTRATES USED FOR PRODUCTION OF BIOTECHNOLOGICAL/BIOLOGICAL PRODUCTS*. 1997.
188. Browne, S.M. and M. Al-Rubeai, *Selection methods for high-producing mammalian cell lines.* Trends Biotechnol, 2007. **25**(9): p. 425-32.
189. Frye, C., et al., *Industry view on the relative importance of "clonality" of biopharmaceutical-producing cell lines.* Biologicals, 2016. **44**(2): p. 117-22.
190. Barnes, L.M., N. Moy, and A.J. Dickson, *Phenotypic variation during cloning procedures: analysis of the growth behavior of clonal cell lines.* Biotechnol Bioeng, 2006. **94**(3): p. 530-7.
191. Barnes, L.M., C.M. Bentley, and A.J. Dickson, *Molecular definition of predictive indicators of stable protein expression in recombinant NS0 myeloma cells.* Biotechnology and bioengineering, 2004. **85**(2): p. 115-121.
192. Klottrup, K.J., et al., *Measuring the aggregation of CHO cells prior to single cell cloning allows a more accurate determination of the probability of clonality.* Biotechnol Prog, 2017.
193. Davies, S.L., et al., *Functional heterogeneity and heritability in CHO cell populations.* Biotechnol Bioeng, 2013. **110**(1): p. 260-74.
194. Derouazi, M., et al., *Genetic characterization of CHO production host DG44 and derivative recombinant cell lines.* Biochem Biophys Res Commun, 2006. **340**(4): p. 1069-77.
195. Lewis, N.E., et al., *Genomic landscapes of Chinese hamster ovary cell lines as revealed by the Cricetulus griseus draft genome.* Nat Biotechnol, 2013. **31**(8): p. 759-65.
196. Barnes, L.M., C.M. Bentley, and A.J. Dickson, *Characterization of the stability of recombinant protein production in the GS-NS0 expression system.* Biotechnol Bioeng, 2001. **73**(4): p. 261-70.
197. Lee, G.M., A. Varma, and B.O. Palsson, *Application of population balance model to the loss of hybridoma antibody productivity.* Biotechnol Prog, 1991. **7**(1): p. 72-5.
198. Kromenaker, S.J. and F. Srienc, *Stability of producer hybridoma cell lines after cell sorting: a case study.* Biotechnol Prog, 1994. **10**(3): p. 299-307.
199. Krebs, L.E., et al., *Effective and efficient characterization of Chinese hamster ovary production cell lines using automated intracellular staining and statistical modeling.* Biotechnol Prog, 2018. **34**(3): p. 570-583.
200. Pilbrough, W., T. Munro, and P. Gray, *Intraclonal Protein Expression Heterogeneity in Recombinant CHO Cells.* PloS one, 2009. **4**(12).
201. Brock, A., H. Chang, and S. Huang, *Non-genetic heterogeneity--a mutation-independent driving force for the somatic evolution of tumours.* Nat Rev Genet, 2009. **10**(5): p. 336-42.
202. Kim, K., Lee *Clonal variability within dihydrofolatereductase-mediated gene amplified chinese hamster ovary cells: stabilityin the absence of selective pressure.* Biotechnol Bioeng, 1998(60): p. 679-688.
203. Powell, K.T. and J.C. Weaver, *Gel microdroplets and flow cytometry: rapid determination of antibody secretion by individual cells within a cell population.* Bio/technology (Nature Publishing Company), 1990. **8**(4): p. 333-337.
204. Manz, R., et al., *Analysis and sorting of live cells according to secreted molecules, relocated to a cell-surface affinity matrix.* Proceedings of the National Academy of Sciences of the United States of America, 1995. **92**(6): p. 1921-1925.
205. Borth, N., et al., *Efficient selection of high-producing subclones during gene amplification of recombinant Chinese hamster ovary cells by flow cytometry and cell sorting.* Biotechnology and bioengineering, 2000. **71**(4): p. 266-273.
206. Shimizu, T. and T. Azuma, *Detection and isolation of anti-hapten antibody-secreting cells by cellular affinity matrix technology.* J Immunol Methods, 2015. **422**: p. 80-6.
207. Kim, Y.G., et al., *New cell line development for antibody-producing Chinese hamster ovary cells using split green fluorescent protein.* BMC biotechnology, 2012. **12**: p. 24-6750-12-24.
208. Sleiman, R.J., et al., *Accelerated cell line development using two-color fluorescence activated cell sorting to select highly expressing antibody-producing clones.* Biotechnology and bioengineering, 2008. **99**(3): p. 578-587.
209. Mancia, F., et al., *Optimization of protein production in mammalian cells with a coexpressed fluorescent marker.* Structure, 2004. **12**(8): p. 1355-60.
210. Meng, Y.G., et al., *Green fluorescent protein as a second selectable marker for selection of high producing clones from transfected CHO cells.* Gene, 2000. **242**(1-2): p. 201-7.

211. Yu, B., J.M. Wages, and J.W. Larrick, *Antibody-membrane switch (AMS) technology for facile cell line development.* Protein engineering, design & selection : PEDS, 2014. **27**(10): p. 309-315.
212. Lang, S., et al., *Surface display vectors for selective detection and isolation of high level antibody producing cells.* Biotechnology and bioengineering, 2016. **113**(11): p. 2386-2393.
213. Chakrabarti, L., et al., *Amber suppression coupled with inducible surface display identifies cells with high recombinant protein productivity.* Biotechnol Bioeng, 2019. **116**(4): p. 793-804.
214. Okumura, T., et al., *Efficient enrichment of high-producing recombinant Chinese hamster ovary cells for monoclonal antibody by flow cytometry.* J Biosci Bioeng, 2015. **120**(3): p. 340-6.
215. Brezinsky, S.C., et al., *A simple method for enriching populations of transfected CHO cells for cells of higher specific productivity.* Journal of immunological methods, 2003. **277**(1-2): p. 141-155.
216. Shi, S., et al., *A High-throughput Automated Platform for the Development of Manufacturing Cell Lines for Protein Therapeutics.* Journal of visualized experiments, 2011. **55**(3010).
217. DeMaria, C.T., et al., *Accelerated clone selection for recombinant CHO CELLS using a FACS-based high-throughput screen.* Biotechnol Prog, 2007. **23**(2): p. 465-72.
218. Yoshikawa, T., et al., *Flow cytometry: an improved method for the selection of highly productive gene-amplified CHO cells using flow cytometry.* Biotechnol Bioeng, 2001. **74**(5): p. 435-42.
219. Basiji, D.A., et al., *Cellular image analysis and imaging by flow cytometry.* Clin Lab Med, 2007. **27**: p. 653-70, viii.
220. Headland, S.E., et al., *Cutting-edge analysis of extracellular microparticles using ImageStream(X) imaging flow cytometry.* Sci Rep, 2014. **4**: p. 5237.
221. Erdbrugger, U., et al., *Imaging flow cytometry elucidates limitations of microparticle analysis by conventional flow cytometry.* Cytometry A, 2014. **85**(9): p. 756-70.
222. George, T.C., et al., *Quantitative measurement of nuclear translocation events using similarity analysis of multispectral cellular images obtained in flow.* J Immunol Methods, 2006. **311**(1-2): p. 117-29.
223. George, T.C., et al., *Distinguishing modes of cell death using the ImageStream multispectral imaging flow cytometer.* Cytometry A, 2004. **59**(2): p. 237-45.
224. Pietkiewicz, S., J.H. Schmidt, and I.N. Lavrik, *Quantification of apoptosis and necroptosis at the single cell level by a combination of Imaging Flow Cytometry with classical Annexin V/propidium iodide staining.* J Immunol Methods, 2015. **423**: p. 99-103.
225. Henery, S., et al., *Quantitative image based apoptotic index measurement using multispectral imaging flow cytometry: a comparison with standard photometric methods.* Apoptosis, 2008. **13**(8): p. 1054-63.
226. Barteneva, N.S., E. Fasler-Kan, and I.A. Vorobjev, *Imaging flow cytometry: coping with heterogeneity in biological systems.* J Histochem Cytochem, 2012. **60**(10): p. 723-33.
227. Schmittgen, T.D. and K.J. Livak, *Analyzing real-time PCR data by the comparative C(T) method.* Nat Protoc, 2008. **3**(6): p. 1101-8.
228. Xu, D., et al., *Quantitative analysis of a biopharmaceutical protein in cell culture samples using automated capillary electrophoresis (CE) western blot.* J Pharm Biomed Anal, 2017. **145**: p. 10-15.
229. Xu, X., et al., *The genomic sequence of the Chinese hamster ovary (CHO)-K1 cell line.* Nature biotechnology, 2011. **29**(8): p. 735-741.
230. Dobin, A., et al., *STAR: ultrafast universal RNA-seq aligner.* Bioinformatics, 2013. **29**(1): p. 15-21.
231. Li, H., et al., *The Sequence Alignment/Map format and SAMtools.* Bioinformatics, 2009. **25**(16): p. 2078-9.
232. Patro, R., et al., *Salmon provides fast and bias-aware quantification of transcript expression.* Nat Methods, 2017. **14**(4): p. 417-419.
233. Liao, Y., G.K. Smyth, and W. Shi, *featureCounts: an efficient general purpose program for assigning sequence reads to genomic features.* Bioinformatics, 2014. **30**(7): p. 923-30.
234. Robinson, M.D., D.J. McCarthy, and G.K. Smyth, *edgeR: a Bioconductor package for differential expression analysis of digital gene expression data.* Bioinformatics, 2010. **26**(1): p. 139-40.
235. Love, M.I., W. Huber, and S. Anders, *Moderated estimation of fold change and dispersion for RNA-seq data with DESeq2.* Genome Biol, 2014. **15**(12): p. 550.
236. Huber, W., et al., *Orchestrating high-throughput genomic analysis with Bioconductor.* Nat Methods, 2015. **12**(2): p. 115-21.
237. D'Andrea, D., et al., *FIDEA: a server for the functional interpretation of differential expression analysis.* Nucleic Acids Res, 2013. **41**(Web Server issue): p. W84-8.

238. Benjamini, Y., Hochberg Y. , *Controlling the False Discovery Rate: A Practical and Powerful Approach to Multiple Testing.* Journal of the Royal Statistical Society: Series B (Methodological) banner, 1995. **51**(1): p. 289-300.
239. Povey, J.F., et al., *Rapid high-throughput characterisation, classification and selection of recombinant mammalian cell line phenotypes using intact cell MALDI-ToF mass spectrometry fingerprinting and PLS-DA modelling.* Journal of Biotechnology, 2014. **184**: p. 84-93.
240. Misaghi, S., et al., *Slashing the timelines: Opting to generate high-titer clonal lines faster via viability-based single cell sorting.* Biotechnology progress, 2016. **32**(1): p. 198-207.
241. Fieder, J., et al., *A single-step FACS sorting strategy in conjunction with fluorescent vital dye imaging efficiently assures clonality of biopharmaceutical production cell lines.* Biotechnol J, 2017. **12**(6).
242. Powell, K.T. and J.C. Weaver, *Gel microdroplets and flow cytometry: rapid determination of antibody secretion by individual cells within a cell population.* Biotechnology (N Y), 1990. **8**(4): p. 333-7.
243. Tsao, Y.S., et al., *Monitoring Chinese hamster ovary cell culture by the analysis of glucose and lactate metabolism.* J Biotechnol, 2005. **118**(3): p. 316-27.
244. Gagnon, M., et al., *High-end pH-controlled delivery of glucose effectively suppresses lactate accumulation in CHO fed-batch cultures.* Biotechnol Bioeng, 2011. **108**(6): p. 1328-37.
245. Mulukutla, B.C., et al., *Multiplicity of steady states in glycolysis and shift of metabolic state in cultured mammalian cells.* PLoS One, 2015. **10**(3): p. e0121561.
246. Hartley, F., et al., *Mechanisms driving the lactate switch in Chinese hamster ovary cells.* Biotechnol Bioeng, 2018. **115**(8): p. 1890-1903.
247. Zagari, F., et al., *Lactate metabolism shift in CHO cell culture: the role of mitochondrial oxidative activity.* N Biotechnol, 2013. **30**(2): p. 238-45.
248. Mariati, et al., *Toward stable gene expression in CHO cells.* Bioengineered, 2014. **5**(5): p. 340-5.
249. Sellick, C.A., et al., *Metabolite profiling of recombinant CHO cells: designing tailored feeding regimes that enhance recombinant antibody production.* Biotechnology and bioengineering, 2011. **108**(12): p. 3025-3031.
250. Tastanova, A., et al., *Overexpression of YY1 increases the protein production in mammalian cells.* Journal of Biotechnology, 2016. **219**: p. 72-85.
251. Nitta, N., et al., *Intelligent Image-Activated Cell Sorting.* Cell, 2018. **175**(1): p. 266-276 e13.
252. Edros, R.Z., S. McDonnell, and M. Al-Rubeai, *Using molecular markers to characterize productivity in Chinese hamster ovary cell lines.* PloS one, 2013. **8**(10): p. e75935.
253. Borth, N., et al., *Comparison of the production of a human monoclonal antibody against HIV-1 by heterohybridoma cells and recombinant CHO cells: A flow cytometric study.* Cytotechnology, 1996. **22**(1-3): p. 129-38.
254. O'Callaghan, P.M., et al., *Cell line-specific control of recombinant monoclonal antibody production by CHO cells.* Biotechnology and bioengineering, 2010. **106**(6): p. 938-951.
255. Dorai, H., et al., *Correlation of heavy and light chain mRNA copy numbers to antibody productivity in mouse myeloma production cell lines.* Hybridoma (2005), 2006. **25**(1): p. 1-9.
256. Strutzenberger, K., et al., *Changes during subclone development and ageing of human antibody-producing recombinant CHO cells.* J Biotechnol, 1999. **69**(2-3): p. 215-26.
257. Chromikova, V., et al., *Evaluating the bottlenecks of recombinant IgM production in mammalian cells.* Cytotechnology, 2015. **67**(2): p. 343-356.
258. Technologies, E.L., *Mito-ID red detection kit*, E.L. Technologies, Editor. 2019.
259. Technologies, E.L., *Golgi-ID Green assay kit*, E.L. Technologies, Editor. 2019.
260. Hinterkorner, G., et al., *Improvement of the energy metabolism of recombinant CHO cells by cell sorting for reduced mitochondrial membrane potential.* J Biotechnol, 2007. **129**(4): p. 651-7.
261. Chakrabarti, L., et al., *Mitochondrial membrane potential identifies cells with high recombinant protein productivity.* J Immunol Methods, 2018.
262. Borth, N., G. Kral, and H. Katinger, *Rhodamine 123 fluorescence of immortal hybridoma cell lines as a function of glucose concentration.* Cytometry, 1993. **14**(1): p. 70-3.
263. O'Callaghan, P.M., et al., *Diversity in host clone performance within a Chinese hamster ovary cell line.* Biotechnology progress, 2015. **31**(5): p. 1187-1200.
264. Roy, G., et al., *Development of a fluorescent reporter system for monitoring ER stress in Chinese hamster ovary cells and its application for therapeutic protein production.* PLoS One, 2017. **12**(8): p. e0183694.
265. Carroll, S. and M. Al-Rubeai, *The selection of high-producing cell lines using flow cytometry and cell sorting.* Expert opinion on biological therapy, 2004. **4**(11): p. 1821-1829.

266. Mony, V.K., S. Benjamin, and E.J. O'Rourke, *A lysosome-centered view of nutrient homeostasis.* Autophagy, 2016. **12**(4): p. 619-31.
267. Baek, E., et al., *Chemical inhibition of autophagy: Examining its potential to increase the specific productivity of recombinant CHO cell lines.* Biotechnology and bioengineering, 2016. **113**(9): p. 1953-1961.
268. Bi, J.X., J. Shuttleworth, and M. Al-Rubeai, *Uncoupling of cell growth and proliferation results in enhancement of productivity in p21CIP1-arrested CHO cells.* Biotechnol Bioeng, 2004. **85**(7): p. 741-9.
269. Itakura, E. and N. Mizushima, *p62 Targeting to the autophagosome formation site requires self-oligomerization but not LC3 binding.* J Cell Biol, 2011. **192**(1): p. 17-27.
270. Kabeya, Y., et al., *LC3, a mammalian homologue of yeast Apg8p, is localized in autophagosome membranes after processing.* EMBO J, 2000. **19**(21): p. 5720-8.
271. Mizushima, N. and T. Yoshimori, *How to interpret LC3 immunoblotting.* Autophagy, 2007. **3**(6): p. 542-5.
272. Haller, M., et al., *Ubiquitination and proteasomal degradation of ATG12 regulates its proapoptotic activity.* Autophagy, 2014. **10**(12): p. 2269-78.
273. Huynh, K.K., et al., *LAMP proteins are required for fusion of lysosomes with phagosomes.* EMBO J, 2007. **26**(2): p. 313-24.
274. Kapuy, O., P.K. Vinod, and G. Banhegyi, *mTOR inhibition increases cell viability via autophagy induction during endoplasmic reticulum stress - An experimental and modeling study.* FEBS Open Bio, 2014. **4**: p. 704-13.
275. Chiang, G.G. and R.T. Abraham, *Phosphorylation of mammalian target of rapamycin (mTOR) at Ser-2448 is mediated by p70S6 kinase.* J Biol Chem, 2005. **280**(27): p. 25485-90.
276. de Araujo, M.E.G., et al., *Crystal structure of the human lysosomal mTORC1 scaffold complex and its impact on signaling.* Science, 2017. **358**(6361): p. 377-381.
277. Mu, Z., et al., *Structural insight into the Ragulator complex which anchors mTORC1 to the lysosomal membrane.* Cell Discov, 2017. **3**: p. 17049.
278. Bohm, E., et al., *Screening for improved cell performance: selection of subclones with altered production kinetics or improved stability by cell sorting.* Biotechnol Bioeng, 2004. **88**(6): p. 699-706.
279. Pichler, J., et al., *Selection of CHO host cell subclones with increased specific antibody production rates by repeated cycles of transient transfection and cell sorting.* Biotechnol Bioeng, 2011. **108**(2): p. 386-94.
280. Freimark, D., V. Jerome, and R. Freitag, *A GFP-based method facilitates clonal selection of transfected CHO cells.* Biotechnol J, 2010. **5**(1): p. 24-31.
281. Mollet, M., et al., *Computer simulations of the energy dissipation rate in a fluorescence-activated cell sorter: Implications to cells.* Biotechnol Bioeng, 2008. **100**(2): p. 260-72.
282. Mollet, M., et al., *Acute hydrodynamic forces and apoptosis: a complex question.* Biotechnol Bioeng, 2007. **98**(4): p. 772-88.
283. Ashcroft, R.G. and P.A. Lopez, *Commercial high speed machines open new opportunities in high throughput flow cytometry (HTFC).* J Immunol Methods, 2000. **243**(1-2): p. 13-24.
284. Richardson, G.M., J. Lannigan, and I.G. Macara, *Does FACS perturb gene expression?* Cytometry A, 2015. **87**(2): p. 166-75.
285. Bar-Even, A., et al., *Noise in protein expression scales with natural protein abundance.* Nat Genet, 2006. **38**(6): p. 636-43.
286. Phillips, N.E., et al., *Memory and relatedness of transcriptional activity in mammalian cell lineages.* Nat Commun, 2019. **10**(1): p. 1208.
287. Chang, H.H., et al., *Transcriptome-wide noise controls lineage choice in mammalian progenitor cells.* Nature, 2008. **453**(7194): p. 544-7.
288. Heffner, K.M., et al., *Lessons from the Hamster: Cricetulus griseus Tissue and CHO Cell Line Proteome Comparison.* J Proteome Res, 2017. **16**(10): p. 3672-3687.
289. Du, Z., et al., *Analysis of heterogeneity and Instability of Stable mAb-expressing CHO Cells.* biotechnology and bioprocess engineering, 2013. **18**: p. 419.
290. Feichtinger, J., et al., *Comprehensive genome and epigenome characterization of CHO cells in response to evolutionary pressures and over time.* Biotechnol Bioeng, 2016. **113**(10): p. 2241-53.
291. Vcelar, S., et al., *Changes in Chromosome Counts and Patterns in CHO Cell Lines upon Generation of Recombinant Cell Lines and Subcloning.* Biotechnol J, 2018. **13**(3): p. e1700495.
292. Masek, T., L. Valasek, and M. Pospisek, *Polysome analysis and RNA purification from sucrose gradients.* Methods Mol Biol, 2011. **703**: p. 293-309.

293. Heyer, E.E. and M.J. Moore, *Redefining the Translational Status of 80S Monosomes.* Cell, 2016. **164**(4): p. 757-69.
294. Simpson, N.H., et al., *Bcl-2 over-expression reduces growth rate and prolongs G1 phase in continuous chemostat cultures of hybridoma cells.* Biotechnol Bioeng, 1999. **64**(2): p. 174-86.
295. Ramirez, O.T. and R. Mutharasan, *Cell cycle- and growth phase-dependent variations in size distribution, antibody productivity, and oxygen demand in hybridoma cultures.* Biotechnol Bioeng, 1990. **36**(8): p. 839-48.
296. Suzuki, E. and D.F. Ollis, *Cell cycle model for antibody production kinetics.* Biotechnol Bioeng, 1989. **34**(11): p. 1398-402.
297. Jenkins, N. and A. Hovey, *Temperature control of growth and productivity in mutant Chinese hamster ovary cells synthesizing a recombinant protein.* Biotechnol Bioeng, 1993. **42**(9): p. 1029-36.
298. Veraitch, F.S. and M. Al-Rubeai, *Enhanced growth in NS0 cells expressing aminoglycoside phosphotransferase is associated with changes in metabolism, productivity, and apoptosis.* Biotechnol Bioeng, 2005. **92**(5): p. 589-99.
299. Itoh, Y., H. Ueda, and E. Suzuki, *Overexpression of bcl-2, apoptosis suppressing gene: Prolonged viable culture period of hybridoma and enhanced antibody production.* Biotechnol Bioeng, 1995. **48**(2): p. 118-22.
300. Fassnacht, D., et al., *Influence of bcl-2 on antibody productivity in high cell density perfusion cultures of hybridoma.* Cytotechnology, 1999. **30**(1-3): p. 95-106.
301. Simpson, N.H., A.E. Milner, and M. Al-Rubeai, *Prevention of hybridoma cell death by bcl-2 during suboptimal culture conditions.* Biotechnol Bioeng, 1997. **54**(1): p. 1-16.
302. Fassnacht, D., et al., *Effect of bcl-2 expression on hybridoma cell growth in serum-supplemented, protein-free and diluted media.* Cytotechnology, 1998. **26**(3): p. 219-25.
303. Tey, B.T., et al., *Bcl-2 mediated suppression of apoptosis in myeloma NS0 cultures.* J Biotechnol, 2000. **79**(2): p. 147-59.
304. Carlage, T., et al., *Proteomic profiling of a high-producing Chinese hamster ovary cell culture.* Anal Chem, 2009. **81**: p. 7357-7362.
305. Chiang, G.G. and W.P. Sisk, *Bcl-x(L) mediates increased production of humanized monoclonal antibodies in Chinese hamster ovary cells.* Biotechnol Bioeng, 2005. **91**(7): p. 779-92.
306. Tizei, P.A., et al., *Selection platforms for directed evolution in synthetic biology.* Biochem Soc Trans, 2016. **44**(4): p. 1165-75.
307. Pourmir, A. and T.W. Johannes, *Directed evolution: selection of the host organism.* Comput Struct Biotechnol J, 2012. **2**: p. e201209012.
308. Yuan, L., et al., *Laboratory-directed protein evolution.* Microbiol Mol Biol Rev, 2005. **69**(3): p. 373-92.
309. Wackett, L.P., *Directed evolution of new enzymes and pathways for environmental biocatalysis.* Ann N Y Acad Sci, 1998. **864**: p. 142-52.
310. Chen, C.P., et al., *ECSTASY, an adjustable membrane-tethered/soluble protein expression system for the directed evolution of mammalian proteins.* Protein Eng Des Sel, 2012. **25**(7): p. 367-75.
311. Majors, B.S., et al., *Directed evolution of mammalian anti-apoptosis proteins by somatic hypermutation.* Protein Eng Des Sel, 2012. **25**(1): p. 27-38.
312. Arakawa, H., et al., *Protein evolution by hypermutation and selection in the B cell line DT40.* Nucleic Acids Res, 2008. **36**(1): p. e1.
313. Kim, C., et al., *Basic amino-acid side chains regulate transmembrane integrin signalling.* Nature, 2011. **481**(7380): p. 209-13.
314. Stanley, P., et al., *Lectin-resistant CHO cells: selection of seven new mutants resistant to ricin.* Somat Cell Mol Genet, 1990. **16**(3): p. 211-23.
315. Homewood, C.A., et al., *Lysosomes, pH and the anti-malarial action of chloroquine.* Nature, 1972. **235**(5332): p. 50-2.
316. Solomon, V.R. and H. Lee, *Chloroquine and its analogs: a new promise of an old drug for effective and safe cancer therapies.* Eur J Pharmacol, 2009. **625**(1-3): p. 220-33.
317. Weber, S.M. and S.M. Levitz, *Chloroquine interferes with lipopolysaccharide-induced TNF-alpha gene expression by a nonlysosomotropic mechanism.* Journal of immunology (Baltimore, Md.: 1950), 2000. **165**(3): p. 1534-1540.
318. Zhao, H., et al., *Chloroquine-mediated radiosensitization is due to the destabilization of the lysosomal membrane and subsequent induction of cell death by necrosis.* Radiat Res, 2005. **164**(3): p. 250-7.
319. Hostetler, K.Y., M. Reasor, and P.J. Yazaki, *Chloroquine-induced phospholipid fatty liver. Measurement of drug and lipid concentrations in rat liver lysosomes.* J Biol Chem, 1985. **260**(1): p. 215-9.

320. Jeong, J.Y. and D.M. Jue, *Chloroquine inhibits processing of tumor necrosis factor in lipopolysaccharide-stimulated RAW 264.7 macrophages.* Journal of immunology (Baltimore, Md.: 1950), 1997. **158**(10): p. 4901-4907.
321. Mauthe, M., et al., *Chloroquine inhibits autophagic flux by decreasing autophagosome-lysosome fusion.* Autophagy, 2018. **14**(8): p. 1435-1455.
322. Redmann, M., et al., *Inhibition of autophagy with bafilomycin and chloroquine decreases mitochondrial quality and bioenergetic function in primary neurons.* Redox biology, 2017. **11**: p. 73-81.
323. Yoon, Y.H., et al., *Induction of lysosomal dilatation, arrested autophagy, and cell death by chloroquine in cultured ARPE-19 cells.* Invest Ophthalmol Vis Sci, 2010. **51**(11): p. 6030-7.
324. Li, M., et al., *Suppression of lysosome function induces autophagy via a feedback down-regulation of MTOR complex 1 (MTORC1) activity.* J Biol Chem, 2013. **288**(50): p. 35769-80.
325. Pi, H., et al., *Enhancing lysosomal biogenesis and autophagic flux by activating the transcription factor EB protects against cadmium-induced neurotoxicity.* Sci Rep, 2017. **7**: p. 43466.
326. Kwakye-Berko, F. and S.R. Meshnick, *Binding of chloroquine to DNA.* Mol Biochem Parasitol, 1989. **35**(1): p. 51-5.
327. Projean, D., et al., *In vitro metabolism of chloroquine: identification of CYP2C8, CYP3A4, and CYP2D6 as the main isoforms catalyzing N-desethylchloroquine formation.* Drug metabolism and disposition: the biological fate of chemicals, 2003. **31**(6): p. 748-754.
328. Hu, T., et al., *Chloroquine inhibits hepatocellular carcinoma cell growth in vitro and in vivo.* Oncol Rep, 2016. **35**(1): p. 43-9.
329. Hamm, M., Y. Wang, and R.R. Rustandi, *Characterization of N-Linked Glycosylation in a Monoclonal Antibody Produced in NS0 Cells Using Capillary Electrophoresis with Laser-Induced Fluorescence Detection.* Pharmaceuticals (Basel), 2013. **6**(3): p. 393-406.
330. Cymer, F., et al., *Therapeutic monoclonal antibody N-glycosylation - Structure, function and therapeutic potential.* Biologicals, 2018. **52**: p. 1-11.
331. Werner, R.G., K. Kopp, and M. Schlueter, *Glycosylation of therapeutic proteins in different production systems.* Acta Paediatr, 2007. **96**(455): p. 17-22.
332. Townsend, D.M., K.D. Tew, and H. Tapiero, *The importance of glutathione in human disease.* Biomed Pharmacother, 2003. **57**(3-4): p. 145-55.
333. Zitka, O., et al., *Redox status expressed as GSH:GSSG ratio as a marker for oxidative stress in paediatric tumour patients.* Oncol Lett, 2012. **4**(6): p. 1247-1253.
334. Projean, D., et al., *In vitro metabolism of chloroquine: identification of CYP2C8, CYP3A4, and CYP2D6 as the main isoforms catalyzing N-desethylchloroquine formation.* Drug Metab Dispos, 2003. **31**(6): p. 748-54.
335. Weber, S.M. and S.M. Levitz, *Chloroquine interferes with lipopolysaccharide-induced TNF-alpha gene expression by a nonlysosomotropic mechanism.* J Immunol, 2000. **165**(3): p. 1534-40.
336. Park, J.H., et al., *Proteomic Analysis of Host Cell Protein Dynamics in the Culture Supernatants of Antibody-Producing CHO Cells.* Sci Rep, 2017. **7**: p. 44246.
337. Migani, D., C.M. Smales, and D.G. Bracewell, *Effects of lysosomal biotherapeutic recombinant protein expression on cell stress and protease and general host cell protein release in Chinese hamster ovary cells.* Biotechnol Prog, 2017. **33**(3): p. 666-676.
338. Slater, A.F., *Chloroquine: mechanism of drug action and resistance in Plasmodium falciparum.* Pharmacol Ther, 1993. **57**(2-3): p. 203-35.
339. Sullivan, D.J., Jr., et al., *On the molecular mechanism of chloroquine's antimalarial action.* Proc Natl Acad Sci U S A, 1996. **93**(21): p. 11865-70.
340. Antony, H.A., et al., *Transcriptomic Analysis of Chloroquine-Sensitive and Chloroquine-Resistant Strains of Plasmodium falciparum: Toward Malaria Diagnostics and Therapeutics for Global Health.* OMICS, 2016. **20**(7): p. 424-32.
341. Gunasekera, A.M., et al., *Plasmodium falciparum: genome wide perturbations in transcript profiles among mixed stage cultures after chloroquine treatment.* Exp Parasitol, 2007. **117**(1): p. 87-92.
342. Gunasekera, A.M., et al., *Drug-induced alterations in gene expression of the asexual blood forms of Plasmodium falciparum.* Mol Microbiol, 2003. **50**(4): p. 1229-39.
343. Lappi, A.K. and L.W. Ruddock, *Reexamination of the role of interplay between glutathione and protein disulfide isomerase.* J Mol Biol, 2011. **409**(2): p. 238-49.
344. Chakravarthi, S., C.E. Jessop, and N.J. Bulleid, *The role of glutathione in disulphide bond formation and endoplasmic-reticulum-generated oxidative stress.* EMBO Rep, 2006. **7**(3): p. 271-5.

345. Handlogten, M.W., M. Zhu, and S. Ahuja, *Glutathione and thioredoxin systems contribute to recombinant monoclonal antibody interchain disulfide bond reduction during bioprocessing.* Biotechnol Bioeng, 2017. **114**(7): p. 1469-1477.
346. Averill-Bates, D.A. and E. Przybytkowski, *The role of glucose in cellular defences against cytotoxicity of hydrogen peroxide in Chinese hamster ovary cells.* Arch Biochem Biophys, 1994. **312**(1): p. 52-8.
347. Przybytkowski, E. and D.A. Averill-Bates, *Correlation between glutathione and stimulation of the pentose phosphate cycle in situ in Chinese hamster ovary cells exposed to hydrogen peroxide.* Arch Biochem Biophys, 1996. **325**(1): p. 91-8.
348. Luperchio, S., S. Tamir, and S.R. Tannenbaum, *NO-induced oxidative stress and glutathione metabolism in rodent and human cells.* Free Radic Biol Med, 1996. **21**(4): p. 513-9.
349. Freeman, M.L., A.W. Malcolm, and M.J. Meredith, *Role of glutathione in cell survival after hyperthermic treatment of Chinese hamster ovary cells.* Cancer Res, 1985. **45**(12 Pt 1): p. 6308-13.
350. Orellana, C.A., et al., *High-antibody-producing Chinese hamster ovary cells up-regulate intracellular protein transport and glutathione synthesis.* J Proteome Res, 2015. **14**(2): p. 609-18.
351. Orellana, C.A., et al., *Overexpression of the regulatory subunit of glutamate-cysteine ligase enhances monoclonal antibody production in CHO cells.* Biotechnol Bioeng, 2017. **114**(8): p. 1825-1836.
352. Shridhar, S., et al., *Transcriptomic changes in CHO cells after adaptation to suspension growth in protein-free medium analysed by a species-specific microarray.* J Biotechnol, 2017. **257**: p. 13-21.
353. Templeton, N., et al., *Peak antibody production is associated with increased oxidative metabolism in an industrially relevant fed-batch CHO cell culture.* Biotechnol Bioeng, 2013. **110**(7): p. 2013-24.
354. Guerrero-Gomez, D., et al., *Loss of glutathione redox homeostasis impairs proteostasis by inhibiting autophagy-dependent protein degradation.* Cell Death Differ, 2019.
355. Desideri, E., G. Filomeni, and M.R. Ciriolo, *Glutathione participates in the modulation of starvation-induced autophagy in carcinoma cells.* Autophagy, 2012. **8**(12): p. 1769-81.
356. Voehringer, D.W., *BCL-2 and glutathione: alterations in cellular redox state that regulate apoptosis sensitivity.* Free Radic Biol Med, 1999. **27**(9-10): p. 945-50.
357. Voehringer, D.W., et al., *Bcl-2 expression causes redistribution of glutathione to the nucleus.* Proc Natl Acad Sci U S A, 1998. **95**(6): p. 2956-60.
358. Meredith, M.J., et al., *Expression of Bcl-2 increases intracellular glutathione by inhibiting methionine-dependent GSH efflux.* Biochem Biophys Res Commun, 1998. **248**(3): p. 458-63.
359. Nasseri, S.S.G., N.; Braasch, K.; Jardon, M.A.; Butler, M.; Kennard, M.; Gapaluni, B.; Piret, J.M., *Increased CHO cell fed-batch monoclonal antibody production using the autophagy inhibitor 3-MA or gradually increasing osmolality.* Biochemical Engineering Journal, 2014. **91**: p. 37-45.
360. Su, M.Y., et al., *Hybrid Structure of the RagA/C-Ragulator mTORC1 Activation Complex.* Mol Cell, 2017. **68**(5): p. 835-846 e3.
361. Malek, M., et al., *LAMTOR1 depletion induces p53-dependent apoptosis via aberrant lysosomal activation.* Cell Death Dis, 2012. **3**: p. e300.
362. Hosokawa, T., et al., *Lamtor1 Is Critically Required for CD4(+) T Cell Proliferation and Regulatory T Cell Suppressive Function.* J Immunol, 2017. **199**(6): p. 2008-2019.
363. Xu, J., et al., *Systematic development of temperature shift strategies for Chinese Hamster ovary cells based on short duration cultures and kinitic modeling*. mAbs, 2019. **11**(1): p.191-204.
364. Kumar, N., et al., *Differential protein expression following low temperature culture of suspension CHO-K1 cells*. BMC Biotechnology, 2008. **8**

Appendix A

RESEARCH ARTICLE

Application of Imaging Flow Cytometry for the Characterization of Intracellular Attributes in Chinese Hamster Ovary Cell Lines at the Single-Cell Level

Eva Pekle, Andrew Smith, Guglielmo Rosignoli, Christopher Sellick, C. M. Smales,* and Claire Pearce

Biopharmaceutical manufacturing using Chinese hamster ovary (CHO) cells requires the generation of high-producing clonal cell lines. During cell line development, cell cloning using fluorescence-activated cell sorting (FACS) has the potential to combine isolation of single cells with sorting based on specific cellular attributes that correlate with productivity and/or growth, identifying cell lines with desirable phenotypes for manufacturing. This study describes the application of imaging flow cytometry (IFC) to characterize recombinant cell lines at the single-cell level to identify cell attributes predictive of productivity. IFC assays are developed to quantify the organelle content and recombinant heavy-chain (HC) and light-chain (LC) polypeptide as well as messenger RNA (mRNA) amounts in single cells. The assays are then validated against orthogonal standard flow cytometry, western blot, and quantitative reverse transcription polymerase chain reaction (qRT-PCR) methods. The authors describe how these IFC assays may be used in cell line development and show how cellular properties can be correlated with productivity at the single-cell level, allowing the isolation of such cells during the cloning process. From the analysis, HC polypeptide and mRNA are found to be predictive of productivity early in the culture; however, specific organelle content did not show any correlation with productivity.

1. Introduction

Mammalian cells are the expression system of choice for the manufacture of therapeutic glycoproteins, such as monoclonal antibodies (mAbs), with over 70% being produced using Chinese hamster ovary (CHO) cells.[1] During cell line development, random integration of the expression plasmid and host cell heterogeneity results in varied expression levels, requiring extensive screening to identify highly productive clones.[2–4] Strategies to identify cells with increased probability of a high final titer at the cloning step could reduce timelines and diminish the total number of cell lines required to be screened at later stages to isolate such clones. Fluorescence-activated cell sorting (FACS) is commonly used for cell cloning in cell line development, and has the advantage of being a high-throughput method that can deposit single cells into wells of multiwell plates, meeting the regulatory demands for clonality and assess cellular characteristics at the single-cell level. Combining FACS with postsorting visualization by fluorescent imaging showed that >99.5% of cells were clonal.[5,6]

Various flow cytometry-based screening methods have been developed to enable

selective isolation of high-producing clones. These include the capture of secreted mAb via binding to the cell surface using microbead technology,[7] surface affinity matrix,[8] introducing fluorescent markers into the vector,[9] and vector modifications to enable secreted mAb to bind to cell surface proteins.[10,11] Although such approaches enrich high-producing clones, they tend to be labor intensive and time-consuming.

Recent advances in flow cytometry have been made with the development of a novel imaging flow cytometer (IFC), ImageStream ([IS]; Amnis/Merck). A key feature of IS is that it combines the workflow and high throughput of conventional flow cytometers with the acquisition of up to 12 images per cell, enabling the spatial resolution and determination of quantitative morphology that can be achieved with microscopy.[12] IFC images that may be obtained include side-scatter, bright field, and up to nine fluorescent images, and such data have been used in a range of studies, including assessment of nuclear translocation,[13] detection and discrimination of tumor cells, and fluorescence in situ hybridization studies.[12] The current study describes a novel approach to study recombinant CHO cell lines using IFC technology to identify the cellular characteristics that correlate with productivity at the single-cell level.

2. Experimental Section

2.1. Cell Culture

CHO cell lines stably expressing a recombinant immunoglobulin G1κ (IgG1κ) were grown in proprietary medium supplemented with 50 μM methionine sulfoximine (SigmaAldrich) and routinely subcultured as previously described.[14]

2.2. mAb Quantitation

The IgG content in the clarified culture medium was quantified by protein-A high-performance liquid affinity chromatography on an Agilent HP1100 instrument (Agilent Technologies).

2.3. Intracellular (IC) Heavy Chain (HC) and Light Chain (LC) Quantification by Western Blot

The IC polypeptide was assessed using standard western analysis.[14] Membranes were incubated overnight with an anti-IgG (FC) antibody conjugated to horseradish peroxidase (HRP) or anti-κ conjugated to HRP diluted at 1:10 000 (both from The Binding Site). A rabbit anti-glyceraldehyde 3phosphate dehydrogenase (GAPDH) antibody (Cell Signaling Technology) with a secondary anti-rabbit antibody conjugated to HRP (Jackson ImmunoResearch) was used to detect GAPDH. Blots were developed by incubation with enhanced chemiluminescence reagent (GE Healthcare Life Sciences) which was also used to measure the band intensity for semiquantitation of proteins.

2.4. HC and LC Messenger RNA (mRNA) Quantitative Polymerase Chain Reaction (qPCR)

Total RNA was extracted using an RNeasy kit and treated with DNase (Qiagen). Quantitative reverse transcription PCR (qRT-

PCR) was performed as previously reported.[14]

2.5. Flow Cytometry Assays

For the HC and LC protein assay, cells (1×10^6) were fixed using a 1:1 solution of Fixation Medium A (Invitrogen) and flow cytometry buffer (phosphate-buffered saline with 5% bovine serum albumin) for 15 min at room temperature and then incubated with Permeabilization Medium B (Invitrogen) containing 1:20 goat $f(ab')_2$ anti-human IgG Alexa Fluor conjugated to 488 (Invitrogen; excitation/emission: ≈500/ 520 nm) and goat $f(ab')_2$ anti-human kappa conjugated to allophycocyanin (Biolegend, excitation/emission: ≈650/675 nm) for 15 min, before being washed and analyzed. HC and LC mRNA were investigated using a PrimeFlow RNA kit with custom probes (Affymetrix, Merck) following the manufacturer's protocol. Quantitation of organelles was performed by staining with Golgi-ID Green (excitation/emission: ≈450/ 530 nm), ER-ID red (excitation/emission: ≈580/660 nm), Mito-ID red (excitation/emission: ≈558/690 nm; all from Enzo Life Sciences), and MitoTracker Deep Red (excitation/ emission: ≈644/665 nm; Invitrogen) using the manufacturers' protocols. 4',6-Diamidino-2-phenylindole (DAPI; excitation/emisssion: ≈340/450 nm) or Sytox nuclear (excitation/emission: ≈444/480 nm) counterstain was used for nuclear localization.

2.6. Flow Cytometry

Flow cytometry was performed on a BD Canto flow cytometer with the BD FACSDiva software. Cells were stained with DAPI and MitoTracker and excited with a violet (405 nm) and red (633 nm) laser, and 10 000 events were acquired for each sample. Doublets and debris were removed by gating on forward- and side-scatter dot plots. FlowJo software was used for statistical analysis.

2.7. Imaging Flow Cytometer

An IS IFC (Merck) with INSPIRE software was used to collect 10 000 events (or 10 min acquisition time). Images of each event were captured using a ×60 objective with 405 nm, 488 nm, and 658 nm lasers, collecting fluorescent images in channels 7, 2, and 5, respectively, along with channels 1 and 9 for bright field and channel 6 for the dark field. The cell classifier was set to 50 on area-lower limit on the bright field channel to avoid debris acquisition. The analysis was performed using IDEAS software (v6.2). Compensation settings were calculated using the built-in software algorithm in the best-fit mode and refined manually. Focused cells were gated using the plot of contrast vs gradient root mean squared features and single cells were gated using a dot plot of the aspect ratio vs cell area for the bright field channel.

3. Results and Discussion

The first step in this study was to develop IFC assays to determine the contents of IC HC and LC polypeptide, HC and LC mRNA, and specific cellular organelles (Figure 1A). The key features of the IFC software are functions that enable spot counting (Figure 1B) to quantify punctate staining, such as the Golgi, and masking to determine the cell or organelle size by creating a mask on the bright field image (Figure 1C). Additionally, colocalization between two signals can also be determined (Figure 1D).

Standard flow cytometry is widely accepted as a robust method for investigating cellular attributes; however, IFC is a relatively new technology and has not been extensively used. We therefore assessed the reproducibility and consistency of results between standard flow cytometry and IFC. To do this, three separate vials of a recombinant CHO cell line were thawed and independently cultured in shake flasks. After the first passage, triplicate samples were taken from each flask on three separate days and

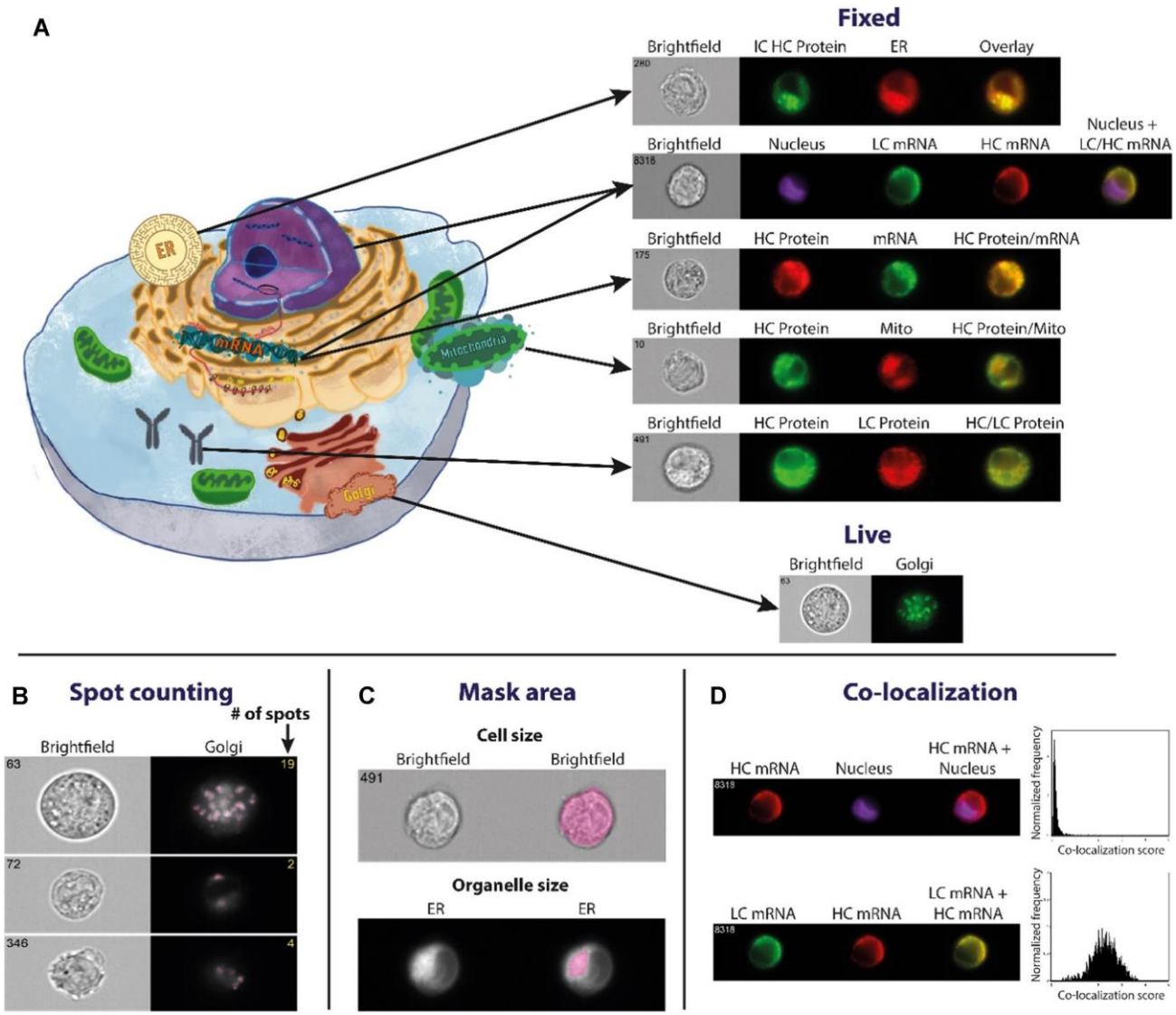

Figure 1. Sample images of the assays developed on the IS. A) Assays were developed in fixed cells for multiplexing with HC protein detection. The assays include ER LC and HC mRNA, LC and HC polypeptide, and mitochondria. The Golgi assay was developed in live cells. Images show bright field, fluorescent staining, and an overlay of the staining. B) Sample images featuring spot counting of the Golgi apparatus, with bright field and fluorescent channel images with the number of spots on the right corner of the image. C) Masking of the cell size based on the bright field image, and of the organelle size based on the threshold of the ER intensity. D) Colocalization of HC mRNA and nucleus, which shows no colocalization, and HC and LC mRNA, which show strong colocalization.

stained with MitoTracker and DAPI (Figure 2A). The percentage of double-positive cells across instruments and days ranged from 94.8% to 100% (Figure 2B,C). The

intensity of nuclear and mitochondrial staining was consistent across instruments (Figure 2D–G), with a good correlation between the signal intensity recorded by the different instruments for both dyes (Figure 2H,I; R^2 = 0.42 DAPI and 0.97 MitoTracker), assuring that observations by IFC could be transferred to standard flow cytometry.

To investigate the cellular differences between high/lowproducing cell lines, and correlations between the organelle content and cell culture parameters, a panel of 19 cell lines expressing a model IgG1 mAb with a range of titers, specific productivities and growth in fed-batch culture was used (Table 1, Supporting Information). The IC HC and LC polypeptide contents and mRNA expression not only varied across the cell lines but also within individual cell lines at different time points of fed-batch culture (Figure 3; Table 2, Supporting Information). The amounts of HC polypeptide and mRNA on day 4, as

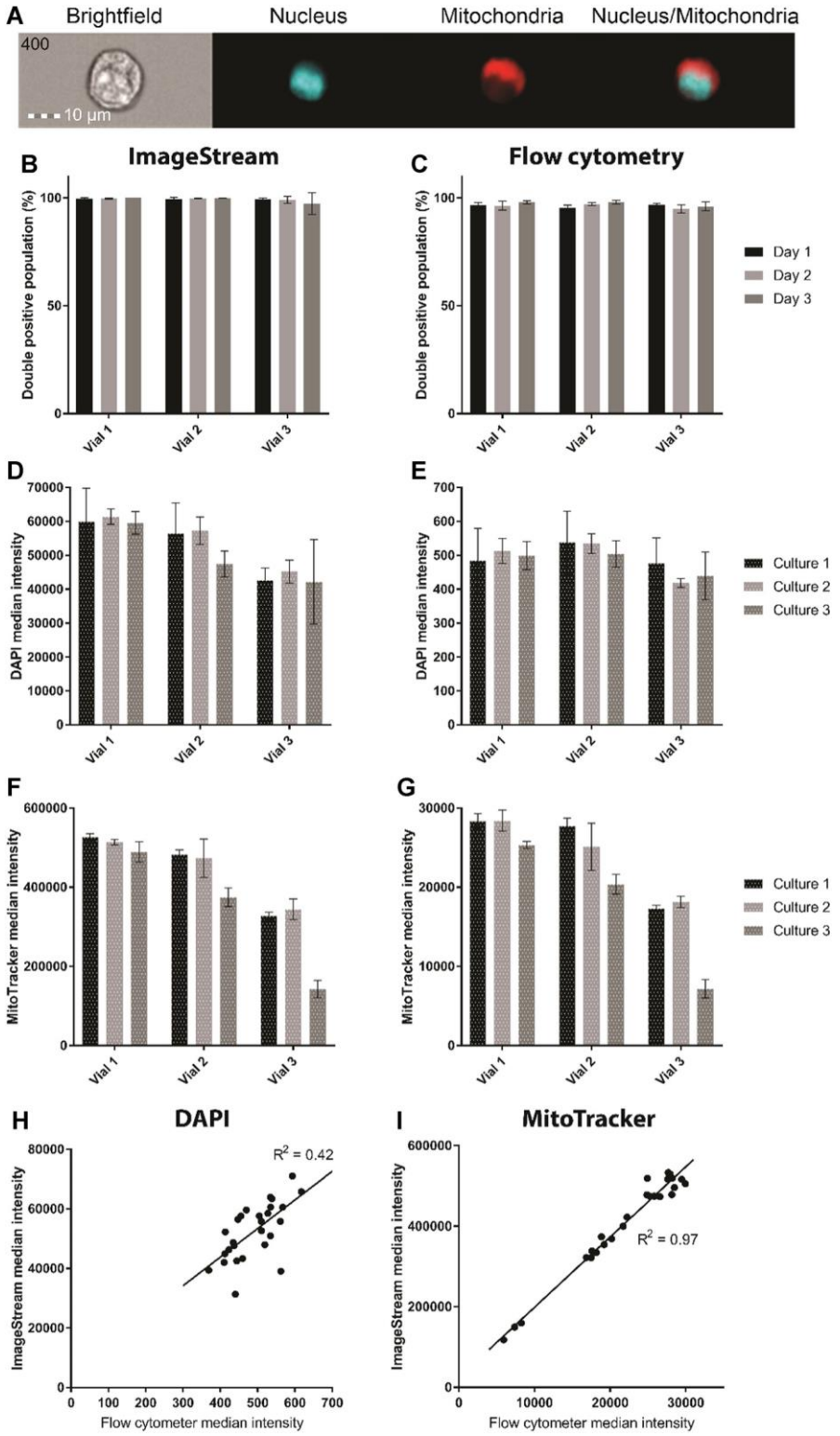

Figure 2 Continued.

determined by western blotting and qPCR, respectively, were both predictive of the final titer (Figure 3A,B), as well as the overall qP (data not shown), HC polypeptide and qP, Pearson's correlation coefficient R = 0.77, and for

HC mRNA, R = 0.82). No correlation was found between the titer and the LC content (data not shown) or between the HC polypeptide and the titer later in the culture (days 7 and 9). From these results, it is evident that the IC HC polypeptide, and mRNA on day 4 could be used as markers of cellular productivity.

The IC HC and LC polypeptide as wel as mRNA contents were then assessed using IFC. The HC polypeptide and mRNA contents on day 3 showed a strong correlation with the final titer (Figure 3C,D), but at later time points (days 6

and 10), no such correlation was found. This suggests that the IC HC polypeptide and mRNA contents are predictive of the final titer early in the fed-batch culture; however, this predictive power is lost as the culture progresses as other factors begin to play a role in determining the final titer, e.g., availability of translation machinery, folding/secretion, and energy status of cells. The LC polypeptide amounts showed no correlation with the final titer or qP, although the LC mRNA content showed a positive correlation with the final titer (R = 0.73 on day 3). Overall, these results are consistent with previous reports that the IC HC polypeptide and mRNA contents show a stronger correlation with mAb productivity than the LC content, indicating that HC can be a limiting factor for the final titer.[15–20] Although the correlation with LC was lower, there was some correlation between LC transcript and the final titer; this is not unexpected as LC polypeptide is necessary to drive HC constant domain 1 (CH1) folding, mAb assembly, and secretion.[21,22] The reported differences as to whether HC or LC are limiting may reflect molecule- and host cell-dependent differences. We note that the cell line with the highest HC mRNA content on day 3 did not have the highest titer. This cell line also had a high amount of LC mRNA on day 6, suggesting that above a certain transcript threshold, there might be potential bottlenecks further down the translðation and secretion pathways.[14,16,23]

Next, we investigated multiplexing HC mRNA and HC polypeptide assays at the single-cell level. This revealed a positive correlation with the titer, similar to that seen at the population level with qRT-PCR and western blotting assays (Figure 3E). IFC images revealed differential cytoplasmic localization of the HC polypeptide and HC mRNA, consistent with the previous findings of HC polypeptide residing in the endoplasmic reticulum (ER) and Golgi,[24] and mRNA localized with ribosomes on the ER surface (Figure 3F). As both the HC mRNA and polypeptide show a positive correlation with the final titer early in culture and with each other, HC polypeptide was selected as the marker of productivity at the single-cell level as the assay is more time- and cost-efficient than that for mRNA. The HC polypeptide was then multiplexed with assays for different organelles.

The differences in productivity between cell lines can be explained not only by a diverse range of mRNA levels, but also by differences in the cellular properties that govern the growth and biosynthetic capacities of individual clones. Energy metabolism[25] and protein synthesis,[16] folding,[26] and secretion[27] pathways can influence the final production and secretion of mAb. We therefore investigated with IS whether productivity differences observed between cell lines were correlated

with variations in the mitochondria, ER, and Golgi content of cells, as well as HC and LC polypeptide and mRNA. Correlations were investigated at the population (population median intensity vs final titer for all cell lines) and the singlecell (intensity organelle vs intensity HC) level (Table 2, Supporting Information). No linear correlations were found for individual cell lines between the mitochondrial content and HC polypeptide or mRNA amounts at the single-cell level on any sampled days. Moreover, no relationships were found at the population level between mitochondrial content and productivity, or specific productivity on any of the days investigated. Mitochondrial content itself is not always reflective of cellular metabolism, as significant changes in the mitochondrial membrane potential (MMP) can occur without fluctuations in mitochondria numbers.[28–30] Studies have linked either high[29] or low[28] MMP with increased final titer; however, we only considered mitochondrial biomass in this study.

Additionally, no correlations were observed between the HC content and the ER content at the single-cell level or at the population level between the ER or Golgi content and titer or specific productivity (Table 2, Supporting Information). Other studies report similar findings during the growth phase,[1,15] while our results show that neither the ER content nor the Golgi content correlates with productivity during the growth phase or at later stages of batch culture. We note reports that host cells with higher ER content prior to transfection result in the isolation of recombinant cells with higher titer.[31]

IFC currently has limitations in its application to sorting and isolation of cells in a cell line construction process. Currently, IFC does not offer a high spatial resolution compared to traditional microscopes, which also allow for time-lapse experiments and spatial-temporal analysis of the sample.[32] A further limitation of IFC is its maximum speed

Figure 2. A) Sample IS images showing the bright field, nuclear staining (DAPI), mitochondria staining (MitoTracker), and composite images. B,C) Average percentage of cells positive for both nuclear and mitochondrial staining for each vial on different days on IS B) and flow cytometry C). D–G) Average of DAPI median intensity D,E) and MitoTracker median intensity F,G) of individual shake flasks on day 3, representative of observations on other days, for IS D,F) and flow cytometry E,G). The intensity of the nuclear staining was consistent between instruments and between shake flasks originating from the same vial, showing no statistical difference (Figure 2D,E). For the mitochondrial staining, differences in intensity were present between shake flasks originating from the same vial and between vials, which could be due to intrinsic differences between cultures (Figure 2F,G). Cultures were prepared and analyzed in a different order to avoid order bias. Overall, there was a strong correlation between the signals measured by both instruments (Pearson's correlation coefficient R = 0.65 for nuclear stain and R = 0.98 for mitochondrial stain). (H&I) DAPI median intensity of individual samples from day 3 H) and MitoTracker I) from flow cytometer vs IS, with the R^2 values (coefficient of determination) on the graph and Pearson's correlation coefficients of 0.65 and 0.98, respectively.

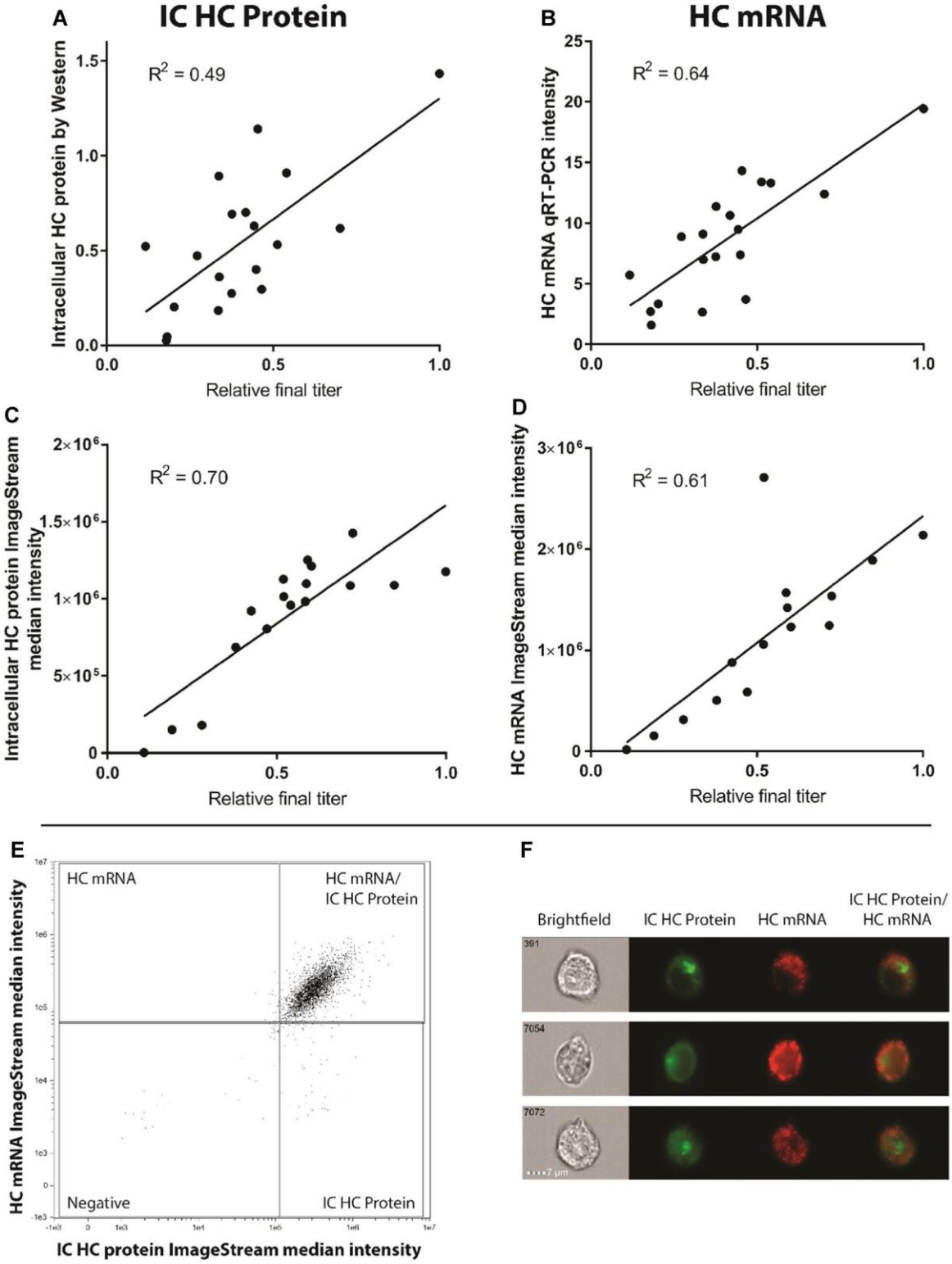

Figure 3. Correlation between titer and IC HC protein measured by A) western blotting and C) IFC (R^2 = 0.84 where R^2 is the coefficient of determination). B,D) Correlation between titer and HC mRNA measured by qRT-PCR B) and IFC D) (R = 0.79). E,F) Multiplexing of HC mRNA and polypeptide with IFC (R = 0.65 for E).

of 300 events s^{-1}, which can only be reached with a high sample concentration of 10^8 cells mL^{-1}. This is quite different to the high throughput of standard flow cytometry. The slow acquisition is mostly the result of limitations in focusing of cells, as out-of-focus cells are excluded from analysis.[32] Finally, there are currently no commercially available IFCs that have the ability to sort cells based on image features, although that may change in the near future following the recent work by Nitta et al.[33] on intelligent image-activated cell sorting.

While the limitations are evident, the powerful IFC approach described here has the potential to identify novel cellular attributes that could be implemented to select for high-producing cells (and eventually cells that have optimal growth profiles and specific product quality profiles) during the cell line development process. Single-cell analysis by IFC could be combined with other approaches such as Opropargyl-puromycin labeling to investigate correlations between the organelle content, the HC and LC transcript and polypeptide, and the total protein synthesis rate.[34] As new live cell assays become available, further characterization of other cell characteristics can be investigated and correlated with desirable cell culture attributes such as productivity, growth, or product quality.

In this study of a panel of 19 cell lines, no differences in the organelle content were observed between high and low producers of a model mAb that is considered easy-to-express. However, it is possible that cellular organelle amounts might differentiate between productivity capabilities of cell lines making more difficult-to-express molecules. Moreover, the IFC tools described here could be applied to the characterization of host cell populations and to identify potential targets for host cell engineering. Consistent with previous reports, we show that the HC protein and mRNA are markers of productivity early in culture—this highlights a need for the development of new flow cytometric methods that allow the measurement of HC polypeptide or mRNA amounts in live cells, which could be used to enrich the proportion of high producers and improve the efficiency of cell line development.

Supporting Information

Supporting Information is available from the Wiley Online Library or from the author.

Acknowledgements

The authors would like to acknowledge Dr. Sarah Dunn for stable cell line generation, Dr. Charlotte Godfrey for initial characterization of the cell lines, and Dr. Diane Hatton for reviewing the manuscript .

Conflict of Interest

The authors declare no conflict of interest.

Keywords

Chinese hamster ovary (CHO) cells, imaging flow cytometry, organelles, single-cell imaging
Received: November 5, 2018

Appendix B

Revised: January 21, 2019

Published online: May 2, 2019

[1] D. Reinhart, L. Damjanovic, C. Kaisermayer, R. Kunert, Appl. Microbiol. Biotechnol. 2015, 99, 4645.
[2] S. Misaghi, D. Shaw, S. Louie, A. Nava, L. Simmons, B. Snedecor, C. Poon, J. S. Paw, L. Gilmour-Appling, J. E. Cupp, Biotechnol. Prog. 2016, 32, 198.
[3] W. Pilbrough, T. P. Munro, P. Gray, PloS ONE 2009, 4, e8432.
[4] J. F. Povey, C. J. O'malley, T. Root, E. B. Martin, G. A. Montague, M. Feary, C. Trim, D. A. Lang, R. Alldread, A. J. Racher, C. M. Smales, J. Biotechnol. 2014, 184, 84.
[5] J. Fieder, P. Schulz, I. Gorr, H. Bradl, T. Wenger, Biotechnol J 2017, 12, 1700002.
[6] K. Evans, T. Albanetti, R. Venkat, R. Schoner, J. Savery, G. Miro-Quesada, B. Rajan, C. Groves, Biotechnol. Prog. 2015, 31, 1172.
[7] K. T. Powell, J. C. Weaver, Biotechnol. 1990, 8, 333.
[8] R. Manz, M. Assenmacher, E. Pfluger, S. Miltenyi, A. Radbruch, Proc. Natl. Acad. Sci. U. S. A. 1995, 92, 1921.
[9] R. J. Sleiman, P. P. Gray, M. N. McCall, J. Codamo, N. A. S. Sunstrom, Biotechnol. Bioeng. 2008, 99, 578. [10] B. Yu, J. M. Wages, J. W. Larrick, Protein Eng., Des. Sel. 2014, 27, 309.
[11] S. Lang, D. Drewello, J. Wichter, A. Nommay, B. Wilms, H. P. Knopf, T. Jostock, Biotechnol. Bioeng. 2016, 113, 2386.
[12] D. A. Basiji, W. E. Ortyn, L. Liang, V. Venkatachalam, P. Morrissey, Clin. Lab. Med. 2007, 27, 653.
[13] T. C. George, S. L. Fanning, P. Fitzgeral-Bocarsly, R. B. Medeiros, S. Highfill, Y. Shimizu, B. E. Hall, K. Frost, D. Basiji, W. E. Ortyn, P. J. Morrissey, D. H. Lynch, J. Immunol. Methods 2006, 311, 117.
[14] C. L. Godfrey, E. J. Mead, O. Daramola, S. Dunn, D. Hatton, R. Field, G. Pettman, C. M. Smales, Biotechnol. J 2017, 12, 1700177. [15] R. Z. Edros, S. McDonnell, M. Al-Rubeai, PloS ONE 2013, 8, e75935.
[16] E. J. Mead, R. J. Masterton, M. Feary, O. Obrezanova, L. Zhang, R. Young, C. M. Smales, Biochem. J. 2015, 472, 261.
[17] N. Borth, K. Strutzenberger, U. Donalies, R. Kunert, H. Katinger, Cytotechnology 1996, 22, 129.
[18] J. McLeod, P. M. O'Callaghan, L. P. Pybus, S. J. Wilkinson, T. Root, A. J. Racher, D. C. James, Biotechnol. Bioeng. 2011, 108, 2193.
[19] P. M. O'Callaghan, J. McLeod, L. P. Pybus, C. S. Lovelady, S. J. Wilkinson, A. J. Racher, A. Porter, D. C. James, Biotechnol. Bioeng. 2010, 106, 938.
[20] N. Borth, D. Mattanovich, R. Kunert, H. Katinger, Biotechnol. Prog. 2005, 21, 106.
[21] H. Dorai, B. Csirke, B. Scallon, S. Ganguly, Hybridoma 2006, 25, 1.
[22] K. Strutzenberger, N. Borth, R. Kunert, W. Steinfellner, H. Katinger, J. Biotechnol. 1999, 69, 215.
[23] V. Chromikova, A. Mader, W. Steinfellner, R. Kunert, Cytotechnology 2015, 67, 343.
[24] S. Mathias, S. Fischer, R. Handrick, J. Fieder, P. Schulz, H. Bradl, I. Gorr, M. Gamer, K. Otte, J. Biotechnol. 2018, 271, 47.
[25] C. A. Sellick, A. S. Croxford, A. R. Maqsood, G. Stephens, H. V. Westerhoff, R. Goodacre, A. J. Dickson, Biotechnol. Bioeng. 2011, 108, 3025.
[26] C. Mohan, G. M. Lee, Biotechnol. Bioeng. 2010, 107, 337.
[27] A. Tastanova, A. Schulz, M. Folcher, A. Tolstrup, A. Puklowski, H. Kaufmann, M. Fussenegger, J. Biotechnol. 2016, 219, 72.
[28] G. Hinterkörner, G. Brugger, D. Müller, F. Hesse, R. Kunert, H. Katinger, N. Borth, J. Biotechnol. 2007, 129, 651. [29] L. Chakrabarti, A. Mathew, L. Li, S. Han, J. Klover, T. Albanetti, P. Hawley-Nelson, J. Immunol. Methods 2018, 464, 31 pii: S00221759(18)30192-3
[30] N. Borth, G. Kral, H. Katinger, Cytometry 1993, 14, 70.
[31] P. M. O'Callaghan, M. E. Berthelot, R. J. Young, J. W. A. Graham, A. J. Racher, D. Aldana, Biotechnol. Progr. 2015, 31, 1187.
[32] N. S. Barteneva, E. Fasler-Kan, I. A. Vorobjev, J. Histochem. Cytochem. 2012, 60, 723.
[33] N. Nitta, T. Sugimura, A. Isozaki, H. Mikami, K. Hiraki, S. Sakuma, T. Iino, F. Arai, T. Endo, Y. Fujiwaki, H. Fukuzawa, M. Hase, T. Hayakawa, K. Hiramatsu, Y. Hoshino, M. Inaba, T. Ito, H. Karakawa, Y. Kasai, K. Koizumi, S. Lee, C. Lei, M. Li, T. Maeno, S. Matsusaka, D. Murakami, A. Nakagawa, Y. Oguchi, M. Oikawa, T. Ota, K. Shiba, H. Shintaku, Y. Shirasaki, K. Suga, Y. Suzukiet al.N. Suzuki, Cell 2018, 175, 266.
[34] F. Nagelreiter, M. T. Coats, G. Klanert, E. Gludovacz, N. Borth, J. Grillari, M. Schosserer, Biotechnol. J 2018, 13, e1700492.

Appendix B

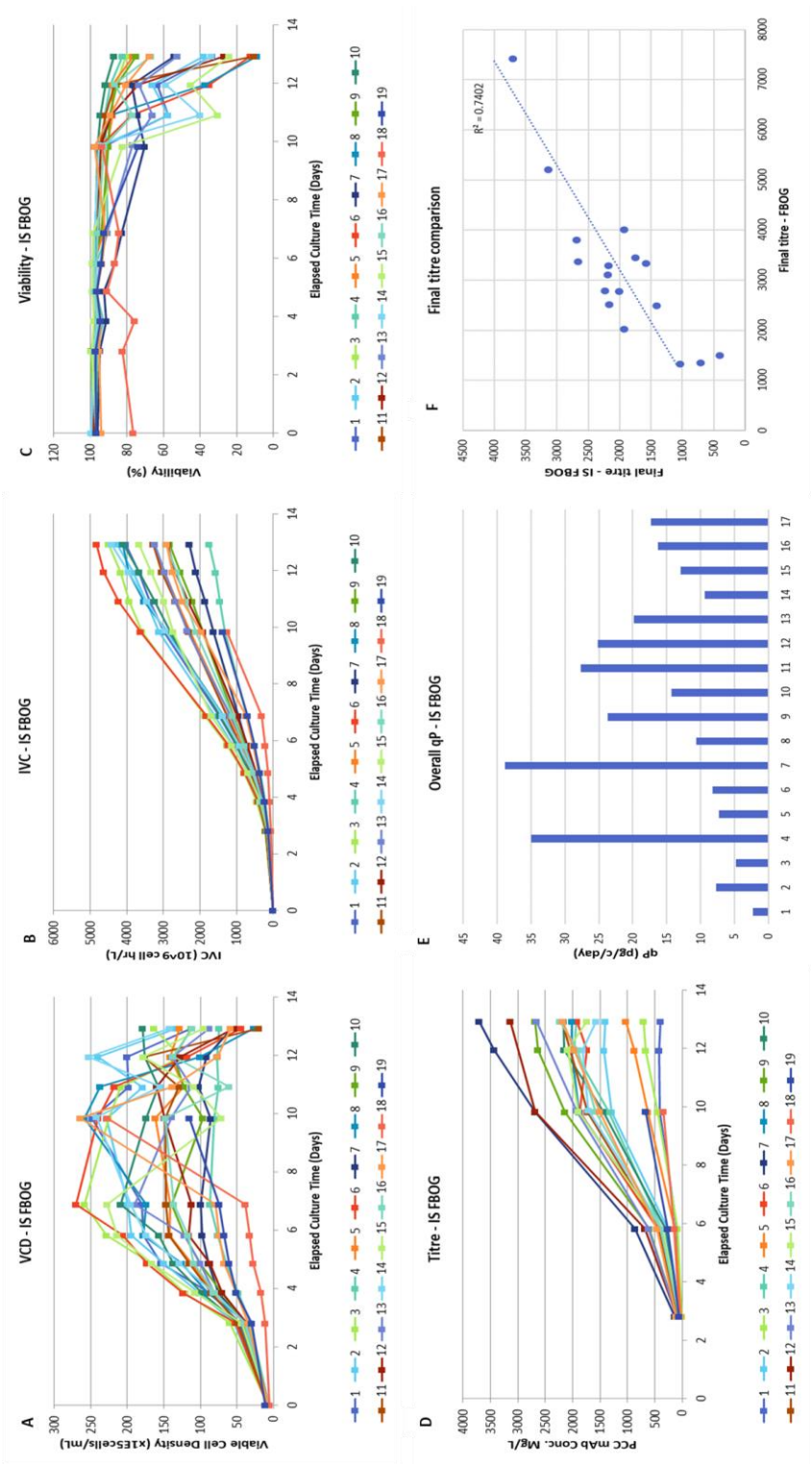

Figure 2 Cell culture data from the repeat of the BSF FBOG, with IS sampling. A) VCD, B) IVC, C) viability, D) titre, E) overall qP and F) comparison of the initial BSF FBOG and the IS FBOG.

Table 1 Values for the overall qP, final titre and final IVC for the cell lines in BSF.

Cell line	qP (pg / cell / day)	Titer (mg / L)	Final IVC (*10^6 cells / ml)
1	4.87	1496	303
2	10.76	2485	237
3	6.39	1343	224
4	28.78	2014	83
5	9.91	1326	153
6	24.25	4007	167
7	74.52	7418	118
8	8.63	2778	324
9	34.11	3800	127
10	14.87	2505	152
11	21.97	3098	163
12	27.8	5201	206
13	18.77	3364	188
14	11.33	3327	325
15	12.35	3450	319
16	20.68	2789	155
17	31.03	3281	127
18	28.79	2494	94
19	10.16	859	67

Table 2 Correlation at the single cell level for individual cell line between mitochondrial content and HC protein, ER content and HC protein, LC protein and HC protein

	1	2	3	4	5	6	7	8	9	10	11	12	13	14	15	16	17	18	19	Range
Mitochondrial content																				
d3	0.44	0.49	0.26	0.19	0.02	0.31	0.15	0.40	0.29	0.35	0.24	0.26	0.26	0.46	0.37	0.25	0.16	0.22	0.28	0.03 to 0.52
d6	0.28	0.40	0.22	0.16	0.02	0.40	0.15	0.45	0.39	0.38	0.39	0.52	0.25	0.43	0.41	0.32	0.17	0.21	0.22	0.02 to 0.46
d10	0.07	0.30	0.05	0.15	0.00	0.30	0.02	0.51	0.29	0.48	0.22	0.13	0.11	0.27	0.19	-0.02	0.08	N/A	N/A	-0.03 to 0.49
ER content																				
d3	0.21	0.57	0.29	0.21	-0.08	0.35	0.17	0.41	0.35	0.43	0.34	0.42	0.30	0.55	0.41	0.33	0.20	0.23	0.27	-0.08 to 0.57
d6	0.21	0.43	0.22	0.17	-0.09	0.46	0.20	0.51	0.41	0.39	0.39	0.51	0.36	0.46	0.41	0.34	0.48	0.25	0.26	-0.9 to 0.51
d10	0.00	0.36	0.07	0.17	-0.06	0.35	N/A	0.52	0.30	0.42	0.34	0.41	0.05	0.11	0.24	0.33	0.21	N/A	N/A	-0.06 to 0.52
LC protein																				
d3	0.91	0.90	0.88	0.92	0.91	0.93	0.92	0.92	0.90	0.90	0.81	0.92	0.91	0.93	0.92	0.91	0.92	0.71	0.92	0.71 to 0.93
d6	0.89	0.86	0.58	0.88	0.80	0.88	0.89	0.88	0.85	0.89	0.84	0.86	0.89	0.88	0.88	0.86	0.89	0.89	0.87	0.57 to 0.89
d10	0.88	0.88	0.47	0.87	0.82	0.90	N/A	0.89	0.86	0.89	0.89	0.89	0.83	0.87	0.88	0.85	0.91	N/A	N/A	0.47 to 0.91

Table 3 Results from the PCA analysis, showing the importance of the different variables towards each of the components

Variables	PC1	PC2	PC3	PC4
HC mRNA	0.41	0.15	-0.14	-0.22
LC mRNA	0.35	0.26	-0.21	-0.31
HC / LC mRNA	0.25	-0.31	0.54	0.17
HC protein	0.36	-0.29	-0.10	0.22
LC protein	0.34	-0.30	-0.10	0.32
HC / LC protein	0.33	-1.70	0.37	-0.56
Lysosome	0.32	0.20	0.00	0.49
Cell size	0.18	0.41	0.25	0.27
ER	0.14	0.40	0.47	-0.07
Mitochondria	-0.70	0.48	-0.01	0.13
HC/ER colocalization	-0.36	-0.07	0.44	0.09

Appendix C

Table 1 Gene list of genes up-regulated in the control compared to the CQ-evolved cells, with the log2 fold change (Log2 FC) and the adjusted p-value of the change (Adj p-value).

Gene name	Log2 FC	Adj p-value
Hsd11b1	5.93	1.29E-06
Cd9	5.39	2.45E-06
Lamb3	4.80	1.21E-05
Mir3102	4.40	4.36E-04
Lingo1	4.18	9.63E-04
ENSCGRG00001002410	4.11	1.26E-02
Etl4	3.95	2.79E-50
P2ry2	3.57	4.76E-263
Arhgef17	3.44	4.95E-261
ENSCGRG00001001630	3.35	9.70E-16
Slc14a1	3.34	1.40E-21
Trem1	3.26	2.86E-03
Fchsd2	3.08	2.62E-116
ENSCGRG00001011776	3.05	1.70E-23
Apbb1	3.04	0.00E+00
Fam168a	3.01	6.10E-114
Nrg1	2.98	2.11E-04
Atg16l2	2.94	1.68E-59
Rab6a	2.82	8.28E-77
Dnajb13	2.79	3.50E-67
Col1a2	2.77	3.80E-02
Relt	2.77	6.99E-134
Areg	2.75	3.89E-51
Smpd1	2.70	1.78E-53
Moxd1	2.70	7.93E-04
Rgs16	2.66	2.14E-13
Cacna1b	2.64	3.36E-03
Ucp3	2.62	6.48E-03
Plekhb1	2.61	4.37E-12
Coa4	2.60	5.91E-70
Mrpl48	2.52	1.06E-98
Cavin4	2.44	4.55E-10
Cdhr4	2.42	1.95E-02
Gucy2d	2.41	1.30E-03
Ereg	2.31	3.11E-05
ENSCGRG00001018176	2.24	2.94E-117
Adgrf1	2.14	3.33E-38
Jakmip2	2.13	3.52E-02

Gene name	Log2 FC	Adj p-value
Ptgir	2.11	2.64E-07
Sh3gl2	2.07	2.12E-13
Il1r2	2.06	1.44E-02
Calcr	2.06	3.97E-04
Sorl1	1.91	2.15E-02
Obscn	1.90	1.84E-02
Egr3	1.89	1.12E-17
Rhox12	1.88	1.01E-09
Btbd11	1.87	2.78E-02
Aqp1	1.86	2.78E-02
Ggta1	1.84	3.86E-03
Arrb1	1.79	6.81E-07
Ccdc170	1.73	1.13E-28
S100a4	1.71	8.38E-20
Klhl38	1.71	9.71E-05
Cavin3	1.71	3.54E-49
Folr1	1.69	7.63E-06
Col6a2	1.68	3.38E-05
Macrod2	1.64	1.65E-02
Fam160a2	1.62	2.75E-158
Inppl1	1.61	4.48E-201
Gdpd5	1.59	3.17E-71
Cd7	1.56	8.40E-03
Fes	1.55	3.63E-08
Cadps	1.55	7.07E-04
ENSCGRG00001000057	1.54	3.50E-02
Numa1	1.52	1.56E-27
Ptpre	1.50	3.18E-03
Slc7a11	1.50	6.69E-03
Dpysl3	1.50	1.17E-02
Tmcc3	1.49	3.08E-02
ENSCGRG00001011331	1.48	7.54E-06
Gstp3	1.48	4.26E-05
Clpb	1.45	1.52E-54
Cmklr1	1.45	1.93E-02
Slc39a2	1.43	2.62E-04
Cnga4	1.42	4.54E-08
Arap1	1.41	1.31E-101
Mefv	1.39	1.02E-04
Stambpl1	1.36	3.36E-02
Ncf4	1.35	2.76E-02
Flt1	1.35	1.02E-06
Add2	1.33	2.70E-02
Ccl2	1.33	4.10E-07
S100a5	1.32	6.16E-07
Acy3	1.32	8.10E-14
Tenm2	1.32	9.91E-06

Gene name	Log2 FC	Adj p-value
ENSCGRG00001011604	1.28	1.10E-02
Rnf121	1.27	9.69E-89
Akr1b7	1.27	3.07E-04
Hmga2	1.26	2.92E-02
Neu3	1.25	4.05E-20
Flnc	1.25	1.33E-03
Tmem178	1.25	2.41E-05
Tbxa2r	1.23	1.11E-09
Cyp4b1	1.22	4.33E-05
Tmem40	1.22	4.92E-03
Rap1gap2	1.20	2.71E-02
Epb41l4a	1.19	4.45E-02
Pold3	1.19	1.86E-08
Tsku	1.19	6.83E-14
Il18bp	1.18	1.34E-05
Grin2d	1.18	2.82E-02
ENSCGRG00001011191	1.17	1.39E-09
Sulf2	1.17	2.94E-05
Itpripl2	1.17	3.73E-02
Pgm2l1	1.16	8.40E-05
ENSCGRG00001016425	1.15	6.83E-07
Map3k2	1.15	3.92E-02
ENSCGRG00001012091	1.14	4.81E-34
Kynu	1.14	2.71E-02
Cd82	1.14	4.55E-12
ENSCGRG00001018722	1.14	3.62E-02
ENSCGRG00001015719	1.14	7.48E-22
Lamtor1	1.14	1.44E-46
Anapc15	1.12	3.25E-13
Thbs1	1.11	4.84E-02
Rnf125	1.10	5.79E-37
Lrrc51	1.10	2.03E-11
Zfp532	1.09	1.38E-09
Olfm1	1.09	9.57E-13
Tcf4	1.07	7.00E-05
2010109I03Rik	1.07	2.86E-02
ENSCGRG00001019427	1.07	8.13E-03
Megf11	1.06	4.40E-02
ENSCGRG00001004748	1.05	2.30E-22
ENSCGRG00001001317	1.05	4.57E-10
Cntn1	1.05	7.03E-06
Acer3	1.04	6.86E-07
Nhsl2	1.03	2.96E-02
Sdk2	1.02	4.48E-23
Trim36	1.02	2.27E-03
Stard4	1.02	2.21E-02
ENSCGRG00001010021	1.01	6.65E-22

Gene name	Log2 FC	Adj p-value
ENSCGRG00001006147	1.01	6.24E-04
Pecam1	1.01	2.58E-02
Fam83a	1.00	6.26E-18
ENSCGRG00001018251	0.99	6.65E-22
Dmxl1	0.99	4.96E-04
Adam19	0.98	1.46E-12
C1qtnf1	0.98	1.45E-05
ENSCGRG00001005533	0.98	2.67E-03
Wdr7	0.97	5.72E-05
ENSCGRG00001010009	0.97	3.44E-04
ENSCGRG00001022855	0.97	4.92E-02
Mbd1	0.97	4.70E-07
B4galt6	0.97	2.71E-04
Kctd14	0.97	3.00E-04
ENSCGRG00001014048	0.97	3.49E-05
Ccr7	0.96	6.43E-06
Igf2bp3	0.96	1.88E-06
Ptprj	0.96	2.41E-02
Ier3	0.96	3.98E-18
Kdm7a	0.96	3.00E-02
ENSCGRG00001013667	0.94	2.16E-23
Tmem176a	0.94	1.87E-03
ENSCGRG00001017591	0.94	2.44E-02
Trim6	0.93	6.20E-09
St14	0.93	5.23E-18
Fgd3	0.92	4.42E-04
Gramd1b	0.91	5.74E-05
Il11	0.90	5.94E-05
Usp35	0.88	2.35E-12
Cited1	0.88	3.17E-04
Acsl6	0.88	1.70E-02
Adamts4	0.88	1.19E-02
ENSCGRG00001024542	0.87	4.80E-03
Tnfaip8	0.87	1.50E-19
Zfp952	0.86	5.46E-05
Hipk2	0.86	3.38E-02
Etv5	0.85	2.43E-15
Apc	0.85	8.96E-11
Neu2	0.85	3.64E-02
Mro	0.84	2.68E-02
RF00554-ENSCGRG00001002240	0.84	2.93E-03
Eif1a	0.84	9.28E-03
Thbd	0.83	2.18E-04
Diaph1	0.83	3.80E-04
Tns3	0.83	2.93E-03
ENSCGRG00001017407	0.83	1.39E-36

Gene name	Log2 FC	Adj p-value
Sh3pxd2a	0.83	1.69E-02
Ube2l6	0.83	6.76E-04
Ntn4	0.83	1.40E-03
Hivep3	0.82	4.31E-09
P4ha3	0.82	1.33E-04
Slc12a2	0.82	1.57E-05
Fam53c	0.82	4.79E-05
Robo2	0.81	4.36E-04
Car5b	0.81	1.36E-16
Atp10a	0.81	1.22E-14
Mmp12	0.81	1.12E-08
Ss18	0.80	4.76E-07
Synpo	0.80	2.25E-02
BC031181	0.80	1.17E-03
4930523C07Rik	0.80	2.84E-04
Arhgef16	0.79	1.91E-16
Aqp11	0.79	6.49E-06
Prickle1	0.79	3.34E-05
Kdm3b	0.79	5.19E-05
Rbm27	0.78	9.17E-03
Etv4	0.78	1.35E-12
Slpi	0.78	1.19E-12
Mmd	0.77	2.75E-03
Prdm2	0.77	3.67E-24
Malrd1	0.77	1.55E-03
Xiap	0.77	3.00E-40
ENSCGRG00001007108	0.77	7.34E-04
ENSCGRG00001002393	0.77	4.61E-03
Ppargc1b	0.77	2.08E-02
ENSCGRG00001009554	0.77	3.05E-02
Nrp2	0.77	6.43E-06
ENSCGRG00001010283	0.76	1.80E-09
8030462N17Rik	0.76	1.96E-02
ENSCGRG00001000882	0.75	2.29E-06
Tgm2	0.75	1.81E-03
Tmem176b	0.75	2.26E-03
Taf4b	0.75	5.46E-05
AW554918	0.75	1.64E-03
Mex3c	0.75	1.15E-07
ENSCGRG00001017909	0.74	2.26E-03
Rnf138	0.74	2.43E-09
Kctd21	0.74	2.57E-03
Ankhd1	0.74	1.39E-12
Ndst1	0.74	1.14E-06
Tpgs2	0.74	4.61E-03
Notch1	0.73	1.14E-04
Alg8	0.73	1.11E-17

Gene name	Log2 FC	Adj p-value
Ints4	0.73	5.10E-08
Arhgef25	0.73	4.87E-07
ENSCGRG00001020498	0.73	2.52E-09
Pkib	0.73	1.10E-06
Etv1	0.73	1.39E-04
ENSCGRG00001017325	0.72	7.17E-10
Atp2b1	0.72	6.13E-03
Cdc23	0.72	8.03E-11
Junb	0.71	3.70E-03
ENSCGRG00001000591	0.71	1.31E-02
Abcb1b	0.71	6.40E-11
Hmgxb3	0.71	9.45E-56
Fbxo32	0.71	3.86E-03
Anxa8	0.71	1.39E-02
Zfp36l2	0.70	1.14E-03
Rab27b	0.70	4.67E-06
Map1a	0.70	5.85E-14
Wdr36	0.70	7.73E-03
Atp6v1h	0.70	3.53E-57
Kcnn4	0.70	6.00E-03
ENSCGRG00001011066	0.70	2.32E-03
Pik3c3	0.70	3.78E-09
Adssl1	0.70	6.41E-04
Dusp6	0.69	3.73E-02
Scn3a	0.69	1.69E-03
Sertad2	0.69	3.38E-02
Nr2f1	0.69	2.79E-02
Iws1	0.68	9.58E-11
Hip1	0.68	4.86E-02
ENSCGRG00001016962	0.68	7.62E-04
Arap3	0.68	3.03E-24
Tmed7	0.68	5.39E-35
Slc24a3	0.67	2.58E-02
ENSCGRG00001015991	0.67	4.30E-02
C77080	0.67	1.66E-08
Ndufc2	0.67	4.39E-13
Socs5	0.67	2.52E-02
Ccdc112	0.67	2.26E-06
ENSCGRG00001006024	0.66	2.76E-09
Rb1cc1	0.66	3.90E-21
Garem1	0.66	5.13E-12
Rnmt	0.66	4.55E-06
Mmp9	0.66	7.47E-03
Gypc	0.66	1.36E-06
Rprd1a	0.65	5.52E-05
Pias2	0.65	2.80E-07
Rsf1	0.65	5.02E-05

Gene name	Log2 FC	Adj p-value
Lman1	0.65	2.01E-03
Elk4	0.64	1.90E-02
Ptpn2	0.64	6.97E-10
Zfhx3	0.64	2.01E-04
Exph5	0.64	4.25E-02
Pstpip1	0.64	1.11E-04
Mbd2	0.64	5.85E-05
Socs3	0.64	1.21E-03
Pdzd2	0.63	1.86E-02
Vstm4	0.63	2.03E-03
ENSCGRG00001000991	0.63	1.04E-06
Camta1	0.63	1.77E-02
Ythdc2	0.63	1.93E-10
Clns1a	0.63	1.45E-07
Nr3c1	0.62	1.15E-12
Pde1b	0.62	3.36E-03
Cped1	0.62	7.05E-07
Trappc8	0.62	2.35E-07
ENSCGRG00001016918	0.62	6.53E-03
Atp5a1	0.62	4.84E-12
ENSCGRG00001008041	0.62	4.18E-11
Bcl2l11	0.62	5.71E-10
Bahcc1	0.62	3.04E-02
Sap130	0.61	2.21E-13
Dctn4	0.61	1.72E-12
Malt1	0.61	1.67E-03
Csnk1a1	0.61	7.58E-03
Tlr3	0.61	1.29E-04
Smad2	0.61	5.15E-04
Tcof1	0.61	5.95E-09
Prelid3a	0.61	1.02E-02
Gnpda1	0.60	5.74E-09
Slc25a46	0.60	2.29E-03
Ino80c	0.60	6.47E-10
Fem1c	0.59	1.24E-02
0610009O20Rik	0.59	2.34E-08
Aqp3	0.59	1.54E-03
Nav2	0.59	4.12E-03
ENSCGRG00001016215	0.59	2.19E-04
Zfp608	0.59	1.22E-03
Pfdn1	0.58	1.16E-08
Cnksr1	0.58	6.89E-03
Cdsn	0.58	6.41E-03
Akr1b8	0.58	3.11E-04
Neurl1a	0.58	1.92E-05
Gpr3	0.58	2.13E-02

Table 2 Gene list of genes down-regulated in the control compared to the CQ-evolved cells, with the log2 fold change (Log2 FC) and the adjusted p-value of the change (Adj p-value).

Gene name	Log2 FC	Adj p-value
Hecw1	-4.45	9.11E-05
Tll2	-3.09	2.32E-04
Svop	-2.73	9.04E-03
Clec3b	-2.73	2.09E-05
Prlh	-2.29	9.03E-03
Fbln1	-1.96	4.16E-02
Postn	-1.83	4.02E-02
Kif26b	-1.83	1.22E-04
Edn1	-1.82	1.75E-05
C1qtnf6	-1.81	4.25E-02
Gpx3	-1.68	4.42E-04
Pinlyp	-1.64	3.28E-02
Ankrd55	-1.60	2.12E-02
Gstm3	-1.59	4.09E-05
Cxcl12	-1.57	3.50E-08
Ces1d	-1.48	3.82E-02
Clmp	-1.48	1.02E-02
Zp1	-1.44	4.18E-02
Cda	-1.43	2.04E-16
Pald1	-1.40	3.32E-03
Map3k7cl	-1.37	2.53E-05
ENSCGRG00001012226	-1.34	1.36E-05
Aldh3b1	-1.34	1.93E-03
Coro2a	-1.32	5.69E-03
ENSCGRG00001024803	-1.29	1.33E-20
Ckb	-1.26	5.63E-04
Nedd9	-1.26	2.93E-03
Mb	-1.23	2.34E-11
Col3a1	-1.17	7.19E-04
Gap43	-1.17	4.10E-07
4930407I10Rik	-1.13	4.57E-03
Gpr37l1	-1.13	2.45E-02
Oit3	-1.13	1.47E-02
Slc22a3	-1.12	5.83E-10
Wt1	-1.10	3.83E-06
Lrp2	-1.09	1.61E-02
Ncald	-1.08	1.24E-04
1700008O03Rik	-1.00	4.29E-02
Alox5	-1.00	1.67E-04
Manba	-0.99	3.27E-05
Apba2	-0.97	1.23E-06
Sprr3	-0.97	9.63E-04
Styxl1	-0.97	1.56E-02
Abca4	-0.94	1.02E-02

Gene name	Log2 FC	Adj p-value
Vsnl1	-0.94	1.13E-02
Angptl4	-0.94	7.11E-03
Ikzf3	-0.93	1.35E-03
9130409I23Rik	-0.92	2.40E-02
Aebp1	-0.90	1.96E-02
Col4a1	-0.90	3.28E-03
Fam26e	-0.89	6.75E-05
Vegfd	-0.89	4.00E-02
Carmil2	-0.88	1.11E-02
Zfp90	-0.88	2.86E-02
Gpr162	-0.88	1.19E-02
Cxcl10	-0.87	4.01E-02
Itga9	-0.87	2.02E-02
Slc1a3	-0.85	9.87E-19
Gstm7	-0.85	2.85E-43
Arhgef10l	-0.84	2.02E-08
Ldhd	-0.83	3.25E-05
Dnaic2	-0.82	2.80E-07
Nmnat2	-0.82	4.21E-02
Slc22a15	-0.81	4.92E-13
Antxr1	-0.81	1.89E-03
Hoxa4	-0.80	1.04E-03
Fam189a2	-0.80	9.92E-13
1700007K13Rik	-0.79	2.64E-02
Star	-0.78	1.12E-03
Rcc2	-0.76	7.61E-09
Tenm3	-0.75	4.76E-08
Angptl6	-0.72	3.81E-05
Fn1	-0.72	3.87E-03
Ankrd1	-0.72	1.79E-02
Osr1	-0.72	4.81E-03
Filip1l	-0.72	9.56E-03
Fhl1	-0.71	2.58E-12
Tcea2	-0.71	1.62E-12
Gm19410	-0.71	3.58E-05
ENSCGRG00001011871	-0.69	2.07E-02
Pkp2	-0.69	4.57E-03
ENSCGRG00001015782	-0.68	1.10E-02
Olfml3	-0.68	1.52E-04
ND3	-0.68	2.59E-03
Rapgef3	-0.67	4.09E-03
Plekha6	-0.65	4.21E-02
Deup1	-0.65	4.33E-39
Wdfy4	-0.64	4.13E-06
Axin2	-0.63	2.35E-12
Gmpr	-0.62	5.23E-04
Banp	-0.62	7.47E-20

Gene name	Log2 FC	Adj p-value
Noxo1	-0.62	7.60E-03
ENSCGRG00001000005	-0.61	3.62E-02
Bcat1	-0.60	4.48E-03